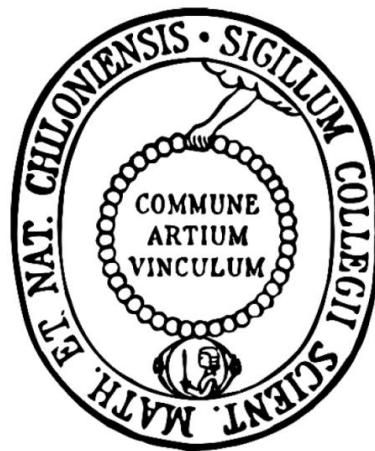


PARTICLE-PARTICLE INTERACTIONS
BETWEEN TAILORED MANNITOL CARRIER
PARTICLES AND DRUG PARTICLES FOR
INHALATION



DOCTORAL THESIS
SUBMITTED IN THE FULFILLMENT OF THE REQUIREMENTS
FOR THE DEGREE OF
DOCTOR IN NATURAL SCIENCES
AT
KIEL UNIVERSITY,
GERMANY

BY

MATHIAS WILLI MÖNCKEDIECK

KIEL 2016

Referee: Prof. Dr. Hartwig Steckel

Co-Referee: Prof. Dr. Thomas Kunze

Date of Exam: 23.09.2016

Accepted for Publication: 23.09.2016

Prof. Dr. N. Oppelt

(Dekanin)

Published research articles:

- Mönckedieck, M., Kamplade, J., Fakner, P., Scherließ, R., Walzel, P. and Steckel, H., The Impact of Particle Shape on the Dry Powder Inhaler Performance of Spray Dried Mannitol Carrier Particles, in: Dalby, R.N. (Ed.), RDD Europe 2015, Antibes, France, 265-268 (2015)
- Mönckedieck, M., Kamplade, J., Littringer, E.M., Mescher, A., Gopireddy, S., Hertel, M., Gutheil, E., Walzel, P., Urbanetz, N.A., Köster, M., Steckel, H., Scherließ, R., Spray drying tailored mannitol carrier particles for dry powder inhalation with differently shaped active pharmaceutical ingredients, in: Fritsching, U. (Ed.), Process Spray – Functional Particles Produced in Spray Processes, Springer Verlag, ISBN: 978-3-319-32368-8, (2016)

Conference contributions:

Oral Presentations:

- Mönckedieck, M., Kamplade, J., Walzel, P., Urbanetz, N., Steckel, H., Scherließ, R., Influence of mannitol carrier morphology on the DPI performance of different APIs, 26th Drug Delivery to the Lungs Conference, Edinburgh, Scotland, 13.12.2015, Pat Burnell New Investigator Award Nominee
- Mönckedieck, M.; Kamplade, J.; Fakner, P.; Steckel, H.; Walzel, P.: Spray drying of tailor-made mannitol carrier particles for dry powder inhalers, 26th European Conference on Liquid Atomization & Spray Systems, Bremen, Germany, 08.09.2014
- Mönckedieck, M.; Kamplade, J.; Fakner, P.; Steckel, H.; Walzel, P.: DPI performance of tailor-made spray dried mannitol and salbutamol sulphate particles, 6th International Congress on Pharmaceutical Engineering, Graz, Austria, 16.06.2014

Posters Presentations:

- Mönckedieck, M., Kamplade J., Walzel, P., Urbanetz, N., Steckel, H., Scherließ, R., Spray dried mannitol carriers in inhalation – the influence of surface energy and API distribution on drug detachment, 10th World Meeting on Pharmaceutics, Biopharmaceutics and Technology, Glasgow, Scotland, April 2016

- Mönckedieck, M., Kamplade, J., Fakner, P., Scherließ, R., Walzel, P. and Steckel, H., Impact of size and surface morphology of mannitol carrier particles on the FPF of DPI formulations, 20th Congress of the Aerosol Society for Aerosols in Medicine, Munich, Germany, June 2015
- Mönckedieck, M., Kamplade, J., Fakner, P., Scherließ, R., Walzel, P. and Steckel, H., The Impact of Particle Shape on the Dry Powder Inhaler Performance of Spray Dried Mannitol Carrier Particles, in: Dalby, R.N. (Ed.), RDD Europe, Antibes, France, May 2015
- Mönckedieck, M., Kamplade, J., Fakner, P., Steckel, H., Walzel, P.: Influence of particle shape of spray-dried mannitol carriers on powder flow and aerodynamic properties, 25th Drug Delivery to the Lungs Conference, Edinburgh, Scotland, December 2014
- Mönckedieck, M., Steckel, H., Urbanetz, N.: Tailored salbutamol sulphate particles for dry powder inhalation by adjusting spray drying parameters, 9th World Meeting on Pharmaceutics, Biopharmaceutics and Technology, Lisbon, Portugal, April 2014
- Mönckedieck, M., Steckel, H., Urbanetz, N.: Alteration of spray drying parameters for tailored salbutamol sulphate particles, Controlled Release Society, German Local Chapter, Kiel, Germany, February 2014

Learn from yesterday,
live for today,
hope for tomorrow.
The important thing is
not to stop questioning.

Albert Einstein (German Noble Laureat)

Meiner Familie gewidmet

Lack of a specific mark or a reference to a trademark or a patent does not imply that this work or part of it can be used or copied without copyright permission.

Table of contents

1	<u>INTRODUCTION AND OBJECTIVES</u>	1
1.1	INTRODUCTION	1
1.2	OBJECTIVES	2
2	<u>THEORETICAL BACKGROUND</u>	5
2.1	INHALATION THERAPY	5
2.1.1	HUMAN RESPIRATORY TRACT	5
2.1.2	TARGETS OF INHALATION THERAPY	7
2.1.3	FORMULATION STRATEGIES	8
2.1.4	MARKET REVIEW	10
2.2	DRY POWDER FORMULATIONS	11
2.2.1	CHALLENGES IN THE DEVELOPMENT OF DRY POWDER FORMULATIONS	12
2.2.2	DEVICES FOR DRY POWDER INHALATION	13
2.3	PARTICLE-PARTICLE INTERACTIONS	15
2.3.1	PARTICLE SIZE	17
2.3.2	PARTICLE MORPHOLOGY	18
2.3.3	INTRINSIC PARTICLE PROPERTIES	19
2.4	PARTICLE ENGINEERING	20
2.4.1	CARRIER PREPARATION	21
2.4.2	DRUG PREPARATION	24
3	<u>MATERIALS AND METHODS</u>	27
3.1	MATERIALS	27
3.1.1	D-MANNITOL	27
3.1.2	SALBUTAMOL SULPHATE	27
3.1.3	TIOTROPIUM BROMIDE	29

3.1.4	BUDESONIDE.....	29
3.1.5	FORMOTEROL FUMARATE	30
3.1.6	FURTHER REAGENTS.....	30
3.2	DESIGN OF EXPERIMENTS.....	31
3.3	PREPARATIVE METHODS	34
3.3.1	PREPARATION OF ENGINEERED CARRIERS.....	34
3.3.2	SALBUTAMOL SULPHATE.....	36
3.3.3	BUDESONIDE.....	39
3.3.4	FORMOTEROL FUMARATE	39
3.3.5	TIOTROPIUM BROMIDE.....	39
3.3.6	MANNITOL FINES.....	40
3.3.7	PREPARATION OF POWDER BLENDS	40
3.4	ANALYTICAL METHODS	42
3.4.1	PARTICLE SIZE.....	42
3.4.2	IMAGING TECHNIQUES	47
3.4.3	FLOWABILITY.....	54
3.4.4	SURFACE ANALYTICS.....	56
3.4.5	CRYSTAL LATTICE	60
3.4.6	DRUG QUANTIFICATION	60
4	<u>RESULTS & DISCUSSION.....</u>	63
4.1	SPRAY DRIED ENGINEERED CARRIERS.....	63
4.1.1	CARRIER STORAGE STABILITY.....	63
4.1.2	DESIGN OF EXPERIMENTS.....	65
4.1.3	PARTICLE SIZE.....	67
4.1.4	PARTICLE MORPHOLOGY	72
4.1.5	INFLUENCE OF OUTLET TEMPERATURE	82
4.1.6	FLOWABILITY.....	83

4.1.7	BET SURFACE AREA	86
4.1.8	SURFACE ENERGY	88
4.2	PREPARATION OF MODEL DRUGS	91
4.2.1	DESIGN OF EXPERIMENTS.....	93
4.2.2	PARTICLE SIZE.....	95
4.2.3	DRUG SHAPE	96
4.2.4	DRUG STORAGE STABILITY	98
4.2.5	SURFACE ENERGY	102
4.3	AERODYNAMIC CHARACTERISATION – INVESTIGATION OF PARTICLE-PARTICLE INTERACTIONS	103
4.3.1	PARTICLE SHAPE	106
4.3.2	SURFACE ROUGHNESS	117
4.3.3	PARTICLE SIZE	119
4.3.4	DRUG HYDROPHILICITY	122
4.3.5	CRYSTALLINITY	124
4.3.6	FLOWABILITY	125
4.3.7	SURFACE ENERGY	126
4.3.8	INFLUENCE OF FINES.....	126
4.3.9	IMPACT OF THE DEVICE	129
5	<u>OVERALL FINDINGS AND FUTURE PERSPECTIVES</u>	<u>132</u>
6	<u>SUMMARY.....</u>	<u>134</u>
7	<u>SUMMARY (GERMAN).....</u>	<u>138</u>
8	<u>APPENDIX.....</u>	<u>142</u>
8.1	HPLC METHODS	142
8.1.1	SALBUTAMOL SULPHATE.....	142
8.1.2	TIOTROPIUM BROMIDE.....	142

8.1.3	BUDESONIDE.....	143
8.1.4	FORMOTEROL FUMARATE	144
8.2	MATERIALS.....	145
8.3	ABBREVIATIONS.....	146
8.4	VARIABLES.....	148
	<u>REFERENCES</u>	<u>150</u>

1 Introduction and Objectives

1.1 Introduction

Drug delivery to the lung is the most relevant route in the local treatment of respiratory diseases like bronchial asthma or chronic obstructive pulmonary disease (COPD) and is in the focus of research for local drug administration e.g. in cystic fibrosis [1–3]. Reduction of drug related side effects by local treatment and high efficacy compared to other administration routes favour inhalation therapy. Drug particles entrained by the airflow during inhalation are directed straight to their therapeutic target resulting in a faster clinical response and higher drug concentrations in the target tissue than for the oral or intravenous routes [4,5].

Large lung surface area and adequate membrane permeability accompanied by exclusion of the first-pass metabolism, improve therapeutic effects not only locally but facilitate an attractive administration route for systemic delivery of drugs [4,5]. Several formulations for systemic use were approved by the US Food and Drug Administration (FDA) and the European Medicines Agency (EMA) recently. Adasuve[®] (Lorazepam, Alexza Pharmaceuticals Inc., California, USA) for the treatment of acute agitation associated with schizophrenia or bipolar disorder, Afrezza[®] (FDA-approved only, MannKind Corp., California, USA), marketed as inhalable insulin to treat insulin-dependent diabetes mellitus and Tyvaso[®] (Tadalafil, FDA-approved only, United Therapeutics Corp., Maryland, USA) as used against pulmonary arterial hypertension are only forerunners for several inhalable drugs for systemic use that are still under investigation.

Apparently, there is a tremendous potential to develop inhalable pharmaceuticals against all kinds of local or systemic diseases. Many current investigations focus on the development of dry powders for inhalation (DPI) since such formulations provide the highest chemical stability over time especially compared to liquid formulations. This makes the inhalation therapy even conceivable for peptides or proteins (as applied for inhalable insulin) [6].

Marketed DPIs are most often carrier-based systems with a sugar as a coarse carrier for fine drug particles as this approach helps to overcome size-dependent cohesion forces of drug-only formulations. Larger drug agglomerates are divided into smaller agglomerates or single particles during blending. The formulation of a new inhalation product is always a complex task that covers the consideration of many factors that might affect aerodynamic performance during inhalation and with this the effective amount of drug [7]. Diverse particle-particle interactions between carrier and drug, carrier and carrier as well as drug and drug need to be controlled to ensure consistent product quality. Apart from these, it is further

important to adapt the dry powder formulation to the dispersing mechanism of the necessarily required inhaler device. Particle-wall interactions as well as the design of the inhaler itself can crucially impact the aerodynamic performance of products for inhalation [8]. The challenges derived from carrier particle engineering via spray drying and the use of mannitol that has not yet been used as a carrier in marketed formulations will be targeted and discussed in this thesis and further be related to particle-particle interactions that arise from different carrier and drug properties to examine their effect on the respirable fraction of various drug particles.

1.2 Objectives

This thesis focusses on the preparation of dry powder formulations and the investigation of the complex mechanisms that affect the dispersion during inhalation. Despite several years of research on particle-particle interactions that occur in carrier-based systems, there are still essential issues that remain unclear [9,10]. The experimental design was geared to enable fundamental control over carrier and drug properties during preparation and was paired with advanced powder characterisations to improve the mechanistic understanding of drug detachment and dispersion during impaction analysis.

This project was admitted to the priority program “Process Spray” (SPP-1423) funded by the German Research Foundation (DFG), which was mainly dealing with the atomisation of sprays and its applications. Spray drying was chosen as technique of choice with respect to the magnificent control over product properties by adaption of the spraying parameters [11,12]. Collaboration with the Technical University in Dortmund, Germany facilitated the carrier preparation with a self-constructed spray tower that was equipped with a special laminar rotary atomiser targeting the production of particularly narrow particle size distributions as this reduced particle size variability within single batches [13–15]. A design of experiments was implemented to gain profound knowledge about the drying history of solute-water droplets since particle properties can be derived from the drying process and in the best case be correlated to particle-particle interactions between drug and carrier. Mannitol served as a carrier contrary to marketed products that mostly contain lactose monohydrate as this contributes to the storage stability due to the crystalline appearance of mannitol upon spray drying [16,17].

Drug particles were generated with a wide range of different properties since those properties are known to crucially affect the respirable fraction [18]. Spray drying was applied as a reliable technique to prepare a set of four drugs (salbutamol sulphate, tiotropium bromide, budesonide, formoterol fumarate) that appeared similar in particle size and shape but different in hydrophilicity as this enabled to investigate the influence of van der Waals forces or hydrogen bonds on the particle-particle interactions between drug and drug or

carrier and drug. Further, drug particles were spray dried with different sizes and particle shapes as controlled by the drying parameters to examine its effects on the aerodynamic performance [19,20]. Spray dried drugs were supplemented by jet-milled qualities to compare spherical drug particles with needle-like or unevenly shaped ones as well as amorphous state with mostly crystalline structures.

Dry powder analytics were applied for carrier and drug particles but also for interactive powder blends of both to understand the drying process of mannitol-water droplets [21–23] but also to generate profound knowledge about particle-particle interactions as these are based on respective powder characteristics [10,24–26]. Some supplementary experiments were introduced to compare the influences of different inhaler devices (Novolizer[®] and Easyhaler[®]), but also to investigate the impact of fines on the dispersion of powder blends with spray dried mannitol as carrier [27,28].

The overall experimental setup covers all steps from accurate carrier and drug preparation, over the blending procedure to the required powder analytics to enable considerable control over particle and blend characteristics but also to gain insight into the complex mechanisms that affect the aerodynamic performance of interactive powder blends during inhalation.

2 Theoretical Background

2.1 Inhalation Therapy

2.1.1 Human respiratory tract

The human respiratory tract can anatomically be divided into three different parts. The upper airways include the nasal passages, throat and pharynx. The lower respiratory tract is subdivided into passage zone, transition zone and respiratory zone with respect to the functional background (Figure 2.1) [29].

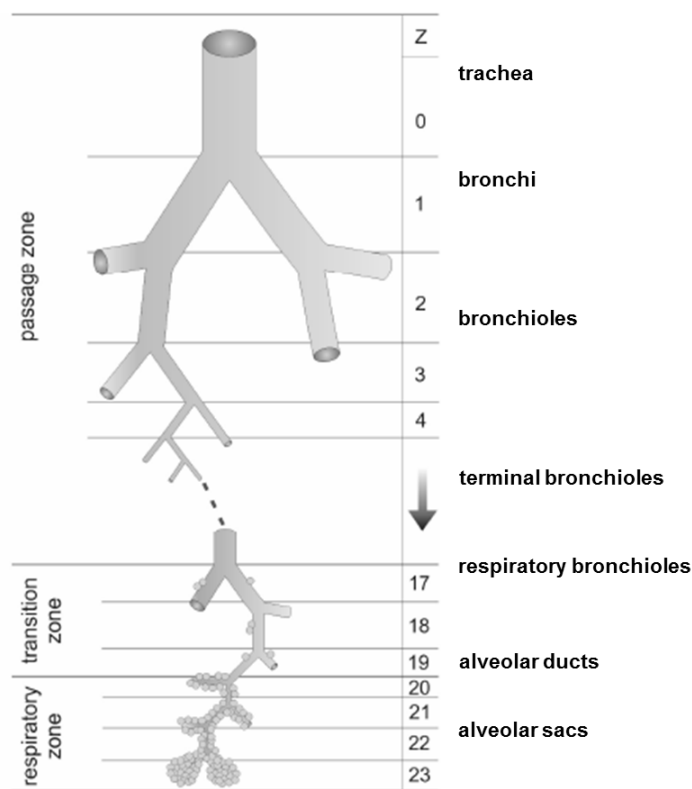


Figure 2.1 – Division of the lower respiratory tract, adapted from [30] with z = number of branches

The passage zone consisting of larynx, trachea, bronchi and bronchioles conducts air to transition and respiratory zone that include respiratory bronchioles, alveolar ducts and alveolar sacs. The trachea splits up into two bronchi that enter the right and left lung before they branch up into bronchioles and later alveolar ducts to finally terminate in the alveolar sacs [31]. Gas exchange between air and lung as the primary function of the lungs occurs in blood vessel-covered respiratory bronchioles, alveolar ducts, but mainly in alveolar sacs which likewise cover the main part of the total surface area of the lungs (total area of 80 – 90 m²) [29,31].

Based on the branched lung structure, inhaled particles are deposited at different places depending on particle size and density. Higher flow velocities in the bronchi and for the first branches of bronchioles trigger inertial impaction of inhaled material, whereas reduction of flow resistance by vastly increased total diameter of the airways reduced the flow velocities to finally reason sedimentation of smaller particles and diffusion of smallest particles with respect to the aerodynamic diameter (d_{dyn}) of those particles (Figure 2.2) [4,31].

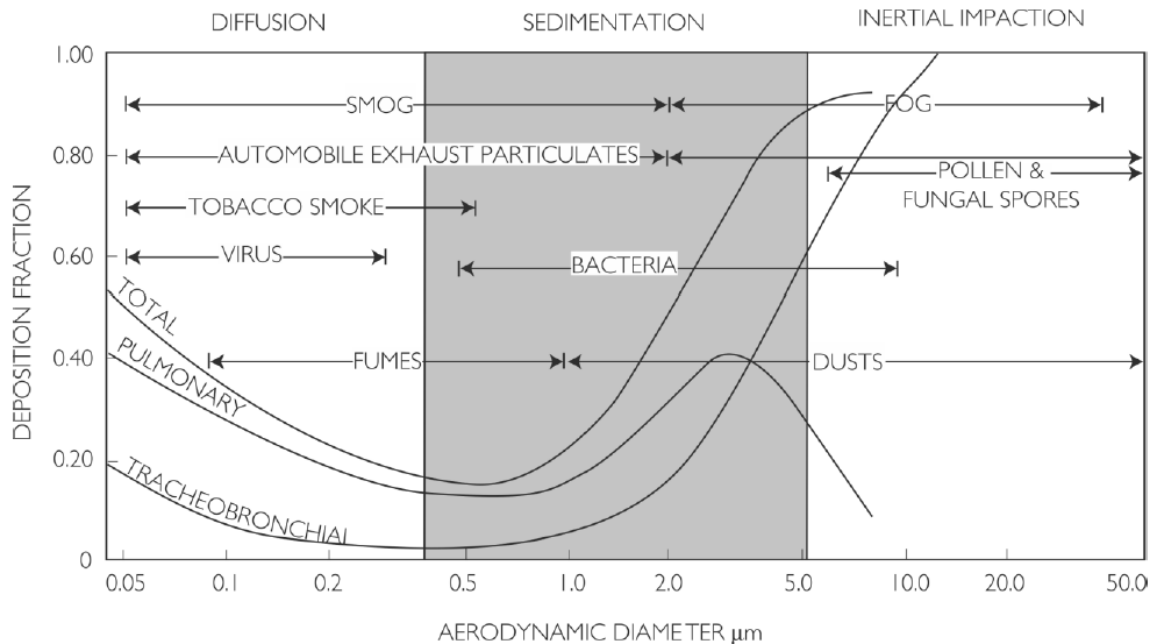


Figure 2.2 – Influence of the aerodynamic diameter (d_{dyn}) on the lung deposition of inhaled material (reprinted from Labiris and Dolovich [4])

This is of special interest for the inhalation of an aerosol consisting of droplets or particles dispersed in a gas phase. Particles with a d_{dyn} above 5 μm will preferably deposit in trachea or bronchi since high air flow velocity in connection to appropriate particle mass results in inertial impaction (Figure 2.3 – A). Materials stick to mucus-covered walls and are mainly removed by ciliary clearance to subsequently be swallowed and digested [4,9].

Smaller particles with a d_{dyn} ranging from 0.5 – 5 μm deposit by sedimentation in the respiratory zone with its alveolar ducts and sacs (Figure 2.3 – B) [32]. This fraction of particles, so called Fine Particle Fraction (FPF), is likewise the fraction of interest for all drugs administered to the lungs [33].

Lung deposition of the finest particles ($d_{dyn} < 0.5 \mu\text{m}$) is mainly affected by Brownian motion and, therefore, by diffusion (Figure 2.3 – C). However, only small amounts will get attached to the lung tissue, while most particles will be exhaled.

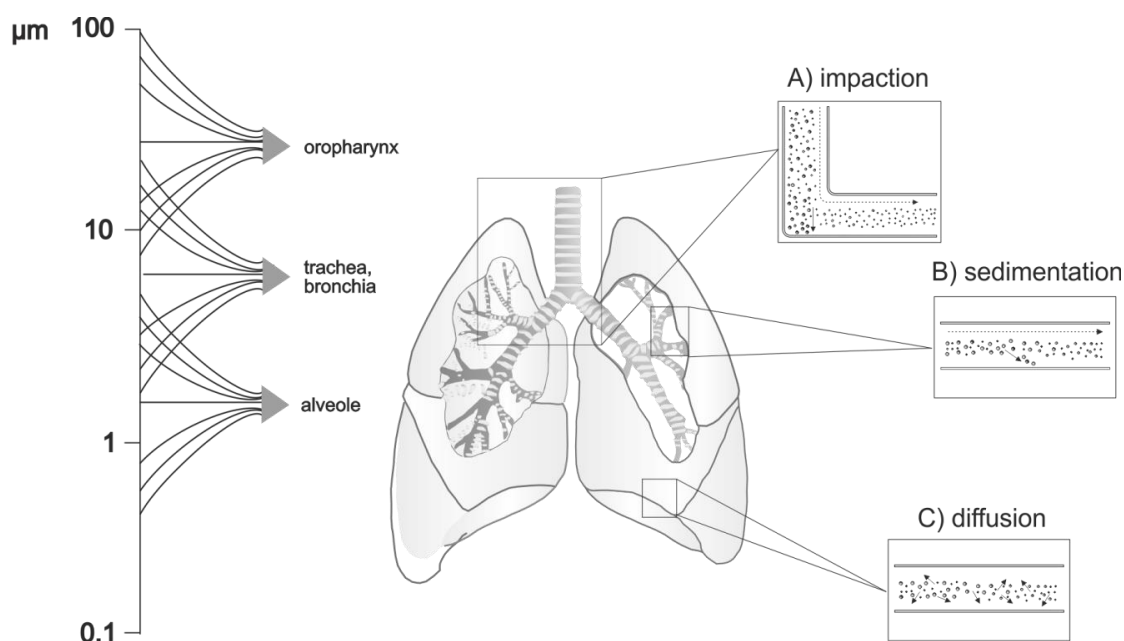


Figure 2.3 – Mechanism of lung deposition in relation to aerodynamic diameter (reprinted from Frömring et. al [34])

2.1.2 Targets of Inhalation Therapy

Inhalation of drugs has successfully been established to locally treat lung diseases. Several marketed products contain a wide range of different drugs for the treatment of asthma or COPD as the lung diseases with the highest prevalence [35,36]. Current research is further focussing on the therapy of cystic fibrosis and lung cancer or the vaccination via the lungs since the lung provides the bronchus associated lymphoid tissue (BALT) that enables mucosal vaccinations [2,37,38].

Systemically, inhalation therapy is of great interest as active pharmaceutical ingredients (APIs) or proteins delivered to the lungs avoid the hepatic first-pass effect and degradation in the gastro intestinal tract. Some marketed products proved this concept and raised hope for the development of pharmaceuticals objected to all kinds of diseases [6,39,40].

Different drugs used in this project are all known from asthma or COPD therapy guidelines. The Global Initiative for Asthma (GINA) and the Global Initiative for Chronic Obstructive Lung Disease (GOLD) release guidelines based on the latest state of the art and suggest the drug therapy with respect to disease severity [41–44].

The lung is mainly targeted by inhalation as local therapy was found to be the most effective route of drug delivery for those diseases. Drug classes for inhalation cover short or long acting β_2 -agonists (SABA / LABA), inhaled corticosteroids (ICS), anticholinergics, leukotriene receptor antagonists (LTRA, inhalation under investigation, marketed as oral formulation) as well as oral theophylline [29,41].

β_2 receptor agonists are used to mainly trigger bronchodilation. SABA like SBS are used as reliever in case of an exacerbation, while LABA like FOR are used as controller of the asthmatic symptoms. Muscarinic M_3 receptors are further targeted to also result in bronchodilation. This drug class is represented by TIO in this project. BUD that belongs to the ICS is regularly applied to control inflammation associated with asthma or COPD. A combination of BUD and FOR can also serve as a reliever due to the fast onset of the β_2 receptor agonist, when applied in asthma therapy of higher severity [29,41,42,44].

2.1.3 Formulation Strategies

All formulations for inhalation require dry or liquid particles (or agglomerates) of $d_{aer} < 5 \mu\text{m}$ to penetrate the deeper airways as described earlier (Section 2.1.1). Currently, four different device classes that are all based on different formulations are described by the European Pharmacopeia (Ph. Eur) [45].

2.1.3.1 Nebulisers

Nebulisers provide drug delivery to the lungs by conversion of drug solutions or suspensions into an aerosol. The devices use vibrating meshes, ultrasonic transducer or simply pressurised air for atomisation (air jet nebuliser) to generate droplets of appropriate size [46,47]. The emerging aerosol is then inhaled over a mouthpiece or a facemask. Virtually any soluble drug or mixture of different drugs and in any dose can be administered by nebulisation, which favours them for infant therapy [1]. Nebulisers can further be used for ventilated patients or those suffering from diseases like dementia or Alzheimer since no specific coordination or device actuation is needed.

At the same time, those device systems are quite cost-intensive, bulky and require a consistent power supply, which limits the use in everyday life [46]. Single dose delivery covers prolonged treatment times compared to pMDIs or DPIs and is reported to shift in droplet size over time [48,49]. Hence, other devices are preferred for standard therapy of asthma or COPD.

2.1.3.2 Pressurised Metered-Dose Inhalers (pMDI)

Pressurised metered-dose inhalers (pMDIs) are portable devices that provide the aerosolisation of drug solutions or suspensions upon actuation by the patient. The drugs are therefore either dispersed in the propellant to form a suspension or dissolved in the propellant to build a drug solution [50]. MDIs have been invented in the 1950s [46] based on chlorofluorocarbon propellants (CFCs) that have mostly been replaced by environmentally less harmful hydrofluoroalkanes (HFAs) at current stage [51]. The formulation, often

supplemented by stabilising or performance modifying excipients, is added to a can with metering valve to ensure adequate dosing.

A single dose is released from the inhaler device upon actuation forcing the drug solution or suspension through a spray orifice to generate an aerosol. The propellant evaporates rapidly to leave solid particles of adequate size (0.5 – 5 μm) that are subsequently inhaled by the patient [46].

For pMDIs, very short treatment times, low production costs and fine particles of the emerging aerosol contrast to stability concerns of the dissolved or suspended drug and high aerosol cloud velocities that result in remarkable particle depositions in the oropharynx when misapplied by the patient [52,53]. However, pMDIs are typically known to enable high FPFs, while reduced lung deposition is further supplemented by issues with the coordination of pMDI actuation and simultaneous inspiration, which results in dose variability and low lung doses as reported in several studies [54]. Spacers that reduce inhalation variability based on easier coordination during inhalation are rather applied for infants or elder people and help to overcome coordination and oropharynx deposition issues. However, they are not routinely used with respect to higher costs.

Breath-actuated devices like the Autohaler[®] have been invented to overcome coordination issues as the aerosol cloud is released upon inhalation. Accordingly, patient-to-patient variability is decreased for those devices.

2.1.3.3 Non-Pressurised Metered Dose Inhalers

Non-pressurised metered-dose inhalers or so-called soft mist inhalers (SMIs) as invented with Boehringer Ingelheim's Respimat[®] generate a low velocity spray from aqueous or ethanolic drug solutions that are forced through a nozzle system. Administration of the drug dose is actuated by the patient and independent from the inspiratory effort. Coordination between inhalation and actuation is simplified due to prolonged treatment times based on lower spray velocities, which in turn results in higher respirable fractions and lower dose variability due to less deposition in the oropharynx compared to pMDIs [46,55,56]. Nevertheless, the use of the Respimat[®] is restricted as only aqueous or ethanolic drug solutions but no suspensions can be delivered, which might change for future devices with adapted dispersion mechanism. Currently, SMIs are designed as a non-reusable devices resulting in remarkably higher costs compared to simple pMDIs [46].

Excellent inhalation performance contrasts to stability concerns and the low number of drugs that can be used for SMIs, which favours dry powder formulations for adequate drug delivery to the lungs as will be discussed in the following sections.

2.1.3.4 Dry Powder Inhalers (DPIs)

Dry powder formulations were initially invented in the 1970s, where the first capsule-based inhaler device (Spinhaler®), containing sodium cromoglycate as a drug, was marketed [57]. Portable DPI devices combine several advantages such as prolonged long-term stability of drugs, higher drug contents per dose or increased respirable drug fractions compared to pMDIs [46]. Marketed inhaler devices work breath-actuated and use the inspiratory forces of the patient for particle dispersion, which results in reduced aerosol velocities and lower oropharyngeal drug depositions that in turn induce higher respirable fractions than gained for pMDIs [58]. DPIs are further beneficial to nebulisers or pMDIs as no propellants or external power sources are demanded to disperse the drug particles [46].

Formulations are packed in capsules, reservoir containers or blister stripes, which further protect them from moisture uptake. Dose adaptations can easily be implemented by replacing capsule sizes and capsule cavity, blister cavity volume or the dosing cavity of a container-based multi dose inhaler by another one [32].

Nevertheless, it needs to be mentioned that despite better results in the overall inhalative dispersing mechanism differences from patient to patient can be observed with respect to the applied inspiratory airflow. Especially, elder people or those suffering from severe asthma or COPD are known to not sufficiently inhale drugs with a DPI, which is reflected in the respirable fraction of drug [59].

The aerodynamic performance of any dry powder for inhalation is a combination of powder properties, inhaler device and the patient habits [59].

2.1.4 Market Review

Despite their advantages or disadvantages, all mentioned devices are currently marketed all over the earth. Lavorini et al. examined the overall retail sales between 2002 and 2008 retrospectively for sixteen European countries to discover the dispensing habits regarding nebulisers, pMDIs and DPIs [60]. They found that more than 75 % of the respiratory drugs prescribed in the UK were applied with pMDIs, while at the same time more than 80 % of the patients in Sweden used DPIs for their inhalation therapy. Germany ranged in the midfield with < 40 % pMDIs and > 45 % DPIs in respiratory use [60].

The large number of sold pMDIs, especially for the use of SABA and ICS containing inhalers [60], can be attributed to low costs for the healthcare system, but also to SABA containing formulations that are commonly used as favourable rescue medication. Figure 2.4 illustrates those discrepancies as the sales volume of DPIs covers less than 25 % of the totally sold respiratory formulations but demands almost half of the costs of all formulations, while pMDIs

as the cheapest marketed devices make up over 60 % of the total sales volume, but only 20 % of the associated costs [61].

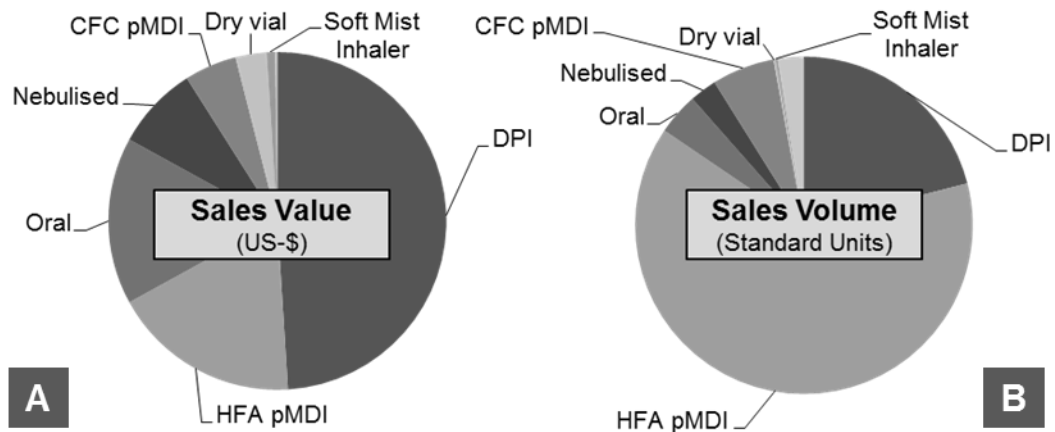


Figure 2.4 – Market review of medicine sold in asthma therapy A: sales values by device / formulation in % (US-\$) for the six major markets (US, France, Germany, Italy, Spain and the UK) and B: sales volumes by device / formulation in standard units for the same markets in 2009 [61]

Nevertheless, it is beneficial to support inhalation therapy based on DPIs with respect to adequate and reliable lung depositions due to convenient handling even though single unit costs exceed pMDI expenses.

Future trends in respiratory drug therapy predict increasing sales values for the following decade. Current sales values of 14,740m US-\$ (2013) in asthma therapy are awaited to reach 17,689m US-\$ in 2021, while COPD therapy is predicted to increase from 8,395m US-\$ (2013) to 9,464m US-\$ in 2021. Most recent launches, such as Spiolto[®] (olodaterol and tiotropium bromide) or Striverdi[®] (olodaterol), were applying the Respimat[®] for administration, while others such as Breo[®] or Relvar[®] (both fluticasone furoate and vilanterol trifenate) using an Ellipta[®] DPI device or Eklira[®] (aclidinium bromide) administered with a Genuair[®] inhaler device were based on dry powder formulations. Accordingly, market growth will most likely be accompanied by further shift towards modern inhaler devices with respective dispersion mechanisms.

2.2 Dry Powder Formulations

The development of new formulations for DPI use requires the consideration of a large number of factors that might influence the overall aerodynamic performance of the new product. Not only particle properties of all components including the drug itself, particle-particle interactions between all components or particle-wall interactions between formulation and inhaler device, but also the choice for the best inhaler device with its associated dispersing mechanism is of importance.

2.2.1 Challenges in the Development of Dry Powder Formulations

Based on the lung anatomy, drug particle size is known as the critical factor for the lung deposition of inhaled formulations (see Section 2.1.1). Aerodynamic particles sizes of $d_{dyn} = 0.5 - 5 \mu\text{m}$ are required for adequate deposition in transition or respiratory zone of the lungs [32]. In these days, drug particles are mainly prepared by micronisation [62], whereas other techniques like spray drying [16,63–65], freeze drying or the micronisation from super critical fluids [66] have also shown to be applicable for these size ranges [32,62]. However, drug particle engineering demands the control of physicochemical characteristics as properties might shift over storage time as will be discussed later [67].

Cohesiveness of drug particles is by far the main challenge in dry powder formulations. A pronounced tendency to build drug agglomerates can be attributed to the sum of adhesion forces (e.g. van der Waals forces, capillary forces or dielectric forces) as associated to increased specific surface area that dominates gravitational forces due to low mass of single drug particles. Drug bulk flowability is massively decreased for those small particles, which renders adequate dosing impossible for pre-metered capsules or blister stripes but also for container based devices.

Different engineering techniques have been applied to overcome those issues. Some formulations target the preparation of size-controlled agglomerates (soft pellets) that size-dependently provide adequate flow characteristics and, thus, appropriate dosing quality. Those agglomerates require dispersion by inspiratory shear forces to enable penetration of the lungs [68]. Another concept has been implemented with the PulmoSphere[®] technique which is based on the preparation of low density spheres by a spray drying approach. The spheres are larger than commonly applied drug particles which triggers adequate powder flow and impact in the respiratory zone of the lung due to low density and, hence, reduced inertial forces [69,70].

Most launched products apply larger carrier particles to improve powder flow and dosing accuracy. Those binary so-called interactive powder blends usually consist of coarse carbohydrate particles and small drug particles, but can be supplemented by fine sugar particles (so-called fines) to receive ternary interactive powder blends [27,32]. Figure 2.5 illustrates the preparation and inhalation of binary interactive powder blends. Carrier particles, mostly consisting of lactose monohydrate with sizes ranging from 50 – 200 μm are blended with drug particles in micrometre range (0.5 – 5 μm) to evenly distribute the drug on the carrier surface. The improved powder flow enables accurate dosing for all kinds of inhaler devices and inspiratory shear forces ensure the detachment of single drug particles or small drug agglomerates from the carrier surface to get entrained by the airflow to penetrate the lungs [46].

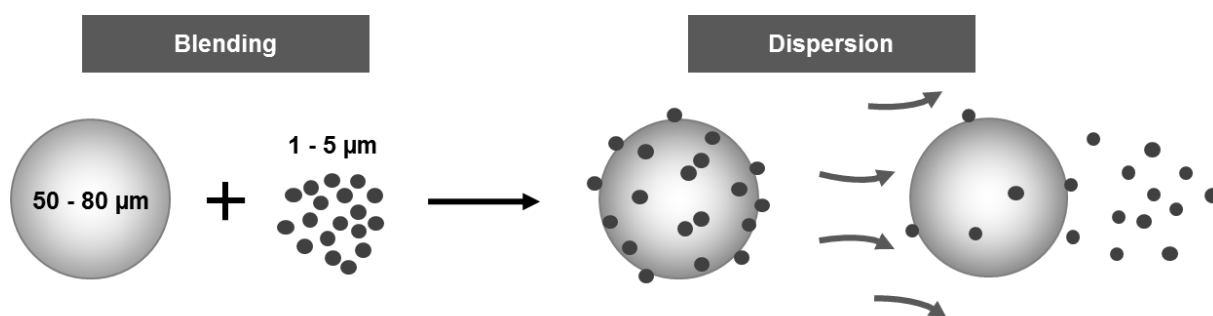


Figure 2.5 – Blending of binary powder blends and dispersion during inhalation

Further, several marketed dry powder formulations and studies published in literature involve fines (further component smaller in size than the carrier) added to the formulation to gain ternary powder blends [7,27]. Lactose fines with a size slightly larger than the drug were described to be beneficial for the respirable drug fraction. Grasmeijer et al. mentioned different theories with positive effect on the inhalative performance such as the buffer theory for which slightly larger mannitol fines protect drug particles from press-on forces [24,27], the agglomeration theory that suggests small agglomerates of drug and fines for easier detachment [7,71] or the active-sites theory which describes that fines preferably bind to highly active sites on the carrier to result in simplified release of drug particles [28,71,72].

Profound knowledge about particle-particle interactions that occur during all stages from preparation of single excipients, over blending and storage to the inhalative usage becomes evident for all kinds of dry powder formulation concepts, but requires supplementary information about the impact of the inhaler device as this is necessarily used to administer those formulations.

2.2.2 Devices for Dry Powder Inhalation

The de-agglomeration of interactive powder blends requires energy provided by inhalation with an inhaler device to overcome interparticulate forces and to result in adequate lung deposition as mainly assured by detachment and dispersion of drug agglomerates. The aerodynamic performance of the powder formulation is therefore strongly depending on the dose metering system and the mechanism to disperse the powder [46,73].

The first modern DPI device invented by Fisons Laboratories was marketed in 1969 with the sodium cromoglycate containing Spinhaler[®] as a passively-used capsule-based unit dose inhaler [57]. Several innovative inhaler devices were designed during the following decades to result in quite different device classes.

Most of the devices marketed for inhalation therapy are passive DPIs that deliver drug particles breath-actuated by inspiratory forces of the patient [46]. Some recent products, especially for systemic therapies, use an active dispersing system to de-agglomerate the dry

powder formulation (Afreeza®). Active DPIs are rather developed for APIs with low therapeutic index (such as insulin in Afreeza®) due to dosing variability that is present in passive devices based on differences in the inspiratory flow rate by the patient [74]. Active DPIs ensure accurate drug dispersion by the device itself and limit patient to patient variabilities. Further, they can be applied to boost the dispersion of those powders that are difficult to disperse.

Passive DPIs as implemented for inhalation therapy against pulmonary diseases comprise a broad range of different inhaler classes. Capsule-based unit dose inhaler such as Cyclohaler® or Handihaler® or multiple unit dose devices based on blister stripes (Diskus®) are designed as pre-metered dose inhalers that attain the lowest dosing variability of all devices. Devices applied in this thesis belong to the group of reservoir-based multi-dose DPIs that administer the drug upon a volume-based on-site metering of each dose with a respective dosing cavity. Adequate flowability is essential for formulations dispersed with a reservoir-based inhaler system to ensure suitably low dosing variability.

Reservoir-based multi-dose inhaler systems, first invented with the Turbohaler® in 1988, consist of powder reservoir, a dosing cavity adaptable in volume and different kinds of dispersing approaches [68]. Experiments performed in the framework of this project were mainly based on the Novolizer® (Figure 2.6). The device was designed and experimentally investigated by de Boer et al. [75]. Here, the fluidised powder dose was stressed by cyclone and impaction walls to disintegrate the interactive powder blends.

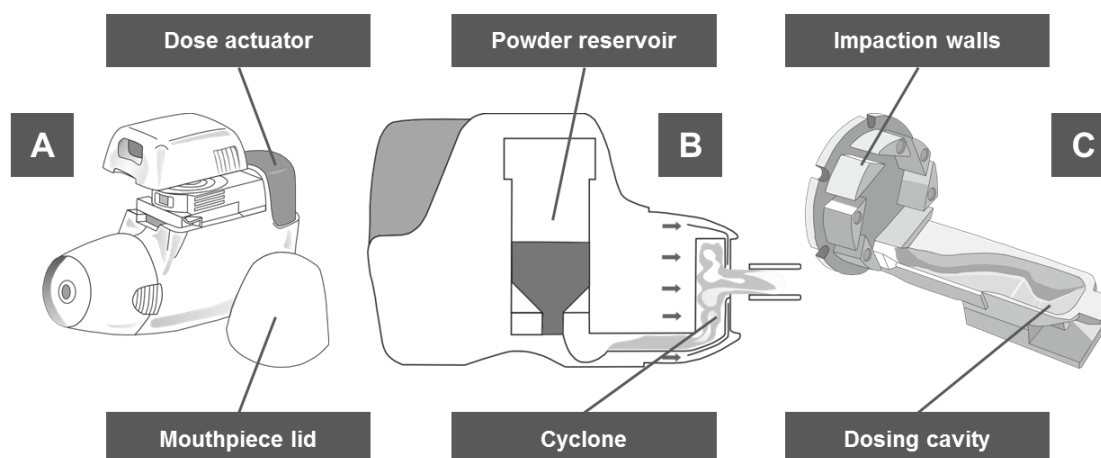


Figure 2.6 – Scheme of the Novolizer®; A: 3D scheme of the Novolizer® with mouthpiece lid, powder reservoir and dose actuator; B: 2D scheme of the Novolizer® with powder reservoir, dosing pocket and cyclone; C: 3D scheme of the dosing slide with dosing pocket and impaction walls [75]

Inhalation procedure starts with an initial dosing step performed by the patient via the dose actuator. Dispersion of the powder happens upon patient inhalation through the device and is supported by increased shear forces gained from the cyclone. This device was mainly designed for large solid carrier particles of higher true density as this results in inertial

impaction to impaction walls rather than for small or hollow particles. Inertial forces cause collisions of carriers to the impaction walls to enforce further drug detachment from the carrier surface [76].

This device was explicitly convenient for purposes in this project as it provides high detachment rates based on its dispersing mechanism, which allow easier detection of slight differences in the aerodynamic performances of different powder blends. Nevertheless, spray dried carrier particles used here comprise quite low bulk densities compared to milled or sieved qualities, which might reduce the impaction forces during inhalation.

The Easyhaler[®] (Figure 2.7) is another container-based multi-dose device that was tested to examine the applicability of results gained with the Novolizer[®] for other inhaler systems [77]. Here, inhaler design is kept very simple as only dose actuator with a spring, powder reservoir and dosing wheel were introduced without having an extra effect on the dispersion of the dry powder formulation. Respirable fractions were most likely expected to be lower than for the Novolizer[®] as cyclone or impaction walls are missing.

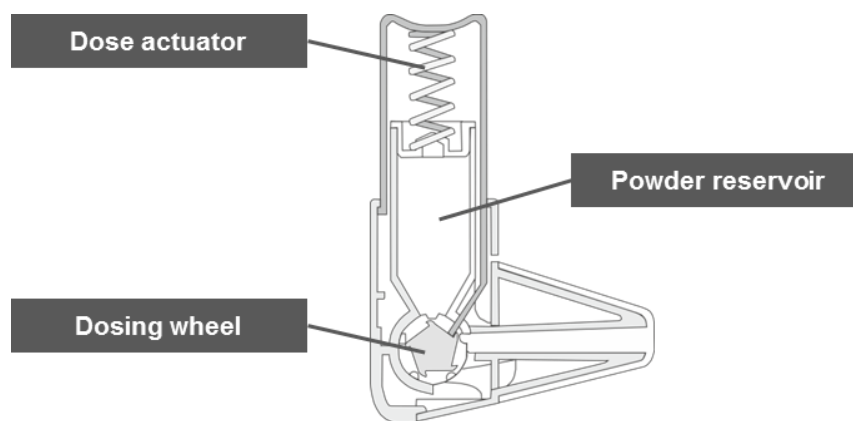


Figure 2.7 – Scheme of the Easyhaler[®] with dose actuator, powder reservoir and dosing wheel

2.3 Particle-Particle Interactions

Efficient drug dispersion during inhalation is governed by several factors that can coherently be described as particle-particle interactions. The energy transferred from inspiratory forces to the powder blends needs to exceed the energy that arises from particle-particle interactions to effectively disperse drug and carrier particles (plus eventually fines). Major forces that are described in literature (Figure 2.8) include those being dominated by physical forces without material bridges such as mechanical interlocking of particles in surface asperities (c), electrostatic charging by acceptor and donor charge transfers or tribo-electrification due to collision or friction of particles (d) and van der Waals forces that occur when dipoles are induced (f) [58].

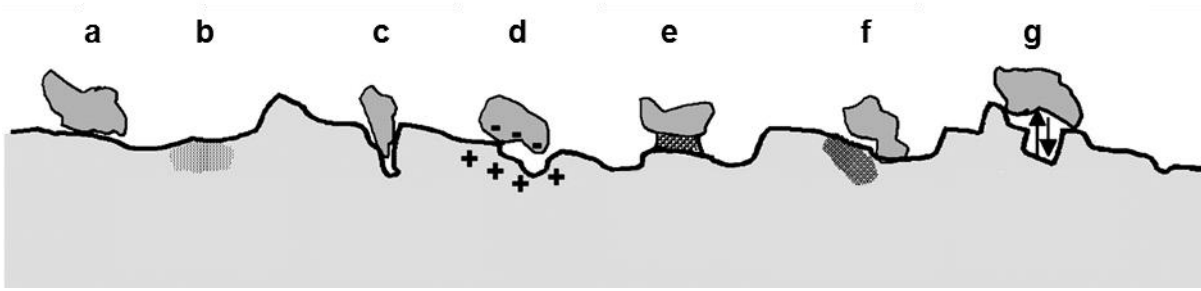


Figure 2.8 – Particle-particle interactions between carrier surface and small particles adhered to the surface modified from Hickey et al. [58]

Even stronger interactions arise from methods or ambient conditions that enforce material bridges as observed for liquid films or solid bridges. The presence of moisture at the interface of two particles induces capillary forces (e), while sintering of particles as caused by higher temperatures (a) or the recrystallisation of amorphous spots on the surface (b) triggers solid bridges between particles [58].

Further, acid-base interactions or hydrogen bonds (g) are mentioned as chemical properties that impact on particle-particle interactions. Particle properties like particle size, morphology or the porosity are therefore important as they impact on these interparticulate forces (Figure 2.9). A lot of work has been done earlier to discover dependencies between particle characteristics and performance during inhalation. Impaction analysis as a technique to study the detachment and dispersion of drug particles upon device actuation was introduced to investigate these dependencies and is required by the Ph. Eur. to assess the fine particle dose (FPD) of any formulation applied for inhalation [78]. The following sections will briefly summarise the main issues based on carrier and drug properties.

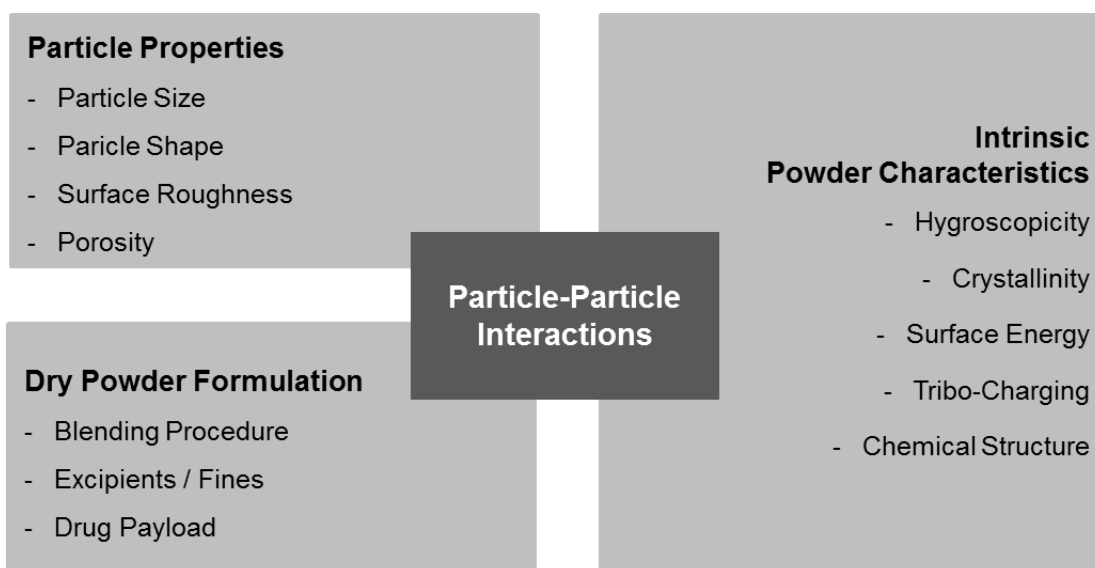


Figure 2.9 – Factors with impact on particle-particle interactions in interactive powder blends

2.3.1 Particle Size

Major impact on particle-particle interactions results from drug or carrier size, but can also be attributed to the addition of fines in so-called ternary powder blends as will be described later [79]. Adhesion of e.g. drug particles on the surface of a carrier or cohesion between particles consisting of the same material correlates to the ratio of interparticulate forces and weight forces that in turn depend on particle size and its bulk density (Figure 2.10). Interparticulate forces such as mechanical interlocking, capillary forces, electrostatic forces or van der Waals forces need to exceed the weight forces to enable attachment of drug particles on the carrier surface, but need to be small enough to ensure detachment by inspiratory forces [58]. At the same time, carrier particles require particle sizes that prevent agglomeration as carrier flow is crucial for adequate powder handling, filling and dosing [79].

Carrier sizes of 50 – 200 μm are required to generate adequate powder flow, but smaller carriers were found to perform better than larger ones [80,81]. The perfect carrier size is determined by low cohesion forces between single particles to prevent agglomerates and preferably low particle mass since this impacts press-on forces that press drug particles on the carrier surface during blending. The smallest carriers with the lowest mass and the least press-on forces that concurrently provide adequate powder flow are preferred for dry powder formulations.

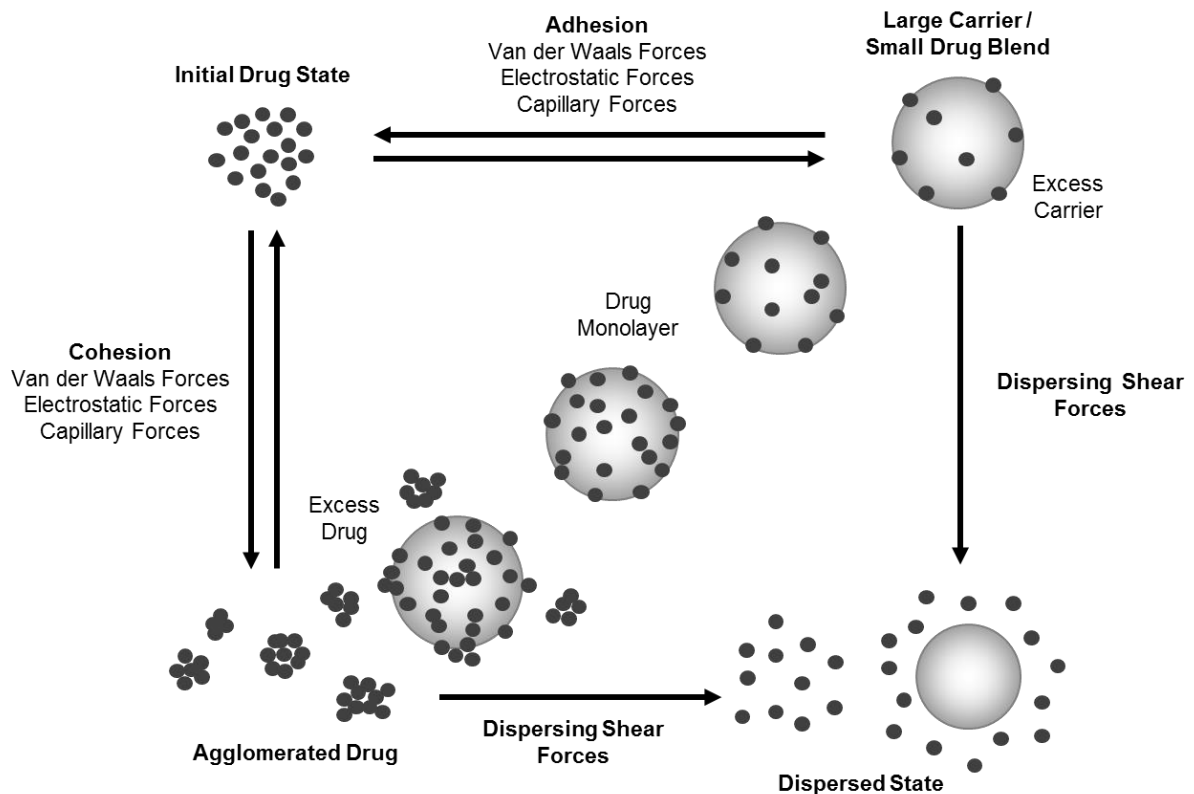


Figure 2.10 – Particle-particle interactions between carrier (large light grey particles) and drug particles (dark grey particles) modified from Steckel [48]

Drug particles are desired to penetrate the deeper airways of the lungs, which limits their suitable particle size. The inspiratory airflow detaches larger particles more easily than small ones with respect to a lower adhesion forces to mass ratio. However, improved drug dispersion contrasts to the targeted drug size that enables impaction in the deeper airways of the lung. Drug particles of perfect size are large enough to enable easy detachment, but small enough to penetrate the lungs to reach the respiratory zone (0.5 – 5 µm). Dispersion of interactive powder blends is further governed by the tendency to build agglomerates that consist of fine drug particles attached to each other by cohesion forces. However, agglomerates are not necessarily disadvantageous since dispersion enforces the generation of smaller agglomerates or single drug particles depending on agglomerate strength and inspiratory forces. High agglomerate strength or large single drug particles cause reduced respirable fractions.

A variety of different engineering approaches is conceivable for particle preparation of virtually any size required for inhalation purposes as introduced in Section 2.4, but demands the consideration of particle morphology as different particle shapes or surface structures influence particle-particle interactions (Section 2.3.2).

2.3.2 Particle Morphology

Particle-particle interactions arising from the particle surface are a measure of contact area and mechanical interlocking. The particle morphology of either carrier or drug particles is known to affect the dispersion of interactive powder blends. In accordance to marketed products, most of the studies published in the scope of interactive powder blends and dependencies on particle morphology are based on lactose monohydrate qualities, but have been extended to mannitol by Maas et al. [82,83] and Littringer et al. earlier within this project [16,20,22,23,64].

Former work targeted the optimisation of carrier properties by e.g. the controlled solvation of the carriers to generate smoother surfaces [84] or carrier modification upon milling or sieving [85]. Littringer et al. were the first focussing on the inhalation of spray dried mannitol carrier particles within this project. Mostly spherical particles were investigated and the impaction results were evaluated with respect to the particle morphology of the carriers [16,23].

In general, adhesion forces that arise from the effective contact area between carrier and drug correlate to the respirable fraction. The larger the contact area, the lower appears the drug fraction of interest. This correlation is apparently not only a function of carrier smoothness but also of drug shape as both interact with each other. Littringer et al. mentioned rough carrier surfaces to be beneficial for dispersion of micronised drugs due to an increased number of contact points, but a decreased total effective contact area [23].

When investigating the particle morphology it is crucial to differentiate between surface asperities that are assigned to surface roughness and those that describe the overall shape of the particle. Surface smoothing reduces the surface roughness but might also remove indentions that initially provide space for drug particles. Indentions or edges as e.g. gained by milling can enable mechanical interlocking and entrapment of particles resulting in lowered respirable fractions [86]. Mechanical interlocking can further impact on the flowability of a bulk as spherical particles provide the conceivably best flow properties.

The differentiation between particle shape and surface roughness was implemented for spray dried mannitol carriers to distinguish effects on the impaction analysis. Further, drug particles of alternating shapes were investigated to not only cover carrier morphology but also drug shape. All carriers or drugs used in this thesis were prepared by appropriate engineering approaches as introduced in Section 2.4.

2.3.3 Intrinsic particle properties

Particle-particle interactions arise not only from individually adjustable particle characteristics like size or morphology, but also from intrinsic particle properties that are dedicated to chemical structure, the engineering approach or to storage conditions.

The chemical structure of a material is the basis for other intrinsic particles properties such as the hydrophilicity [32]. It enables to determine the octanol-water-coefficient or so-called $\log P$ value as a measure of hydrophilicity. Low values indicate a material to be hydrophilic, while higher values are assigned to lipophilic substances. Long hydrocarbon chains or aromatic compounds as contained in substances with high $\log P$ values are attributed to the ability to build low energy van der Waals bonds, whereas nitrogen or oxygen containing functional groups support high energy hydrogen bonds in accordance to lower $\log P$ values and appropriate solubility in water, but are not the only factors affecting $\log P$ values. The effect of hydrophilicity on the DPI performance was investigated by implementation of drugs with different $\log P$ values to discover effects on particle-particle interactions between drug and hydrophilic mannitol carrier surface.

Substances purchased as pure organic material are usually crystalline, indicating that molecules are arranged in an ordered repeating pattern that forms the crystal lattice based on several non-covalent interactions [58]. Most solids exist in more than one crystal form. This so-called polymorphism implies one crystal modification to be the thermodynamically most stable one, while others tend to change to the thermodynamically more stable one based on the ambient conditions. Depending on the processing method, some substances even occur as non-crystalline or amorphous solid without long-range order. Crystal modifications are material-specific. Spray dried mannitol normally appears in the most-stable β -modification as proved by Littringer et al. earlier, whereas most drug substances result in

unstable amorphous structures upon rapid drying [16,87–89]. Optimally, excipients or drugs used for pharmaceutical products are used in the most stable modification to avoid stability issues. However, in some cases other modifications or amorphous materials may be beneficial in therapeutic use due to improved solubility especially of sparingly soluble drugs [90] or possibly enhanced dispersion during inhalation as will be examined in this project.

Handling stability issues was one of the main targets when working with spray dried drugs. Polymorphs differ not only in density, melting point or solubility, but also in the ability to absorb water. The capacity to absorb moisture in correlation to the ambient relative humidity (rH) is correlated to the crystal modification [67]. Amorphous products with high free Gibbs energies absorb more moisture than crystalline modifications of lower energy, but tend to transition into lower energy states upon moisture uptake or in correlation to the ambient temperature [32]. As this might trigger particle growth and, therefore, reduced respirable fractions, stability of the product during storage and handling is one of the main tasks.

Capillary forces are prominent for those particles that have absorbed moisture from the ambient air. Hydrogen bonds and capillary forces arising from absorbed moisture evoke quite strong particle-particle interactions that might further reduce the FPF during inhalation. Controlled moisture contents are required to enable repeatable results especially for thermodynamically instable products [32,58].

However, electrostatic charging of particle surfaces needs to be considered when reducing the ambient relative humidity. Some factors such as atmospheric ionisation, contact with charged objects, the chemical composition or triboelectric charges that arise from motion or wall friction of blend and device, generate electrostatic charges which might influence the inhalation performance as published by Karner et al. earlier within this project [91–93]. Nevertheless, charging can be reduced by adequate deionisation with respective instruments as performed in this thesis, but is not applicable in every-day life.

Particle properties might influence dry powder inhalation crucially, but can be controlled by the right choice of particle engineering, constant ambient conditions or adequate deionisation.

2.4 Particle Engineering

Current research and development projects in pharmaceutical industry require maximum control over the engineering processes of all excipients used for formulations as this determines their particle properties. Most components used in dry powder formulations are limited in over-all particle properties as most marketed products consist of sieved or milled lactose blended with micronised drug particles of undefined shape. This section gives an

introduction to different engineering approaches possibly used to prepare carrier or drug particles for inhalation.

2.4.1 Carrier Preparation

Carbohydrates for dry powder formulations demand the fulfilment of high quality standards since small differences in particle properties might vastly influence the aerodynamic behaviour. Carrier engineering is therefore targeting narrow particle size distributions (PSDs) and reproducible morphologies.

2.4.1.1 Recrystallisation and Sieving

Marketed products specialised for inhalation purposes are mainly based on sieved lactose monohydrate qualities e.g. InhaLac[®]. The crystalline raw material has previously been recrystallised by cooling the dissolved sugar and separating emerging particles from the solvent [94]. Sieving steps are mandatory to receive PSDs of adequate width. Different sieve fractions are applicable for inhalation with respect to several factors such as the inhaler device, the dry powder formulation or the purpose (carrier or fines). Sugar fines require an additional milling step to reach their final particle size.

Mannitol used here is usually gained by catalytic hydrogenation from mannose and recrystallised to end up with a raw product of wide PSD that requires sieving steps to achieve carrier qualities of controlled particle sizes.

For both, sieving of lactose monohydrate or mannitol, the sieving method can serve as a critical step during preparation as it might impact on the carrier surface. Especially, lactose monohydrate is susceptible to the generation of amorphous spots that might affect the inhalation performance.

Standard sieving methods are restricted by the flow characteristics of the bulk. The preparation of smaller particles like fines as added to ternary powder blends requires other approaches like milling to further grind the particles (Section 2.4.2.1).

2.4.1.2 Spray Drying

Another approach for carrier particle engineering in a size range applicable for inhalation is to spray dry dissolved sugar alcohols with a spray drier of appropriate size [11,12,16]. The surface expansion during spray generation enables efficient drying of droplets due to the large partial pressure gradient of solvents in a heated drying air stream. Nozzles, such as twin fluid nozzles or single substance pressure nozzles, or rotary atomisers are most commonly applied for atomisation of dissolved substances [95]. Process control is vital for droplet generation as every single droplet gives rise to a single product particle. Spray towers are restricted to a maximum droplet size or amount of water that can be evaporated with

respect to the chosen drying temperature, so that the drying capacity can be derived from tower size, drying temperature, air stream volume and droplet size. Parameters like mass concentration, drying temperature, rotation speed or volume of the drying gas are conceivable to affect the particle properties [16].

Rotary atomisers as applied for the preparation of carrier particles in this project accelerate the feed by centrifugal forces. The emerging lamella or threads disintegrate to droplets upon interaction with the heated drying air. The droplet size can be controlled by the rotation speed of the rotary wheel since higher acceleration reduces the filament diameter and thus the initial droplet size [96].

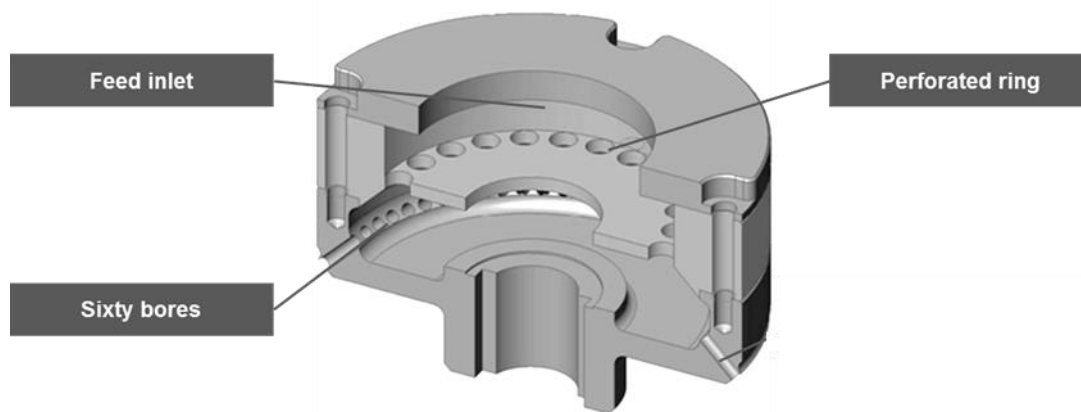


Figure 2.11 – Cross section of the LamRot atomiser with feed inlet, perforated ring and sixty bores for generation of laminar threads [97]

A special self-constructed laminar rotary atomiser (LamRot) was applied for experiments described here to particularly target narrow PDSs (Figure 2.11) [15,98]. The feed enters the atomiser at the top to experience homogeneous distribution by a perforated ring. A total of sixty bores are located at the bottom-side of the atomiser to release the liquid as single laminar threads that get further stretched by acceleration to disintegrate following the principle of Rayleigh (Figure 2.11) [14,99,100]. The gas distribution system constructed by Mescher et al. was implemented to overcome those challenges [15]. Uncontrolled thread disruption (green arrows) as suggested for the axial drying air stream (red arrows) – still applied as the main drying source – has been reduced by adding a second so-called swirl air stream (blue arrows) to the tower (Figure 2.12).

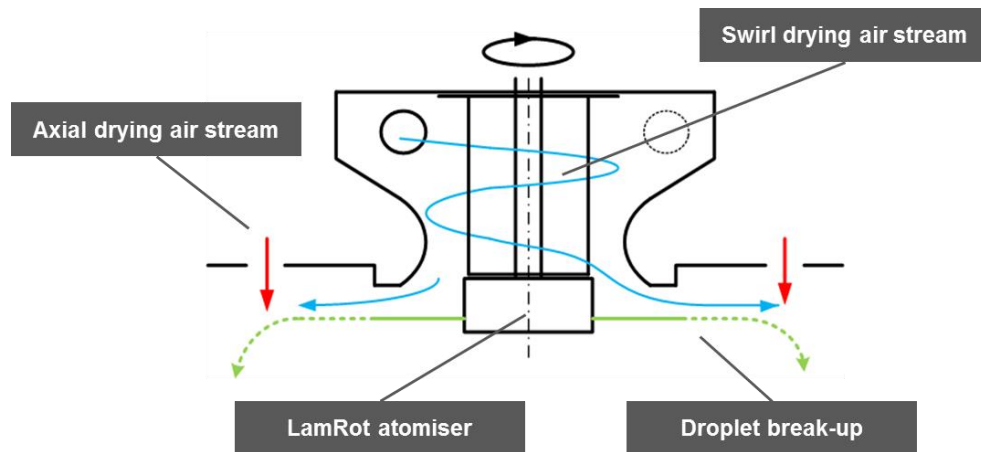


Figure 2.12 – Scheme of the gas distribution of the self-constructed spray tower used for spray drying of carrier particles

The velocity of the swirl air stream was adjusted to meet the velocity of the emerging threads targeting low relative velocities between air and threads, which results in almost perfect Rayleigh break-up [14,99]. The main air stream is hitting the droplets beyond the break-up zone and deflects them to prevent wall collisions. Studies performed on the basis of polyvinyl pyrrolidone (PVP) by Mescher et al. proved this concept as particle span was reduced compared to experiments without the swirl air stream [14].

It is generally known from literature that spray drying is applicable to control particle morphology [11,64,101,102]. Most spray dried substances, such as lactose monohydrate or SBS, are gained as almost spherical particles with respect to the shape of the droplet from which the particles emerge, while others are reported with wrinkled shape as e.g. observed for spray dried trileucine [11,103]. Earlier experiments performed on mannitol in the framework of this priority program revealed particle shape to depend on the drying temperatures. Mostly spherical particles were gained for lower drying temperatures, while increase of drying temperature correlated to the occurrence of indentions [16,64,82].

The equipment used for carrier drying experiments was improved by heater batteries for the swirl air stream to enable maximum control and the lowest batch-to-batch variation for particles dried at the same conditions.

The drying of particles during spray drying processes can be described by the Peclet number (Pe) as a dimensionless value based on the diffusion ability of the solute in the solvent with respect to the chosen drying rate [11]. Pe values below 1 indicate rapid diffusion of the solute. Evaporation of solvent appears slow enough to avoid the formation of concentration gradients within the droplet. Pe values that exceed 1 predict an enrichment of the solute at the droplet surface which most likely results in a shell formation and hollow particles [11,104]. Pe numbers vary depending on the drying rate, which enables correlations to the particle size as will be discussed in this thesis [11].

Marketed spray dried sugar alcohols such as the mannitol equivalents Pearlitol® 200SD (Roquette Frères, Lestrem, France) or spray granulated Partec® M200 (Merck, Darmstadt, Germany) are commonly used for tableting processes due to excellent compression abilities.

The applicability of spray granulated particle engineered mannitol qualities in inhalation therapy is currently tested in a project performed by Rhein et al. targeting at the first marketed mannitol quality for inhalation purposes [105].

2.4.2 Drug Preparation

The preparation of drug particles meant for inhalation purposes demands particles with a d_{aer} of 0.5 to 5 μm as described earlier. Several approaches have been introduced to target this size range, but only a few are currently used for marketed products. Micronisation techniques published in literature suggest freeze drying, micronisation from supercritical fluids or air jet milling to be applicable for drug preparation since all techniques provide particles with respective size and appropriate aerodynamic behaviour.

This thesis compares spray dried drug particles of four different model drugs with jet-milled qualities of a choice of two model drugs.

2.4.2.1 Air Jet Milling

Micronisation by air jet milling is the most commonly used method to prepare particles for inhalation purposes. The process appears cost-effective and is reliable with regards to batch-to-batch variations.

The crystalline raw materials are introduced into a grinding chamber and grinded by high pressure nozzles using an inert gas. The resulting particle size is determined by the chosen grinding pressure since fine particles are separated based on the inert gas velocity in the chamber. It has been reported that micronised materials comprise amorphous spots on the surface due to the high energy input during micronisation. Drawbacks are not only related to amorphous spots that might recrystallise during storage due to their high free Gibbs energy but also to drug particle shape [106]. Most substances appear with unevenly shaped particles upon jet milling [18], so that particle adherence to carrier particles cannot be derived from distinct controlled product properties.

Spray drying approaches overcome those challenges as this technique is known for its homogeneous overall particle shape.

2.4.2.2 Spray Drying

Spray drying of drug particles for inhalation follows the theory described in Section 2.4.1.2 but is rather based on twin fluid nozzles or even ultrasonic meshes than on rotary

atomisers. The maximum rotation speed of the rotary wheel limits the minimum droplet size and, therefore, the particle size.

However, twin fluid nozzles or ultrasonic meshes can easily be applied to control drug particles in size based on mass fraction and spraying gas or mesh size, respectively. The liquid is therefore disintegrated by spraying gas or vibration induced by a piezo crystal.

The overall appearance of the particles is homogenous contrary to jet milled qualities as described above. Papers published earlier, found SBS, BUD and FOR particles to appear mostly spherical in shape, which most likely is beneficial for the development of new formulations due to maximum control in drug shape [20,88]. However, the crystal habitus of spray dried drugs has been studied likewise indicating all products to be fully amorphous when analysed by X-Ray powder diffraction (XRPD). This suggests a crucial lack in storage stability since most products tend to recrystallise when exposed to higher ambient relative humidity and / or temperatures [88,89].

Nevertheless, amorphous contents in drug particles might be beneficial for sparingly soluble drugs as mentioned earlier. Experiments performed here will focus on the preparation of carrier and drug particles with controlled particle properties by appropriate methods and the physico-chemical analysis of those as described in the following.

3 Materials and Methods

3.1 Materials

3.1.1 D-Mannitol

D-mannitol ($C_6H_{14}O_6$) is a white, crystalline powder of $182.2 \text{ g} \cdot \text{mol}^{-1}$ in molecular mass and with the melting point at $T_m = 168 \text{ }^\circ\text{C}$, which is classified as polyol due to its chemical structure (Figure 3.1) and belongs to the sugar alcohols since it is derived from a sugar. Its solubility in water is reported to be $216 \text{ g} \cdot \text{L}^{-1}$ [107] and hydrophilicity is claimed with a log P of - 3.7 [108]. Mannitol can be gained from mannose by reduction and belongs to the group of non-reducing sugar alcohols, which accounts mannitol to be compatible for molecules containing amide-bonds e.g. proteins [109] due to low reactivity with other molecules. Three different modifications (α , β , γ) are known from literature, where the β -modification is mentioned to be the most stable one [87]. Mannitol has been reported to initially recrystallise during spray drying due to a very low T_g ($T_g \approx 30 \text{ }^\circ\text{C}$), but might be prepared in other crystalline states by e.g. freeze drying [110].

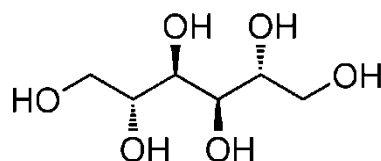


Figure 3.1 – Chemical structure of D-mannitol [111]

In these experiments mannitol was applied for the spray drying of carrier particles and the preparation of mannitol fines for use in ternary powder blends. Pearlitol[®] 160C, which served as raw material for all investigations, was kindly provided by Roquette Frères (Lestrem, France) as a crystalline quality of mannitol.

3.1.2 Salbutamol Sulphate

Salbutamol sulphate is typically used for the treatment of asthma or COPD and is listed on the World Health Organisation List of Essential Medicines [112]. Drug delivery to the lungs by inhalation is the most common application route. SBS serves as a short-acting β_2 selective adrenergic receptor agonist which causes relaxation of smooth muscles and therefore dilation of bronchial passages as well as vasodilation in muscle and liver [113].

Table 3.1 – Chemical, physical and pharmacological drug properties [107,114–117]

Drug	SBS	TIO	BUD	FOR
Molecular weight, g • mol ⁻¹	239.3	472.4	430.5	344.4
Melting point, °C	157 – 158	217 – 227	226	138 – 140
Log <i>P</i>	0.64	- 1.80	1.90	2.20
Solubility in H ₂ O	Sparingly soluble	Sparingly soluble	Insoluble	Poorly soluble
Drug class	Short-acting β ₂ agonist	M ₃ receptor antagonist	Glucocorticoid	Long-acting β ₂ agonist
Standard dose, μg [35]	100 - 200	9 - 18	200 - 400	6 – 12

The drug molecule (C₁₃H₂₁NO₃) belongs to the resorcinol derivatives, is used as a racemic mixture of *R*- and *S*-enantiomer with chemical, physical and pharmacological properties as mentioned in Table 3.1.

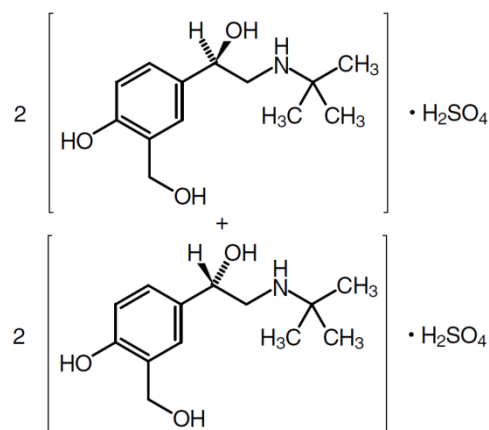


Figure 3.2 – Chemical structures of the *R*- and *S*-enantiomer of salbutamol sulphate [111]

This project applied SBS as one of the two hydrophilic model drugs ($\log P = 0.64$). The drug was initially spray dried in the framework of a design of experiments to discover the effect of drying parameters on the particle properties to then use spray dried and jet-milled qualities for powder blends with mannitol carrier particles. Raw SBS was purchased from Selectchemie AG (Zürich, Switzerland) and modified as described in Section 3.1.2 to generate the desired drug particle size and shape.

3.1.3 Tiotropium Bromide

Tiotropium bromide is usually applied for the maintenance treatment of COPD or as add-on controller for asthma. The muscarinic receptor antagonist mediates a bronchodilatory effect acting on muscarinic acetylcholine receptors (M_3) located on smooth muscles or submucosal glands [113].

Chemically, TIO ($C_{19}H_{22}BrNO_4S_2$) belongs to the N-quaternary anticholinergic derivatives with an ionic structure, so that it cannot pass the blood brain barrier. The chemical, physical and pharmacological properties are summarised in Table 3.1.

TIO used for this study was gained from Hangzhou Hyper Chemicals Ltd. (Zhejiang, China) and was spray dried for further use in binary interactive powder blends with mannitol carrier particles. Preparation of particles for inhalation is further described in Section 3.3.5.

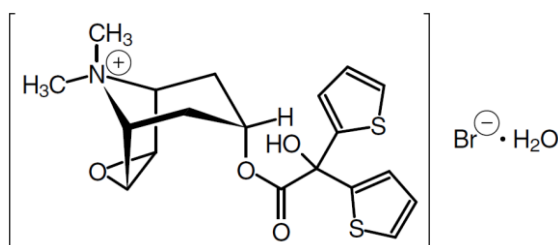


Figure 3.3 – Chemical structure of tiotropium bromide [111]

3.1.4 Budesonide

Budesonide serves as anti-inflammatory drug in the long term management of asthma and COPD when administered to the lung or against allergic rhinitis and nasal polyps when deposited in the nose. It belongs to the steroid derivatives and is also listed on the World Health Organisation's List of Essential Medicines [112].

Its common use in inhalative therapy of pulmonic diseases is mainly based on high receptor affinity, lipophilic character and, therefore, low systemic bioavailability of 10 – 20 % [118]. The chemical, physical and pharmacological properties of this racemic mixture are depicted in Table 3.1.

This study applied BUD purchased from Minakem SAS (Dunkerque, France) in micronised quality ($d_{50.3} = 1.81 \mu\text{m}$) as gained from the vendor and spray dried quality prepared as depicted in Section 3.3.3 to investigate the aerodynamic behaviour of binary interactive powder blends of BUD and mannitol carrier particles.

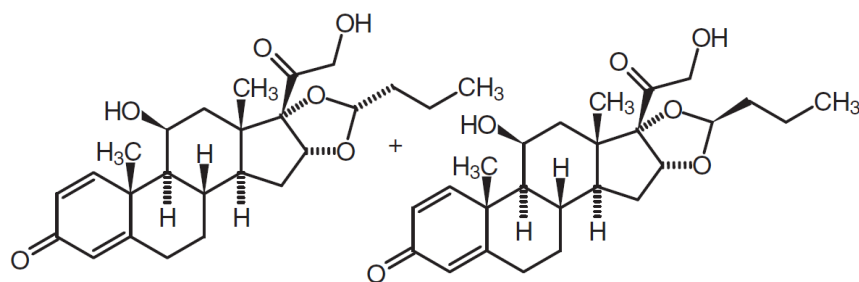


Figure 3.4 – Chemical structure of the *R*- and *S*-enantiomer of budesonide [111]

3.1.5 Formoterol Fumarate

Similarly to SBS, formoterol fumarate belongs to the group of β_2 selective adrenergic receptor agonists but is applied in therapy as a long-acting derivate with prolonged duration of action. It is commonly used to treat the pulmonic diseases asthma and COPD as it provokes bronchodilation by relaxing smooth muscles.

FOR appears as racemic mixture with the chemical, physical and pharmacological properties summarised in Table 3.1.

The raw material provided from Vamsi Labs Ltd. (Maharashtra, India) was used to prepare spray dried drug particles of lipophilic quality and defined shape as further described in Section 3.3.4.

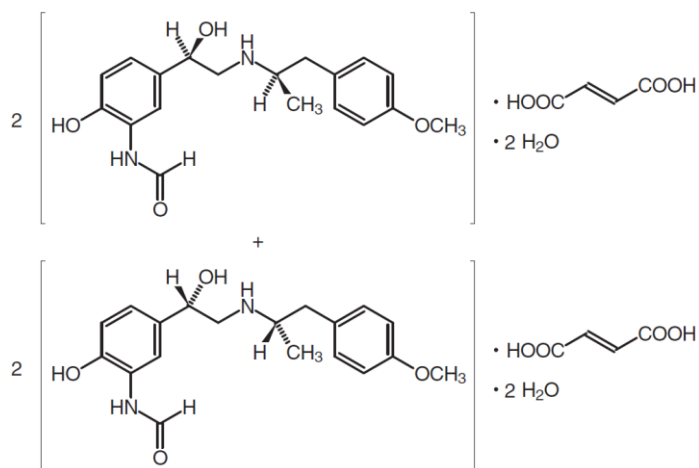


Figure 3.5 – Chemical structure of the *R*- and *S*-enantiomer of formoterol fumarate [111]

3.1.6 Further Reagents

All further reagents as necessary for analytics are further listed in Section 8.2.

3.2 Design of Experiments

A Design of Experiments (DoE) with a defined set of conditions was applied for the spray drying of mannitol carrier particles and SBS drug particles to investigate influences of drying conditions on the product properties. In general, DoE optimises the number of required experiments with respect to the underlying statistics [119–121] and enable predictions for follow-up experiments, when significant models are found.

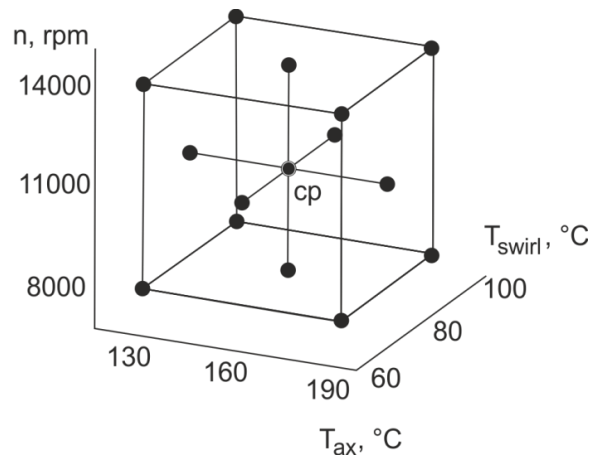


Figure 3.6 – CCF design with three factors (rotary speed, n ; axial air stream temperature, T_{ax} ; swirl air stream temperature, T_{swirl}) on three levels for spray drying of mannitol in the framework of a DoE. The cube shows 15 different experimental setups, for which the center point (cp) was repeated five times.

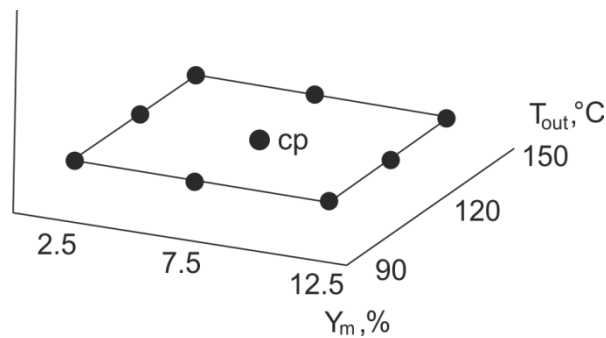


Figure 3.7 – CCF design with two factors (mass fraction, Y_m ; outlet temperature, T_{out}) on three levels for the spray drying of SBS in the framework of a DoE. The cube shows 9 different experimental setups, for which the center point (CP) was repeated five times

A large number of different designs is available to cover a broad range of purposes. This study applied a face-centred central composite (CCF) response surface designs which covers a 3D cube for three different factors and a 2D plane for two different factors as illustrated in Figure 3.6 and Figure 3.7. The final number of experiments can be calculated according to Equation (3.1).

$$N = 2^f + 2f + cp \quad (3.1)$$

N	Total number of experiments
f	Number of factors
cp	Number of centre points

Both DoE varied the factors on three equidistant levels, which allowed the investigation of linear and quadratic terms. The centre point of the designs was repeated five times in order to gain information about reproducibility and validity of the chosen design and to improve prediction abilities. Factors including the levels of interest of both DoE were summarised in Section 3.3.1 and Section 3.3.2.1.

Resulting particle properties were evaluated as responses (y) to the chosen factor levels. Every potential term, which might affect the appropriate response, was included for the evaluation initially, which results in the following equation representing a design for three factors:

$$y = a_0 + a_1 f_1 + a_2 f_2 + a_3 f_3 + a_4 f_1^2 + a_5 f_2^2 + a_6 f_3^2 + a_7 f_1 f_2 + a_8 f_1 f_3 + a_9 f_2 f_3 \quad (3.2)$$

y	Response to the chosen factors
a_i	Coefficient (displaying the statistical significance of the term)
f_x	Factor level

Based on the design, a model was fitted to every single response by neglecting insignificant terms in a backward regression. The resulting equations describe correlations between alteration of factors and effects on the response coherently and are depicted in the results sections for valid models. Respective coefficients are given as scaled and centred values which indicate the physical effect on a response when the appropriate factor is increased by one level.

All models were checked for adequate model quality on the basis of four quality parameters: The percent of variation explained by the model (R^2) which estimates how well the model fits the data; the prediction quality (Q^2) which measures the predictive power of the model; the

validity of the model (p -value) and the reproducibility (RP) which illustrates the variation of experiments that were conducted at the same conditions (centre points). Plausibility of the model is related to appropriate limits of these quality parameters. The best model quality is generally illustrated by a value of 1. For R^2 and Q^2 limit of acceptance was set to 0.5 at minimum, which represents a well fitted model with good predictive qualities. Model validity must exceed 0.25 to indicate that the lack of fit for single measurements occurs smaller than the pure error given by RP . This includes that models might show reduced model validities due to extraordinarily good RP values which in turn is known as artificial lack of fit due to the very small experimental (pure) error. Nevertheless, RP was desired to reach values close to 1 to display how well experiments can be repeated [122].

In general, the DoE was created and evaluated with the DoE software Modde (Version 10.1.1, Umetrics AB, Umeå, Sweden) by using the Multi Linear Regression (MLR) method.

3.3 Preparative Methods

3.3.1 Preparation of Engineered Carriers

Mannitol carrier particles were prepared by spray drying a bi-component solution of mannitol and water with a self-constructed spray tower located at the Technical University in Dortmund, Germany (group of Prof. Walzel).

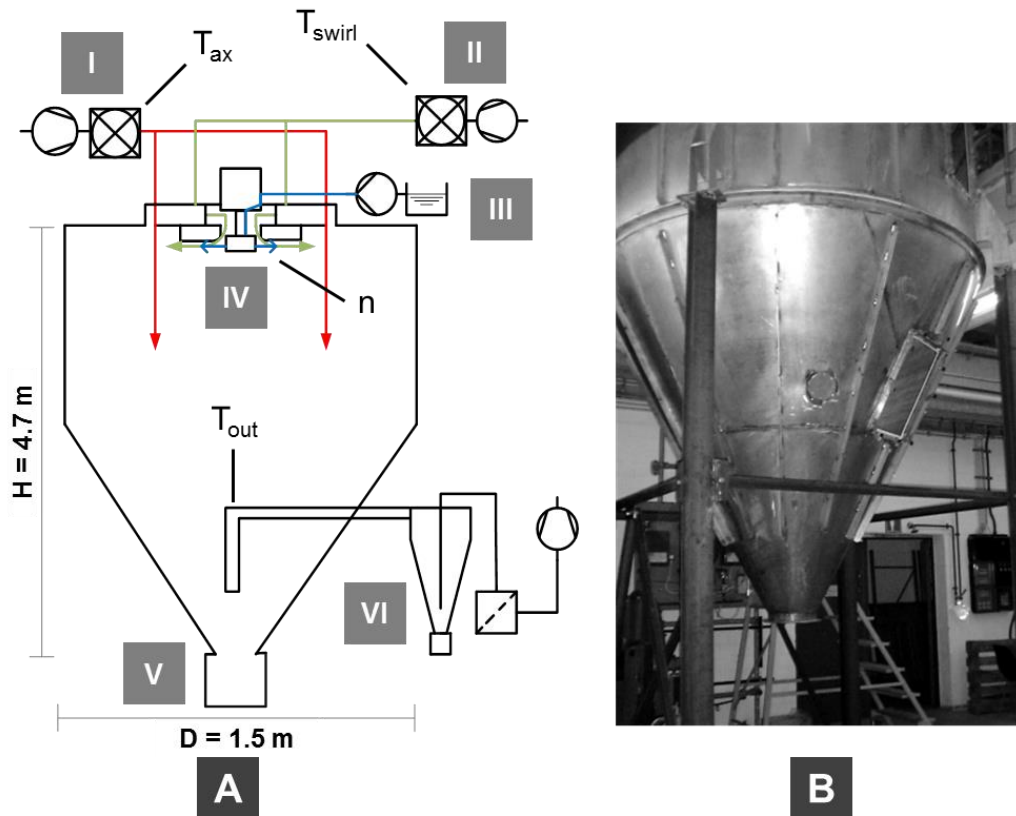


Figure 3.8 – A: Scheme of the self-constructed spray tower with (I) axial inlet air stream and the point of measure for T_{ax} , (II) swirl inlet air stream and point of measure for T_{swirl} , (III) heated feed stock vessel, (IV) LamRot atomiser with rotation speed n , (V) collecting vessel and (VI) cyclone; the tower has a height H of 4.7 m and a diameter D of 1.5 m, B: photograph of the conical part of the spray tower [123]

The tower consists of a cylindrical upper part ($H = 2.5$ m) and a conical lower part ($H = 2.2$ m) with a total height of $H = 4.7$ m and a diameter of $D = 1.5$ m (Figure 3.8). The mannitol solution was fed to the drying chamber with a special laminar rotary atomiser (LamRot, Figure 3.9) which was designed to generate products of narrow PSDs. The bi-component solution was added to the atomiser centrally to be distributed to the inner wall of the LamRot atomiser. Droplets emerged from sixty bores around the rotating LamRot atomiser (Figure 3.9) and got redirected towards the tower bottom by an axial air stream that entered the tower at the top (Figure 3.8, red arrows). A swirl air stream (Figure 3.8, green arrows) was applied to the spray tower to improve controlled droplet break-up and to govern the temperature next to the rotary atomiser separated from the axial inlet air stream [14,15]. Both

inlet air streams were heated by heater batteries and could be adjusted in volume per time. The main collecting vessel was attached at the bottom of the tower. The drying air stream left the drying chamber concentrically and was directed to a cyclone, which was applied to separate fines. A filter was assembled to clean the exhaust air from finest particles.

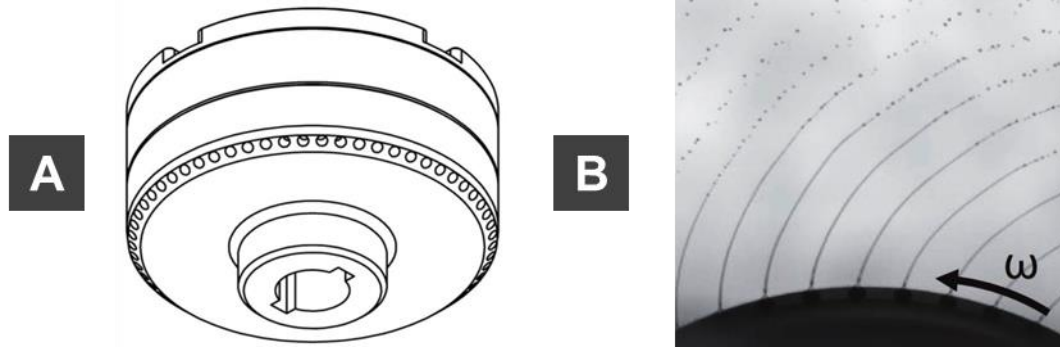


Figure 3.9 – A: Scheme of the LamRot atomiser with sixty bores; B: Photograph of mannitol-water filaments emerging from the atomiser [123]

Spray drying took place in the framework of a CCF design as described in Section 3.2. T_{ax} , T_{swirl} and n were chosen as factors, which were altered on three levels (-1, 0, +1) to generate a broad set of mannitol batches with various particle properties (Table 3.2).

Rotation speed was chosen with regard to droplet size distribution experiments in an off-site setup, where the effect of different LamRot velocities on the droplet size was tested by laser diffraction (Malvern Spraytec, Malvern Instruments, Worcestershire, UK). Mannitol with a feed concentration of 10 % [w/w] was fed to the atomiser with a feed rate of $10 \text{ L} \cdot \text{h}^{-1}$ to mimic the standard spraying conditions in the pilot scale spray tower. Those experiments were mainly conducted to estimate resulting particle sizes from the observed droplet sizes to finally generate carrier particles between $50 \mu\text{m}$ and $80 \mu\text{m}$.

Table 3.2 – Displays the three levels of the factors chosen for the CCF design of spray drying mannitol; *marks the center point conditions, which were repeated five times

Factor	- 1	0*	+ 1
Rotary speed, n , rpm	8,000	11,000	14,000
Axial air stream temperature, T_{ax} , °C	130	160	190
Swirl air stream temperature, T_{swirl} , °C	60	80	100

Drying temperature was chosen to be varied for both inlet air streams in contrast to earlier experiments by Littringer et al. [16,23,23]. The temperatures were set with respect to T_{out} since a minimum drying temperature is required to generate dry particles. The axial air stream dealt as the main drying air stream with the larger volume per time ($V_{ax} = 1000 \text{ m}^3 \cdot$

h^{-1}) for these experiments and was varied from $T_{ax} = 130\text{ }^{\circ}\text{C}$ to $190\text{ }^{\circ}\text{C}$. T_{swirl} of the swirl air stream ($V_{swirl} = 400\text{ m}^3 \bullet \text{h}^{-1}$) was kept between $60\text{ }^{\circ}\text{C}$ and $100\text{ }^{\circ}\text{C}$ due to heat limitations of the used equipment.

Several further parameters were kept at constant levels (Table 3.3). The mannitol was dissolved in purified water to reach a feed concentration of 15 % [w/w] and preheated to $T_{feed} = 25\text{ }^{\circ}\text{C}$ in a closed feed stock vessel prior to the experiment. The bi-component solution was fed to the LamRot atomiser with a feed rate of $V_{feed} = 10\text{ L} \bullet \text{h}^{-1}$ by the use of a peristaltic pump. The swirl air stream volume was kept at $V_{swirl} = 400\text{ m}^3 \bullet \text{h}^{-1}$, for which the gas velocity corresponds to the circumferential velocity of medium rotary speeds. The particles collected in the main collecting vessel were dried at $100\text{ }^{\circ}\text{C}$ in a compartment drier for at least 1 h to remove residual moisture and to prevent agglomeration. Product caught in the cyclone was not employed for further analysis.

The resulting nineteen batches were analysed by various techniques as described in Section 3.4. A selection of these mannitol carriers was used for the preparation of interactive powder blends (Section 3.3.7).

Table 3.3 – Constant parameters during the spray drying process

Constant Parameter	Process Condition
V_{ax}	$1000\text{ m}^3 \bullet \text{h}^{-1}$
V_{swirl}	$400\text{ m}^3 \bullet \text{h}^{-1}$
C_{feed}	15 % [w/w]
T_{feed}	$25\text{ }^{\circ}\text{C}$
V_{feed}	$10\text{ L} \bullet \text{h}^{-1}$

3.3.2 Salbutamol Sulphate

The hydrophilic model drug SBS ($\log P = 0.64$) was used in micronised quality with an irregular shape and spray dried quality with spherical particles to discover the effect of drug shape on the particle-particle interactions.

3.3.2.1 Spray drying of SBS

Spray drying of SBS was conducted with a commercially available lab scale spray dryer (Büchi Mini Spray Dryer B-290, Büchi Labortechnik AG, Flawil, Switzerland) to generate particles of spherical shape.

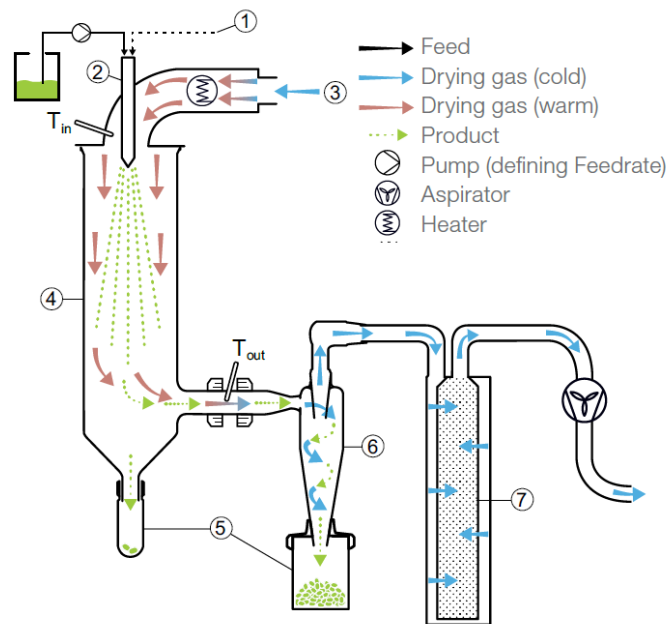


Figure 3.10 –Scheme of the Büchi Mini Spray Dryer B-290 as used for aqueous solutions with open cycle [124]

Figure 3.10 shows a scheme of the dryer. The prepared stock solution of salbutamol sulphate in bi-distilled H_2O was passed through a peristaltic pump and fed to the main drying chamber over a two-fluid nozzle (①, ②, $d = 2$ mm). The aspirator set to 100 % for all experiments was used to suck ambient air into the system (③). The air was preheated by a heater and introduced to the spray tower at the top, where T_{in} was measured. Droplets were dried in the drying chamber (④) and particles were collected in the product vessel (⑤) after separation by the cyclone (⑥). T_{out} was determined in the bypass between drying chamber and cyclone. The air was finally sucked through a filter to be cleared from fine particles (⑦).

The spray drying of SBS was used to investigate the influence of drying parameters on the drug properties. SBS concentration (Y_m) in bi-distilled H_2O and T_{out} were chosen as factors to be varied on three levels in the framework of a DoE. A total of 13 batches including the center point batch, which was repeated five times, were dried with the lab scale spray dryer. The feed concentration Y_m was set between 2.5 % and 12.5 %, while T_{out} was varied linearly at a range from 90 °C to 150 °C (Table 3.4). The inlet temperature was set to $T_{in} = T_{out} + 60$ °C. T_{out} as a function of the inlet temperature and the amount of solution spray dried per time was controlled by the chosen feed rate. Further parameters like the aspirator capacity (100 %, $38 \text{ m}^3 \cdot \text{h}^{-1}$) and the spraying air (40 mm, $666 \text{ L} \cdot \text{h}^{-1}$) [124], which controls the droplet and by this the particle size, were kept constant for these experiments. The product was collected from the vessel beneath the cyclone and stored in a desiccator upon blue gel (Sigma Aldrich Chemie GmbH, Munich, Germany) until further analysis to ensure the stability of the product.

Table 3.4 – Three levels of the chosen factors for the spray drying of SBS. *marks the conditions of the center point experiments

Factor	- 1	0*	+ 1
SBS concentration, Y_m % [w/w]	2.5	7.5	12.5
Outlet temperature, T_{out} , °C	90	120	150

3.3.2.2 Jet-Milling of SBS

Micronisation of SBS was performed to generate unevenly shaped drug particles of inhalable size. Jet milling was chosen for this task as a reliable technique to generate micronised materials with quite narrow particle size distributions. Cracking of particles by particle-particle collisions or particle-wall collisions facilitates decrease in size that can be controlled by the chosen micronising conditions. An air Jet-O-Nizer Modell 00 (Figure 3.11, Fluid Energy Aljet, Plumsteadville, USA) with nitrogen 2.8 (Linde AG, Hamburg, Germany) as inert gas was applied to run the process.

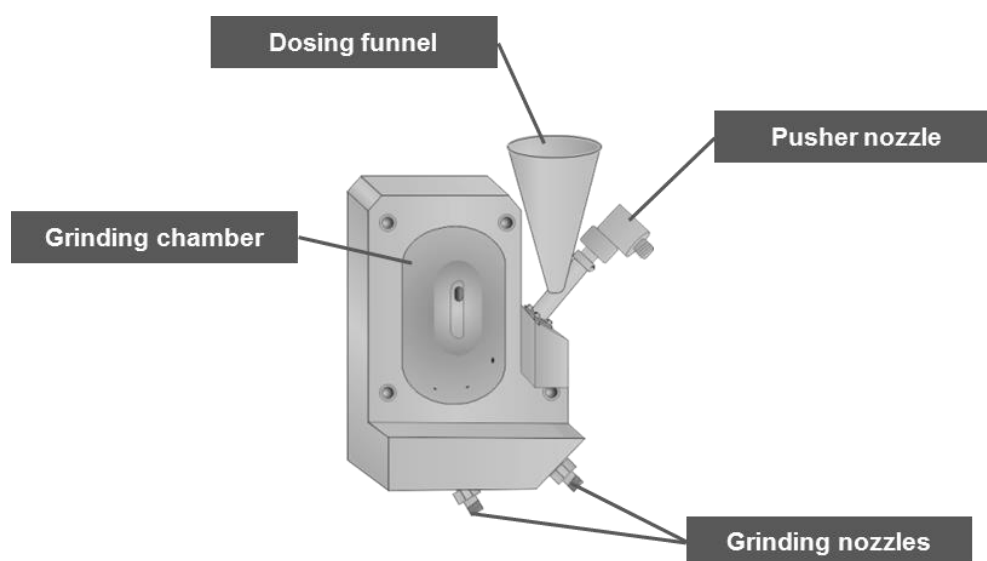


Figure 3.11 – Scheme of the jet mill used for grinding of SBS and mannitol (Pearlitol® 160C)

Grinding pressure was set to 6.0 bar while injection pressure was 7.0 bar to ensure the feeding of SBS. The raw material was fed at a feed rate of approximately $1 \text{ g} \cdot \text{min}^{-1}$ and product was collected in a filter pocket right after leaving the grinding chamber. Jet-milled SBS was stored in a desiccator upon blue gel as jet milling may create small amorphous regions which might recrystallise under ambient conditions [67].

3.3.3 Budesonide

BUD, which served as a lipophilic model drug ($\log P = 1.9$) in this project, was used in spray dried and micronised quality. Micronised BUD was supplied by Minakem SAS (Dunkerque, France) and was used without further treatment ($d_{50.3} = 1.81 \mu\text{m}$). The spray dried quality was prepared with the Büchi B-290 Mini Spray Dryer as described earlier (Section 3.3.2.1). The inert loop modul Büchi B-295 (Büchi Labortechnik AG, Flawil, Switzerland) was applied to overcome explosion hazards of methylene chloride in ambient air. The closed cycle was operated with Nitrogen 5.0 as spraying gas to ensure that oxygen is excluded during the drying process.

A feed concentration of 7 % BUD in methylene chloride was chosen to generate particles of 2.0 – 2.5 μm in size. The spraying gas was adjusted to 35 mm on the Büchi scale, which corresponds to $538 \text{ L} \bullet \text{h}^{-1}$, respectively, [124] and drying temperature was set to $T_{in} = 100 \text{ }^\circ\text{C}$ prior to the experiment. Spray drying was started at constant conditions with a feed rate of 8 %. The product was collected in the small vessel beneath the cyclone and stored upon silica gel in a desiccator until further analysis.

3.3.4 Formoterol Fumarate

FOR was used as a lipophilic model drug ($\log P = 2.2$) in this project. The spray dried quality was prepared with a Büchi B-290 Mini Spray Dryer in connection with the inert loop module Büchi B-295 as formoterol was dissolved in methanol prior to drying. The closed loop enables the recovery of methanol by condensation and diminishes explosion hazards.

Spray drying conditions were chosen based on earlier experiments (data not shown) aiming at particles of 2.0 – 2.5 μm in size. The feed concentration was set to 4.8 % [w/w] FOR dissolved in methanol. The feed vessel was sealed with parafilm to prohibit evaporation of solvent. Spraying air was set to 33 mm on the Büchi scale corresponding to $\approx 498 \text{ L} \bullet \text{h}^{-1}$. The inlet temperature was kept at $100 \text{ }^\circ\text{C}$ during the drying process, which resulted in an outlet temperature of approximately 60 – 62 $^\circ\text{C}$. Particles collected in the vessel beneath the cyclone were stored upon silica gel in a desiccator to guarantee stability of the product.

3.3.5 Tiotropium Bromide

Spray dried TIO particles ($\log P = -1.8$) were gained as described for SBS earlier (Section 3.3.2.1). The Mini Büchi B-290 was set to an inlet temperature of $T_{in} = 150 \text{ }^\circ\text{C}$ which resulted in a temperature of approximately $T_{out} = 81 - 83 \text{ }^\circ\text{C}$. 2 % [w/w] TIO were dissolved in bi-distilled H_2O and conveyed with a feed rate of 10 %. A spraying air of 40 mm or $667 \text{ L} \bullet \text{h}^{-1}$ was applied in order to generate particles with a size of 2.0 to 2.5 μm . The product was stored upon silica gel until further analysis.

3.3.6 Mannitol Fines

Apart from drug particles, mannitol fines were needed for further trials. Jet milling was chosen to comminute Pearlitol[®] 160C as raw material to a desired final particle size of 4 – 5 µm. Micronisation was performed according to Section 3.3.2.2. With respect to the desired final particle size grinding pressure was set to 5.5 bar while the pusher nozzle was run at 6.5 bar. The final product collected with the filter pockets was stored at ambient conditions as mannitol was found to be stable at these conditions (Section 4.1.1).

3.3.7 Preparation of Powder Blends

Interactive powder blends of mannitol carrier particles and fine drug particles were prepared with a Turbula[®] blender (Figure 3.12, Typ T2C, Willy A. Bachhofen AG, Basel, Switzerland). A total of six mannitol batches was chosen with regard to different particle shapes and sizes as generated in the framework of the DoE (Section 4.1, Table 4.1). Blending procedures were adapted for different drug particles to overcome stability concerns with regards to recrystallisation of amorphous contents or the elimination of drug agglomerates as will be described in this section.

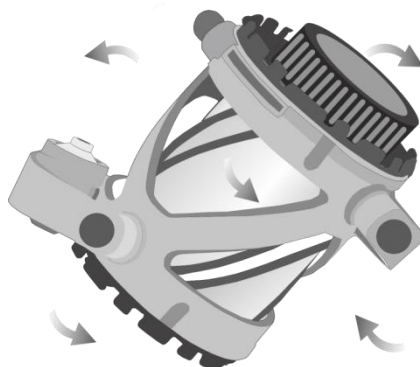


Figure 3.12 – Scheme of the Turbula[®] blender as a free fall blender

Blending of all powder blends was performed under controlled conditions in a climatic chamber (Imtech Deutschland GmbH & Co KG, Hamburg, Germany). Relative humidity was kept as low as necessary to ensure stability of amorphous contents and as high as possible to prevent electrostatic charging of powder blends during preparation or blending. A stainless steel sieve with a mesh size of 355 µm was used for all drugs and mannitol batches to remove agglomerates manually prior to blending. Each interactive powder blend consisted of 14.85 g mannitol (99 % [w/w]) and 0.15 g drug (1 % [w/w]), which resulted in 30 – 40 % filling volume of the stainless steel vessel used for blending. With respect to blend homogeneity a double sandwich weighing method was applied for mannitol carrier and drug containing blends starting with 4.95 g ($\frac{1}{3}$) mannitol plus 0.075 g ($\frac{1}{2}$) of drug followed by another 4.95 g ($\frac{1}{3}$) mannitol, 0.075 g ($\frac{1}{2}$) of drug and 4.95 g ($\frac{1}{3}$) of mannitol. The blending vessel was then fixed

into the Turbula[®] blender (Figure 3.12) and blended for appropriate blending times. Sieving steps were introduced to eliminate agglomerates. Ten samples were randomly taken from different positions of the finished product to check for homogeneity. A drug recovery of 90 – 110 % and a relative standard deviation below 5 % were set as limits for further analysis. Samples were dissolved in appropriate solvents and drug content analysed via reversed phase high performance liquid chromatography (RP-HPLC) as described in Section 3.4.6. The finished product was stored upon silica gel in a desiccator until further analysis.

The blending procedures were adapted in terms of climatic conditions or blending steps to meet requirements for the blend quality.

SBS containing blends were prepared at 21 °C and 35 % rH, which prevents the recrystallisation of amorphous structures of the drug particles while keeping electrostatic charging as low as possible. Blending was performed for 2 x 15 min with one in-between sieving step. Rotation speed of the Turbula[®] blender was kept at 42 rpm. SBS was used in spray dried and micronised quality.

BUD containing blends were produced at the same climatic conditions (21 °C, 35 % rH) but demanded another blending step to fulfil the homogeneity requirements. The blending procedure was extended to 3 x 15 min including two in-between sieving steps. Rotation speed was kept on the same level for both spray dried and micronised BUD qualities.

FOR handling was performed at 21 °C and 35 % rH to keep amorphous contents stable. Carrier and drug were blended for 2 x 15 min, but with increased rotation speed of 90 rpm, as higher energy input was necessary to eliminate FOR agglomerates and to accomplish homogeneity requirements. FOR was only used in spray dried quality.

TIO containing powder blends were prepared at lower relative humidity (21 °C, 25 % rH) as TIO is known to be hygroscopic (Section 4.2.4). Blending was performed for 3 x 15 min at 42 rpm including two in-between sieving steps.

SBS and Fines were blended with conditions according to powder blends only containing mannitol carrier and SBS particles. Mannitol fines were added first in different concentrations (0 % to 15 %) following the sandwich weighing method mentioned above. The drug particles were then added after the first blending step instead of sieving the initial blend of mannitol carrier and fines. The drug was therefore separated in several small portions to be added to different spots in the mixing vessel. Sieving was conducted between second and third blending step.

3.4 Analytical Methods

3.4.1 Particle Size

Particle size can be described by several different particle diameters with regard to the technique chosen and the purpose of the analysis. In general, three dimensions (length, width, depth) are mandatory to define a particle by size. Ferret's or Martin's diameter are exemplary for two-dimensional measurements as performed with a microscope while a broad range of different equivalent diameters refer to corresponding spherical particles. Results presented here are either corresponding to the volume based equivalent diameter ($d_{50.3}$) which describes the diameter of a sphere with the same volume as the particle or the aerodynamic equivalent diameter (d_{adyn}) representing the diameter of a spherical particle with the density $1 \text{ g} \cdot \text{cm}^{-3}$ and the same settling velocity as the (irregular) particle of interest [125].

Various techniques can be used to determine the desired diameters. Laser diffraction as a standard method for dry powder analytics was applied to measure the volume based diameters ($d_{50.3}$). Aerodynamic diameters (d_{adyn}) of drug particles for inhalation were gained by impaction analysis as described in Section 3.4.1.2.

3.4.1.1 Laser Diffraction

Volume based equivalent diameters were determined by laser light scattering. The laser diffraction technique relies on the characteristic diffraction pattern of incident laser light by the particles of interest. The diffraction angles are inversely proportional to the size. Small particles cause large diffraction rings with low intensity, while small diffraction rings of high intensity refer to large particles. The according diffraction pattern is evaluated based on the Mie theory or the Fraunhofer approximation resulting in the volume based equivalent diameter. It needs to be considered that both calculations assume that the particles to measure are of spherical shape [125].

Prior to final product determinations a Malvern laser diffraction system (STP 5921, Malvern Spraytec, Malvern Instruments, Worcesterchire, UK) was applied to measure the initial droplet size distributions of the droplets emerging from the LamRot atomizer in an off-site setup. The effect of rotation speed (n) on the droplet size was tested by increasing n from 3,000 rpm to 14,000 rpm. Feed concentration (15 % [w/w]) of mannitol in water and feed rate ($10 \text{ L} \cdot \text{h}^{-1}$) were selected with respect to the spray drying conditions chosen for the DoE.

Droplet sizes were used to calculate resulting particle sizes based on a shift factor, which was determined according to an approach invented by Maas et al. [82]. Shift factor was set to 1.73 with respect to initial density of mannitol in water (15 % [w/w], $1030 \text{ kg} \cdot \text{m}^{-3}$), the

bulk density of mannitol ($1200 \text{ kg} \cdot \text{m}^{-3}$) and an assumed final porosity of 50 %. The final particle size can then be calculated from the measured droplet size as follows:

$$d_{50.3}(\text{particle size}) = \frac{d_{50.3}(\text{droplet size})}{1.73} \quad (3.3)$$

Laser diffraction was further used for particle size investigations of dry carrier and drug particles in this thesis. For both, the HELOS laser diffraction system (Sympatec GmbH, Clausthal-Zellerfeld, Germany) equipped with a helium neon laser ($\lambda = 623.8 \text{ nm}$) was used in connection with the RODOS dry dispersing unit (Sympatec GmbH, Clausthal-Zellerfeld, Germany). Pressurised air was applied to deagglomerate the samples. The dispersing pressure was chosen with respect to the breaking strength of the particles [126]. Mannitol carrier batches were measured with a dispersing pressure of $p_{abs} = 1.2 \text{ bar}$ to prevent particle break-up. Smaller drug samples were dispersed at $p_{abs} = 4.0 \text{ bar}$ due to their cohesiveness and facilitated by their higher physical stability. All samples were fed to the dispenser manually to reach a minimum optical density of 1 %. Samples were measured in triplicate and evaluated with the Windox software (Version 5.4.2.0, Sympatec GmbH, Clausthal-Zellerfeld, Germany). Results were gained as volume based equivalent diameters, for which the cumulative distribution and density distribution were plotted. The median ($d_{50.3}$) as well as the 10 % ($d_{10.3}$) and 90 % ($d_{90.3}$) quantile were used for further analysis.

$$\text{span} = \frac{(d_{90.3} - d_{10.3})}{d_{50.3}} \quad (3.4)$$

span	width of PSD
$d_{90.3}$	volume-based 90 % quantile of the PSD
$d_{50.3}$	volume-based 50 % quantile of the PSD
$d_{10.3}$	volume-based 10 % quantile of the PSD

Span values were calculated according to Equation (3.4) to assess the width of the PSDs [126].

3.4.1.2 Next Generation Pharmaceutical Impactor (NGI)

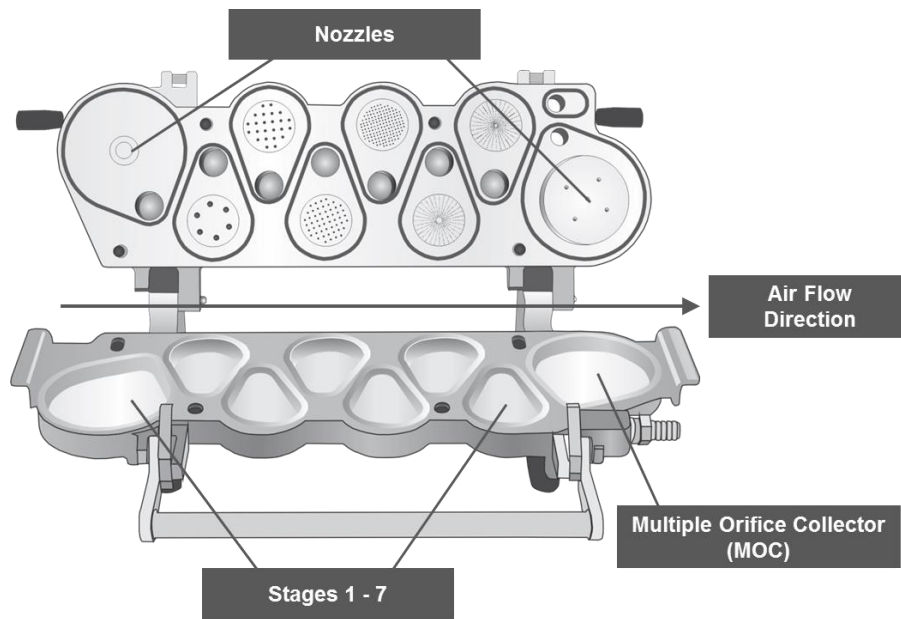


Figure 3.13 – Scheme of the opened Next Generation Pharmaceutical Impactor (NGI) with seven stages and the Multiple Orifice Collector (MOC) at the bottom and the appropriate nozzles in the lid

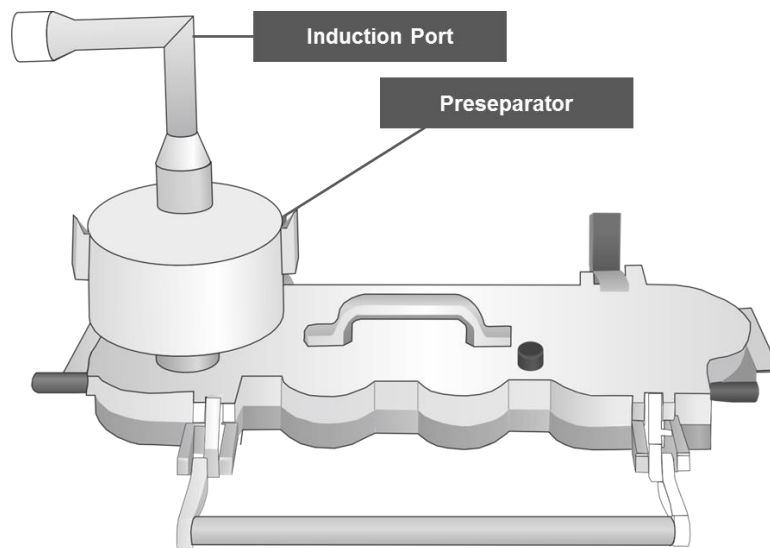


Figure 3.14 – Scheme of the closed Next Generation Pharmaceutical Impactor (NGI) with a throat-like tube connected to the preseparator and the stages and nozzles at the bottom (see Figure 3.13)

Aerodynamic equivalent diameters are commonly evaluated by cascade impaction. This covers the impact of particle shape and density as particles with lower densities behave aerodynamically as though they are smaller than their physical size and vice versa. Impaction analysis enables to assess the fine particle fraction and provides useful information about the aerodynamic behaviour of the particles. Cascade impactors are built of one or more stages with nozzles of defined diameters and cups beyond the nozzles to collect the droplets or particles. The Ph. Eur. lists three different impactors to determine the “Fine

Particle Fraction” of dry powders according to “Preparations for inhalation – aerodynamic assessment of fine particles” (Apparatus C, D, E, Ph.Eur. 2.9.18) [127].

In this thesis the aerodynamic characterisation of interactive powder blends was examined with the Next Generation Pharmaceutical Impactor (NGI, Apparatus E, Pharmacopeia Europaea, 2.9.18, Copley Scientific, Nottingham, UK) [127]. The impactor was equipped with an induction port to attach appropriate mouth pieces for all types of inhalation devices and a preseparator for the deposition of larger particles. Seven stages and a multiple orifice collector (MOC), which served as filter for the smallest particles, were applied for the accurate assessment of fine particles (Figure 3.13, Figure 3.14).

The Ph. Eur. requires a pressure drop of 4 kPa over the inhaler device and an inhaled volume of 4 L which corresponds to the standard lung volume of an adult [127]. The appropriate pressure drop was implemented by adjusting the volumetric flow rate (Q) as measured with the digital flowmeter (DFM3, Copley Scientific, Nottingham, UK). The opening times (T_{inh}) of the solenoid valves of the critical flowmeter (TPK, Copley Scientific, Nottingham, UK) were calculated according to Equation (3.5) to ensure an inhaled volume of $V_{inh} = 4$ L.

$$T_{inh} = \frac{V_{inh}}{Q} \quad (3.5)$$

T_{inh}	Valve opening time, s
V_{inh}	Absoulte inhaled volume, 4 L
Q	Volumetric flow rate, L • min ⁻¹

Table 3.5 shows the respective parameters as used for analysis with two chosen commercial inhaler devices, Novolizer[®] (Meda Pharma, Bad Homburg, Germany) and Easyhaler[®] (Figure 2.7).

Table 3.5 – Device-dependent parameters for impaction analysis with the NGI using the Novolizer[®] and Easyhaler[®] as devices

	Novolizer [®]	Easyhaler [®]
Volumetric flow rate, Q , L • min ⁻¹	78.2	45.0
Valve opening time, T_{inh} , s	3.1	5.3

The collection cups including preseparator and MOC of the NGI were coated with a special stage coating consisting of ethanol, Brij[®] 35 and glycerol (51:15:34 [w/w]) prior to every measurement to minimise bouncing of particles. The container of the appropriate inhaler device was filled with 1.0 g of interactive powder blend. An external collection tube with a suitable mouthpiece adapter was applied for priming the inhaler device. Initially, twenty doses (doses 1 – 20) were discharged into the tube. Inhalation was triggered by opening the solenoid valve of the critical flowmeter for the calculated timeframe. The following doses were administered with the inhaler device connected to the induction port.

All experiments performed with the Easyhaler[®] were conducted with SBS, while the Novolizer[®] was used for impaction analysis with SBS, BUD, TIO and FOR. The number of doses discharged to the impactor was varied with respect to the maximum load of the collection cups. The Novolizer[®] was actuated ten times for SBS, TIO and FOR (doses 21-30) and five times for BUD (doses 21-25) to generate appropriate drug concentrations for quantification. Induction port (including mouthpiece), preseparator, seven stages and the MOC were sampled separately. The deposited drug was dissolved with predefined volumes of the appropriate solvent and distinct rinsing times to avoid undissolved drug residues.

The results of the aerodynamic characterisations as gained by drug quantification by reversed phase high pressure liquid chromatography (RP-HPLC, Section 3.4.6) were evaluated with the Copley Inhaler Testing Data Analysis Software (Copley Scientific, Nottingham, UK). The total drug content detected in the impactor from mouthpiece to MOC was defined as emitted dose (ED) released by the inhaler device. The cut-off diameters of the stages which depend on nozzle diameter and the chosen flow rate determine the fraction of particles with a median mass aerodynamic diameter (MMAD) of < 5 µm, which represents the d_{50} of the cumulative aerodynamic PSD. The fine particle dose (FPD) is defined as the mass of drug particles with a MMAD < 5 µm, while the fine particle fraction (FPF) is calculated as the fraction of particles with a MMAD < 5 µm in % referring to the ED (Equation (3.6)) [46].

$$FPF = \frac{FPD}{ED} \times 100 \% \quad (3.6)$$

FPF	Fine Particle Fraction, %
FPD	Fine Particle Dose, μg
ED	Emitted Dose, μg

All adhesive mixtures were measured in triplicate and results were given as mean of three \pm standard deviation.

3.4.2 Imaging Techniques

Imaging techniques, as widely employed in pharmaceutical research and development, provide the opportunity to characterise particles with regard to their visual appearance. The morphology of particles is of utmost interest to discover the drying kinetics during spray drying as well as to understand particle-particle interactions in interactive powder blends. Different parameters to describe the morphology can most easily be assessed by different imaging techniques [125]. In this thesis, the morphology of carrier particles was divided into particle shape and surface roughness as these properties can be controlled separately during the spray drying process. Additionally, the drug shape of SBS particles prepared at different conditions was evaluated next to carrier shape and roughness to investigate the effect of drug morphology on the impaction results.

Scanning Electron Microscopy (SEM) was chosen to visualise all carrier and drug particles as well as powder blends prior to and after the aerodynamic characterisation (Section 3.4.2.1). Different surveys were applied to evaluate the particle morphology based on categorisation of these SEM images (Section 3.4.2.2, Section 3.4.2.5). Further, image analysis was performed to discover the sphericity and aspect ratios of the carriers to support the survey results in terms of particle shape.

Surface roughness of the carriers as principally evaluated by categorisation of SEM images was supported by 3D laser scanning microscopy (Section 3.4.2.6) which generates a 3D surface of the carriers.

Further, a special confocal Raman spectroscopy approach which combines surface topography and the according Raman scattering was applied to overcome concerns of the location of drug particles on the carrier surface (Section 3.4.2.7).

3.4.2.1 Scanning Electron Microscopy (SEM)

The SEM technique as the imaging tool with the highest resolution and depth of focus is based on the scattering of an electron beam originated from an electron gun [125]. The electrons are accelerated in correlation to the chosen working voltage, where high working voltages between 10 kV and 15 kV serve the best resolution but cause deeper penetration and degradation of the specimen. Lower working voltages of < 5 kV offer perfect conditions for surface topography investigations due to the low penetration depth. The electrons of the scanning electron beam strike the sample surface which triggers the emission of low energy secondary electrons (SEs) or high energy backscattered electrons. An array of specialised detectors helps to visualise the signals. To minimise beam scattering by gas molecules, SEM analysis is conducted at very high vacuum [125].

This project applied a Zeiss Ultra 55 Plus (Carl Zeiss NTS GmbH, Oberkochen, Germany) for visualisation. All samples were fixed on carbon stickers (Plano GmbH, Wetzlar, Germany) and sputter coated using a Bal-Tec SCP 050 Sputter Coater (Leica Instruments, Wetzlar, Germany) as this ensures conductivity for the analysis of electrically nonconductive organic substances. Sputtering was conducted in an evacuated chamber for 65 s at 50 mA with Argon 5.0 (Linde AG, Hamburg, Germany). Argon ions were accelerated towards a gold target to generate a thin conductive gold layer on the specimen surface. The coated samples were transferred to the SEM chamber and scanned with a working voltage of 2 kV. Images were gained from secondary electrons with the SE-2 detector. All samples were visualised at different magnifications from 100-fold to 10,000-fold when reasonable.

3.4.2.2 Carrier and Drug Shape by Survey

Analysing the shape of particles is still a challenging task as most techniques require appropriate size ranges to provide useful information. A visual evaluation of SEM images by twenty volunteers, who were filling in a survey, was chosen as the principal method to investigate the particle shape of spray dried mannitol carriers and was supported by image analysis (Section 3.4.2.3) and particle cross sections (Section 3.4.2.4). Images of different magnifications (100 fold to 1,000 fold) were chosen to be classified into five categories regarding its particle shape as listed in Table 3.6. Results were analysed as continuous values in the framework of the DoE.

Table 3.6 – Five shape categories as used for the evaluation of the carrier shape by a survey

Category	Description
1	All particles are completely spherical without any indentations.
2	Some particles exhibit single small indentations.
3	Most particles with several small indentations and first single deeper indentations.
4	All particles with at least small indentations, several particles with deep indentations.
5	All particles show many deep indentations.

The shape of spray dried SBS drug particles was examined similarly, as these particles appear even smaller, so that drug shape cannot be assessed by image analysis or cross sections. Five different categories were defined as mentioned in Table 3.7 to evaluate the drug shape in the framework of a survey and based on SEM images of different magnifications (1,000 fold to 5,000 fold). Results were again analysed as continuous values by the DoE software Modde.

Table 3.7 – Five categories for the evaluation of SBS drug shape by a survey

Category	Description
1	No golf ball structure for drug particles of every size (all particles with smooth surface).
2	Only larger particles with a slight golf ball structure, medium and small particles with smooth surface.
3	Medium and large particles with a slight golf ball structure, small particles with smooth surface.
4	Large particles with prominent golf ball structure, medium and small particles with a slight golf ball structure.
5	Prominent golf ball structure for drug particles of every size (all particles with obvious indentations).

3.4.2.3 Image Analysis

Image analysis was implemented targeting the aspect ratio (AR) of particles as a measure to describe particle shape. A high speed camera was used with the QICPIC system (Sympatec GmbH, Clausthal-Zellerfeld, Germany) that provides a 2D visualisation of dispersed particles with a frequency of 450 hz. Appropriate dispersion was ensured by application of the RODOS dry dispersing unit with the same conditions mentioned in Section 3.4.1.1. The carrier particles of six different mannitol batches as used for the preparation of powder blends (Section 4.1.2) were examined to support the data gained by visual categorisation (Section 3.4.2.2, Section 3.4.2.5). The Windox software (Version 5.8.0.0, Sympatec GmbH, Clausthal-Zellerfeld, Germany) was calculating the aspect ratio as depicted in Equation (3.7).

$$AR = \frac{d_{min}}{d_{max}} \quad (3.7)$$

AR	aspect ratio
d_{min}	minimal diameter of a particle with defined orientation, m
d_{max}	maximum diameter of a particle with defined orientation, m

An *AR* of 1 describes a perfect sphere, while indentions or other shapes like platelets or elongated particles lead to a lowered *AR*.

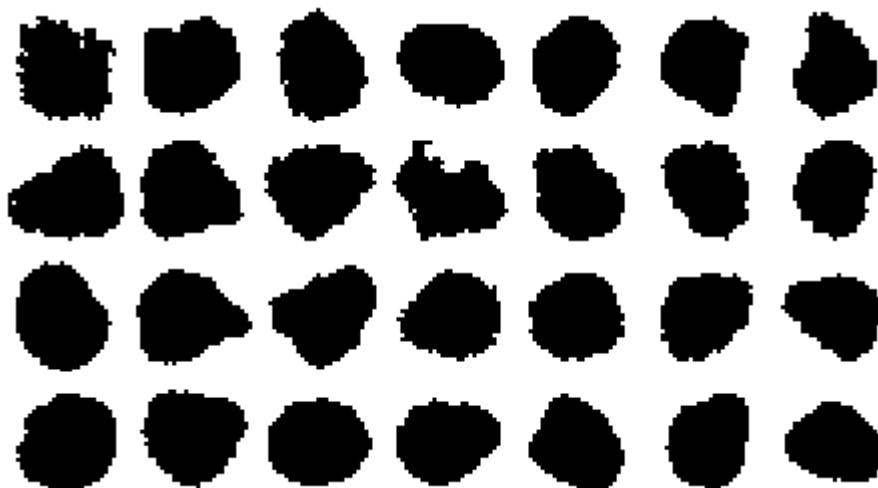


Figure 3.15 – Particle gallery of mannitol particles with a size between 25 μm and 125 μm and the AR above 0.75 as gained by image analysis

The particle gallery was used to set requirements for evaluation (Figure 3.15). An aspect ratio of $AR \geq 0.70$ was demanded to avoid agglomerates and overlaid particles which cause

incorrectly lower aspect ratios. Particle size was chosen as another parameter to exclude large agglomerates. Only particles with an equivalent circle diameter of 25 – 150 μm were taken into account. Smaller particles were excluded since the resolution is not appropriate for accurate evaluation.

3.4.2.4 Particle Cross Sections

As not only the outer shape is of interest for the examination of drying kinetics, particle cross sections were implemented to discover the inner particle structure. Exemplarily, a mostly spherical and an indented mannitol batch were embedded in tissue freezing medium (Tissue-Tek[®], Sakura Finetek, California, USA) at – 25 °C. Slices of 5 μm in thickness were cut with a cryomicrotome (CryoStar NX 70, Thermo Scientific, Waltham, Massachusetts, USA) and placed on the carbon sticker of a SEM sample holder. The cross sections were visualised as described in Section 3.4.2.1.

3.4.2.5 Surface Roughness by Survey

The determination of surface roughness parameters for mostly spherical particles by an analytical method like 3D laser scanning microscopy is challenging due to a number of reasons. The calculation of appropriate values is complicated due to spherical character and occurrence of indentations as results need to be flattened prior to evaluation. Further, only a few single particles can be covered by these approaches. Therefore, visual evaluation of SEM images was selected as the principal method to discover the surface roughness for all spray dried carrier batches. As for the particle shape, twenty volunteers were asked to categorise three SEM images of different magnification into five categories from smooth to crystalline structures with granular accumulations (crystallinity was predetermined by XRPD) as listed in Table 3.8. The results were evaluated as continuous values in the context of the DoE. 3D laser scanning microscopy was performed to support those data (Section 3.4.2.6).

Table 3.8 - Five roughness categories as used for the evaluation of the carrier surface roughness by a survey

Category	Description
1	Surface of all particles completely smooth
2	Some single crystalline structures on the surface
3	Several crystalline structures on the surface
4	Several crystalline structures on the surface including some single granular accumulations
5	All particles with crystalline structures and granular accumulations on the particle surface

3.4.2.6 3D Laser Scanning Microscopy

3D laser scanning microscopy (3D Laser Scanning Microscope VKX-200, Keyence Deutschland GmbH, Neu-Isenburg, Germany) was applied in order to visualise and quantify the roughness of the mannitol carrier surface of six different mannitol carriers (Section 4.1.2). A violet laser ($\lambda = 408 \text{ nm}$) served for a maximum resolution of 1 mega pixel ($135 \mu\text{m} \times 101 \mu\text{m}$) at 100 fold magnification. The particles of interest were placed on a microscope slide and fixed by glue prior to measuring. Surface visualisation was performed with a working distance of 0.3 mm and analysed with the Keyence MultiFile Analyser (Keyence Deutschland GmbH, Neu-Isenburg, Germany). A Gauss filter that describes the maximum altitude recognised as surface roughness was set to $\lambda_c = 0.08 \text{ mm}$ in order to distinguish between surface roughness and particle shape. The bending of the spherical particle shape was further considered for calculation. The surface roughness was calculated as arithmetic average of absolute values (R_a) for one-dimensional values (Equation (3.8)) corresponding to DIN EN ISO 4287 [128] and as arithmetic average of absolute values for an area (S_a) for two-dimensional values (Equation (3.9)).

$$R_a = \frac{1}{l} \sum_0^l |z(x)| dx \quad (3.8)$$

R_a	Arithmetic average of absolute values for a line (1D), μm
l	Length of the line in x direction with deviations in z direction, μm
$z(x)$	(cumulative) deviations in z direction, μm
dx	length of sector x in x direction, μm

Accordingly, R_a corresponds to the sum of all deviations $z(x)$ from the mean line divided by the sampling length l as was further illustrated in Figure 3.16.

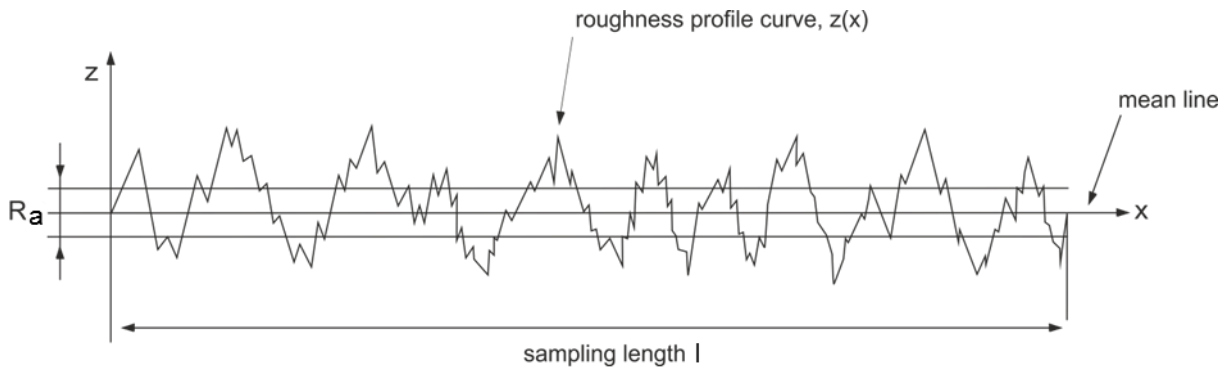


Figure 3.16 – R_a determination according to the roughness profile curve over the chosen sampling length l

The calculation of the arithmetic average of all deviations (S_a) from an area (A) follows the assumptions illustrated for R_a in Figure 3.16 as described by Equation (3.9).

$$S_a = \frac{1}{A} \sum_0^A |z(x,y)| dx dy \quad (3.9)$$

S_a	arithmetic average of all deviations from an area, μm
A	area defined in x and y direction with deviations in z direction, μm^2
$z(x,y)$	cumulative deviations (z direction) of the area (x and y), μm
$dx dy$	size of area covered for the measurements (x and y direction), μm^2

3.4.2.7 Confocal Raman Spectroscopy

A confocal Raman analysis approach was applied to distinguish between drug and carrier particles in interactive powder blends as the detection of drug accumulates with regard to the carrier particle shape was of special interest. Raman spectroscopy studies the inelastic Stokes Raman scattering of monochromatic radiation by a sample.

Experiments were performed with a WITec alpha 300R⁺ (WITec Instruments Corp., Ulm, Germany), which involved a surface topography module to gain a 3D profile of the particles. A green laser light source ($\lambda = 532 \text{ nm}$) was used to excite electrons in mannitol carrier particles as well as micronised BUD particles. Compound identification was based on characteristic Raman shifts at 1656 cm^{-1} for BUD and 875 cm^{-1} for mannitol. The surface topography of each particle was determined under white light in order to gain the height of the surface, which serves as the focal plane for the Raman spectra acquisition. Integration time was set to 0.5 s / line with a step size of $1 \mu\text{m}$. The analysis was performed on powder blends consisting of micronised BUD and two mannitol qualities, a spherical (M71(L)) and an indented one (M97(L)). Five particles were examined per batch. The overlay images were applied for qualitative evaluation of drug localisation after blending.

3.4.3 Flowability

Bulk flowability as a crucial parameter for carrier based powder blends can be determined based on diverse techniques. This project included Carr's Index (CI) as a measure related to analytics described in the Ph. Eur. [129] and the Basic Flowability Energy (BFE) measured with a powder rheometer for evaluation of particle-particle interactions in mannitol carrier samples.

3.4.3.1 Carr Index

CI describes the compressibility of a powder and is often used to classify its overall flow properties. Here, a jolting volumeter (Erweka SVM 121/221, Erweka GmbH, Heusenstamm, Germany) was applied to investigate bulk and tapped density based on Ph. Eur. 2.9.34 [129]. CI was calculated according to the following equation:

$$CI = \left(1 - \frac{\rho_B}{\rho_T}\right) \times 100 \quad (3.10)$$

CI	Carr Index
ρ_B	Bulk Density, $\text{g} \cdot \text{cm}^{-3}$
ρ_T	Tapped Density, $\text{g} \cdot \text{cm}^{-3}$

A small CI ($CI < 20$) represents free-flowing powders as bulk and tapped density will be close in value, while large a CI ($CI > 20$) indicates that more particle-particle interactions occur, which decreases particle flow.

3.4.3.2 Powder Rheometer

In general, rheology analytics are applied to record how the flow behaviour of a test material changes, when different strain rates are used. It is commonly introduced as a routine characterisation technique for liquid and semi-solid systems [130], but has rarely been used for solids like powder particles. Nevertheless, powder rheology approaches provide promising opportunities in order to analyse powder flow and, therefore, interparticulate forces.

An FT-4 Powder Rheometer[®] (Freeman Technology, Gloucestershire, UK) was applied to examine all mannitol batches for the BFE which was used to describe the flow properties within this project. The BFE represents the work which is needed to agitate a twisted blade downwards through a cylindrical borosilicate test vessel filled with the powder to test (Figure 3.17).

All samples were sieved with a 355 μm sieve prior to analysis to avoid agglomerates and discharged with a rod ionisator (S-Line LC, 50 VA, Haug GmbH & Co. KG, Leinfelden-Echterdingen, Germany) to overcome electrostatic forces. The analysis was started with conditioning cycles to induce loosening of the powder by turning the twisted blade clockwise (tip speed = 100 $\text{mm} \cdot \text{s}^{-1}$). This aimed at a standardised packing density and improved comparability of the results. Reversing the direction of the rotating blade (compared to the conditioning cycles) caused compaction of the sample. The force detected versus the distance travelled by the blade during the downward traverse gives the work (BFE) needed to generate a defined flow pattern within the sample [131]. Each measurement was repeated ten times and mean values were evaluated within the scope of the DoE.

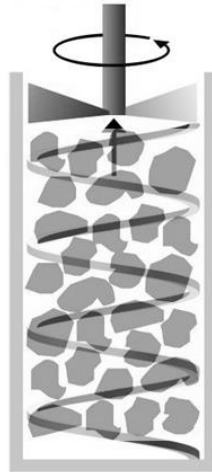


Figure 3.17 – Test vessel of the FT-4 powder rheometer with twisted blade and defined volume of powder particles

In theory, BFE is supposed to be lower for non-cohesive samples with less adhesion forces or mechanical interlocking than for powder batches with more interparticulate forces. The flow properties of a bulk can further be linked to particle characteristics like particle size or morphology as those are known to affect the particle-particle interactions and, therefore, the bulk flowability.

3.4.4 Surface Analytics

3.4.4.1 Surface area

Surface area measurements using the adsorption of an inert gas such as nitrogen, helium or krypton are based on the assumption that the amount of adsorbed gas is proportional to the surface area of the particles to test. Brunauer, Emmet and Teller (BET) introduced the BET equation [132] which can be simplified to the following:

$$S_t = \frac{V_m N_0 A_{cs}}{M_w} \quad (3.11)$$

S_t	total surface area, $\text{m}^2 \text{g}^{-1}$
N_0	Avogadro's number
A_{cs}	cross-sectional area of the adsorbent molecule, m^2
M_w	molecular weight of the adsorbent, $\text{g} \bullet \text{mol}^{-1}$
V_m	volume of gas adsorbed as a monolayer

The specific surface area is then obtained by correlation of S_t and the mass of powder measured. Measurements performed in the framework of this project were performed according to the European Pharmacopeia monograph “Specific surface area by gas adsorption” [133] to support the results gained for particle size and morphology determinations, as the BET surface area is known to be affected by these particle properties [134]. Sample preparation was started one day prior to measuring since samples were subjected to vacuum for > 12 h as a conditioning step (VacPrep 61, Micromeritics Instrument Corporation, Norcross, USA) to avoid unspecific binding of gas molecules on the surface. A Gemini 2360 System (Micromeritics Instrument Corporation, Norcross, USA) was applied for the BET investigations. The samples to test were compared to a reference sample filled with the amount of glass beads, which corresponds to the dead space volume of the sample as measured with a helium pycnometer before. Both sample tubes were cooled to 77 °K by liquid nitrogen during analysis. The dead space of the sample tube was measured with Helium (Quality 5.0, Linde Gas Hamburg, Germany) prior to each measurement. The amount of adsorbed Nitrogen (Quality 5.0, Linde Gas Hamburg, Germany) which was applied as test gas was defined as the volume difference between sample and reference vessel. Specific surface area calculations were based on a multipoint correlation with eleven different relative pressures between 0.05 and 0.3 p/p_0 , which was requiring a correlation coefficient of > 0.999 to be considered for evaluation. Samples were measured in triplicate and interpreted within the scope of the DoE.

3.4.4.2 Specific Surface Energy

Surface energy as determined by inverse gas chromatography (iGC) can be used to explain powder characteristics, such as crystallinity, morphology or the detachment of drug particles from a carrier surface during inhalation. A column packed with the sample to test is investigated with gas probes of known properties. Non-polar eluents are used to examine the dispersive component of the free surface energy (γ_s^d), while polar ones are necessary for the acid-base interactions (γ_s^p). The total surface energy (γ_s) is described by the addition of both, dispersive surface energy and polar surface energy [125,135,136].

Results described in this thesis are gained by non-polar eluents to examine the dispersive surface energy. Dispersive (apolar) interactions, also known as Lifshitz–van der Waals interactions, consist of London interactions which originate from electron density changes (the force between two instantaneously induced dipoles) but may also include both Keesom (the force between two permanent dipoles) and Debye (the force between a permanent dipole and a corresponding induced dipole) interactions. Specific (polar) interactions explain all other types of interactions, but were not measured in this project.

IGC analysis was performed with an SMS iGC (Surface Measurement Systems Ltd., Alperton, UK). Special iGC columns (Surface Measurement Systems Ltd., Alperton, UK) of 3 mm in diameter for drug samples and 4 mm in diameter for mannitol samples were packed and tapped with an iGC Column Packer (Surface Measurement Systems Ltd., Alperton, UK) for 10 min at level 6 to get comparable packing densities for all samples. The powder was fixed in the column by silanised glass wool (Supelco, Bellefonte, USA). Analysis was performed with two different methods, where both methods use Helium at 10 ppm as a carrier gas. First, samples were measured with a series of alkanes (hexane, heptane, octane, nonane, decane) at a vapour concentration of $0.03 p/p_0$, which corresponds to an infinite dilution. This injection concentration can be linearly related to the adsorbed amount as Henry's Law is applicable at this point of the adsorption isotherm [137]. Methane, which shows no interference with the surface of the specimen, was used to determine the death volume ($0.01 p/p_0$). The eluents were detected with a flame ionisation detector (FID) after passing the column. This method was used to calculate the dispersive surface energy (iGC Advanced Analysis Macro V1.41 for Microsoft Excel 2013, Surface Measurement Systems Ltd., Alperton, UK / Microsoft Corporation, Redmond, USA).

The same alkanes were used for further investigations at finite concentration to examine the dispersive surface energy profiles of the mannitol carrier. In theory, probe molecules adhere to high energy spots on the surface prior to low energy ones, when present. Different vapour concentrations from $p/p_0 = 0.03$ to $p/p_0 = 0.95$ were screened to generate an isotherm for each alkane used. The isotherms display that in this setup the Langmuirian adsorption isotherm (Type I) but not Henry's Law is applicable for evaluation [132,138]. This method was used to investigate the heterogeneity of the carrier surfaces, as the surface energy was plotted against the surface loading at different concentrations [138]. The surface was assumed to be homogenous for $\Delta\gamma_s^d < 5$ mJ.

Dispersive surface energy as the free energy of adsorption can be expressed by Equation (3.12), so that $RT \ln V_R^0$ can be plotted against $\sqrt{\gamma_L^d}$ to gain the dispersive surface energy from the slope of a linear correlation ($2N_A \sqrt{\gamma_s^d}$).

$$RT \ln V_R^0 = 2N_A \times a \times \sqrt{\gamma_L^d \times \gamma_S^d} + K \quad (3.12)$$

R	general gas constant, $J \bullet kg^{-1} K^{-1}$
T	temperature, $^{\circ}K$
V_R	net retention volume, m^3
N_A	Avogadro number, $6.022 \times 10^{23} \text{ mol}^{-1}$
a	cross sectional area of the probe molecule, 0.162 nm^2 for N_2
γ_L^d	dispersive surface energy of the liquid phase, $mJ \bullet m^{-2}$
γ_S^d	dispersive surface energy of the solid surface, $mJ \bullet m^{-2}$
K	probe molecule specific constant

3.4.4.3 Dynamic Vapour Sorption

The ability to adsorb water not only on the surface but also absorb it into the material can often be related to amorphous contents, which recrystallise when a distinct content of moisture occurs. The mass of adsorbed and absorbed water depends on the crystal habit of the sample and the relative humidity (p/p_0).

The behaviour of drug particles at defined ambient moisture contents was investigated with a DVS-1 (Surface Measurement Systems Ltd., London, UK) that measures the humidity-dependent increase in mass gravimetrically. According moisture sorption isotherms were recorded for an increase of the p/p_0 value from 0.0 p/p_0 to 0.9 p/p_0 (steps 0.1 p/p_0) and the decrease to 0.0 p/p_0 again. Moisture contents were kept stable for up to 720 min unless change in mass was $< 0.0005 \% \bullet \text{min}^{-1}$. The first cycle was repeated once to enable statements on water uptake during the first cycle as crystallisation events occur irreversibly and do not affect the moisture sorption isotherm of the second cycle.

Mannitol samples were measured accordingly but with a DVS-HT (Surface Measurement Systems Ltd., London, UK) which allowed the determination of up to ten samples simultaneously.

3.4.4.4 Differential Scanning Calorimetry

Differential Scanning Calorimetry (DSC) was applied as a method to examine thermic events that occur during heating a sample. The differential heat flow between sample and reference

cell was investigated with a Perkin Elmer PYRIS Diamond DSC (Perkin Elmer, Waltham, USA) to relate differences to events like melting, recrystallisation or glass transition.

Therefore, 4 – 5 mg of sample was accurately weighed into aluminium DSC pans and the pans were closed with a pierced lid. A temperature-time-program with a heating rate of 10 °C min⁻¹ was applied to sample and reference cell for all samples. The minimum temperature was chosen to be 20 °C, while the maximum temperature was adjusted according to the melting temperature of each sample gained from literature. Measurements were performed at a nitrogen flow of 20 mL • min⁻¹. Calculation of recrystallisation temperature (T_c) and melting temperature (T_m) was performed with PYRIS software 3.8 (Perkin Elmer, Waltham, USA).

3.4.5 Crystal Lattice

X-Ray powder diffraction (XRPD) is known as a method to analyse crystal lattice structures of crystalline samples or to indicate that a product occurs fully amorphous. The according XRPD diffractograms display the intensity of X-Rays in correlation to the detected diffraction angles by the sample of interest.

The X-Rays are generated in an evacuated X-Ray tube. High voltage is applied to a wolfram cathode which accelerates electrons towards the anode. The kinetic energy is mainly converted into thermal energy, but serves to also emit a small amount of X-Rays, which were used for analysis. The X-Rays are directed to the sample to be diffracted by the crystal lattice (when short- or long order appears). The crystal lattice can be derived from diffraction pattern in relation to the respective diffraction angle and peak intensity since different structures and polymorphs refract differently.

Mannitol and drug samples were investigated by XRPD (Stadi P diffractometer, Stoe & Cie GmbH, Darmstadt, Germany) using an acceleration voltage of 40 kV and a current strength of 30 mA applied to the copper anode to emit CuK α_1 X-Rays for interference with the sample. The diffracted beams were measured in the range of $\theta = 8 - 35^\circ$ at a step rate of $2\theta = 0.05^\circ$. For evaluation, diffraction intensity was plotted against bending angle 2θ .

Mannitol diffractograms were further compared to data of the three polymorphs alpha, beta and delta which are known from literature [87].

3.4.6 Drug Quantification

Drug quantification was performed by reversed phase high performance liquid chromatography (RP-HPLC), as this technique is known to generate accurate results for a broad range of concentrations and with a very low limit of detection. In total, four different drugs were analysed. SBS and BUD were quantified using a Waters HPLC system (Waters

Corporation, Milford, USA) and evaluated with Empower[®] Pro 2 software (Waters Corporation, Milford, USA). TIO and FOR samples were investigated with an Agilent HPLC system (Agilent Technologies Inc., Santa Clara, USA). The respective methods are summarised in Section 8.1. The raw materials of each drug served as external standards for a calibration curve that was calculated prior to every test series.

4 Results & Discussion

4.1 Spray Dried Engineered Carriers

The preparation of mannitol carrier particles was performed with a pilot scale spray dryer as used by Littringer et al. and Maas et al. earlier [16,23,82] and described in Section 3.3.1. In total, nineteen different batches were spray dried as part of a DoE to further investigate mannitol carrier properties in dependence of the chosen drying conditions.

4.1.1 Carrier Storage Stability

It is known from literature that mannitol appears in different polymorphs (α , β , δ) depending on preparation, treatment or storage of the sugar alcohol. Investigations on spray dried mannitol as performed by XRPD revealed that all batches prepared within this project consisted of β -mannitol which is likewise the most stable conformation [87]. Figure 4.1 exemplarily shows one batch of the spray dried sugar alcohol, whose peak pattern agrees with the one of β -mannitol as published by Littringer et al. [23] and Fronczek et al. earlier [87].

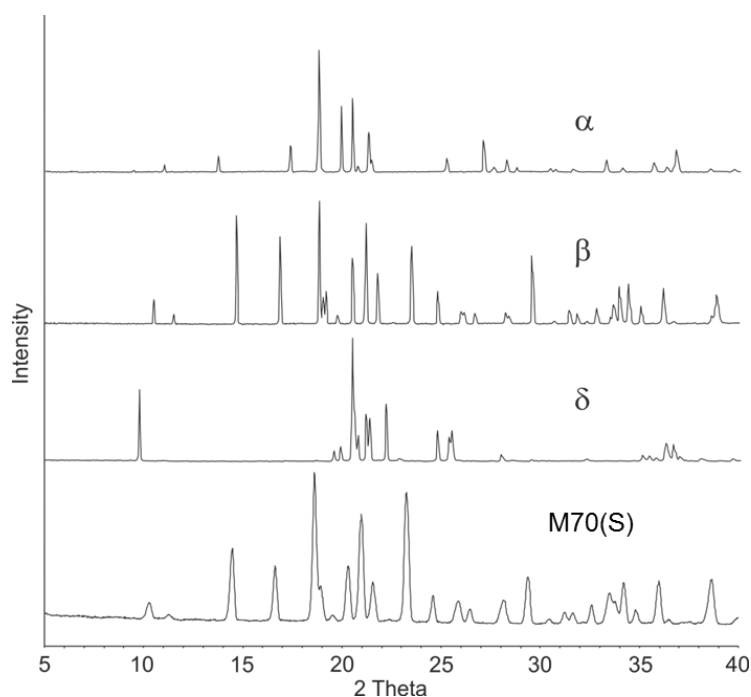


Figure 4.1 – XRPD diffractograms of the three different polymorphs of mannitol (α , β , δ) described in literature [87] and exemplarily one batch (M70(S)) of spray dried mannitol as gained by spray drying with the pilot scale spray dryer

XRPD results were gained to generate qualitative information about the crystallinity. Earlier investigations by Littringer et al. observed that almost 100 % of the spray dried product appears in form of the β -polymorph [23].

Further analysis was performed to test product properties during storage as this might affect the product quality. Figure 4.2 shows the change in mass during a DVS analysis, when the mannitol surrounding moisture content was increased stepwise from 0 % rH to 90 % rH. Differences between first and second cycle, which would indicate recrystallisation by moisture uptake during the first cycle, could not be detected. Sample mass was increased by ~ 1.3 % during both cycles, when moisture was kept at 90 % rH. Data exhibit spray dried mannitol batches to be slightly hygroscopic according to the Ph. Eur. as the amount of moisture uptake was found to be below 2 %, but above 0.2 % [133]. In general, these data support the XRPD results suggesting that the product appeared in the most stable β -polymorph as no recrystallisation events were detected. Crystalline mannitol was most likely observed with respect to the low T_g (≈ 30 °C) that governs instant recrystallisation during the spray drying process [110].

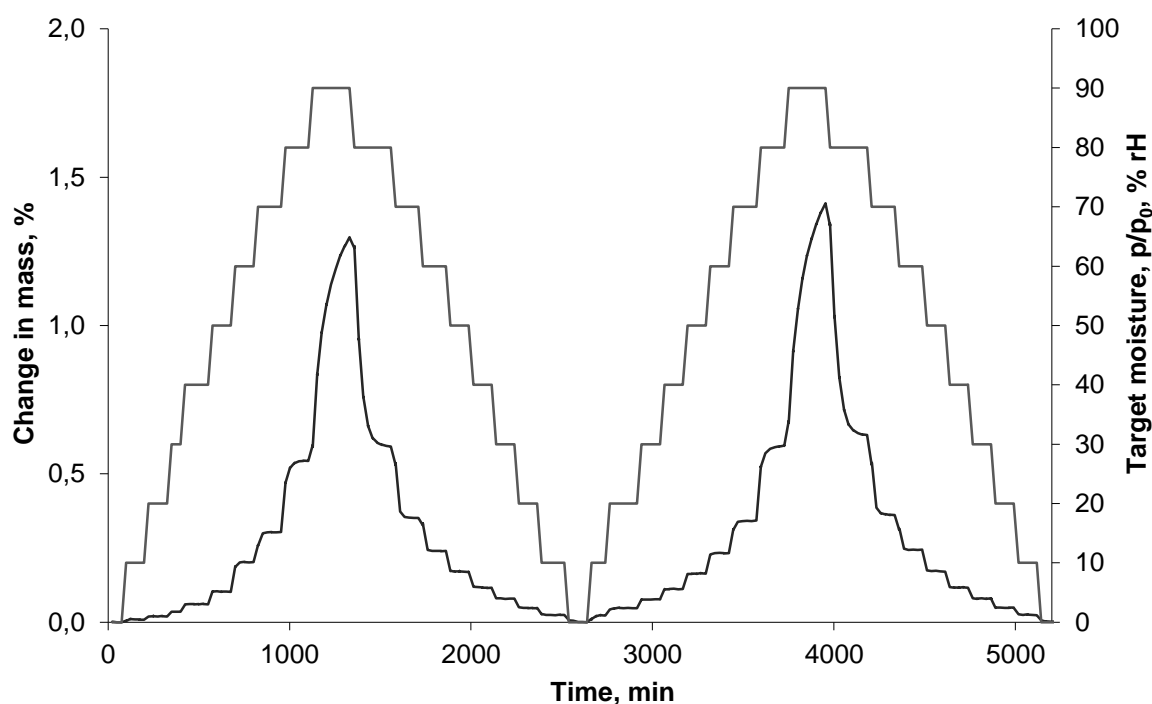


Figure 4.2 – Change in mass plot of the DVS analysis with spray dried mannitol, exemplarily displayed for one batch (Run 15). The x-axis shows the time in minutes. The 1st y-axis displays the change in mass (Δm) in % (lower plot), while the target moisture (p/p_0) in % rH was plotted on the 2nd y-axis.

DSC analysis was performed on spray dried mannitol to finally support the XRPD results along with the examination of its purity. Figure 4.3 displays the DSC plot of mannitol, when the sample was heated from 50 °C to 200 °C. Only a single event was observed for the heat flow which represented the melting point of mannitol at $T_m = 166.1$ °C (Figure 4.3) matching earlier results for the raw material Pearlitol[®] 160C published by Cares-Pacheco et al. [139]. Further events which might indicate recrystallisation of the product were not detected.

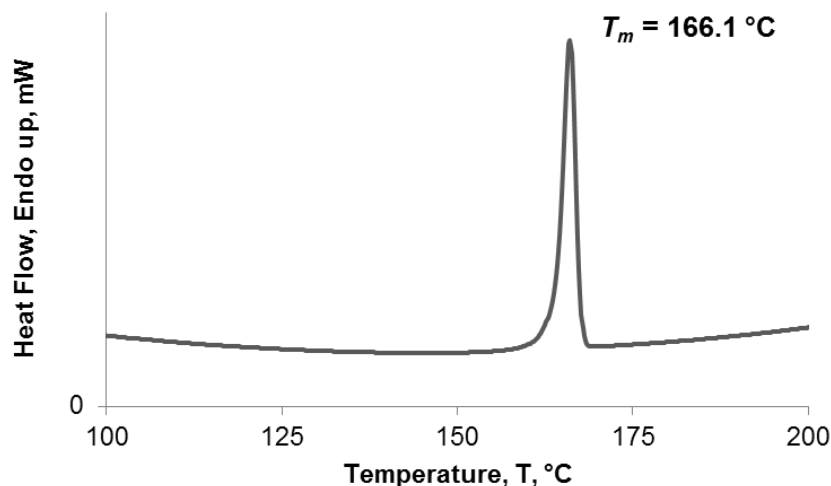


Figure 4.3 – DSC results of spray dried mannitol (M70(S)) with the heat flow in mW (y-axis) plotted against the temperature in °C (x-axis).

Engineered mannitol carrier particles occurred in the β -modification which is supposed to be the most stable one, and were found to sparsely absorb moisture even at high relative humidity, which further supports storage stability as moisture uptake promotes recrystallisation and by this crystal growth.

Stability of the product is of great importance for all formulations in pharmaceutical use. Spray dried mannitol carrier particles were found to be stable at ambient conditions which simplifies the storage over time. All products prepared in the scope of the DoE as described in the following section were stored at room temperature and without further moisture control.

4.1.2 Design of Experiments

The conditions used for the spray drying of nineteen mannitol carrier batches are displayed in Table 4.1 as factors which were altered for three levels (Section 3.3.1). All spray dried mannitol carrier batches were analysed for a broad set of different powder characteristics and evaluated in the framework of the DoE. Results for analyses, which were performed on all mannitol carrier batches generated in this project, are summarised in Table 4.1 as responses. Further, these results were supplemented by further analytics which were only performed on those six batches chosen for the use in interactive powder blends (Table 4.1). The batches were numbered according to the run order given by the DoE. Additional labels were allocated to the six batches that were applied for aerodynamic characterisation, providing further information regarding particle size and morphology of the carrier. The batch labels distinguish between small (S, 45 – 55 μm), medium (M, 55 – 65 μm) and large particles (L, 65 – 75 μm) and inform about the chosen outlet temperature as particle morphology was found to depend on the drying temperature as will be discussed later.

Table 4.1 – Results of powder analytics on nineteen mannitol carrier batches as spray dried in the framework of the DoE.

Sample Name		Spray drying conditions					Particle Properties												
DoE: Naming		Results: Extra Labelling	DoE: Factors			T _{out} , °C	DoE: Responses with significant models					Span	Aspect Ratio	Surface / Line Roughness, S _a / R _a , μm	Tapped Density, g/cm ³	Carrs Index	Surface Energy, mJ/m ²	Porosity	
Run Order	Exp. Name		n, rpm	T _{ax} , °C	T _{swirl} , °C		Particle Size, x50.3, μm	Particle Shape, Cat. 1-5	Surface Roughness, Cat. 1-5	Basic Flow-ability Energy, BFE, mJ	BET surface area, m ² /g								
10	1	M71(L)	8000	130	60	71	68.1	1.4	2.7	91	0.26	0.69	0.8967	0.53 / 0.10	0.49	9.73	47.2	0.62	
19	2		8000	190	60	96	73.6	3.6	3.4	144	0.33	0.69		0.53	13.61			0.60	
15	3		8000	130	100	75	69.2	2.8	3.0	109	0.44	0.72		0.51	11.11			0.60	
11	4	M97(L)	8000	190	100	97	76.8	4.9	4.5	149	0.61	0.71	0.8547	3.02 / 0.37	0.52	9.11	65.2	0.64	
9	5	M70(S)	14000	130	60	70	51.1	1.7	2.2	82	0.44	0.83	0.8866	0.89 / 0.08	0.51	11.97	64.8	0.62	
8	6		14000	190	60	82	65.3	4.5	4.4	102	0.51	0.87		0.50	12.73			0.61	
5	7		14000	130	100	78	57.1	2.9	3.3	94	0.51	0.91		0.54	13.03			0.59	
12	8		14000	190	100	93	64.6	4.6	4.0	95	0.65	0.98		0.50	15.93			0.63	
14	9	M74(M)	11000	130	80	74	57.5	2.5	2.9	98	0.42	0.76	0.8825	0.70 / 0.12	0.51	11.97	61.4	0.50	
7	10		11000	190	80	90	66.3	4.4	4.5	126	0.59	0.83		0.52	15.47			0.61	
17	11		11000	160	60	81	60.8	3.3	3.0	125	0.52	0.85		0.54	14.29			0.61	
6	12		11000	160	100	86	60.7	3.8	3.4	117	0.55	0.75		0.54	13.98			0.60	
18	13		8000	160	80	85	70.7	3.7	3.6	141	0.49	0.79		0.53	11.44			0.59	
13	14	M80(S)	14000	160	80	80	53.7	4.3	3.6	111	0.57	0.83	0.8676	3.57 / 0.23	0.54	16.49	65.0	0.60	
1	15		11000	160	80	81	62.1	3.8	3.2	123	0.56	0.71		0.54	14.29			0.60	
3	16		11000	160	80	81	61.2	3.8	3.8	119	0.56	0.74		0.54	13.03			0.60	
4	17		11000	160	80	80	60.5	3.6	3.9	114	0.53	0.87		0.53	12.71			0.59	
16	18		11000	160	80	81	60.3	4.4	3.8	133	0.55	0.87		0.54	15.04			0.60	
2	19	M80(M)	11000	160	80	80	60.8	3.7	3.9	130	0.55	0.71	0.8661	1.55 / 0.15	0.53	12.71	64.3	0.43	

All analytical results were considered for DoE evaluation but only significant results are shown here. The quality parameters as described in Section 3.2 are displayed in Table 4.2. Models for every single response were gained followed by a backward regression of insignificant terms which resulted in the best fitting model for the evaluated data. Model quality for particle size, particle shape, basic flowability energy and BET surface area was found to be excellent, as the models exhibit optimal fittings to the analytical results (R^2) and allow prediction of particle properties for further experiments (Q^2). Medium but adequate quality was found for all quality parameters of surface roughness as a response.

Table 4.2 – Quality parameters for mannitol properties evaluated within the DoE. First column gives the evaluated quality parameter including the limits of acceptance. Further columns show the responses and the according quality results. *artificial lack of fit due to high reproducibility

quality parameter	particle size $x_{50.3}$, μm	particle shape, Cat. 1-5	particle roughness, Cat. 1-5	basic flowability energy (BFE), mJ	BET surface area, m^2/g
$R^2 (> 0.50)$	0.94	0.90	0.74	0.91	0.94
$Q^2 (> 0.50)$	0.86	0.83	0.61	0.81	0.82
$P (> 0.25)$	0.04*	0.83	0.76	0.94	0.36*
$RP (> 0.50)$	0.99	0.89	0.79	0.84	0.97

DoE quality was examined to ensure that fittings enable interpretations in terms of e.g. drying kinetics during the spray drying of bi-component mannitol water droplets based on profound models. Those results will be discussed in the next sections.

4.1.3 Particle Size

The spray drying technique and its various parameters enable the production of particles with controlled particle sizes. Several factors have been found to significantly influence the size of the finished product. The resulting dimensions are mainly a function of dissolved mass per solvent, spray droplet size and drying temperature. Drying of droplets is further limited by spray tower size and air stream volume as this determines the resident time in the drying chamber and so the maximum droplet size that can be dried adequately. The mass fraction of mannitol to dry, which was 15 % [w/w] and was not altered for the drying of mannitol carriers in the framework of the DoE, theoretically impacts on the size due to the point when saturation occurs on the droplet surface. Saturation solubility is reached earlier when the mannitol concentration in the solvent is higher, which leads to an earlier crystallisation and

larger particles while the solvent gets evaporated [11,22]. However, this aspect was not further covered by this DoE since earlier experiments within the scope of this project were dealing with different mass fractions showing the effects mentioned before.

Three different factors were chosen to be altered on three different levels for this study to examine the influence on mannitol carrier properties. The effect of the LamRot atomiser rotation speed on the droplet size was initially tested in an off-site setup by laser diffraction to calculate the resulting particle sizes, assuming an average porosity of 40 % as mentioned by Littringer et al. [22]. The screening of rotation speeds between 3,000 and 14,000 rpm led to droplets of $d_{50.3} = 200 \mu\text{m}$ when low acceleration forces occurred and to $d_{50.3} = 78 \mu\text{m}$ for the highest rotation speed (Table 4.3). Span values revealed droplets generated at medium rotation speeds (span = 0.40 – 0.45; 5,000 – 10,000 rpm) to have the narrowest droplet size distribution. Calculated particle sizes (Equation (3.3)) suggested particles to have a final volumetric diameter of $d_{50.3} = 45 \mu\text{m}$ to $116 \mu\text{m}$ assuming that all particles have the shape of a perfect sphere. Rotation speed used for the final experiments was varied between 8,000 and 14,000 rpm with respect to earlier experiments performed by Littringer et al, who conducted experiments at 6,300 to 8,100 rpm [16]. Hence, experiments were aiming at particles of smaller size than gained by former studies.

All factors considered here were tested for influences on the final particle size but only rotation speed (n) and axial air stream temperature (T_{ax}) were found to have an effect. Dependencies for particle size as response (y) of the DoE can be displayed by Equation (4.1):

$$y = a_0 + a_1 T_{ax} + a_3 n + a_4 T_{ax}^2 + a_6 n^2 \quad (4.1)$$

which was obtained from Equation (3.2) by neglecting insignificant terms in a backward regression as mentioned in Section 3.2. Remaining terms show a linear term of T_{ax} and n as well as a quadratic correlation of T_{ax} to have a significant effect on the final carrier size. Scaled and centred values for the coefficients given in Table 4.4 assumed that n has the main impact on the final particle size. An increase of n by one level or $n = 3000$ rpm reduces the resulting particle size for about $6.66 \pm 0.59 \mu\text{m}$, while T_{ax} enlarges the carriers by $4.37 \pm 0.59 \mu\text{m}$ per level ($T_{ax} = 30 \text{ }^\circ\text{C}$).

Table 4.3 – Droplet sizes of an aqueous solution of mannitol after atomisation with the LamRot atomiser in an off-site spray experiment

LamRot rotation speed, rpm	Droplet size, $d_{50.3}$, μm	Span, $\frac{(d_{90.3}-d_{10.3})}{d_{50.3}}$	Calculated particle size, $d_{50.3}$, μm
3,000	200	0.53	116
4,000	169	0.48	98
5,000	152	0.45	87
6,000	140	0.44	80
7,000	132	0.41	76
8,000	116	0.43	67
9,000	109	0.42	63
10,000	103	0.43	60
11,000	97	0.46	56
12,000	91	0.5	52
13,000	83	0.55	48
14,000	78	0.78	45

Table 4.4 – Scaled and centred coefficients (\pm standard deviation) for carrier particle size as a response. Values give the effect on the final particle size in μm , when the factor is changed for one level ($T_{ax} = 30\text{ }^\circ\text{C}$; $n = 3,000\text{ rpm}$)

Coefficients	Particle size $d_{50.3}$, μm scaled & centred
a_0	-
T_{ax}	4.37 ± 0.59
n	-6.66 ± 0.59
$T_{ax} \cdot T_{ax}$	2.29 ± 1.05
$n \cdot n$	2.58 ± 1.05

Experiments resulted in final carrier sizes of 51.1 μm to 76.8 μm as summarised in Table 4.1. The effect of T_{ax} and n was further visualised in the contour plot shown in Figure 4.4, which displays that the smallest particles ($d_{50.3} < 55\text{ }\mu\text{m}$) were generated at high rotation speeds ($n = 14,000\text{ rpm}$) and low axial air stream temperatures ($T_{ax} = 130\text{ }^\circ\text{C}$), while the largest

particles ($d_{50.3} > 75 \mu\text{m}$) occurred for low rotation speeds ($n = 8,000 \text{ rpm}$) and high axial air stream temperatures ($T_{ax} = 190 \text{ }^\circ\text{C}$).

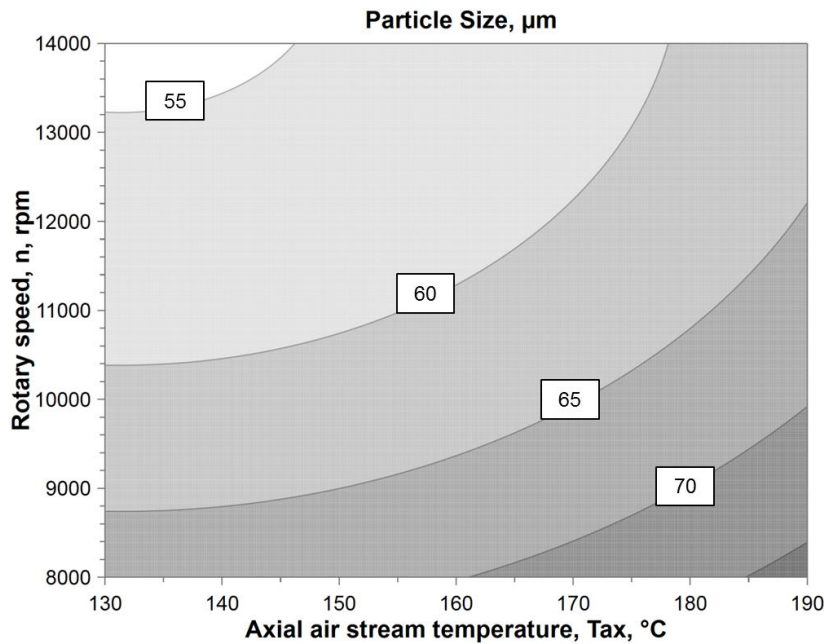


Figure 4.4 – Contour plot of the final particle size as a response of the DoE with the factor rotation speed (n) on the y-axis and the axial air stream temperature (T_{ax}) on the x-axis

The effects observed here prove findings discussed in literature earlier. Rotation speed and its influence on the droplet size have been shown by Littringer et al. within the same project for lower rotation speeds [16,22]. The acceleration of the emerging filaments determines the filament diameter and by this the moment of droplet disruption, which in turn defines the droplet diameter and by this the resulting particle size [14,98].

The way bi-component droplets dry is governed by the interplay of the diffusion of dissolved molecules and the evaporation of its solvent. Results presented here revealed the drying temperature T_{ax} to affect mannitol carrier particle size. In general for the drying of mannitol, evaporation of water molecules exceeds the diffusion of mannitol molecules in an aqueous solution, which reasons that mannitol concentrates on the surface of a droplet during drying [140]. The shell, which was built when saturation solubility was reached on the droplet surface, determined the final particle size. The effect of drying temperature on the shell formation – and by this the particle size – is further displayed in Figure 4.5. The temperature of the ambient drying air also affected the evaporation of water. Higher temperatures cause higher drying rates, which resulted in faster evaporation and surface reduction accompanied by saturation of mannitol on the droplet surface. This led to an earlier shell formation and larger particles compared to droplets dried at moderate conditions as can be seen in Figure 4.4 and Figure 4.5.

This effect can also be explained by the dimensionless Peclet numbers (Pe) which underline the described effect as these numbers depend on the drying velocity. The larger Pe , the faster is the evaporation of water from the surface which in turn results in larger particles. The Pe calculated for an outlet temperature of $T_{out} = 70.2$ °C amounts to $Pe = 139.6$, while the Pe for particles dried at $T_{out} = 97.2$ °C amounts to $Pe = 200.5$, which reflects that higher outlet temperatures indicate an earlier shell formation than lower ones as published by Gopireddy et al. earlier [141]. Diffusion of mannitol from the droplet surface towards the inside proceeds too slow to compensate the diffusion and evaporation of water, which results in rising mannitol surface concentrations and higher Pe numbers, which in turn reasons the earlier shell formation.

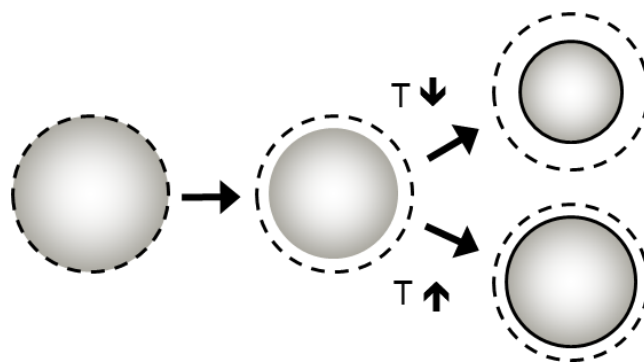


Figure 4.5 – Sketch of the drying of bi-component mannitol-water droplets at different drying temperatures (T)

Further, the mannitol carrier PSD was of interest, as the combination of LamRot atomiser and swirl air stream was designed to control the droplet break-up and by this to lower span values. In fact, all batches dried within the DoE revealed span values < 1.0 (Table 4.1) with the narrowest PSD for some batches dried with a rotation speed of 8000 rpm (Run 1 / 2; $span = 0.69$). Figure 4.6 shows the PSD of DoE Run 2 exemplarily for all other batches, illustrating that spray drying of mannitol lead to monomodal and narrow PSDs, when compared to Pearlitol 160C, which was used as raw material for these experiments. These results can be attributed to the defined diameters of the sixty bores distributed around the LamRot atomizer (Figure 3.9), but also to the swirl air stream, which allows unaffected droplet break-up by the repression of axial forces by the axial air stream.

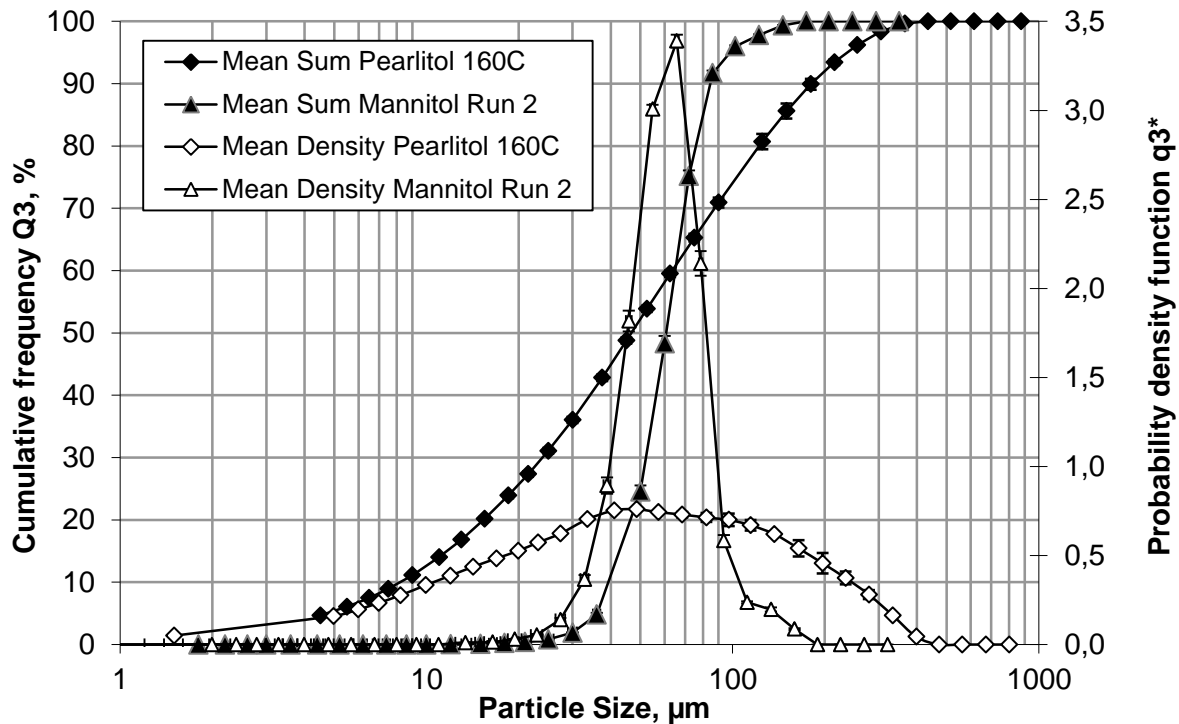


Figure 4.6 - PSDs of spray dried mannitol Run 2 and commercially available Pearlitol 160C as a sieved mannitol quality

A medium span value of 0.79 ± 0.08 was measured for the current nineteen experiments, whilst experiments conducted by Littringer et al. [16] using the same pilot scale spray dryer resulted in an average span of 0.84 ± 0.06 indicating slight improvements, which however were not significant as examined with an unpaired t-test. It can be suggested that control of the swirl air stream volume (V_{swirl}) might further improve the span value of spray dried mannitol particles. Mescher et al. have proved on the drying of PVP that V_{swirl} and the resulting swirl air stream velocity need to meet the acceleration forces of the LamRot atomiser or the droplet velocity, respectively, to generate the best PSD results [15], which was not implemented for mannitol drying to stay with a reasonable number of factors.

With respect to the use in DPIs, particles of 50 – 80 µm as generated by spray drying with the pilot scale spray dryer match the desired size range. Literature mentioned particles with a size > 50 µm to be suitable for carriers with inhalation purpose [16,46].

4.1.4 Particle Morphology

The morphology of carrier particles used for inhalation purposes has been described to impact the inhalation characteristics crucially. The factors used in this study were chosen with respect to earlier studies, which dealt with the spray drying of mannitol and the influence of drying conditions on the appearance of the mannitol carriers [11,16,82].

Morphology was distinguished between particle shape and surface roughness to focus on the drying of bi-component mannitol-water droplets as shape and roughness were believed to arise independently. Further, it was of interest to evaluate the influence of both on the aerodynamic performance of interactive powder blends to discuss the effects separately.

4.1.4.1 Particle Shape

The three factors varied in the framework of the DoE were tested for significant effects on the particle shape, but only T_{ax} and T_{swirl} were found to affect the shape, which results in the following Equation (4.2):

$$y = a_0 + a_1 T_{ax} + a_2 T_{swirl} + a_4 T_{ax}^2 \quad (4.2)$$

which includes T_{ax} and T_{swirl} as linear terms as well as a quadratic term of T_{ax} . Scaled and centred values for the coefficients depicted in this equation revealed T_{ax} to have the main impact on the particle shape as an alteration of the factor T_{ax} for one level ($T_{ax} = 30$ °C) changed the particle shape by 1.065 ± 0.10 categories. The effect of T_{swirl} was less pronounced with only 0.435 ± 0.10 categories per level ($T_{swirl} = 20$ °C). These differences can be attributed to the chosen air stream volumes since V_{swirl} only amounts to 40 % of V_{ax} .

Table 4.5 - Scaled and centred coefficients (\pm standard deviation) for carrier particle shape as a response. Values give the effect on the particle shape in categories (Category 1 – 5), when the factor is changed for one level ($T_{ax} = 30$ °C; $T_{swirl} = 20$ °C)

Coefficients	Particle shape, Cat. 1-5 scaled & centred
a_0	-
T_{ax}	1.065 ± 0.10
T_{swirl}	0.435 ± 0.10
$T_{ax} \cdot T_{ax}$	-0.494 ± 0.15

Experiments resulted in a broad range of differently shaped particles starting from quite spherical particles as scored with an average shape of category 1.4 (Table 4.1, Run 1) up to deeply indented particles with an average shape of category 4.9 (Table 4.1, Run 4) as assessed by visual inspection of SEM images. The whole range of particle shapes with its dependencies in terms of axial or swirl air stream temperature is illustrated in Figure 4.7. Almost perfect spheres (category < 2) occurred, when drying temperatures of both T_{ax} and

T_{swirl} were kept low ($T_{ax} = 130\text{ °C}$; $T_{swirl} = 60\text{ °C}$), which is further depicted by the appropriate SEM image shown in Figure 4.7. In turn, droplets dried at higher temperatures ($T_{ax} = 190\text{ °C}$; $T_{swirl} = 100\text{ °C}$) lead to mannitol particles with deep indentions as displayed by the SEM image in Figure 4.7.

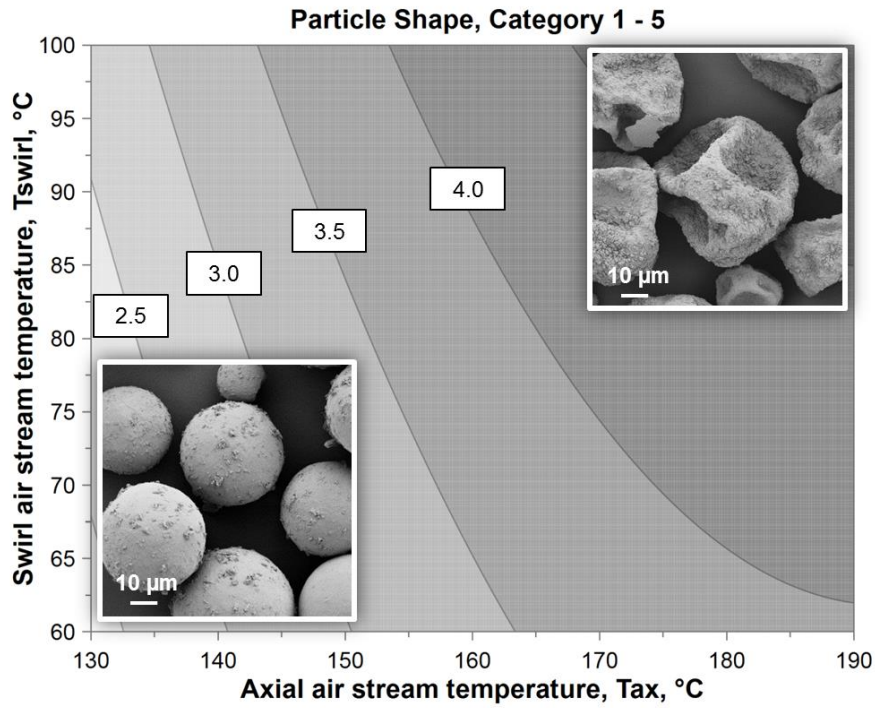


Figure 4.7 – Contour plot of the carrier particle shape as a response of the DoE with the factor swirl air stream temperature (T_{swirl}) on the y-axis and axial air stream temperature (T_{ax}) on the x-axis. Results are given in categories from category 1 (spherical carrier particles, Run 5) to category 5 (deeply indented carrier particles, Run 4) and are visualised exemplarily by two SEM images (1,000 fold magnification)

The evaluation of SEM images in form of a survey used several subjective perspectives to generate an objective view on the particle shape. Image analysis was applied to overcome subjectivity. The mean aspect ratios were measured for six mannitol batches as illustrated in Figure 4.8 for particles from 25 to 150 µm in diameter. Results gained here support the data gained by SEM image evaluation.

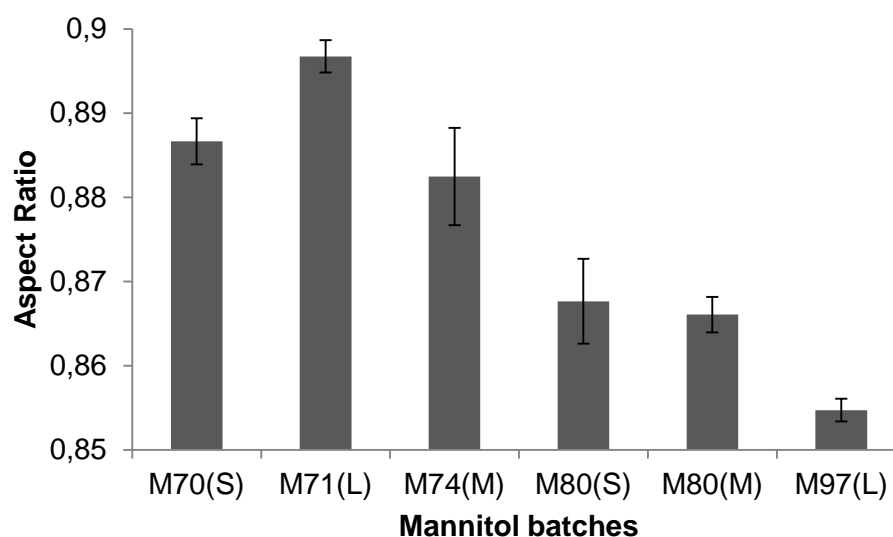


Figure 4.8 – Mean aspect ratios of the six mannitol batches chosen for interactive powder blends ($n=3 \pm$ standard deviation)

Further, two representative mannitol batches were cut using a kryo microtome to complete the results gained by visual inspection of SEM results and image analysis since these cross sections offered the opportunity to examine the inside of the particles, when visualised by SEM analysis.

The SEM images shown here represent the average cross sections of the batches of interest as it was necessary to find particles, which received a centered cut. In fact, cross sections exhibited the same (outer) particle shape as expected with respect to earlier SEM images and aspect ratios. Figure 4.9 – A shows a spherical carrier batch, which comprises an obvious cavity inside the particle, while Figure 4.9 – B reveals indentations in the outer core of the particle and a smaller inner cavity. The crystalline structure of the mannitol shell consisted of smaller and larger crystals involving several pores, which – in conjunction with the inner cavity – led to an appropriate porosity as discussed by Littringer et al. earlier [22]. Noticeably, spherical particles dried at lower drying temperatures consist of both smaller and larger crystals compared to those generated at higher temperatures, which are mostly built of smaller ones, which can be attributed to the increased number of crystal seeds when spray drying is conducted at higher temperatures.

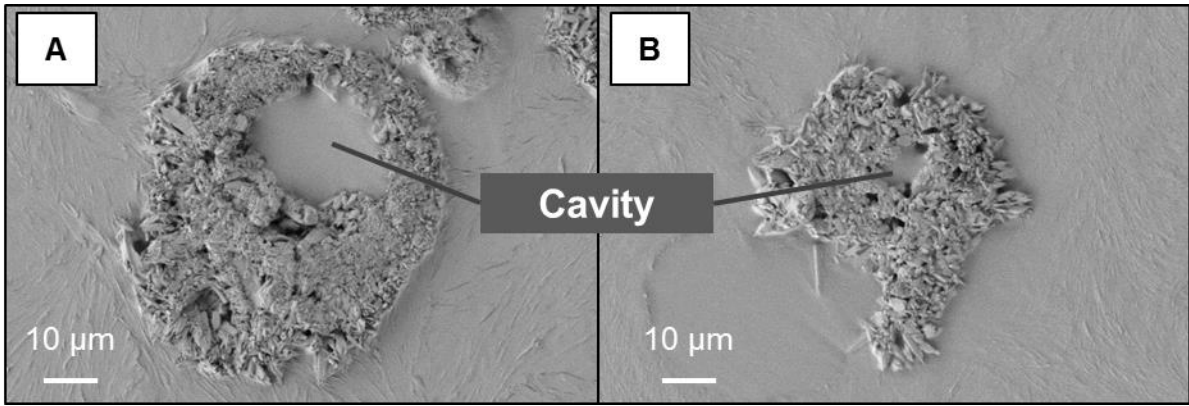


Figure 4.9 – Cross sections of two mannitol carrier batches at 1,000 fold magnification; A: spherical carriers (Run 5); B: indented carriers (Run 4)

The formation of the observed particle shapes can be assessed by the drying history of bi-component mannitol-water droplets. Assumptions were based on earlier studies by Nestic & Vodnik [21] who had been discussing the general principle of solvent evaporation from droplets and its different stages but were not focussing on the drying of mannitol or the generation of different particle shapes. Figure 4.10 displays the different temperatures inside the droplet or early particle over time by proposing five different stages (stage I to V), which are closer depicted in Figure 4.11.

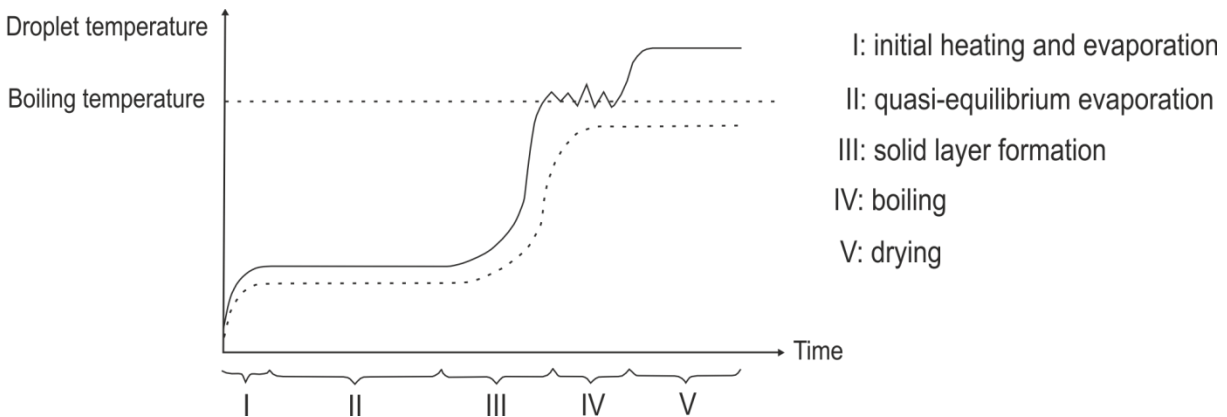


Figure 4.10 – Inner temperature development of bi-component mannitol-water droplets over time as proposed by Nestic and Vodnik [21,142]

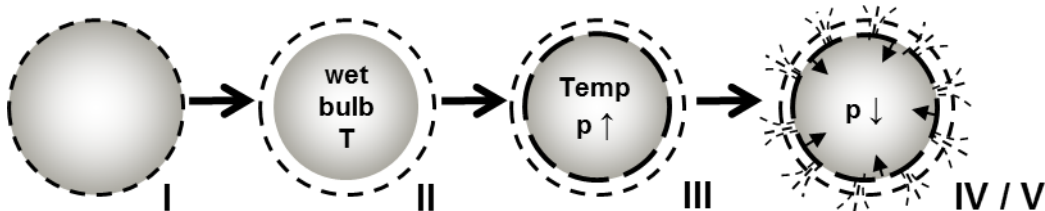


Figure 4.11 – Drying history of bi-component mannitol-water droplets with the inner pressure p

The drying of droplets emerging from the filaments, which left the LamRot atomiser during the process, started with the initial heating and evaporation of water from the droplet surface (stage I). Accordingly, the volume of the droplet decreased, while the temperature of the

droplet increased to reach a plateau at the wet bulb temperature (stage II). Droplet temperature and drying rate (Δ surface area / time) kept constant at quasi-equilibrium until the mannitol concentration exceeded the saturation solubility of the sugar alcohol at the droplet surface. Several crystallisation seeds initiated the formation of a solid layer around the droplet since diffusion of mannitol towards the surface proceeded slower than evaporation of the solvent. The temperature of the solvent inside the early particle started to increase as evaporation of water was hindered due to the shell already being formed (stage III). Consequently, this resulted in rising pressure inside the particle. Pressure differences reasoned both a stabilising effect on the spherical particle shell against external aerodynamic stress and mannitol-water solution being pressed through small pores in the shell to compensate the rising inner pressure. Concurrently, the temperature of the bi-component solution inside the particle rose depending on the chosen drying temperature. Moderate drying conditions caused inner temperatures, which remained below the boiling point of the mannitol solution (Figure 4.10 – dotted line). Harsh conditions with higher drying temperatures could result in inner temperatures, which even exceeded the boiling point (Figure 4.10 – solid line). Accordingly, the weak shell was subjected to a considerably rising pressure inside the particle, which led to the expansion of the particle shell (stage IV). This effect was further observed in levitator experiments in the context of this project, where larger mannitol-water droplets were observed to ‘explode’ due to the spontaneous increase in volume [142]. Single droplets were dried at two different drying temperatures ($T = 80 / 120$ °C) in an ultrasonic field, which kept the droplets in place during the experiment. The corresponding droplet or particle size was tracked via shadowgraphy over drying time and exhibited a vast increase in size for those single droplets dried at higher temperatures ($T = 120$ °C, Figure 4.12) right after the initial shell was built. A stable shell was observed for lower drying temperatures ($T = 80$ °C), where particle size stayed constant after shell formation. These effects occurred similarly for droplets dried with the pilot scale spray drier, but did not lead to particle explosion as the particle volume appeared to be > 300 times smaller than for levitator experiments. Accordingly, the shell was stable enough to hold the inner pressure.

In the last drying stage, particle temperature decreased due to cooling of the ambient air, which led to a slight loss of pressure for moderate drying conditions but a considerable pressure drop for particles with water vapour, which condensated upon cooling (stage V). The vacuum, which is applied to the shell, caused the particles to collapse and to build the observed deep indentions. The lower pressure gradient at moderate drying conditions got compensated by the small pores in the shell as mentioned earlier, which kept those particles spherical and stable against the occurring stress.

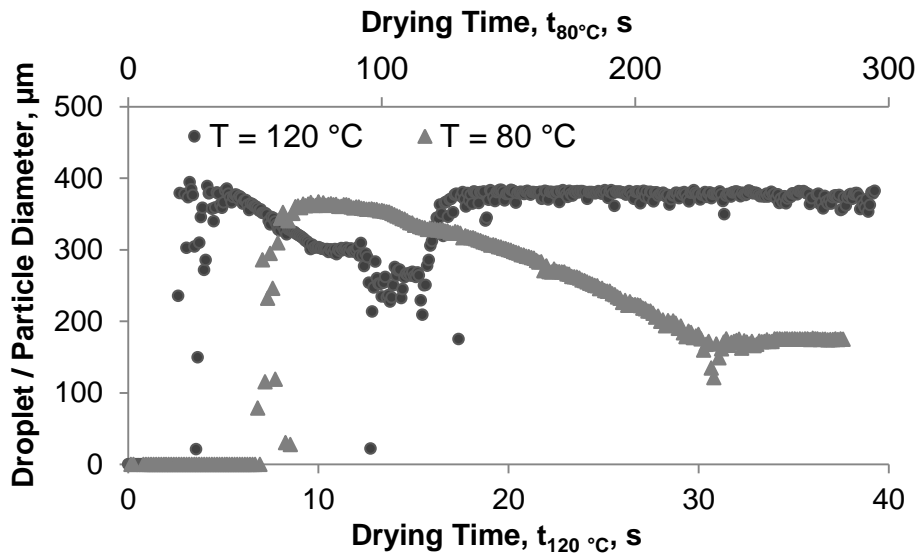


Figure 4.12 – Droplet or particle diameter of bi-component mannitol water droplets dried with a levitator at two different drying temperatures ($T = 80 / 120\text{ }^{\circ}\text{C}$) over time (1st x-axis for $T = 120\text{ }^{\circ}\text{C}$; 2nd x-axis for $T = 80\text{ }^{\circ}\text{C}$) as measured by shadowgraphy – droplets were inserted at $t \approx 10\text{ s}$ (t_{120}) or $t \approx 60\text{ s}$ (t_{80})

To sum up, spray drying can be applied to prepare carrier particles with controlled outer appearance as the particle shape is a function of the chosen drying temperatures. This can be of great interest in the context of inhalation as several earlier studies – mainly based on lactose monohydrate – mentioned the shape of carrier particles to influence the inhalable drug fraction significantly. Optimally, the FPF of any drug can be controlled by adjustment of drying conditions as this controls the occurrence of indentations. The effect of particle shape on the aerodynamic performance during inhalation will be discussed in Section 4.3.1.

4.1.4.2 Surface Roughness

The drying of bi-component mannitol-water droplets was performed with special focus on the microstructure or roughness of the surface. Several earlier studies dealing with the morphology of carrier particles did not distinguish between particle shape and surface roughness but were mainly focussing on a general measure of morphology, when discussing its effect on the aerodynamic performance of these particles. Assessment of roughness was challenging as surface asperities appeared to be quite small in size, which complicated the detection. Nevertheless, surface roughness was evaluated by categorisation of SEM images and 3D laser microscopy to understand why surface asperities occur and connect those irregularities with the drug detachment during impaction analysis (Section 4.3.2).

All nineteen batches of the DoE were evaluated based on SEM images. Obtained results mention the drying temperatures T_{ax} and T_{swirl} to significantly influence the surface roughness, which resulted in the following Equation (4.3):

$$y = a_0 + a_1 T_{ax} + a_2 T_{swirl} \quad (4.3)$$

showing that both factors show a linear correlation (a_1 ; a_2) between drying temperature and resulting surface roughness. The scaled and centred values for the coefficients displaying the model exhibited the surface roughness categories to increase for 0.68 ± 0.11 categories, when T_{ax} was raised for one level ($T_{ax} = 30$ °C), but only for 0.24 ± 0.11 categories when T_{swirl} was raised for one level ($T_{swirl} = 20$ °C). Similarly to particle shape, effects of the axial drying air exceeded those of the swirl air stream since the drying air volumes are different.

Table 4.6 - Scaled and centred coefficients (\pm standard deviation) for carrier surface roughness as a response. Values give the effect on the surface roughness in categories (Category 1 – 5), when the factor is changed for one level ($T_{ax} = 30$ °C; $T_{swirl} = 20$ °C).

Coefficients	Surface roughness, Cat. 1-5 scaled & centred
a_0	-
T_{ax}	0.68 ± 0.11
T_{swirl}	0.24 ± 0.11

The nineteen experiments cover a range from category 2.2 (Table 4.1, M70(S)) to category 4.5 (Table 4.1, M97(L)), which is further displayed by the contour plot in Figure 4.13. This plot illustrates that high drying temperatures caused several surface asperities including granular accumulations on the surface (surface roughness category > 4.0), while moderate drying conditions led to smoother particles, which still showed some smaller surface irregularities (surface roughness category < 3.0). The SEM images (inserts of Figure 4.13) display the visualisation of the smoothest surface (M70(S)) gained by the DoE compared to the roughest surface (M97(L)).

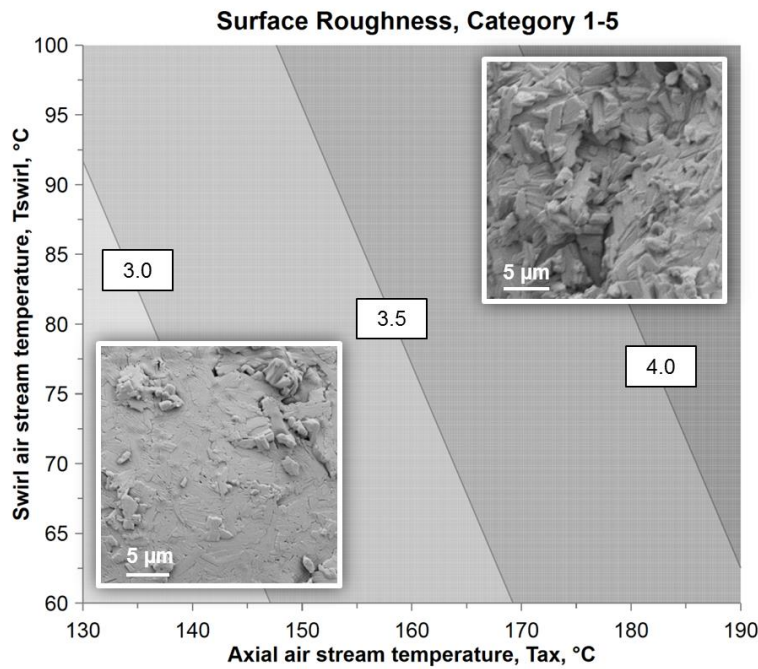


Figure 4.13 - Contour plot of the carrier surface roughness as a response of the DoE with the factor swirl air stream temperature (T_{swirl}) on the y-axis and axial air stream temperature (T_{ax}) on the x-axis. Results are given in categories from category 1 (smooth carrier particles, M70(S)) to category 5 (rough carrier particles with granular accumulations, M97(L)) and are visualised exemplarily by two SEM images (2500 fold magnification)

Further, a 3D laser scanning microscopy tool was applied to objectively evaluate the carrier surface as survey results are based on subjective decisions. Results shown in Figure 4.14 depict both the line roughness R_a and the surface roughness S_a . Evaluation was performed with a special focus on the six mannitol carrier batches, which were used for further characterisation as carriers in interactive powder blends as discussed later. The according images of the carrier particles display exemplarily where surface roughness was measured (line or area roughness). Line roughness was determined with the same orientation for all spherical batches, but was adapted for particles dried at higher temperatures to exclude indentions. Similarly, distinct areas were chosen to avoid indentions for these measurements.

Line roughness R_a was found to be $< 0.11 \mu\text{m}$ for the batches dried at lower temperatures (M70(S); M71(L) and M74(M)) but appeared quite large with $R_a > 0.20 \mu\text{m}$ for two batches dried at higher outlet temperatures (M80(S); M97(L)). Differences in roughness were significant between those two groups of particles, while batch M80(M) revealed a medium roughness, which was not significantly different to other batches except for M97(L).

Similarly, surface roughness S_a was determined and evaluated on the same five particles to evaluate not only a line but an defined surface area. Tendencies found here met the results of R_a evaluations as M70(S); M71(L) and M74(M) appeared with the smoothest surface ($S_a < 1.0 \mu\text{m}$) compared to M80(S) and M97(L) ($S_a > 3.0 \mu\text{m}$).

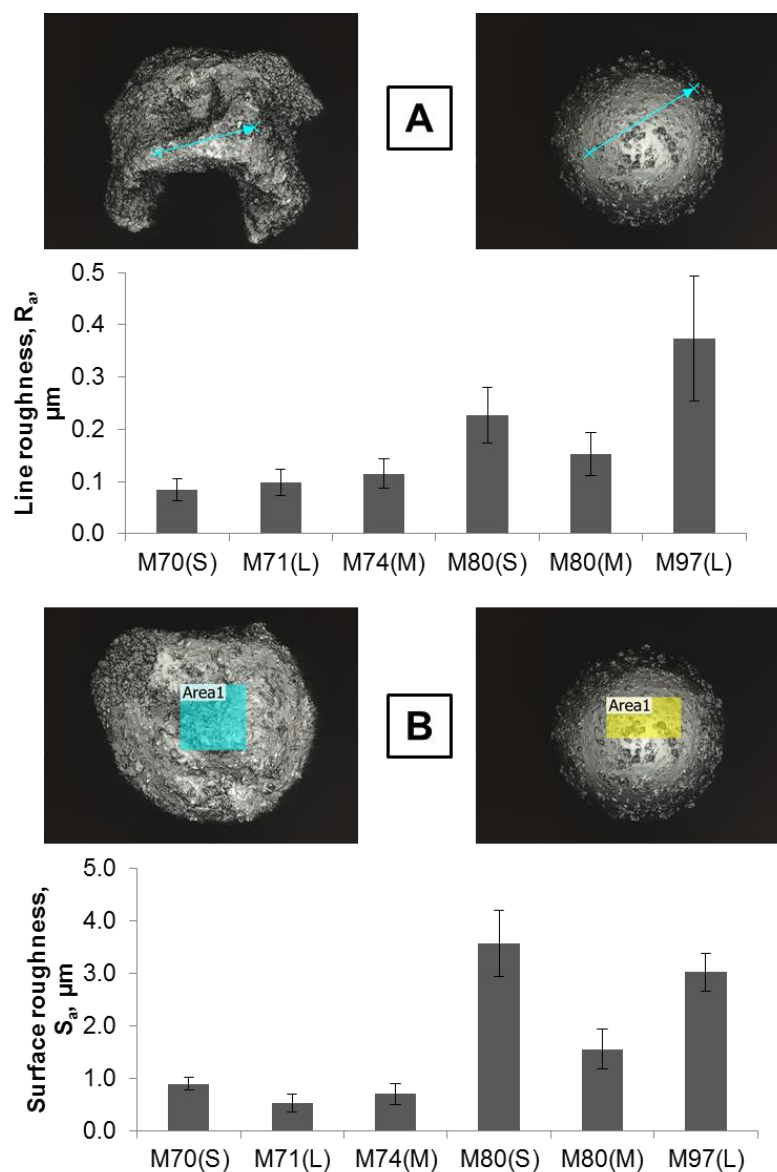


Figure 4.14 – Evaluation of carrier surfaces by 3D laser microscopy; A: images show the surface exemplarily for a particle of the roughest (M70(S)) and the smoothest (M97(L)) carrier batch with the line, for which the line roughness was calculated. The graph displays the line roughness R_a in μm for six mannitol carrier batches ($n = 5 \pm$ standard deviation); B: images show particles of the same batches as for the line roughness, but display the surface for which the surface roughness S_a was calculated. The graph shows the surface roughness S_a in μm for six mannitol carrier batches ($n = 5 \pm$ standard deviation).

Obviously, mannitol carrier particles exhibited more surface asperities, when drying temperatures T_{ax} and T_{swirl} were set to maximum values. This effect went along with the impact of drying temperature on the particle shape and can be explained based on the drying history mentioned in Section 4.1.4. Overlying crystals and granular accumulations originated in drying stage III (Figure 4.10 and Figure 4.11) when an initial shell was formed. The inner pressure rose due to increasing temperatures within the particle. Small pores occurred subsequently to compensate the pressure gradient. Mannitol solution was pressed through the early shell and crystallised on the outside of the particle since the hot surrounding air forced the water to evaporate. This effect was observed for all particles as the inner pressure

is supposed to increase for all different drying temperatures. The probability that surface asperities appear was strongly depending on the drying temperature since this affected the pressure gradient. The higher the pressure gradient, the more pores were formed, the more overlying crystals occurred.

Additionally, crystallisation behaviour during spray drying might affect the microstructure. Even though the final product was generally found to consist of the β -modification as the most stable one, it cannot be precluded that other crystalline structures like the less stable α -modification or amorphous transition states occur during and right after spray drying. Assumptions, that drying temperature might influence the crystallisation behaviour and the microstructure of the mannitol particle surface, are based on the drying velocity. Low drying velocities enable direct crystallisation to gain the β -modification, while fast drying might cause other intermediates, which recrystallise or transform subsequently. This would supplement the results found in this project but needs to be proved by onsite analytics like in-line Raman analysis. Cornel et al. had shown that Raman analysis can be applied to distinguish between three different polymorphs of mannitol and mannitol in solution [143], which needs to be transferred to an in-line spray drying approach.

In summary, spray drying can be used to adjust the surface roughness of mannitol carrier particles. The influence of different microstructures on the drug detachment will be discussed in Section 4.3.2.

Despite of the quite prominent dependencies between drying temperature and particle shape or surface roughness, it was not possible to control those two parameters independently. Spherical particles always exhibited the smoother surfaces than the indented ones.

4.1.5 Influence of Outlet Temperature

All effects regarding particle morphology in terms of particle shape and surface roughness strongly depended on the chosen drying temperatures. T_{ax} and T_{swirl} were found to affect the appearance of the particles with respect to temperature and air stream volumes V_{ax} and V_{swirl} . The inlet temperatures were altered as factors within the scope of the DoE as the spray tower offers to directly control them via the heater batteries. Nevertheless, it was found that effects on the particle morphology can more easily be explained by T_{out} , which combines the impact of T_{ax} , T_{swirl} , V_{ax} and V_{swirl} in one parameter.

Table 4.1 summarises the drying conditions of all spray drying experiments, while Figure 4.15 exhibits the dependencies between T_{out} and the categorisation of carrier particles into particle shape or surface roughness categories. A general trend towards more indentions and rougher surface structures was observed for rising outlet temperatures as mentioned for the data gained for the DoE.

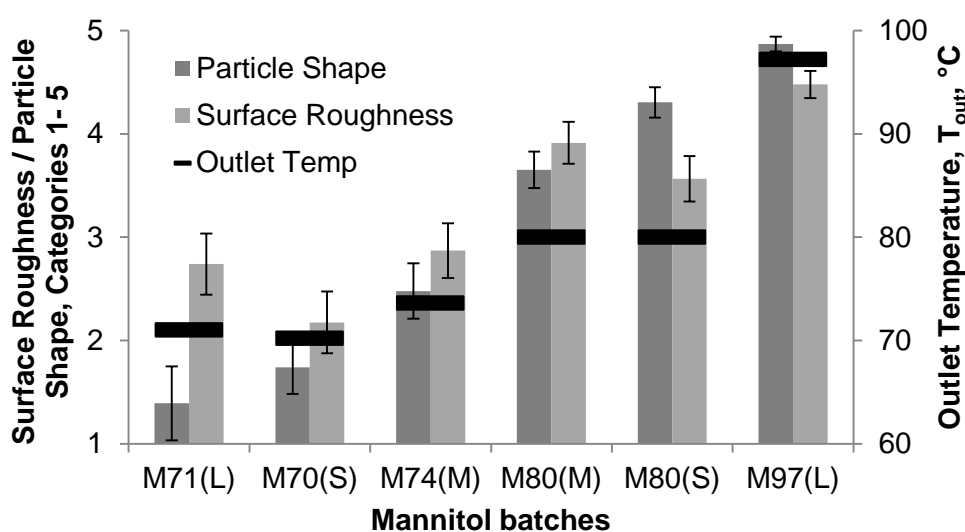


Figure 4.15 – Effect of T_{out} (2nd y-axis in °C displayed by black bars) on particle shape and surface roughness (1st y-axis in Categories 1 to 5 displayed by grey columns, $n=30 \pm$ relative standard deviation) for six spray dried mannitol batches

Based on these correlations, six mannitol batches were chosen with respect to T_{out} and particle size to examine the effects of these properties on the aerodynamic performance during impaction analysis. These batches were labelled according to outlet temperature and particle size and further investigated regarding their properties.

4.1.6 Flowability

Particle size and morphology are particle properties, which are known to affect the flowability of a bulk. Particles designed for use in multi-dose inhalers for dry powder inhalation need to provide good flow properties as this is crucial for accurate dosing of the powder blends.

Flowability was determined to ensure that spray dried mannitol carrier particles meet those requirements. Carr Index and BFE, measured with a powder rheometer, were taken into account for evaluation.

Carr Index as a measure of compressibility, which is often linked to the flowability of a bulk, was determined for all mannitol batches. Results were first evaluated within the scope of the DoE, but did not show any significant dependencies regarding the chosen drying conditions (Table 4.1). This might be attributed to the accuracy of this method as determination of bulk and tapped densities, was not precise enough to detect differences between spray dried mannitol batches. Nevertheless, results enabled to estimate that all batches show good flow properties as Carr Indices were found to be < 16 . Some batches (with larger particles) even revealed Carr Indices below 10, which indicates excellent flow properties (M71(L); M97(L)).

Powder rheology was then performed as a more accurate method to link effects of particle properties like particle size or morphology to the resulting flow properties of the according

mannitol batches. Indeed, an excellent fitted model was gained from the DoE (Section 4.1.2) which resulted in dependencies based on the factors T_{ax} and n as further depicted in Equation (4.4).

$$y = a_0 + a_1 T_{ax} + a_3 n + a_4 T_{ax}^2 + a_8 T_{ax} n \quad (4.4)$$

Coefficients of both factors included linear correlations to the resulting BFE but also an interactive influence of T_{ax} and n as well as a quadratic effect of T_{ax} , which will be explained in the following.

Table 4.7 - Scaled and centred coefficients (\pm standard deviation) for the Basic Flowability Energy (BFE) as a response. Values give the effect on the flowability of the mannitol carrier particles in mJ, when the factor is changed for one level ($T_{ax} = 30$ °C; $n = 3,000$ rpm)

Coefficients	Flowability, Basic flowability energy (BFE), mJ scaled & centered
a_0	-
T_{ax}	14.25 ± 2.04
n	-14.93 ± 2.04
$T_{ax} \cdot T_{ax}$	-14.70 ± 2.96
$T_{ax} \cdot n$	-9.10 ± 2.28

Effects on the BFE arise from alteration of both T_{ax} and n as depicted in Table 4.7. An increase of T_{ax} reasons higher BFEs ($T_{ax} = 14.25 \pm 2.04$), whereas more centrifugal forces and smaller droplets decrease the resulting BFE ($n = -14.93 \pm 2.04$). The negative quadratic effect of T_{ax} ($T_{ax}^2 = -14.70 \pm 2.96$) becomes apparent in the flowability contour plot (Figure 4.16), where particularly low inlet temperatures trigger an effect on the BFE, while the effect was negligible for high drying temperatures. The general decrease of the BFE as detected for a concurrent increase of T_{ax} and n ($T_{ax} \cdot n = -9.10 \pm 2.28$) cannot be gained from the appropriate contour plot.

Mannitol batches generated within the scope of the DoE cover the BFE ranging from 90 mJ to 149 mJ (Table 4.1). Lowest values appear for high LamRot rotation speeds (resulting in small droplets and hence small particles) in accordance with low axial drying temperatures, whereas highest values were found for low rotation speeds and high axial drying

temperatures. Those effects can further be linked to particle properties like particle size and morphology as described in literature [131].

Thus, enhancement of T_{ax} from 130 °C to 160 °C, which caused the appearance of indentions, showed the main effect on the flowability of the mannitol carriers. The twisted paddle of the powder rheometer required the lowest energy when moving through spherical particles dried at the lowest temperatures ($T_{ax} = 130$ °C, BFE = 90 mJ). The resistance increased rapidly towards batches dried at $T_{ax} = 160$ °C (BFE > 140 mJ), whereas the temperature effect was diminished for further increase to $T_{ax} = 190$ °C. Hence, the occurrence of first indentions constituted particle-particle interlocking, which resulted in a first increase of the energy. Further deterioration of the shape ($T_{ax} > 160$ °C) had no effect on the BFE.

In contrast, the effect of n on the BFE was found to be more conspicuous for higher drying temperatures ($T_{ax} = 160 - 190$ °C) than for lower ones. Particle size, as known to be affected by n , can be identified as the reason for differences in the resistance towards the turning powder rheometer paddle. Nevertheless, effects of particle size were only detected for indented particles, whereas the flowability of spherical mannitol carriers was found to not be dependent on particle size. This can easily be attributed to the indentation depth, as smaller particles (BFE < 110 mJ) exhibited smaller indentions than larger ones (BFE > 140 mJ), which in turn affected particle-particle interlocking and so the BFE. Particles without indentions were without particle-particle interlocking.

Additionally, a slight decrease of the BFE was detected from the maximum value between $T_{ax} = 165$ °C and 180 °C towards higher axial drying temperatures. This effect can be attributed to a size effect observed for higher drying temperatures (Section 4.3.3). Increase of drying temperature caused earlier shell formation and larger carrier particles, which in turn showed slightly better flow properties compared to the ones dried at moderate conditions.

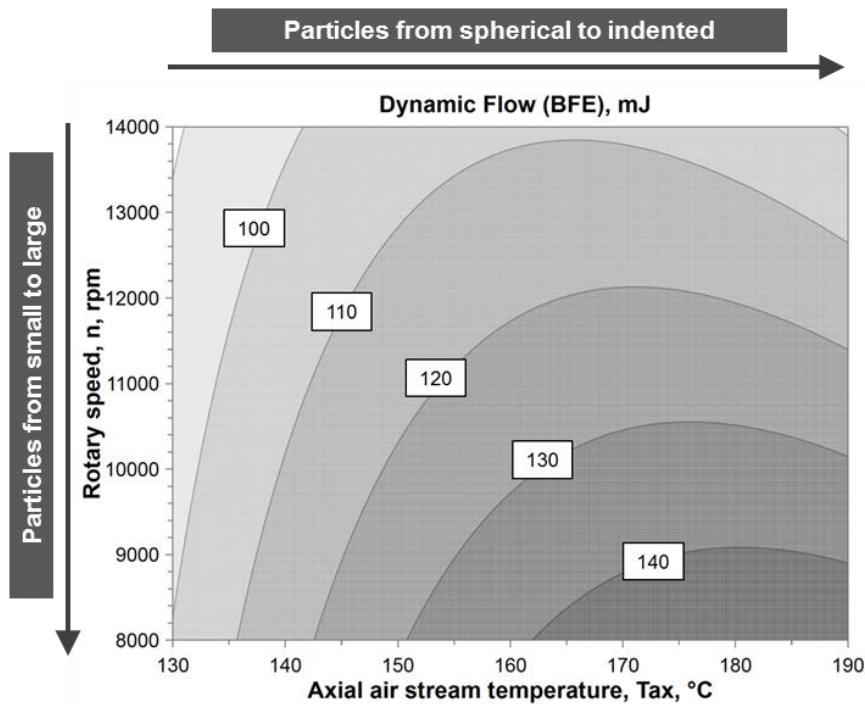


Figure 4.16 - Contour plot of the Basic Flowability Energy (BFE) as a response of the DoE with the factor rotation speed (n) on the y-axis and axial air stream temperature (T_{ax}) on the x-axis. Results are given in mJ

To conclude, mannitol carrier flowability was found to correlate with both axial drying temperature and rotation speed. Small spherical carriers performed better than large indented ones, which is a measure of particle-particle interlocking. Results evaluated in the framework of the DoE revealed that spray drying of mannitol carrier particles enabled the formation of carrier particles with defined flow properties in terms of their primary particle properties particle size and morphology. With respect to the overall size range, all carrier batches gained from the DoE showed proper flow properties for a DPI use. Nevertheless, it needs to be mentioned, that flow properties might change crucially by the addition of fine drug particles or mannitol fines.

4.1.7 BET Surface Area

Determination of the BET surface area was applied as an analytical tool to support and confirm earlier findings as the surface area is able to reflect differences in particle size and morphology. Indeed, evaluation within the frame of the DoE revealed all factors mentioned for particle size (Section 4.1.3), particle shape (Section 4.1.4) and surface roughness (Section 4.1.4.2) to be relevant for the BET surface area (Equation (4.5) after neglecting insignificant terms in a backward regression).

$$y = a_0 + a_1 T_{ax} + a_2 T_{swirl} + a_3 n + a_4 T_{ax}^2 + a_8 T_{ax} n \quad (4.5)$$

BET areas from $0.26 \text{ m}^2 \text{ g}^{-1}$ for low rotation speeds (n) and drying temperatures (T_{ax} / T_{swirl}) to $0.61 \text{ m}^2 \text{ g}^{-1}$ for high rotation speeds (n) and drying temperatures (T_{ax} / T_{swirl}) were observed for these experiments (Table 4.1).

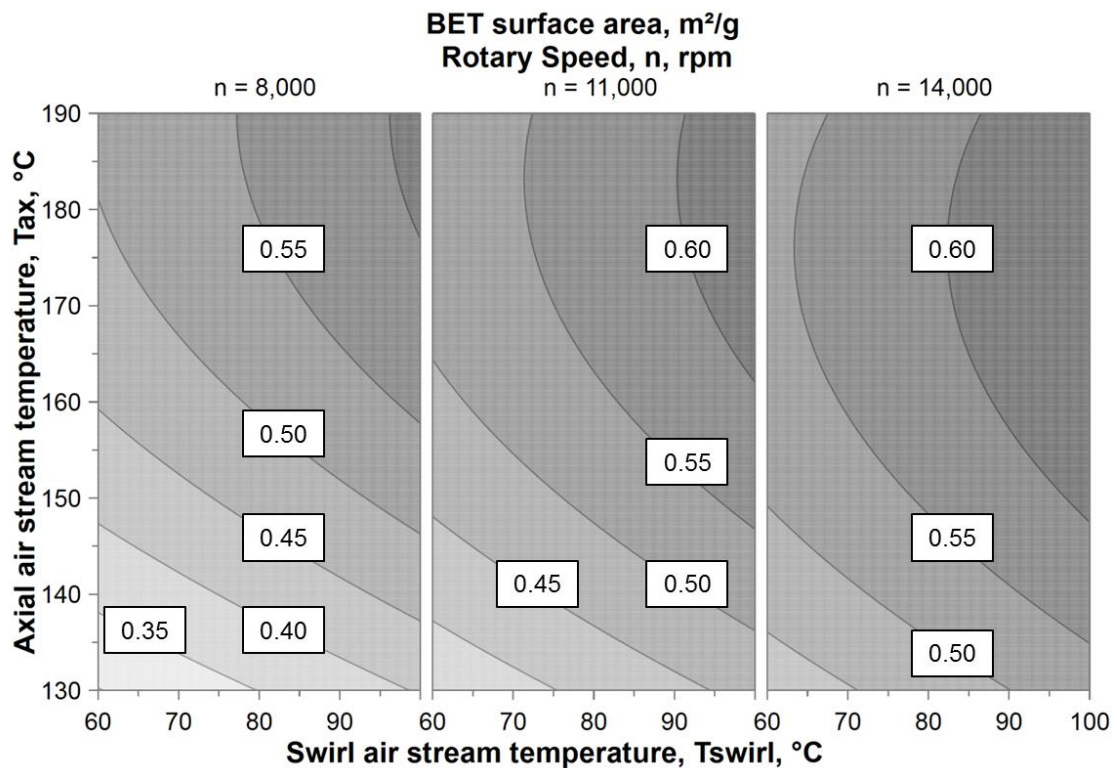


Figure 4.17 - Contour plot of the BET surface area as a response of the DoE with the factor axial air stream temperature (T_{ax}) on the y-axis and axial air stream temperature (T_{swirl}) on the x-axis. The three plots represent the BET surface area at 8,000, 11,000 and 14,000 rpm. Results are given in $\text{m}^2 \cdot \text{g}^{-1}$

The contour plots (Figure 4.17) show a general trend towards larger surface areas for rising drying temperatures (T_{ax} / T_{swirl}), which is more pronounced for T_{ax} . This coincides with the findings gained from categorisation of SEM images, which observed more indentions and rougher surfaces for harsh drying conditions compared to moderate ones in accordance with stronger influence by T_{ax} . Surface asperities as well as all deviations from a perfect sphere increased the surface area of the mannitol batch.

The impact observed by n was mainly attributed to the droplet size, which was affected by the centrifugal forces during spray drying with the LamRot atomiser. BET surface area results agreed with particle size evaluations since higher rotation speeds caused smaller particles and, therefore, larger BET surface areas.

In general, all surface areas determined with nitrogen as test gas were close to detection limit but were measured in triplicate and with respect to good DoE correlation coefficients, which allowed the evaluation of these results.

4.1.8 Surface Energy

Determinations of surface energies of mannitol carrier batches were performed to investigate the influence of drying temperature and droplet size on the surface characteristics. The slope of the straight line gained by plotting $RT \ln V_R^0$ versus $\sqrt{\gamma_L^d}$ was used to calculate the dispersive surface energy. Fittings were excellent for all investigated mannitol carrier batches ($R^2 > 0.99$).

Results summarised in Figure 4.18 exhibited most spray dried mannitol batches with free dispersive surface energies of $\gamma_s^d = 60 - 65 \text{ mJ} \cdot \text{m}^{-2}$. Only commercially available Pearlitol[®] 160C, which served as crystalline raw material for all experiments, and batch M71(L) resulted in lower dispersive surface energies of $\gamma_s^d = 45.6 \pm 1.3 \text{ mJ} \cdot \text{m}^{-2}$ and $\gamma_s^d = 47.2 \pm 0.4 \text{ mJ} \cdot \text{m}^{-2}$, respectively. Results were measured at infinite dilution of the alkanes used ($0.03 p/p_0$) and represent γ_s^d of spots with the highest free dispersive surface energy.

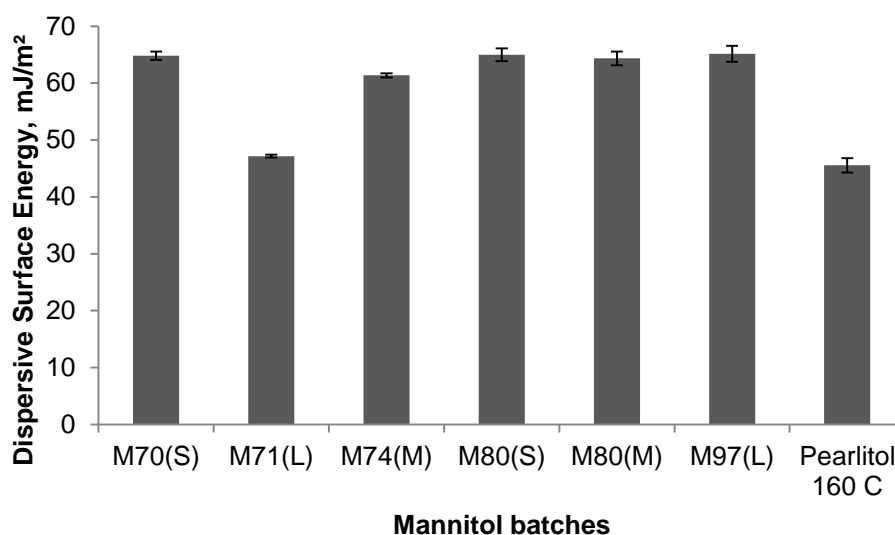


Figure 4.18 – Free dispersive surface energy γ_s^d of six spray dried mannitol qualities and Pearlitol[®] 160C as crystalline raw material ($n=3 \pm$ standard deviation)

In order to investigate the whole surface of spray dried mannitol carrier particles, dispersive surface energy profiles were determined by injecting alkanes with rising injection volumes ($p/p_0 = 0.03$ to 0.95). Figure 4.19, which shows the free dispersive surface energy γ_s^d plotted against the alkane surface coverage, displays the results of mannitol M71(L) and M80(M), for which M80(M) represents the dispersive surface energy profile of all further spray dried qualities as only M71(L) deviated from the general results.

Surface coverage was plotted on two different x-axes due to differences in the maximum coverage of the mannitol batches evaluated here. M71(L) with a maximum alkane surface coverage of $0.15 n/n_m$ exceeded the maximum coverage of M80(M), which covered $0.06 n/n_m$.

when measured at $p/p_0 = 0.95$. This effect can be related to the according BET surface areas as M71(L) revealed a lower BET surface area of $0.26 \text{ m}^2 \cdot \text{g}^{-1}$ than M80(M) with a surface area of $0.55 \text{ m}^2 \cdot \text{g}^{-1}$ (Table 4.1). The lower the surface the less alkanes were needed to reach full coverage, which explains the results found for larger particles (M71(L)) with lower BET surface areas compared to smaller particles.

Dispersive surface energy profiles revealed mannitol M71(L) to have a homogeneous surface as surface energy was found to remain almost similar ($\Delta\gamma_s^d < 5 \text{ mJ} \cdot \text{m}^{-2}$) with rising partial pressures and surface coverages. The experiments performed at finite dilution agreed with results gained at infinite dilution as both calculated a maximum free dispersive energy of $\gamma_s^d \sim 45 \text{ mJ} \cdot \text{m}^{-2}$ measured at $0.03 p/p_0$. In theory, alkane probe molecules adhere to high energy spots first and to areas of lower energy next, when applicable. Here, the whole particle surface was found to have the same energy.

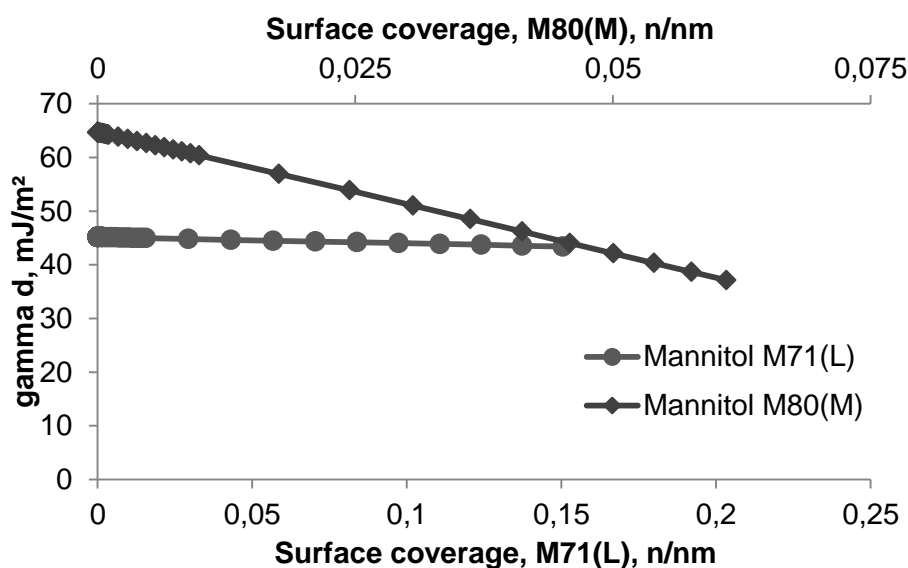


Figure 4.19 – Dispersive surface energy profiles of mannitol M71(L) (spray dried, homogenous surface energy profile) and M80(M) (spray dried, heterogeneous surface energy profile exemplarily for other spray dried qualities) with the surface coverage n/nm

Contrarily, dispersive surface energy profiles of all other mannitol qualities, represented by mannitol M80(M) in Figure 4.19, occurred to be heterogeneous as illustrated by the negative slope of γ_s^d plotted against the surface coverage. The surface revealed spots of high energy with $\gamma_s^d > 60 \text{ mJ} \cdot \text{m}^{-2}$ for $p/p_0 = 0.03$ and the lowest surface coverage, but also spots of low energy with $\gamma_s^d < 40 \text{ mJ} \cdot \text{m}^{-2}$ for higher surface coverage at $p/p_0 = 0.95$. Areas of higher or lower energy are evenly distributed for surface coverages from 0 % to approximately 20 % as depicted by the linear correlation of the plot.

In general, spray drying of sugar alcohols such as lactose monohydrate or mannitol is known to increase surface energies in comparison to crystalline non-spray dried qualities. Most of these results agreed with results published earlier, as spray dried mannitol revealed

dispersive surface energies of $\gamma_s^d > 60 \text{ mJ} \bullet \text{ m}^{-2}$ in contrast to the crystalline quality of Pearlitol® 160C investigated as raw material ($\gamma_s^d = 45.6 \text{ mJ} \bullet \text{ m}^{-2}$). The surface of these samples was more energetic with respect to non-polar London forces [10].

Nevertheless, mannitol batch M71(L), which was one of the batches spray dried at the lowest outlet temperatures and a batch with quite large particles, showed a dispersive surface energy of comparable level to the raw material in accordance to a homogeneous surface energy distribution. These findings could be attributed to spray drying conditions as this batch was dried close to the limits of the spray tower. Large droplets in conjunction with low drying temperatures led to particles, whose drying process was not finally finished, when they were deposited in the collecting vessel. This resulted in small amounts of particles that dried subsequent to the usual drying process on the conical spray tower walls, while most particles were found clumped together in the collecting vessel due to their high residual moisture content. The slow drying and crystallisation process led to surface energies close to raw material level.

In general, the large number of spray dried mannitol batches was found at higher surface energies than the raw material and with heterogeneous dispersive surface energy profiles. This indicates the mannitol carriers to have active sites on the carrier surface that might adhere particles tighter than other spots on the surface. The occurrence of active sites might influence the detachment of drug particles as mentioned by Grasmeijer et al. earlier [72]. Therefore, further experiments were performed with mannitol carrier particles, SBS drug particles and mannitol fines to cover high energy spots with focus on dependencies between drug detachment and added mannitol fines (Section 4.3.8).

4.2 Preparation of Model Drugs

Model drugs were prepared in order to associate effects to either carrier particle properties or drug particle properties. With this target, four different drugs were spray dried to generate particles that were comparable in particle size and shape as this prevented the occurrence of effects that might be related to those drug properties. Observed effects on the aerodynamic performance could therefore directly be correlated to the carrier properties or intrinsic drug properties like hydrophilicity or surface energy. Shape control was provided by the process itself as drug-containing droplets trigger the generation of overall mostly spherical particles.

Further, spray dried SBS was prepared in different sizes (and morphologies) in the scope of a DoE to examine the effects by drug size and morphology. The shape effect was further supplemented by the investigation of jet-milled SBS and BUD qualities which additionally included the examination of influences by crystallinity as spray dried material was used in amorphous state and micronised drugs in mostly crystalline state.

Initially, the effect of spray drying parameters of a standard laboratory spray dryer on SBS particle properties was tested. Table 4.8 lists all experiments performed within the experimental design covering the two factors outlet temperature (T_{out}) and mass fraction (Y_m) and the responses particle size, span and particle shape as will be evaluated in Section 4.2.1.

The spray drying parameters used for BUD, TIO and FOR as well as for SBS batches spray dried for interactive powder blends are coherently summarised in Table 4.8 and were mainly based on investigations performed within the priority program PICO, where spray drying of different drugs for inhalation was treated as part of the project.

Table 4.8 – Summary of spray drying parameters (or factors within the DoE) and resulting particle properties (or responses within the DoE) for all drug batches (including two micronised qualities) investigated in this project. *SBS batches prepared for interactive powder blends were prepared with slightly elevated spraying gas (42 mm instead of 40 mm) to generate smaller drug particles than in die experimental design

Drug	Run / Drug Quality	Factor		Response			
		T_{out} °C	Y_m , %	Particle Size, x_{50} , μm	Particle Span	Particle Shape, Category 1-5	iGC, mJ m^{-2}
SBS in Experimental Design	N1	65	2.5	2.6	2.0	1.1	
	N2	115	2.5	2.7	2.1	3.3	
	N3	65	12.5	4.1	1.9	1.8	
	N4	115	12.5	4.0	1.7	3.9	
	N5	65	7.5	3.7	2.1	1.8	
	N6	115	7.5	3.8	2.0	3.8	
	N7	90	2.5	2.6	2.0	1.1	
	N8	90	12.5	4.6	1.9	2.1	
	N9	90	7.5	3.4	2.1	1.5	
	N10	90	7.5	3.6	2.1	2.4	
	N11	90	7.5	3.9	2.0	2.1	
	N12	90	7.5	3.5	2.0	1.9	
	N13	90	7.5	3.5	2.0	2.0	
Drug Batches for Interactive Powder Blends	SBS SD(S)*	90	2.5	2.4	1.8	spherical, golf ball structure	42.17
	SBS SD(M)*	115	7.5	2.8	1.8	spherical, smooth	
	SBS SD(L)*	90	12.5	3.7	1.8	spherical, golf ball structure	
	SBS micro	n.a.	n.a.	2.5	2.8	needle like	44.97
	TIO SD	100	4.8	2.2	2.2	spherical	48.08
	BUD SD	100	4.0	1.8	2.1	spherical	50.53
	BUD micro	n.a.	n.a.	1.4	1.8	uneven	60.12
FOR SD	100	4.8	2.1	1.9	spherical	34.04	

4.2.1 Design of Experiments

A DoE was employed for the preparation of spherical SBS particles but not for BUD, TIO or FOR since only SBS was chosen to be used in different qualities regarding drug size and morphology. The CCF design comprised thirteen experiments for two factors and three levels as summarised in Table 4.8. Each response was evaluated separately to calculate the best fitting models based on a backward regression of insignificant terms.

Drug properties of batches used in interactive powder blends were then adjusted with respect to results presented and discussed in the following. However, drug particles for aerodynamic characterisation were desired to appear from 2.0 to 2.5 μm , which was not covered by the DoE. Those batches were therefore prepared with slightly increased spraying gas (42 mm instead of 40 mm) to match those requirements (Table 4.8).

4.2.1.1 Power of the model

Evaluation of spray dried SBS batches provided significant models with appropriate quality parameters for the control of particle size and particle morphology. The models of both particle properties are featured by well fitted data (R^2 adjusted ≥ 0.88), good predictive power ($Q^2 \geq 0.84$), reliable model validity ($p \geq 0.79$) and optimal reproducibility ($RP \geq 0.88$). Another model calculated for the particle span did not meet the required limits in terms of predictive power and was not taken into account for evaluation.

Table 4.9 - Quality parameters for SBS properties evaluated within the DoE. First column gives the evaluated quality parameter including the limits of acceptance. Further columns show the responses and the according quality results

Quality Parameter	Particle Size	Particle Morphology
R^2 adjusted (> 0.50)	0.88	0.90
Q^2 (> 0.50)	0.84	0.87
P (> 0.25)	0.79	0.89
RP (> 0.50)	0.90	0.88

The good quality parameters enable profound statements on the drying of bi-component SBS-water droplets that can be derived from dependencies between factors and responses as will be discussed in the following (Section 4.2.1.2 and Section 4.2.1.3).

4.2.1.2 Particle Size (SBS)

Preparation of SBS particles for inhalation was performed by spray drying as this technique enables the generation of mostly spherical particles with a $d_{\text{aer}} < 5 \mu\text{m}$ that usually arise in the amorphous state indicating storage stability issues. The factors used here were mainly

chosen with respect to already published effects on the according particle properties [20,63,89]. Particle size was controlled by different mass fractions (Y_m) in this study as illustrated in Figure 4.20. Small mass fractions ($Y_m = 2.5\%$) caused particles of $d_{50.3} < 2.8\ \mu\text{m}$ as measured by laser diffraction, while large mass fractions ($Y_m = 12.5\%$) lead to particles of $d_{50.3} > 4.2\ \mu\text{m}$. The model depicts a linear correlation between mass fraction and particle size without any effect detected for T_{out} .

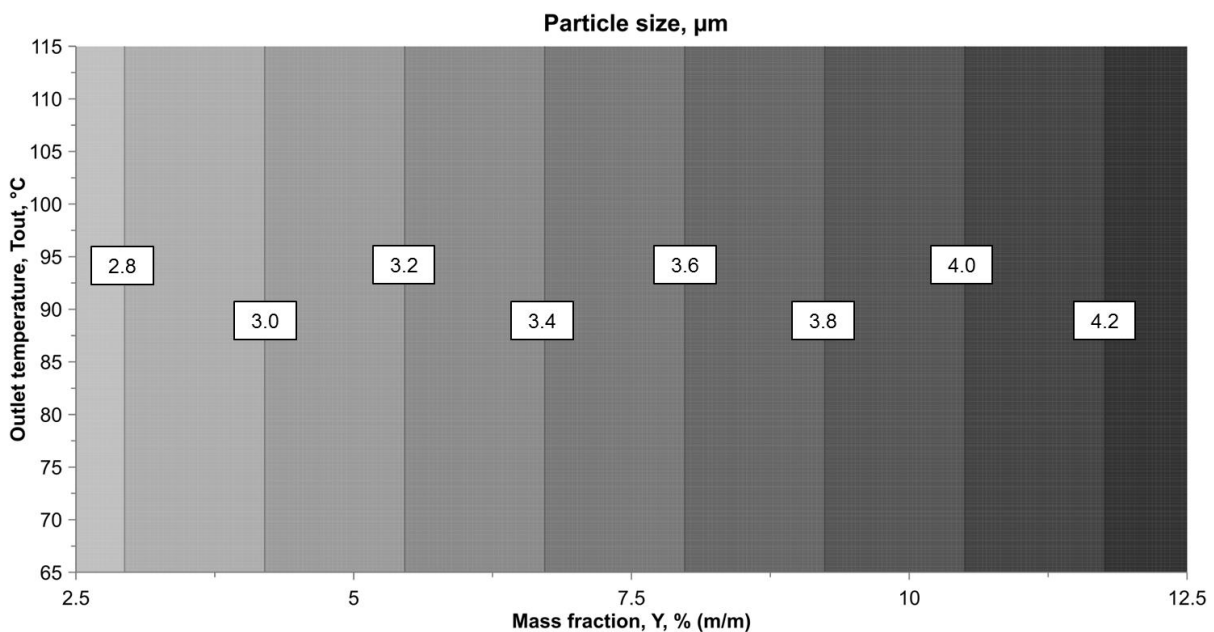


Figure 4.20 - Contour plot of the final SBS particle size as a response of the DoE with the factor outlet temperature (T_{out}) on the y-axis and the mass fraction (Y_m) on the x-axis

Higher mass concentrations trigger earlier crystallisation and, therefore, larger particles. The initial droplet size as another crucial factor for the resulting particle size was kept constant since the spraying gas air flow was not altered for the experimental design. The drying temperature (here T_{out} instead of T_{in}) which was found to affect the particle size of the carrier material did not significantly influence on the size of SBS during drying. Mass fraction as a well-known factor to control particle size defined the moment of shell formation and by this the final particle size.

The preparation of three SBS batches of different sizes was based on these results and is described in Section 3.3.2.1. However, particles prepared within the experimental design were larger than the targeted drug size for the standard powder blends so that spraying gas was elevated from 40 mm to 42 mm for those batches to reduce droplet and by this the resulting particle size.

4.2.1.3 Particle Morphology (SBS)

The overall particle morphology of all SBS batches spray dried in the framework of this DoE was evaluated by categorisation of SEM images into five categories from 1 to 5 as described

earlier. SBS particles were found with a golf ball like structure (Figure 4.21, particle morphology > Category 2.5), when T_{out} was kept low (Figure 4.22 – A / C). Here, drug particles of all sizes appeared with small indentions. Smoother surfaces occurred first for smaller particles, when particles were prepared at higher T_{out} . Further, particles of medium size showed smooth surfaces for rising drying temperatures and only some single larger particles with golf ball like morphology were found for batches dried at $T_{out} = 115\text{ °C}$, which resulted in batches rated as smooth particles (Figure 4.21, Category < 2.5, Figure 4.22 - B). The main effect on the particle morphology arose from drying temperature, but was supplemented by an increase in mass fraction.

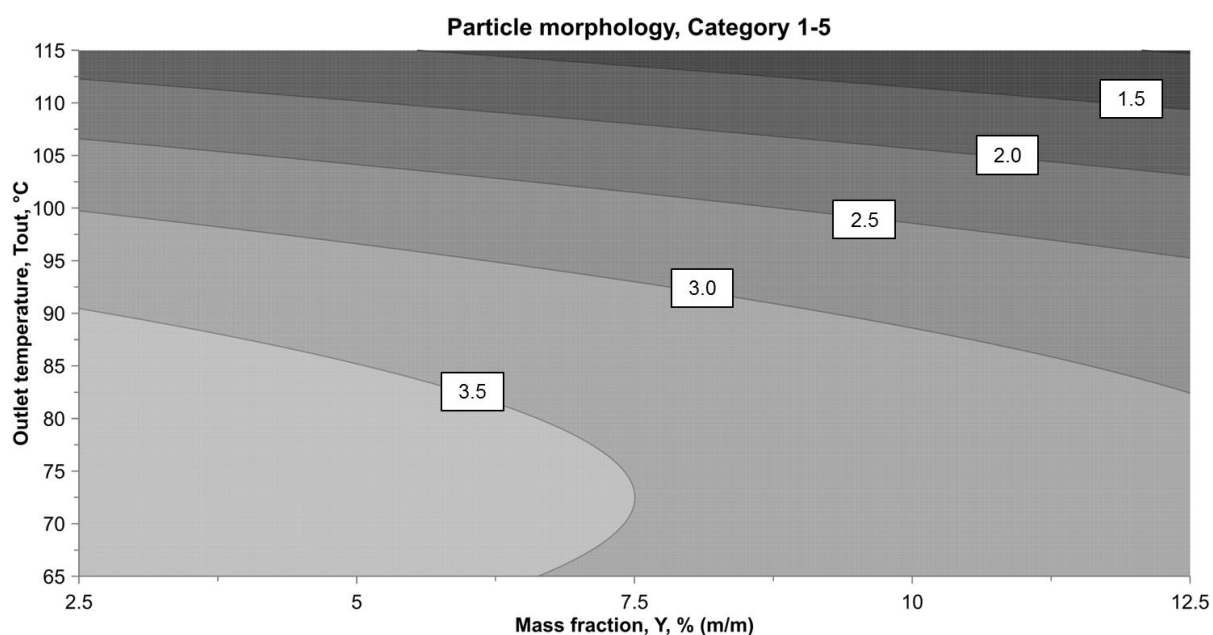


Figure 4.21 – Contour plot of the SBS particle morphology in Categories from 1 (smooth surface, all particles without indentions) to 5 (golf ball like shape for particles of all sizes) as response for a DoE with the factors outlet temperature (T_{out} , y-axis) and mass fraction (Y_m , x-axis)

In general, it was possible to control the particle morphology of spray dried SBS particles by the chosen drying temperature. Harsh conditions generated smoother particles, while lower temperatures caused golf ball like structures.

These findings were taken into account for the preparation of spray dried SBS batches for interactive powder blends as drug shape is known as a factor, which might affect the aerodynamic behaviour of an API crucially. Results will be discussed in Section 4.3.1.2.

4.2.2 Particle Size

Several drug batches were prepared in spray dried and micronised qualities for interactive powder blends and with the intention to reach the respiratory zone of the lungs during inhalation.

Inhalation of drug particles is limited by drug size since size is one of the relevant factors that determine the FPF. A combination of particles with an $d_{50.3} < 2.5 \mu\text{m}$ and a PSDs with span values < 2.5 was chosen to be applicable for these experiments as these limits ensure that most particles have a size suitable to assess the fine airways of the lung or those stages of the NGI that are relevant for the respirable fraction.

Mean particle sizes ($d_{50.3}$) and span values are coherently summarised in Table 4.8. Micronised BUD was purchased and used with a size of $d_{50.3} = 1.4 \mu\text{m}$. The spray dried quality of BUD was applied with a $d_{50.3}$ of $1.8 \mu\text{m}$. This size serves as a compromise between the small micronised BUD purchased by the vendor and all other drug qualities (SBS, TIO, FOR) used ($d_{50.3} = 2.0 - 2.5 \mu\text{m}$).

Spray dried TIO and FOR particles, which were prepared based on parameters investigated in earlier experiments, were applied to interactive powder blends with particle sizes of $d_{50.3} = 2.2 \mu\text{m}$ (TIO) and $d_{50.3} = 2.1 \mu\text{m}$ (FOR). The micronised quality of SBS was jet-milled again to reach a final particle size of $d_{50.3} = 2.5 \mu\text{m}$.

Spray dried SBS was prepared in three qualities, which were different in size (and shape). SBS SD(S) as the standard batch used for all SBS investigations (including addition of fines and comparison of Novolizer[®] and Easyhaler[®] performance) represented the smallest SBS batch with an $d_{50.3}$ of $2.4 \mu\text{m}$. SBS SD(M) was slightly larger ($d_{50.3} = 2.8 \mu\text{m}$), while SBS SD(L) ($d_{50.3} = 3.7 \mu\text{m}$) was used as the largest drug batch within this project.

All span values were appropriate indicating narrow PSDs for all batches used for aerodynamic characterisations.

4.2.3 Drug Shape

In this study micronised and spray dried drug qualities were used in interactive powder blends to investigate the influence of drug shape on the detachment and dispersion of these drug particles. Jet-milling caused needle-like SBS particles (Figure 4.22 – D), while micronised BUD particles were found with a more uneven shape (Figure 4.23 – B) as purchased from the vendor.

Most spray dried qualities used in this study appeared with spherical character (SBS, Figure 4.22 – A to C; TIO, Figure 4.24 – B; FOR, Figure 4.24 – A). Only spray dried BUD was found with slightly unevenly shaped particles (Figure 4.23 – A) as it was spray dried dissolved in methylene chloride. Surface tension of this solvent is lower than in aqueous solutions as used for SBS which makes droplets more accessible to turbulences and thus to other morphologies during drying.

Apart from the comparison of needle-like or unevenly shaped micronised drug particles and spherical spray dried ones, this study applied two different qualities of spray dried SBS

particles. Two out of three SBS batches appeared with golf-ball like structure (SBS SD(S), Figure 4.22 – A and SBS SD(L), Figure 4.22 – C), while one was dried with a smoother surface (SBS SD(M), Figure 4.22 – B).

All different drug qualities were blended with the six chosen mannitol qualities to further investigate the impact of particle properties on the drug detachment and FPF.

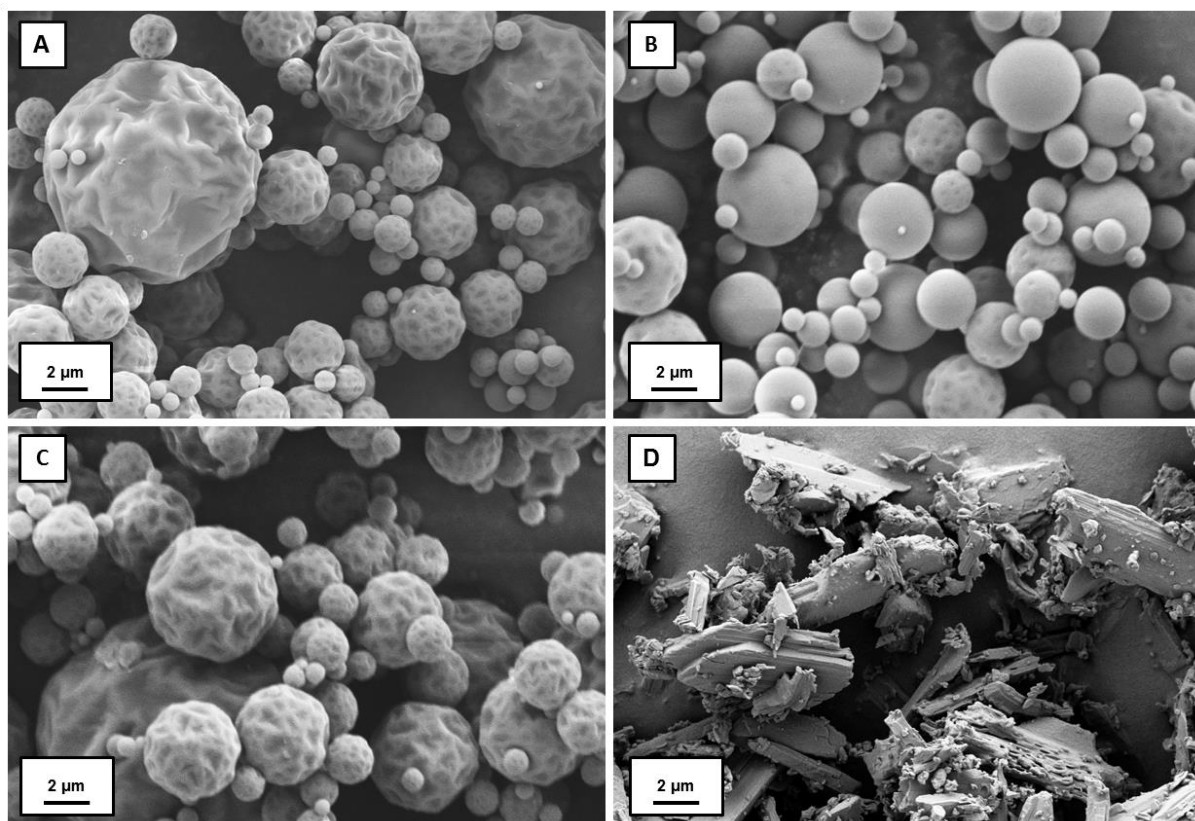


Figure 4.22 – SEM images of spray dried SBS particles (A: SBS SD(S), B: SBS SD(M), C: SBS SD(L)) and micronised SBS particles (D: SBS micronised) at 5,000 fold magnification

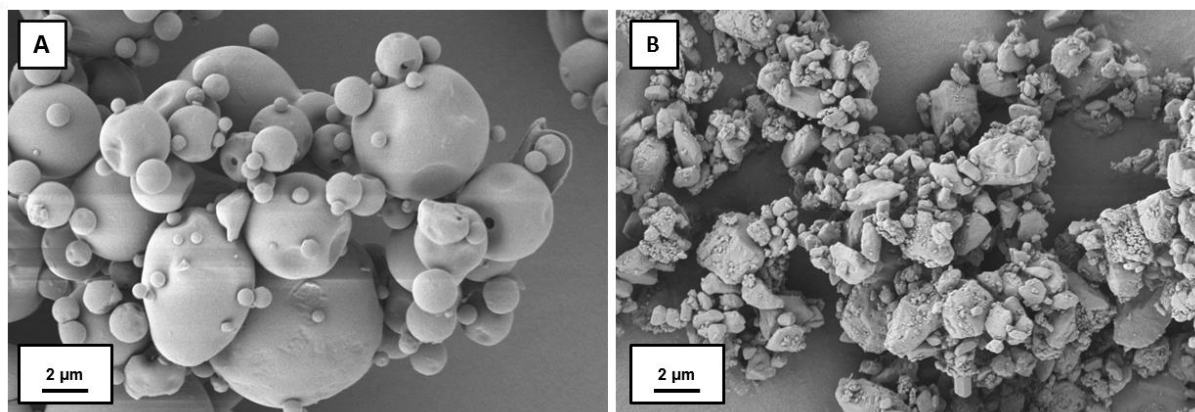


Figure 4.23 – SEM images of A: spray dried BUD and B: micronised BUD at 5,000 fold magnification

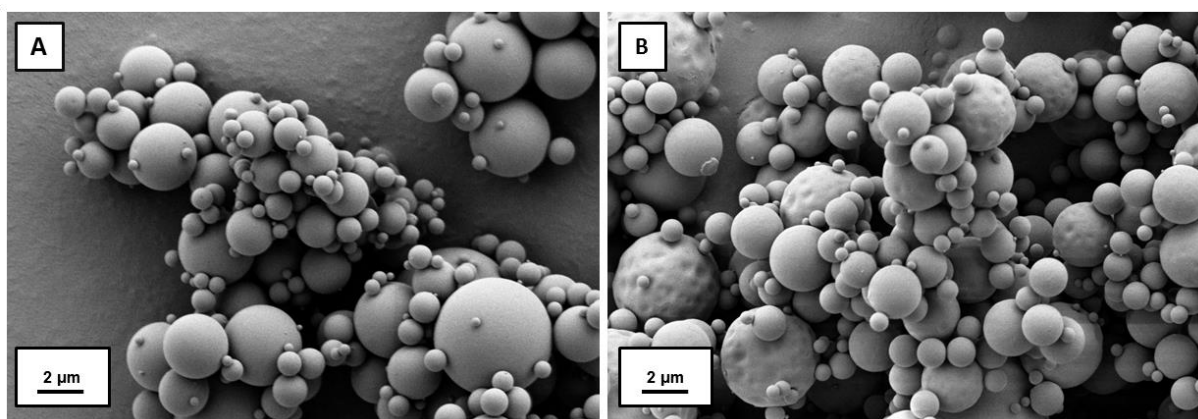


Figure 4.24 – SEM images of A: spray dried FOR and B: spray dried TIO at 5,000 fold magnification

4.2.4 Drug Storage Stability

In general, drugs are known for its ability to modify in crystal lattice structures over time when not initially present in the most stable form. This goes along with a change in the overall particle properties, but can be prevented by the chosen storage conditions. The capability to absorb moisture or physical parameters like the melting point repose on the crystal modification and can be used to determine the moment of recrystallisation at different ambient conditions to draw conclusions regarding the storage stability.

First of all, drug storage stability can be derived from the crystal lattice structure as measured with XRPDx. The inertness at different temperatures was tested by DSC analysis, while DVS was applied to approve stability of the products at higher relative humidity. All results together provide an overview over the suggested storage stability during handling and storage.

Figure 4.25 gives the XRPD diffractograms of SBS and BUD in micronised and spray dried quality. Crystalline structures were found for the micronised qualities of both drugs, while amorphous material without crystal lattice was detected right after spray drying.

The technique of XRPD allows to state that spray dried SBS and BUD batches appear almost completely amorphous as only a halo was detected, but prohibits statements about the ratio of crystalline and amorphous contents unless quantification with samples of known amount of crystalline and amorphous contents would be performed. Samples investigated here showed that crystalline structures appear. Nevertheless, it is known from literature that micronised materials most probably comprise amorphous spots after preparation. Similar results were published for FOR [88]. XRPD indicated spray dried FOR particles to be amorphous, while micronised FOR exhibited characteristic XRPD peaks [88].

Appropriate storage conditions are necessary for all drugs to avoid recrystallisation as this might cause crystal growth or built solid bridges between drug particles resulting in reduced

respirable fractions during inhalation. Additionally, drug particles might stick to the carrier surface (in interactive powder blends) upon recrystallisation, which might affect drug detachment crucially.

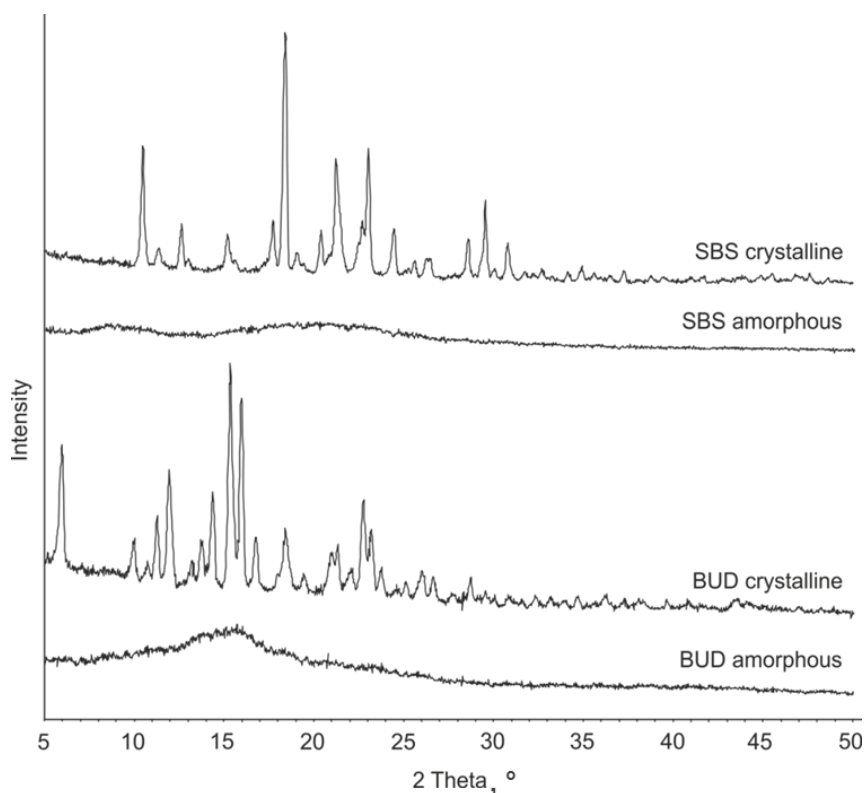


Figure 4.25 – XRPD diffractograms of SBS and BUD in spray dried amorphous quality and micronised quality with crystalline structures

Moisture uptake at different relative humidity was discovered by DVS analysis for SBS SD and TIO SD (Figure 4.26 and Figure 4.27). The change in mass increased steadily for SBS SD, when humidity was raised to 40 % rH, but increased rapidly above 40 % rH (change in mass > 12 %) to spontaneously release large amounts of water at 70 % rH. This step indicates recrystallisation of the spray dried material. Almost no moisture uptake was observed for the second increase of surrounding relative moisture, which substantiates that the whole spray dried material recrystallised during the first DVS cycle.

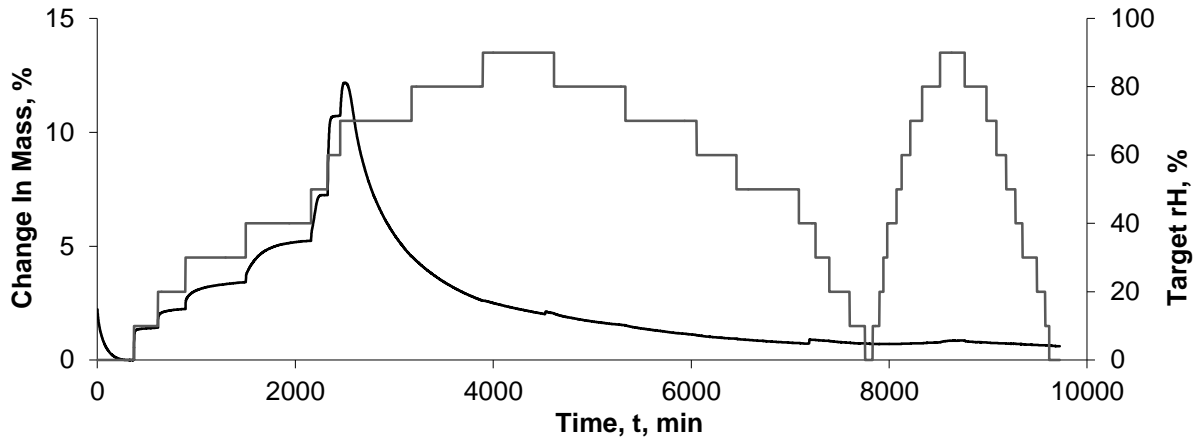


Figure 4.26 – DVS change in mass plot of spray dried SBS for relative humidities from 0 % rH to 90 % rH (2nd y-axis) and the according moisture uptake in % (1st y-axis)

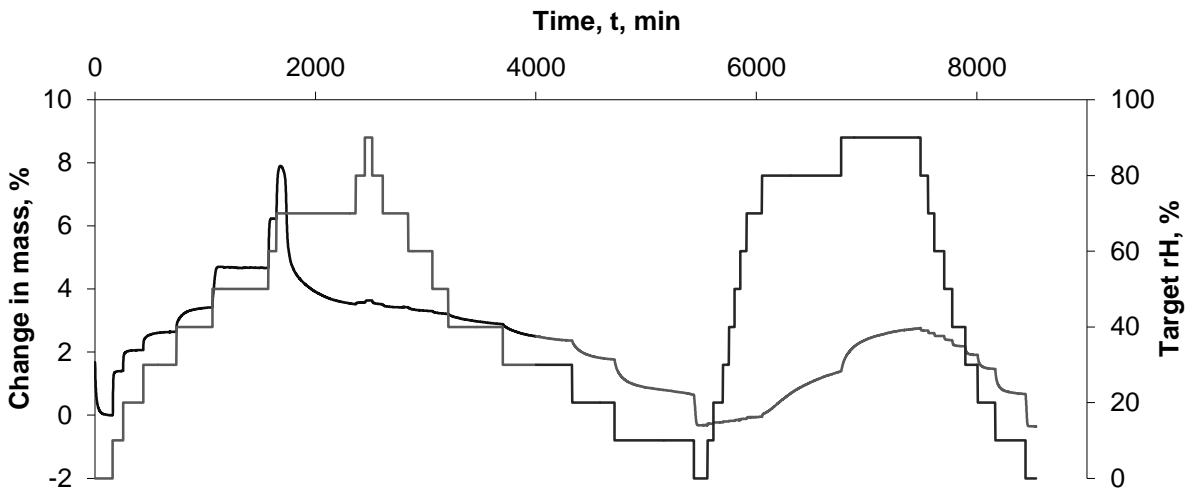


Figure 4.27 – DVS change in mass plot of TIO SD for relative humidities from 0 % rH to 90 % rH (2nd y-axis) and the according moisture uptake in % (1st axis)

Similarly, the uptake of moisture recorded for TIO SD exhibited slight uptake of moisture for the first steps of the analysis, but rapid increase, when moisture was set above 60 % rH to release larger amounts of water at an rH of 70 % rH. Again, this indicates recrystallisation of the spray dried material, which was again proved by a lower moisture uptake during the second cycle.

DVS results need to be considered for storage conditions and experimental work as they assume both spray dried APIs to be unstable for higher relative humidity. Handling of SBS SD or TIO SD should be performed below 40 % rH to avoid severe moisture uptake or even recrystallisation. As a result, preparation of interactive powder blends and impaction analysis were performed under controlled conditions at 35 % rH. Dry powder formulations that are used in every-day life would require desiccants to ensure stability of the product.

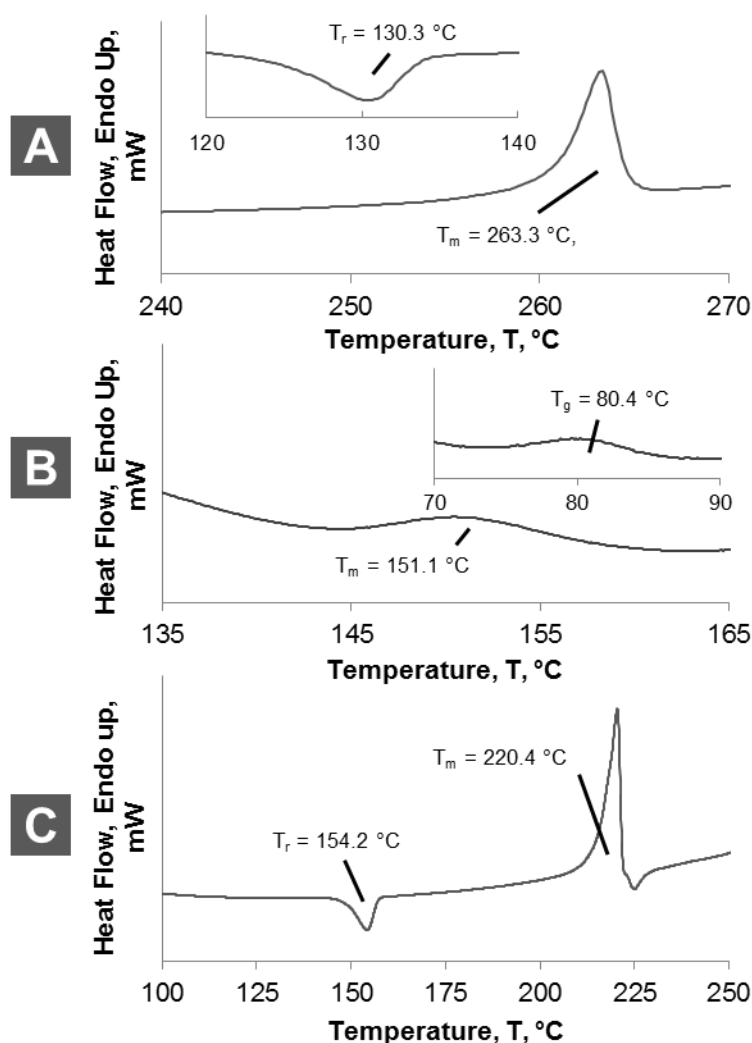


Figure 4.28 – DSC analysis of different drug qualities; A: BUD SD; B: FOR SD; C: TIO SD.

DSC analysis was further applied to BUD SD, FOR SD and TIO SD as not only humidity but also temperature might affect the stability of a product. Results obtained several thermic events that occurred at temperatures far away from standard laboratory conditions (Figure 4.28). BUD SD showed an exothermic event at $T_r = 130.3\text{ °C}$ representing the recrystallisation of the spray dried product and the melting point at $T_m = 263.3\text{ °C}$ which agrees with findings in literature [88]. A glass transition was not observed, but has been mentioned for $T_g = 89.5\text{ °C}$ by Tajber et al. earlier. FOR SD revealed a small endothermic event at $T_p = 80.4\text{ °C}$ that was suggested as glass transition by Tajber et al. and another endothermic event displaying the melting point at $T_m = 151.1\text{ °C}$. Recrystallisation was not detected as a thermic event here, but by Tajber et al. at $T_r = 126\text{ °C}$ [88]. TIO SD was found with a typical recrystallisation event at $T_r = 154.2\text{ °C}$ followed by the melting point at $T_m = 220.4\text{ °C}$. DSC analysis of SBS SD (not shown here) obtained a glass transition at $T_g = 113.1\text{ °C}$, but no further thermic events up to 250 °C.

All DSC results found that spray dried drug particles are stable at 20 °C as the chosen conditions for these experiments. Drug storage stability was proved for all drug particles used in these studies at the chosen conditions.

4.2.5 Surface Energy

Dispersive surface energy of all drug qualities used for interactive powder blends was determined to discover the potential to form non-polar particle-particle interactions. Results summarised in Table 4.8 and illustrated in Figure 4.29 exhibit that drug batches cover a range from $\gamma_s^d = 30 \text{ mJ} \bullet \text{m}^{-2}$ to $\gamma_s^d = 60 \text{ mJ} \bullet \text{m}^{-2}$.

Spray dried qualities of SBS and BUD were found with lower dispersive surface energy than their micronised counterparts. Amorphous material exhibited reduced non-polar interactions between particle surface and eluent compared to crystalline structures that occur for jet-milled materials resulting in lower dispersive surface energies as illustrated in Figure 4.29.

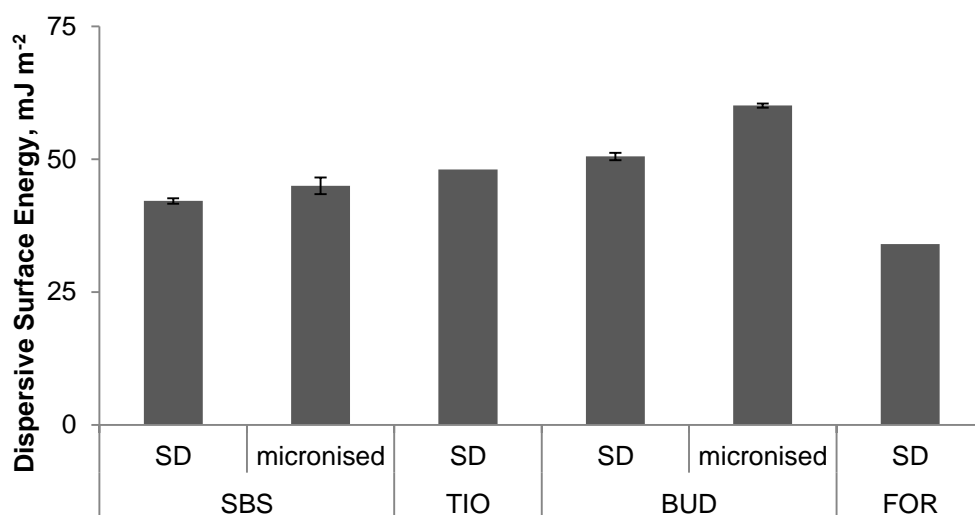


Figure 4.29 – Dispersive surface energy of different drug qualities used in these studies

The comparison of all spray dried drug particles revealed lipophilic FOR SD to have the lowest dispersive surface energy with $\gamma_s^d = 34.0 \text{ mJ} \bullet \text{m}^{-2}$ and lipophilic BUD SD to show the highest dispersive surface energy with $\gamma_s^d = 50.5 \text{ mJ} \bullet \text{m}^{-2}$. The hydrophilic drug batches SBS SD ($\gamma_s^d = 42.2 \text{ mJ} \bullet \text{m}^{-2}$) and TIO SD ($\gamma_s^d = 48.1 \text{ mJ} \bullet \text{m}^{-2}$) were found between those values, which leads to the conclusion, that dispersive surface energy does not appear to be a measure of hydrophilicity.

Dispersive surface energy has earlier been used to correlate differences in surface characteristics and resulting FPFs, which will be discussed in Section 4.3.7.

4.3 Aerodynamic Characterisation – Investigation of Particle-Particle Interactions

Engineered mannitol particles as investigated in Section 4.1 and the drug particles described in Section 4.2 were blended to generate carrier-based interactive powder blends that were examined for their aerodynamic performance by impaction analysis as will be discussed in this section. The quality of a powder blend is determined by several parameters such as the ability to be dispersed by the inhaler device during inhalation or the facilitation of drug deagglomeration resulting in adequate fine particle fractions (FPFs). Impaction results can further be linked to carrier and drug properties since detachment and dispersion of single drug particles or agglomerates are known to be affected by those characteristics. This section will approach blend quality and impaction results first and discuss the findings in the scope of particle-particle interactions subsequently.

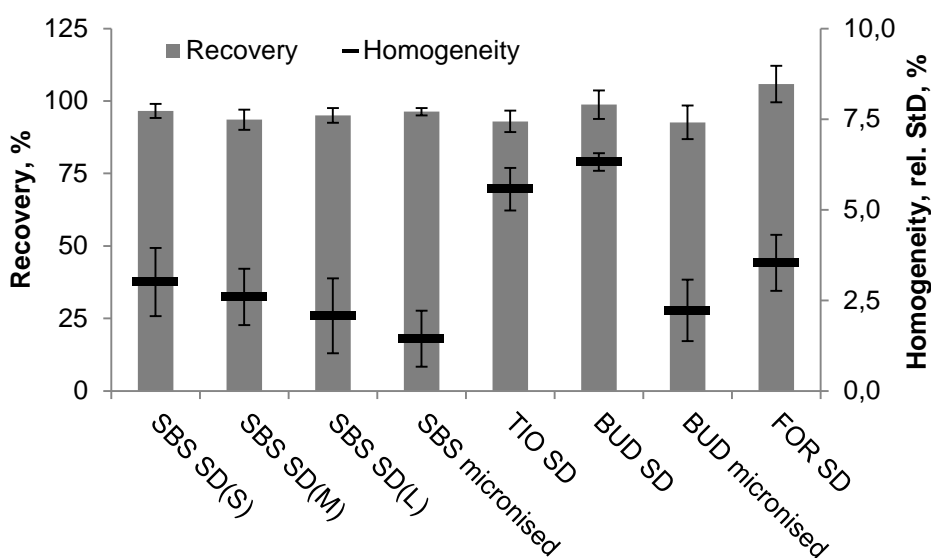


Figure 4.30 – Recovery and blend homogeneity averaged for all drug qualities as blended with six different mannitol carrier qualities

Initially, powder blends were tested for its drug recovery and homogeneity as those quality parameters build the basis for all further experiments (Figure 4.30). Most powder blends met the defined limits for recovery (> 90 %) and homogeneity (relative StD < 5 %). Only the spray dried qualities of TIO and BUD were found with decreased homogeneity as relative standard deviation was found above the 5 % limit, which was mainly due to tribo-charging effects that could not efficiently be reduced by deionisation prior and during the blending procedure. Charges were only observed for these two drug qualities where drug particles got stuck to the vessel wall after blending indicating that this affected the homogeneity of those blends. Further, powder blend homogeneity of blends prepared with the most spherical carrier particles (M71(L)) was reduced for TIO SD, BUD SD and FOR SD compared to those

batches with slight indentions which indicated SBS SD to adhere tighter as will be discussed later in this section. The recovery of all blends was evaluated with reasonable measures of > 90 %.

Impaction analysis was then performed with the NGI resulting in deposition profiles like exemplarily depicted for powder blends consisting of SBS SD(S) and the six chosen mannitol qualities in Figure 4.31. Results exhibited that most of the administered drug deposited in throat or preseparator, which indicates that large amounts of drug particles were not well dispersed during inhalation or stayed attached to the mannitol carrier, which most likely impacted in the preseparator. The following stages showed a maximum SBS deposition on Stage 2, which gradually decreased towards the following stages.

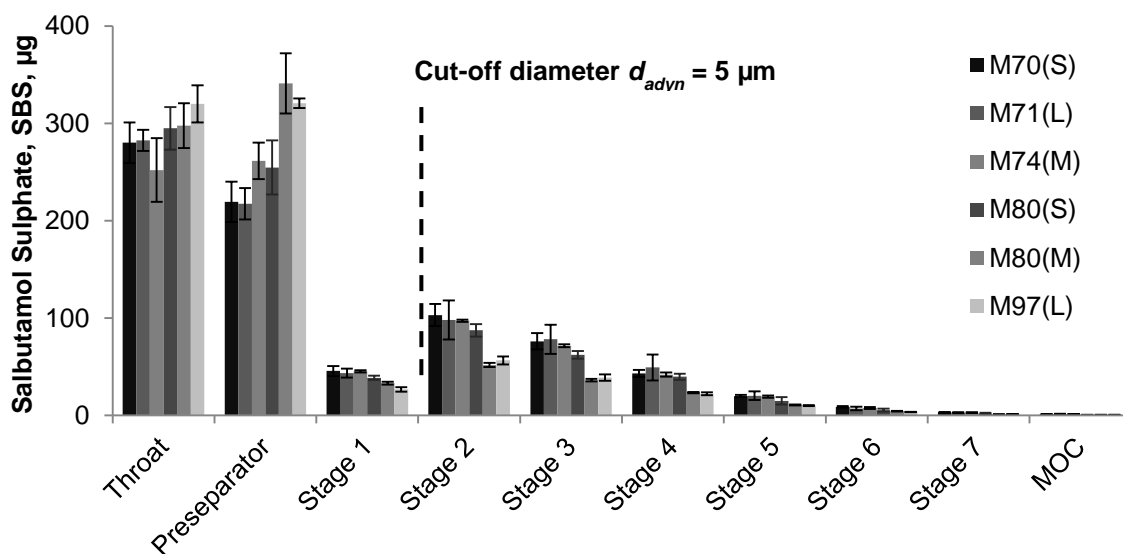


Figure 4.31 – SBS in $\mu\text{g} \pm \text{StD}$ (y-axis) as deposited on the different stages of the NGI (x-axis) after administration of ten doses with the Novolizer[®] for powder blends with six different mannitol batches and SBS SD(S) (n=3)

Apart from this overall description, mannitol batches differ in the deposition on single stages. Significant differences were observed for the comparison of M70(S)/M71(L) and M80(M)/M97(L). Blends prepared with carriers dried at lower outlet temperatures (M(70S)/M71(L)/M74(M)) were found with less deposition in the preseparator, but with more SBS on the stages, while those batches prepared with carriers dried at higher outlet temperatures (M80(S)/M80(M)/M97(L)) revealed more SBS deposited in the preseparator and less on the stages.

The cut-off diameter for particles with a $d_{advn} < 5 \mu\text{m}$ was located between Stage 1 and 2 for a flow rate of 78.2 L min^{-1} (as illustrated in Figure 4.31) as necessary for the Novolizer[®], so that the respective FPF is based on an extrapolation. The resulting FPFs are summarised in Table 4.10, which displays the FPFs of powder blends containing one of the four SBS qualities and the chosen mannitol carrier batches. The observed respirable fractions agree

with the respective deposition profiles since batches with more deposition on the stages resulted in higher FPFs than those with more deposition in preseparator and throat.

Results shown here covered an overall range from 11.1 % to 35.0 % with the highest FPFs detected for the micronised SBS quality. Detachment and dispersion of spray dried SBS was generally lower than for micronised SBS since the according FPFs ranged from 11.1 % to 27.3 %, while the micronised drug caused FPFs ranging from 27.3 % to 35.0 %.

Table 4.10 – FPF ± StD in % of six mannitol batches blended with four different SBS qualities

Mannitol batches			Drug batches							
DoE: Labelling		Results: Extra Labelling	SBS							
Run Order	Exp Name		SBS micronised	Spray Dried						
				SBS SD(S)		SBS SD(M)		SBS SD(L)		
			FPF	StD	FPF	StD	FPF	StD	FPF	StD
Run 9	N5	M70(S)	33.4	0.6	27.3	2.6	26.7	0.5	19.4	0.7
Run 10	N1	M71(L)	35.0	3.2	25.7	3.1	22.4	0.9	15.9	0.3
Run 14	N9	M74(M)	32.6	1.0	23.9	0.8	22.2	1.4	18.7	0.8
Run 13	N14	M80(S)	33.2	1.4	20.9	0.7	21.3	0.8	14.3	0.6
Run 2	N19	M80(M)	27.3	1.8	11.2	0.3	15.4	0.6	11.1	0.5
Run 11	N4	M97(L)	29.4	0.7	12.9	0.7	11.5	1.8	11.7	0.3

Experiments performed with hydrophilic SBS were supplemented by other drugs of different hydrophilicity to SBS. Table 4.11 summarises the FPFs of the aerodynamic characterisation of interactive powder blends with 1 % (w/w) TIO SD, BUD SD, BUD micronised and FOR SD and the six chosen mannitol batches as gained by impaction studies utilising the Novolizer®. Noticeably, results revealed quite different levels for the different drugs and drug qualities. SD TIO exhibited the highest FPFs of all drug batches investigated here with FPF = 32.0 ± 1.2 % to 41.8 ± 1.0 %. Interactive powder blends containing BUD showed quite divergent FPFs for spray dried and micronised drug particles. Contrary to SBS, BUD SD performed much better (FPF = 28.3 ± 1.4 % to 33.6 ± 1.6 %) than the micronised counterpart (FPF = 15.2 ± 2.0 % to 24.2 ± 1.1 %). FOR SD revealed FPFs between 26.6 % and 35.0 %. Contrary to blends consisting of mannitol and SBS SD(S/M/L), M70(S) and M74(M) containing blends with FOR SD resulted in the lowest FPF, while M80(S) and M97(L) caused higher FPFs.

Table 4.11 – FPF ± StD in % of six mannitol batches blended with TIO SD, BUD SD / micronised and FOR SD.

Mannitol batches			Drug batches							
DoE: Naming		Results: Extra Labelling	TIO		BUD				FOR	
Run Order	Exp Name		TIO SD		BUD SD		BUD micronised		FOR SD	
			FPF	StD	FPF	StD	FPF	StD	FPF	StD
Run 9	N5	M70(S)	34.1	1.8	32.1	1.1	15.7	2.0	29.1	1.1
Run 10	N1	M71(L)	35.6	0.2	28.3	1.4	24.2	1.1	35.0	0.5
Run 14	N9	M74(M)	38.2	2.0	33.6	1.6	20.2	1.0	26.6	1.7
Run 13	N14	M80(S)	41.8	1.0	37.2	1.0	15.6	2.0	34.3	1.5
Run 2	N19	M80(M)	32.0	1.2	32.6	0.8	15.2	2.0	31.6	0.7
Run 11	N4	M97(L)	33.4	2.7	33.0	0.9	15.3	1.0	33.7	0.2

Carrier-containing interactive powder blends as applied here are based on particle-particle interactions that cause adhesion or cohesion between particles. Experiments performed in this project were designed to cover numerous particle properties of both carrier and drug particles and its effect on the dispersion during impaction analysis to examine effects on particle-particle interactions and respirable fraction and, therefore, on the quality of the product. The following subsections will deal with the correlation of respirable fractions and carrier or drug properties like particle shape (Section 4.3.1), surface roughness (Section 4.3.2), particle size (Section 4.3.3), flowability (Section 4.3.6), surface energy (Section 4.1.8) or also drug hydrophilicity (Section 4.3.4) and crystallinity (Section 4.3.5). Supplementary investigations will further focus on the influence arising from inhaler device (Section 4.3.9) and from the addition of mannitol fines (Section 4.3.8).

4.3.1 Particle Shape

During preparation, both carrier and drug particles were varied in terms of particle shape. Hence, evaluation of the aerodynamic performance was performed divided into carrier shape and drug shape to separate appropriate effects.

4.3.1.1 Carrier Shape

The carrier shape is known to influence the DPI performance of interactive powder blends as it has been reported for lactose monohydrate carriers, but also for mannitol carrier particles earlier in this project (Section 2.3.2). The results gained from impaction analysis with spray dried model drugs and six chosen mannitol carriers demand different descriptions for the

dispersion mechanisms of the applied drugs that are in turn based on different particle-particle interactions.

Evaluation of impaction results will start with results of powder blends containing spray dried SBS and will be followed by powder blends with spray dried BUD and TIO to end up with the evaluation of FOR SD containing blends.

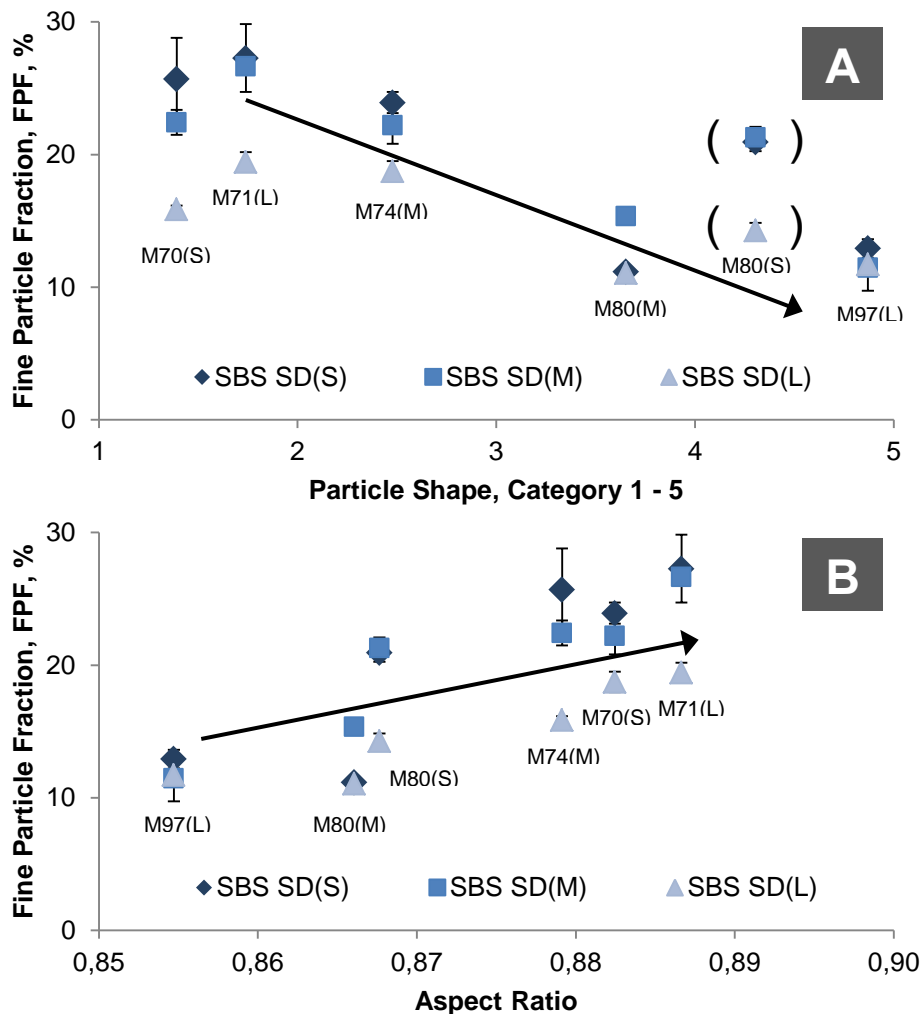


Figure 4.32 – FPF \pm StD in % (y-axis) of powder blends consisting of six chosen mannitol batches (M70(S)/M71(L)/M74(M)/ M80(S)/M80(M)/M97(L)) and SBS SD(S/M/L) related to measurements describing the particle shape: A: particle shape by categorisation of SEM images into five categories from category 1 (spherical) to category 5 (indented); B: aspect ratio measured by image analysis (n=3). Results that do not fit the trend due to effects arising from carrier size are bracketed.

Two different parameters were applied to discover the effect of particle shape. Figure 4.32 – A illustrates the correlation of FPF (y-axis) to particle shape categories (x-axis) as determined with the survey. It was observed that powder blends with more spherical character (shape category < 2.5) led to higher FPFs for all different spray dried SBS qualities (Table 4.10, 18.7 % - 27.3 %) compared to those with more indentions (Table 4.10, 11.1 % -

21.3 %). This effect was even more pronounced for powder blends with SBS SD(S) and SBS SD(M) compared to SBS SD(L) as will be discussed in Section 4.3.3.2.

In more detail, the three mostly spherical carrier batches do not significantly impact on the FPF of SBS drug batches, when compared with each other, but show significantly higher FPFs compared to the three batches prepared with indented carriers ($p < 0.05$). However, blends with mannitol M80(S) (Shape Category 4.3) were found to deviate from the general trend towards lower FPFs for all SBS qualities when more indentions occur. Its respirable fraction was detected to be higher than the one for blends prepared with mannitol M80(M) (Category 3.7, bracketed in Figure 4.32 – A) which will further be explained by effects of carrier size in Section 4.3.3.1.

Supplementary, Figure 4.32 – B gives the FPFs correlated to the aspect ratio of the carrier particles the powder blends were prepared with. Similar trends were found for all these batches as lower aspect ratios (Table 4.1, 0.8967 to 0.8547) generally caused worse DPI performances (FPF = 27.3 % to 11.1 %). Batches M80(S) and M80(M) were evaluated with almost equal aspect ratios, but reveal again significant differences for the respective FPF. As mentioned above, this effect can coherently be described as a factor of particle size in the following.

Figure 4.33 gives the visualisation of four powder blends with mannitol carriers of spherical and indented character as prepared with SBS SD(S). The spray dried drug particles were well spread over the whole surface or build drug bridges between the carrier particles, when carriers are spherical. Drug bridges were mainly detected in powder blends prepared with M70(S) (Figure 4.33 – A) since smaller carrier particles facilitate accumulations due to the lower mass per particle, while the single carrier mass might have been too large for bridges in powder blends consisting of larger M71(L) (Figure 4.33 – B) and SBS SD(S). Nevertheless, performance of both powder blends led to FPFs above 25 %, which suggested that both kinds of drug distribution support adequate drug detachment and agglomerate dispersion.

Particles presented in Figure 4.33 – C/D exhibited indentions that trapped drug particles during blending to enable the generation of drug accumulations. The resulting FPFs decreased with the occurrence of indentions.

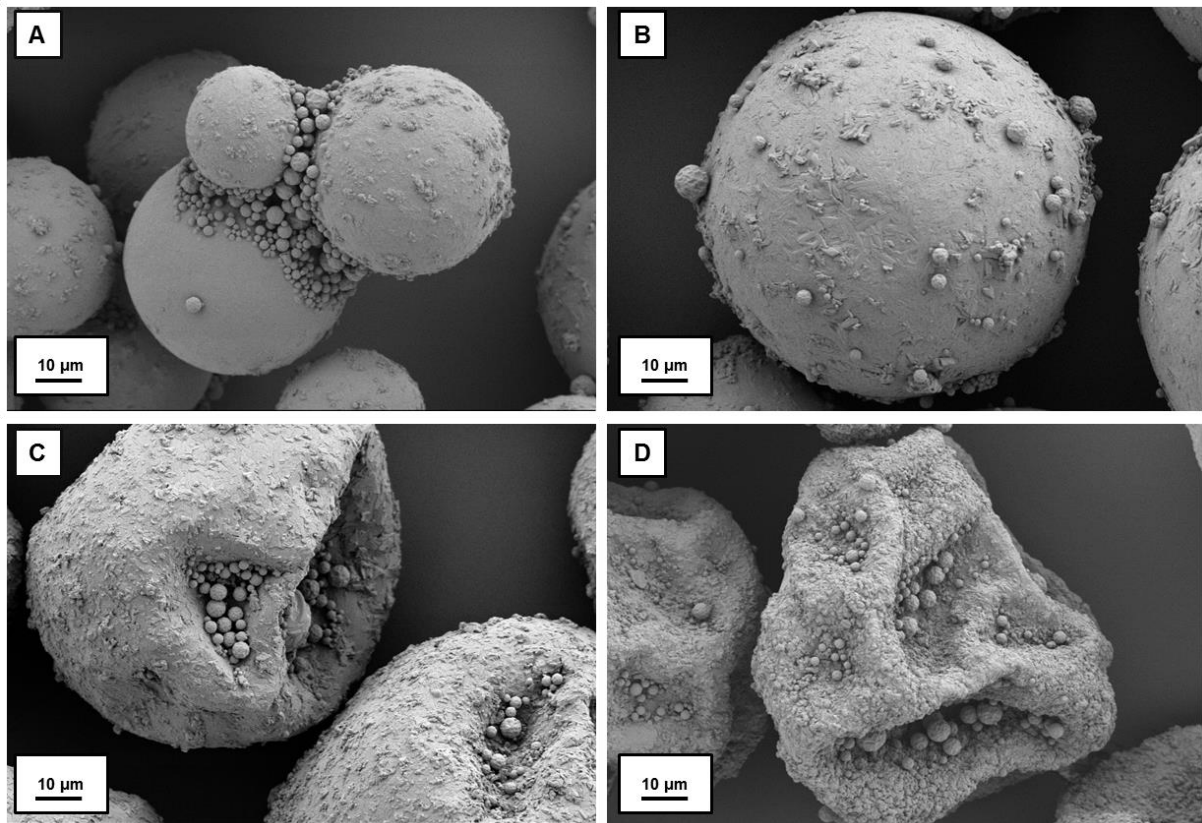


Figure 4.33 - Visualisation of interactive powder blends with SBS SD(S) and different mannitol carrier batches; A: M70(S); B: M71(L); C: M80(S); D: M97(L)

Figure 4.34 gives a more schematic view on the detachment and dispersion of SBS particles from carriers of different shape. Scheme A indicates that spherical carriers facilitate both the generation of drug bridges and drug particles being evenly distributed on the whole carrier surface, while Scheme B illustrates how drug particles get trapped by indented carrier particles. Most of the drug particles get entrained by the air flow and are dispersed by inhalative shear forces, when the carrier appears spherical, but only a few get detached from indented carriers, where several particles remain in the indentations as observed in the experiments discussed before.

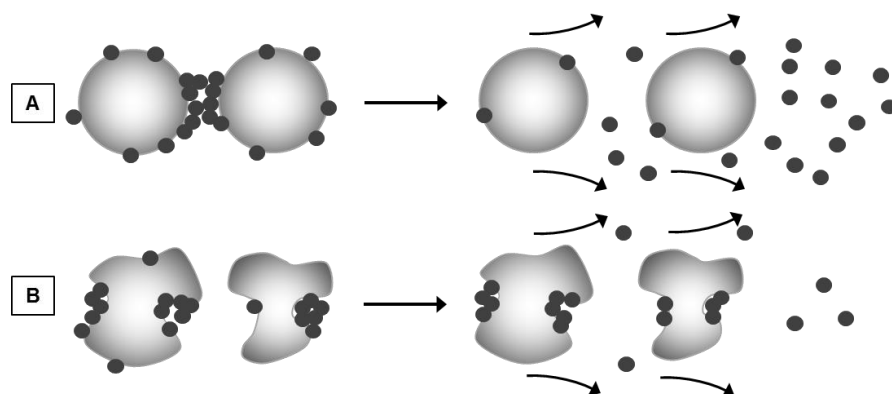


Figure 4.34 – Scheme of the detachment of SBS particles (black) from the carrier (light grey) during inhalation for A: spherical carrier particles and B: indented carrier particles

Drug detachment of TIO SD and BUD SD as measured by impaction analysis resulted in contrary trends compared to SBS SD as illustrated in Figure 4.35. The plot shows the FPFs of both drugs correlated to the according shape categories as evaluated by a survey.

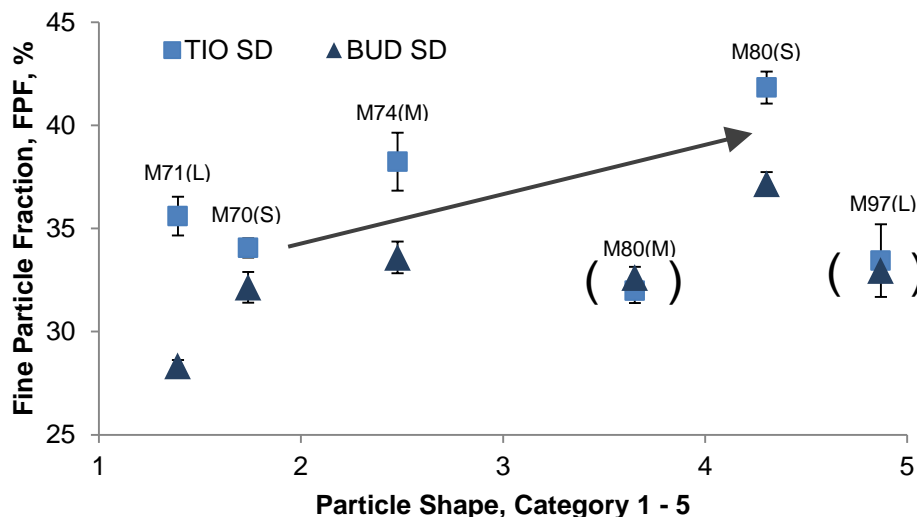


Figure 4.35 - FPF \pm StD in % (y-axis) of powder blends consisting of six chosen mannitol batches (M70(S)/M71(L)/M74(M)/ M80(S)/M80(M)/M97(L)) and TIO SD or BUD SD related to the particle shape as evaluated by categorisation of SEM images into five categories from category 1 (spherical) to category 5 (indented) (n=3). Results that do not fit the trend due to effects arising from carrier size or indentation depth are bracketed.

Most powder blends with TIO SD triggered higher FPFs than with BUD SD (except for M80(M) and M97(L), which were found at the same range), which will be discussed later. With focus on the carrier particle shape, the efficiency of drug dispersion increases significantly with rising shape categories or the occurrence of indentations. Accordingly, the FPFs of powder blends with TIO SD rose from 34.1 ± 1.8 % (M70(S)) to 41.8 ± 1.0 % (M80(S)), while blends prepared with BUD lead to FPFs from 28.3 ± 1.4 % (M71(L)) for spherical carriers to 37.2 ± 1.0 % (M80(S)) for slightly indented ones. For both model drugs, an decrease of the FPF was observed for powder blends containing mannitol M80(M) or M97(L), which will be attributed to the carrier size in the following sections. SEM visualisations in Figure 4.36 give images of powder blends containing of spherical carriers with lower FPF (T1 / B1), of medium indented carriers performing best in impaction analysis (T2 / B2) and of deeply indented carriers with decreased FPF (T3 / B3).

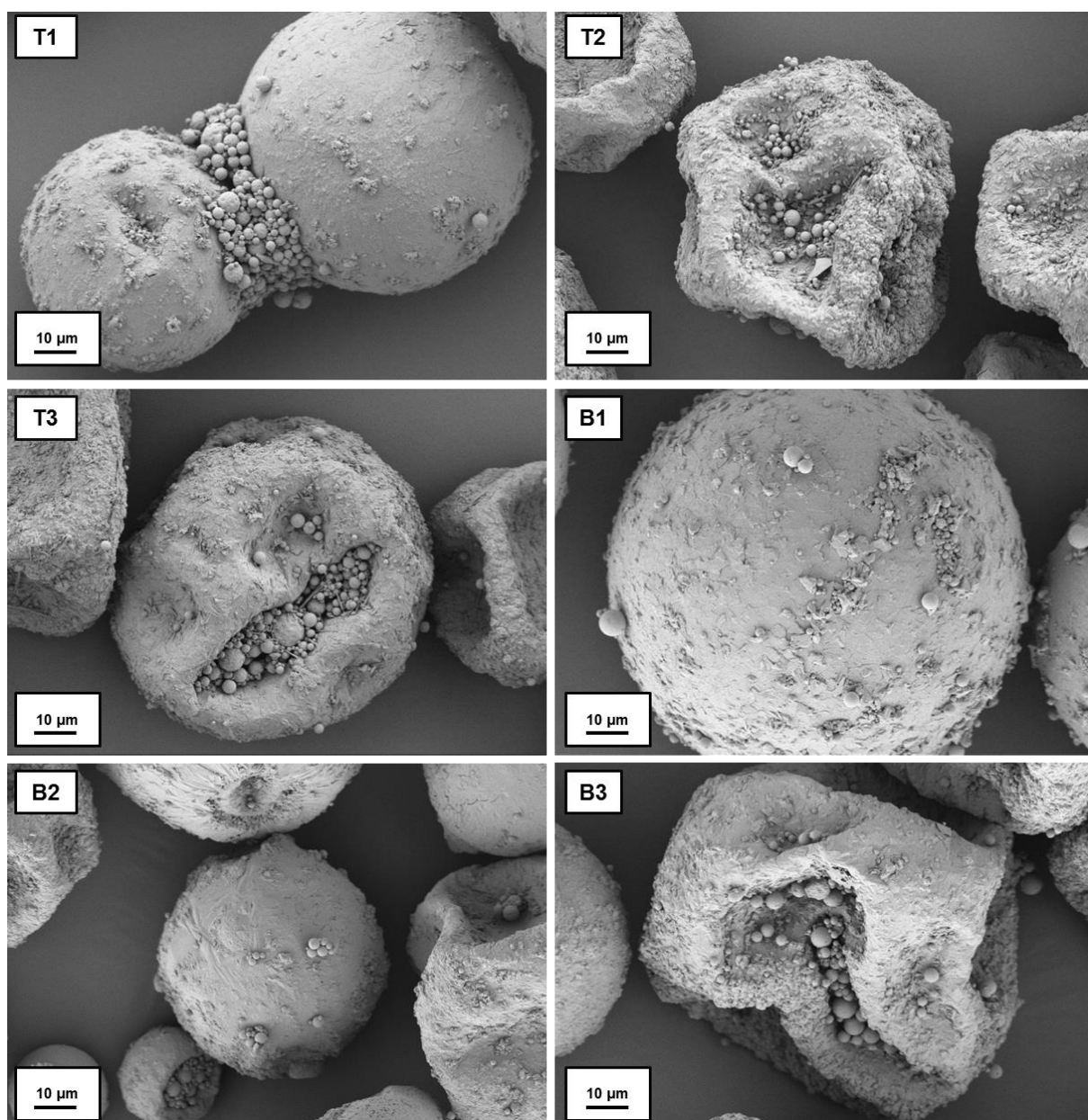


Figure 4.36 – SEM visualisations of powder blends containing TIO SD (T1-3) and BUD SD (B1-3) and the following mannitol qualities: T1: M70(S); T2: M80(S); T3: M97(L); B1: M71(L); B2: M80(S); B3: M97(L).

Again, drug bridges were found between small and spherical carrier particles (T1), while drug particles were evenly distributed on the surface for larger carriers (B1). The batches performing best during impaction analysis exhibited small indentions, which entrap drug particles (T2 / B2). Powder blends with mannitol M97(L) (T3 / B3) revealed several deep indentions that were filled with drug accumulates.

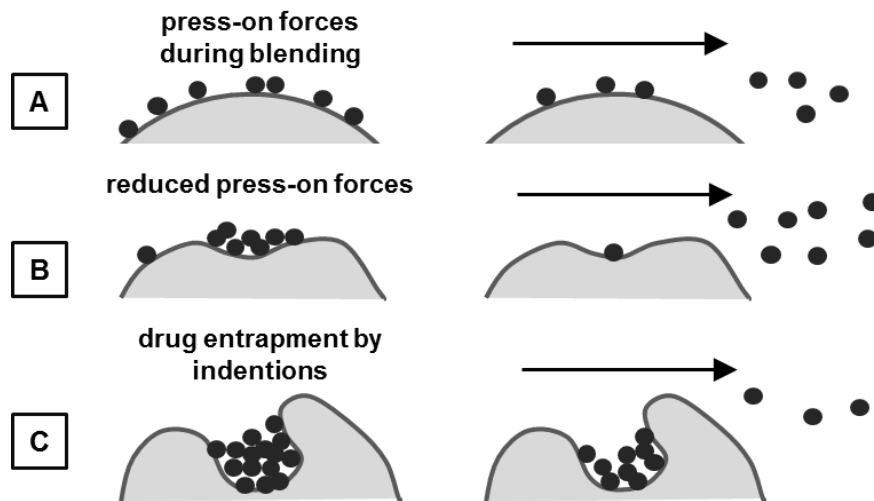


Figure 4.37 – Scheme of the detachment of TIO SD / BUD SD (black) from carriers of different particle shapes (grey), A: spherical carrier; B: slightly indented carrier, C: carrier with deep indentions

The trends observed for idealised spherical drug particles of TIO SD and BUD SD support the theory of press-on forces that occur during blending and handling. Drug particles blended with spherical carrier particles are pressed on the carrier surfaces during the blending procedure as there is no ability to hide in surface irregularities. These press-on forces increase the adhesion forces between drug particles and carrier surface, which decreases the FPF (Figure 4.37 – A). The occurrence of first slight indentations enables drug particles to hide from press-on forces by other carrier particles during blending. Less press-on forces and so less adhesion forces cause easier detachment of drug particles during inhalation, which results in rising respirable fractions for this group of model drugs (Figure 4.37 – B). Only particles with several deep indentions show decreased FPFs since drug particles are hindered to be entrained by the air flow (Figure 4.37 – C).

That this effect is not prominent for the SBS particles as described above might be explained by the tendency to be detached by the air stream. SBS seems to be adhered tighter when caught in even slight indentions compared to BUD or TIO particles. In turn, SBS is not affected by press-on forces as observed for the other two drugs. However, this could not directly be measured in these experiments.

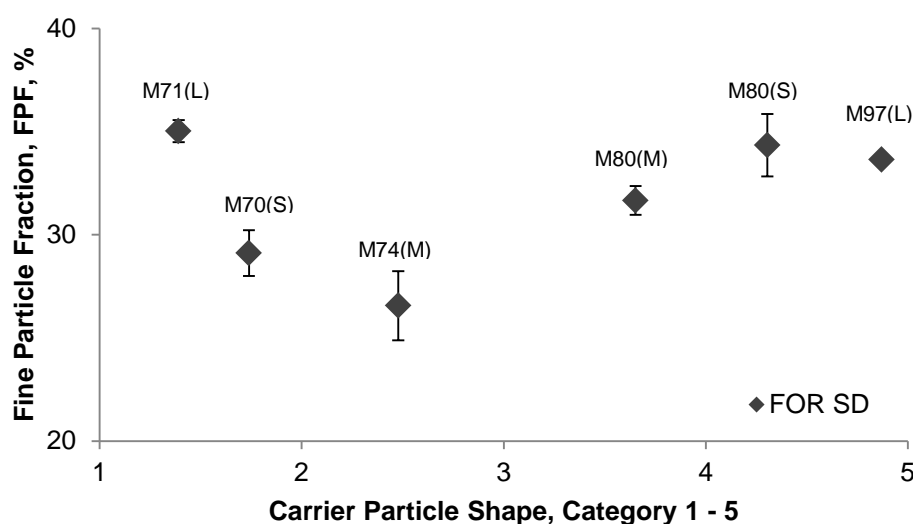


Figure 4.38 - FPF \pm StD in % (y-axis) of powder blends consisting of six chosen mannitol batches (M70(S)/M71(L)/M74(M)/ M80(S)/M80(M)/M97(L)) and FOR SD related to the particle shape as evaluated by categorisation of SEM images into five categories from category 1 (spherical) to category 5 (indented) (n=3)

Experiments performed with lipophilic FOR SD revealed carrier particles with several deep indentions (M80(S)/M97(L)) to trigger the best FPFs, while two batches with more spherical character were found with reduced FPFs (M70(S)/M74(M)). M71(L) as a large and spherical carrier quality deviated from this trend since the FPF was found on the same level than indented carriers M80(S) and M97(L).

Results can be linked to an interplay of carrier particle shape and agglomerate strength which is most likely linked to the drug size. FOR SD was suggested to appear as a quite cohesive drug with high tendency to build agglomerates of remarkable agglomerate strength due to its blending behaviour. The blending process was adapted to faster rotation of the blending vessel to enable homogeneity by destroying these agglomerates. Challenges based on the occurrence of agglomerates help to understand trends in correlation to carrier particle shape observed here.

Carrier particles with a high number of indentions enable adequate drug distribution without the generation of large drug accumulates within these indentions as the sum of indentions provides a lot of space for the low number of drug particles (Figure 4.39 – B). The least indentions occur the higher is the tendency to build larger agglomerates, which hardly get dispersed during inhalation. This reduces the according FPF for M74(M) exemplarily. An additional negative effect can be assumed for batch M70(S) with respect to the small carrier size. As for the other model drugs, FOR SD exhibited a tendency to build drug bridges between those small carrier particles due to the absence or low numbers of indentions (Figure 4.39 – B). These bridges were formed by drug agglomerates that needed to be dispersed during inhalation, which caused a reduction in FPF. The mentioned agglomerates

were not adequately dispersed during impaction analysis, which could be attributed to the possibly more intense agglomerate strength compared to other drugs.

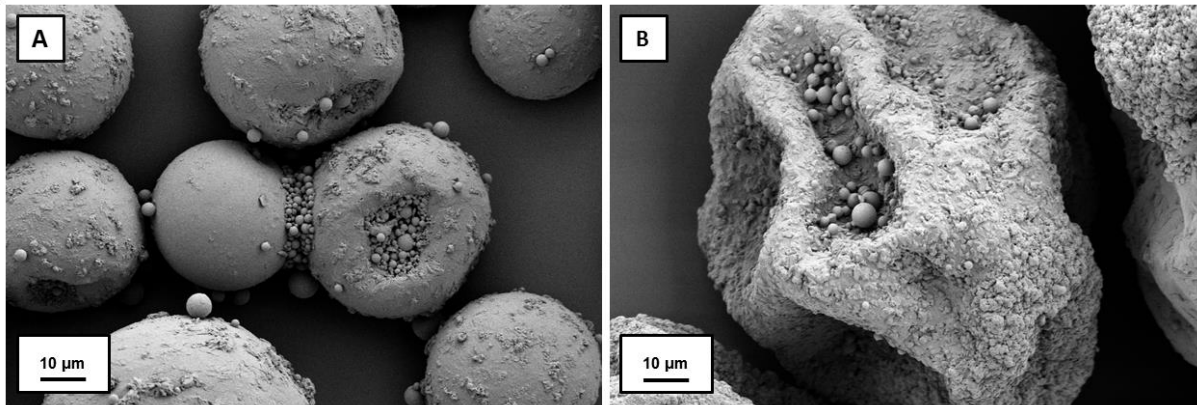


Figure 4.39 – SEM visualisations of powder blends containing FOR SD and A: mannitol M70(S) or B: mannitol M97(L).

Interactive powder blends containing M71(L) and FOR SD lead to significantly higher FPFs compared to blends with M70(S) even though both carriers were of spherical shape. The particle mass of the larger carrier quality avoids the development of drug agglomerates in form of drug bridges, so that the drug was evenly distributed over the whole carrier surface resulting in an easier dispersion during inhalation and appropriate FPFs.

The fact that FOR SD was less entrapped by the deep indentions than e.g. SBS SD can be related to particle-particle interactions between carrier and drug particle as will be discussed in Section 4.3.4.

In general, formulations for DPI use are desired to easily generate high FPFs with adequate reproducibility as this reduces the loss of drug as well as the risk of systemic side effects. Results claim the particle shape to affect the detachment of drug particles since indentions either enable the entrapment of small particles or help to hide from press-on forces. Spray dried carriers need to be spherical (SBS; FOR for large carrier particles), slightly indented (TIO, BUD) or deeply indented (FOR) to trigger the best aerodynamic performance when tested with spray dried drug particles. Mechanisms are based on how well the drug particles get detached from the carrier surface but also on the suggested agglomerate strength of the respective drugs. The development of new dry powder formulations requires new evaluations for every drug as the effect of carrier shape appears to be drug dependent. However, the examination of drug agglomerate strength and adhesion forces requires methods for direct investigations to enable predictions.

4.3.1.2 Drug Shape

Drug shape was of further interest, as not only the carrier might influence particle-particle interactions. Investigations were performed using spray dried and micronised qualities of hydrophilic SBS and lipophilic BUD.

The aerodynamic performance of powder blends containing these drug qualities is summarised in Figure 4.40, which displays the FPFs for six different mannitol batches. Starting with the comparison of both SBS qualities, inhalation of SBS micronised resulted in noticeably higher and mostly similar FPFs (Table 4.10, $FPF = 32.6 \pm 1.0\%$ – $35.0\% \pm 3.2\%$) compared to all spray dried qualities. Only powder blends prepared with M80(M) and M97(L), where carriers exhibited the most indentions, showed slightly decreased values (Table 4.10, $FPF = 27.3 \pm 1.8\%$ – $29.4 \pm 0.7\%$), that might be explained by entrapped drug particles.

Reduced FPFs for spray dried SBS can be attributed to drug shape, but also to crystal structure. Micronised SBS exhibited needle-like particles (Figure 4.22 – D), that align in the air flow after detachment from the carrier. This affects the impaction of drug particles since needles that are entrained by the airflow provide less surface area to be accelerated and impacted. Drug orientation within the airflow supplements this effect as needle-like particles pass the impactor nozzles easier [144].

In fact, SBS SD(S) showed decreasing FPFs, when first slight indentions occurred on the carrier surface, while micronised SBS kept similar FPFs. The needle-like shape prevents those particles from entrapment in small indentions, so that dispersion was not influenced here.

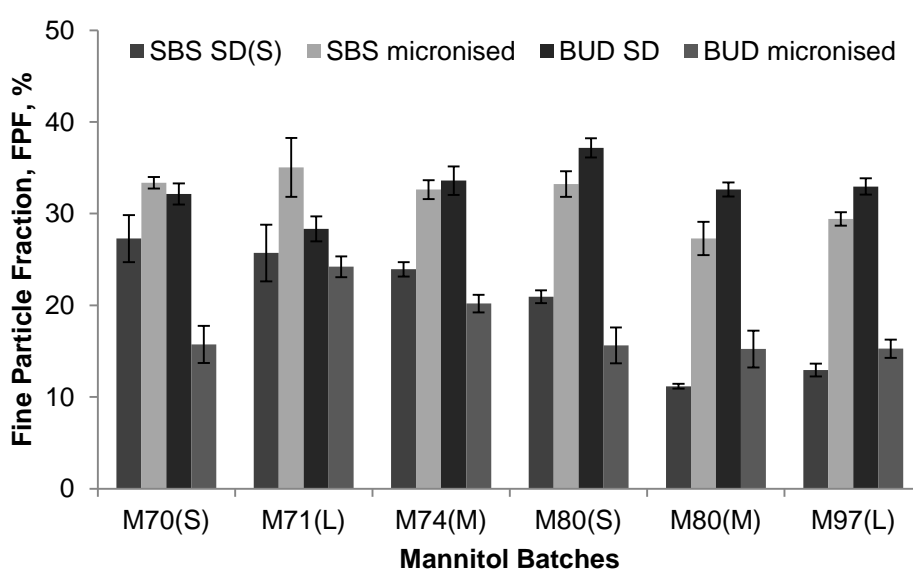


Figure 4.40 - FPF \pm StD in % (y-axis) of six chosen mannitol batches (x-axis) and appropriate powder blends with SBS SD(S), SBS micronised, BUD SD and BUD micronised (n=3)

The comparison of BUD SD and micronised BUD contrasted the findings described before. BUD micronised was found with lower FPFs ($FPF = 15.2 \pm 1.1 \% - 24.2 \pm 1.0 \%$) than the spray dried quality ($FPF = 28.3 \pm 1.4 \% - 37.2 \pm 1.0 \%$). Micronised BUD containing blends were initially investigated with Raman analysis to check for the drug distribution on the surface (Figure 4.41) as micronised drug particles cannot easily be distinguished from surface asperities by SEM.

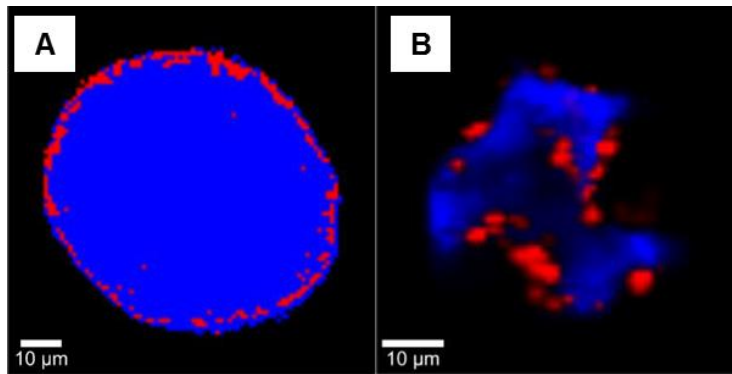


Figure 4.41 – Overlay images of Raman analysis with BUD micronised containing powder blends with A: spherical mannitol carrier particles (M71(L)) and B: indented mannitol carrier particles (M97(L)).

Results revealed that BUD was spread over the surface for spherical carriers and accumulated in indentions, if present, which went along with findings described for SBS or BUD SD. Hence, differences between BUD SD and micronised BUD need to be assigned to further reasons.

Observed effects can be dedicated to the tendency to build agglomerates as well as to the effective contact area of the different BUD drug qualities. Agglomerate strength decreases with larger drug sizes, so that the spray dried quality ($d_{50.3} = 1.8 \mu\text{m}$) was favoured for detachment compared to the micronised one ($d_{50.3} = 1.4 \mu\text{m}$). The contact area between single BUD particles of the same quality decreases and enables easier dispersion. Further, the effective contact area between BUD drug particles of different quality gets impacted by drug shape. Spherical particles have the lowest effective contact area between single particles and, therefore, the lowest particle-particle interactions, which reduces its agglomerate strength and triggers higher FPFs.

The comparison of SBS and BUD qualities provides quite divergent results, which hardly offer overall conclusions for the influence of drug shape on the resulting FPF. Drug orientation in the airflow, agglomerate strength, effective contact area as well as the detachment ability can be taken into account to reason findings of these experiments. However, these characteristics were changed drug specifically and do not show overall dependencies.

4.3.2 Surface Roughness

Carrier surface roughness – also known as the microstructure of the particle surface – was correlated to the impaction results with respect to carrier particle shape since both particle properties could not be adjusted separately. Figure 4.42 gives the FPF in % (y-axis) plotted against the surface roughness in roughness categories (x-axis) from category 1 (smooth) to 5 (rough) for powder blends consisting of six different mannitol qualities and three spray dried SBS batches.

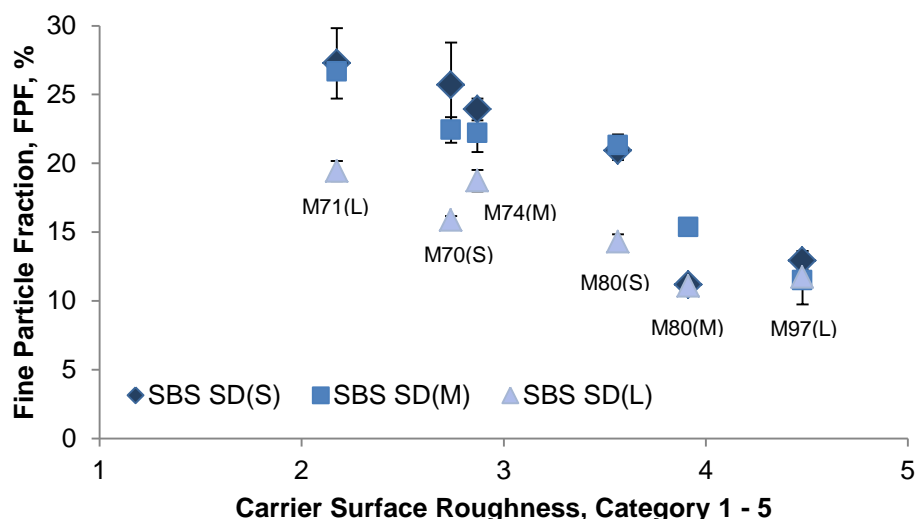


Figure 4.42 - FPF \pm StD in % (y-axis) of powder blends consisting of six chosen mannitol batches (M70(S)/M71(L)/M74(M)/ M80(S)/M80(M)/M97(L)) and three different drug qualities (SBS SD(S/M/L)) related to the surface roughness as evaluated by categorisation of SEM images into five categories from category 1 (smooth) to category 5 (rough) (n=3)

The illustration suggests decreasing FPFs with rising surface roughness categories or rougher carrier surfaces, which needs to be scrutinised since particle shape revealed similar trends for the same powder blends. The main impact on the aerodynamic performance was most likely triggered by particle shape, but supplemented by an additional effect ensuing from the surface roughness.

In more detail, it was found, that the roughest carrier surfaces provided by mannitol M97(L) caused similarly low FPFs for drug particles of all sizes (SBS SD(S/M/L)). Starting from here to smoother surfaces, smaller SBS drug particles performed better than the larger ones. This suggests the surface roughness to impact on powder blends containing SBS batches with a large number of small particles (SBS SD(S/M)) rather than those with larger drug particles (SBS SD(L)).

In fact, SEM images of powder blends containing SBS SD(S) and smooth or rough mannitol carrier particles (Figure 4.43), that were visualised after impaction analysis, obtained fine spray dried SBS particles entrapped by the surface asperities on the mannitol carrier surface.

Images illustrate that remaining drug particles are of small size (below 1 μm). Apparently, rough structures enabled fine drug particles to stay attached during inhalation, so that differences between smooth (Figure 4.43 – A) and rough surface (Figure 4.43 – B) occurred. Only some single spherical drug particles were detected on the smooth surface of mannitol M71(L), while mannitol M97(L) retained several SBS drug particles during impaction analysis. This effect is a factor of the size and number of intermediate spaces between overlying crystalline structures on the carrier surface.

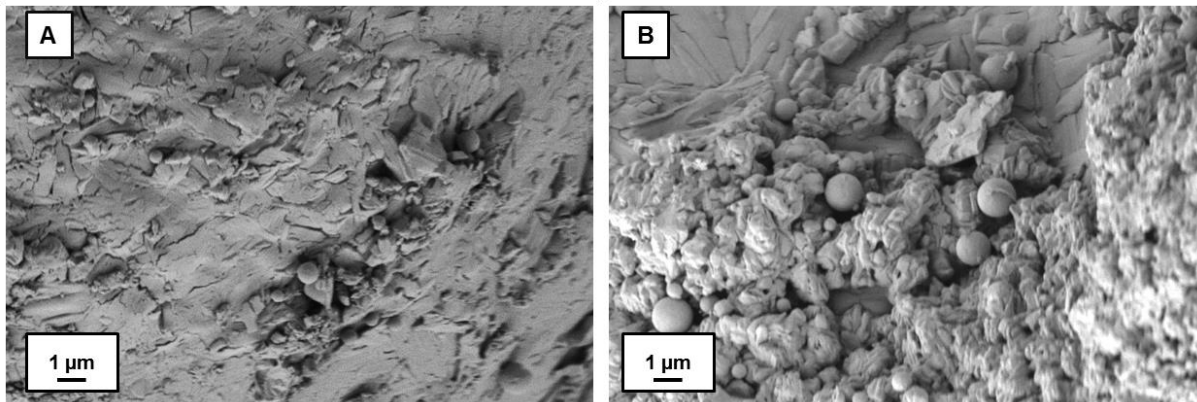


Figure 4.43 – SEM images (5000 fold magnification) of SBS SD(S) attached to the surface of two different mannitol qualities after impaction analysis, A: M71(L); B: M97(L).

Appropriate particle-particle interactions are schematically illustrated in Figure 4.44, which gives a simplified view of either a rough or a smooth surface structure with spherical drug particles of different size attached to the surface. It emphasizes, that smooth carrier surfaces provide the least contact area to spherical drug particles as only a single point of contact exists. Nevertheless, the effective contact area between carrier surface and drug particle needs to be discussed since it strongly depends on the drug size. Larger drug particles exhibit larger effective contact areas per particle than smaller drug particles. The number of contact points increases, when surface asperities occur. This establishes larger effective contact areas for smaller drug particles, but decreases these contact areas for larger drug particles simultaneously as depicted in Figure 4.44.

Not only the effective contact area, but also the ratio of particle mass to effective contact area and with this adhesion forces is of importance to describe particle-particle interactions between drug and carrier. Preferably, smaller particles remain attached to the carrier surface as the ratio mass to effective contact area is low, while the ratio increases rapidly with rising drug particle sizes, which supplements detachment of these particles during inhalation.

Nevertheless, the effect of surface roughness on the inhalation performance of an interactive powder blend is rather low and determined by the size and number of intermediate spaces between rough crystalline structures on the carrier surface.

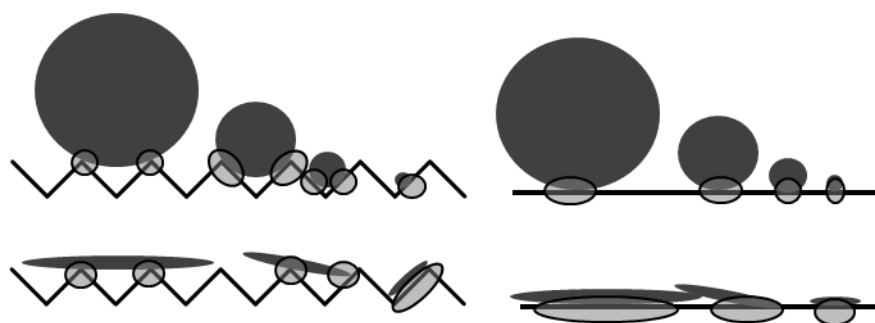


Figure 4.44 – Scheme of contact areas for spherical spray dried API particles (e.g. SBS SD(S/M/L)) of different sizes attached to rough (e.g. M97(L)) or smooth carrier surfaces (e.g. M71(L)) and needle-like jet-milled qualities attached to the same surfaces

Experiments performed here favour smooth surfaces for the hydrophilic model drug SBS since such surfaces reduce the number of contact points for spherical drug particles.

Littringer et al. [20,23] proposed rough surfaces to be advantageous for micronised SBS as this decreases the number of contact points and the effective surface contact area for those needle-like particles, which agrees with the theory displayed here (Figure 4.44). The different drug shape plays an important role for the effective contact area, so that different surface appearances may be beneficial for different drug particles.

To conclude, the connection of aerodynamic performance and surface roughness of a carrier needs to be discussed with respect to the overall shape of a drug particle, but also with focus on the drug shape as both properties influence each other. Surface asperities might hinder the smallest drug particles to be detached from the carrier, but are at the same time beneficial for materials with non-spherical appearance.

4.3.3 Particle size

The particle size was investigated as a parameter for dry powder formulations that has widely been described in literature. This project covered a broad set of different carrier and drug sizes to get a coherent overview about how particle size affects the dispersion of drug particles during inhalation. Necessarily, the observed effects were divided into carrier size and drug size based ones.

4.3.3.1 Carrier Size

Carrier size effects were observed for different model drugs as indicated earlier. Figure 4.45 gives relations between FPF (1st y-axis), mannitol carrier batches (x-axis) and its carrier sizes (2nd y-axis) for four different SBS drug qualities. The four presented mannitol batches were grouped into spherical carriers and indented carriers as not only size, but size in connection to the apparent particle shape was found to affect the impaction results.

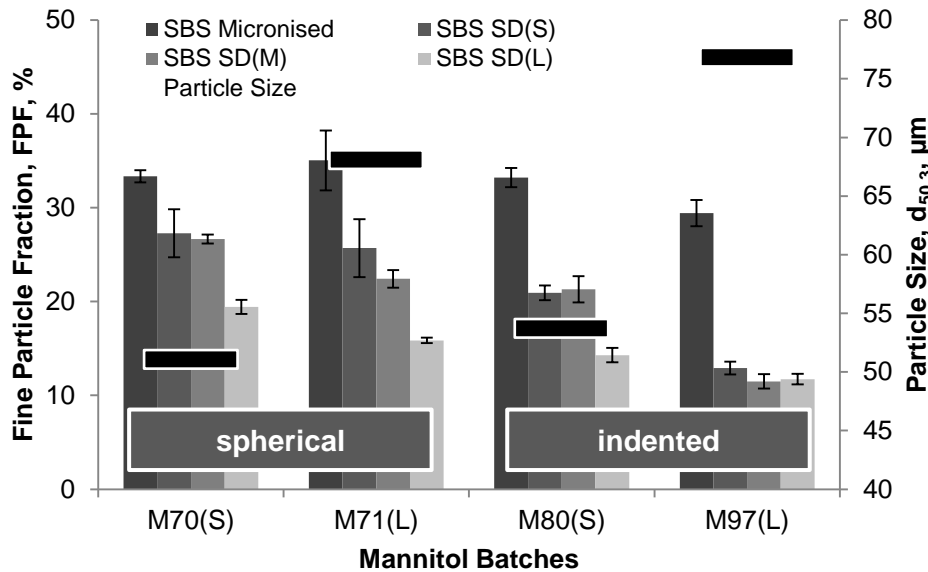


Figure 4.45 - FPF \pm StD in % (1st y-axis, columns of different greyscales) of powder blends consisting of four chosen mannitol batches (M70(S)/M71(L)/M80(S)/M97(L)) and SBS SD(S/M/L) or SBS micronised related to the particle size (black marks) (n=3)

Powder blends investigated here revealed that the FPF of spherical carrier particles was not affected by the carrier size, since the results of blends with SBS micronised, SBS SD(S) and SBS SD(M) do not significantly differ for smaller M70(S) and larger M71(L). In contrast to that, differences in the aerodynamic performance were found for the indented carrier batches M80(S) and M97(L), where the smaller carriers triggered significantly higher FPFs for all SBS qualities, when compared to the larger ones.

The observed effects can be derived from an interplay between carrier size and shape. Obviously, particle size does not affect the dispersion of drug particles, when carriers occur spherical and without indentions, whereas for indented carriers particle size deals as a measure of indentation depth since larger particles are supposed to obtain deeper indentions than smaller ones. In turn, this determines the space provided for drug accumulations in these cavities. Drug particles entrapped in the indentions of smaller particles get easier detached by the airflow than those accumulated in larger ones. This affects the detachment of SBS particles significantly as was observed for small spray dried SBS qualities ($p < 0.01$), but also for SBS SD(L) and SBS micronised ($p < 0.05$).

Similarly, reduced respirable drug fractions of TIO SD or BUD SD were gained from powder blends with the indented carriers M97(L) and M80(M) compared to indented M80(S) as mentioned earlier (Figure 4.35). Slight indentions were suggested to be advantageous for these drugs as they prevent those drug particles from press-on forces. However, deep indentions hinder TIO and BUD particles from being detached during inhalation, which again reduces the FPF for these batches. No carrier size effect was found for lipophilic FOR particles. Results described here agree with findings of Steckel et al. earlier, who mentioned

smaller (lactose monohydrate) carriers to perform better during inhalation than with larger ones [81].

4.3.3.2 Drug Size

Drug size is known to be a crucial parameter that affects the amount of drug, which is enabled to reach the deeper airways of the lung. The FPF as the fraction of particles with an aerodynamic equivalent diameter $< 5 \mu\text{m}$ is strongly depending on the drug size. Three SBS qualities different in size (SBS SD (S/M/L)) were tested by impaction analysis to proof this concept.

Results obtained the smaller SBS batches SBS SD(S) ($d_{50.3} = 2.4 \mu\text{m}$) and SBS SD(M) ($d_{50.3} = 2.8 \mu\text{m}$) to generate larger respirable fractions (FPF = $11.2 \pm 0.3 \%$ – $27.3 \pm 2.6 \%$) compared to the larger SBS batch SBS SD(L) ($d_{50.3} = 3.7 \mu\text{m}$) with the FPF covering a range from $11.1 \pm 0.5 \%$ to $19.4 \pm 0.7 \%$.

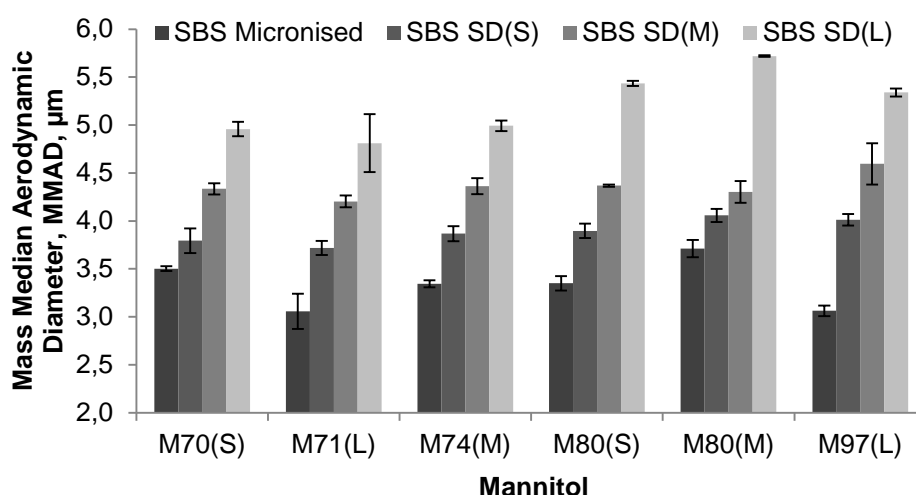


Figure 4.46 – MMAD in $\mu\text{m} \pm \text{StD}$ for four SBS qualities and six chosen mannitol batches

The drugs applied for powder blends differed in size and so in the amount of particles that were below an $d_{50.3} / d_{\text{odyn}}$ of $5 \mu\text{m}$. Laser diffraction analysis found $89.3 \pm 0.5 \%$ of the SBS SD(S) particles below $5 \mu\text{m}$, while only $67.2 \pm 0.2 \%$ of SBS SD(L) remained under the $5 \mu\text{m}$ limit. This corresponds to the MMADs measured for all different SBS drug qualities by impaction analysis (Figure 4.46). SBS SD(S) revealed the lowest values since MMAD was found to range from $3.7 \pm 0.1 \mu\text{m}$ to $4.1 \pm 0.1 \mu\text{m}$ compared to SBS SD(L) that covered MMAD from $4.8 \pm 0.1 \mu\text{m}$ to $5.7 \pm 0.1 \mu\text{m}$.

MMADs were found with larger values compared to the drug sizes measured by laser diffraction. This could be attributed to the tendency to build drug agglomerates that were not dispersed adequately during inhalation. Consequently, those agglomerates impacted earlier mimicking larger particles. Dry dispersion with the dry dispersing unit of the laser

diffraction is recognised to be more efficient than dispersion during inhalation, justifying smaller particle sizes measured with this technique.

The smaller the particles the higher is the tendency to build agglomerates as adhesion forces exceed weight forces. All factors result in higher MMADs compared to the laser diffraction results, even though adequate allocation is not possible.

Accordingly, the inhalable drug fraction can be derived from the initial drug size as larger particles or agglomerates of fine particles impact earlier with respect to their inertial forces as published by Biddiscombe et al. earlier [19].

4.3.4 Drug Hydrophilicity

Four different model drugs that covered a broad range of different $\log P$ values (TIO = -1.8; SBS = 0.6; BUD = 1.9; FOR = 2.2) were compared regarding their aerodynamic performance when blended with the same mannitol carrier particles and investigated by impaction analysis to discover the effect of drug hydrophilicity on particle dispersion.

Results coherently summarised in Section 4.3 revealed drug particles of all model drugs to reach maximum FPFs around 27 – 41 % without any correlation to the respective hydrophilicity. Dependencies were mostly found for drug size or shape or based on the carrier properties as discussed before.

Nevertheless, findings can be related to drug hydrophilicity in terms of detachment behaviour. The chosen model drugs detached in different manners as described above. Hydrophilic SBS was found with strong dependence on the carrier shape with spherical carriers performing best, TIO and BUD were preferably applied with slightly indented carrier particles due to lower press-on forces and FOR particles with either large spherical carriers or indented carriers of every size.

Differences between SBS and FOR detachment can easily be derived from drug hydrophilicity. Particle-particle interactions between carrier and drug are based on several different forces like e.g. polar forces in hydrogen bonds or non-polar van der Waals forces that – in most cases – cannot be quantified by a distinct value yet. Hydrogen bonds as typically observed for molecules with hydrophilic parts or van der Waals forces are of interest for the differentiation of materials with various hydrophilicities. The $\log P$ values of drug and carrier give an idea of the interactions that might occur. The hydrophilic sugar alcohol mannitol ($\log P = -3.1$) can easily build hydrogen bonds but has no hydrophobic parts for appropriate van der Waals forces. TIO ($\log P = -1.8$) or SBS ($\log P = 0.6$) comprise hydrophilic functions that have the ability to build hydrogen bonds, while BUD ($\log P = 1.9$) or FOR ($\log P = 2.2$) are mostly lipophilic with the tendency to interact via weaker van der Waals forces.

Particle-particle interactions observed in these experiments do not provide direct correlations between log P value and detachment manner as not only hydrogen bridge bonds or van der Waals forces but also effects arising from agglomerate strength affect the detachment of drug particles from a carrier. Nevertheless, the values can be applied to make suggestions on the drug detachment.

Figure 4.47 gives an overview over the initial distribution of drug particles on the surface of four different mannitol carriers and the optimal dispersion upon inhalation as most particles got detached in form of single particles. Impaction results suggest different drugs to be affected by different characteristics. SBS particles were easily dispersed even when agglomerates occurred in slight indentions or in form of drug bridges, but were not detached when entrapped in deep indentions. This suggests this drug to build weak drug-to-drug interactions, but to have stronger drug-to-carrier-interactions. Contrary, FOR particles were found to be dispersed best when the occurrence of drug agglomerates was prevented by the carrier choice. Large spherical or deeply indented carriers were beneficial for high FPFs, while agglomerates that occurred for small spherical or slightly indented carriers were not dispersed adequately during inhalation. This behaviour suggests FOR having strong drug-to-drug interactions, but at the same time weak drug-to-carrier interactions as the drug was even detached from deep indentions.

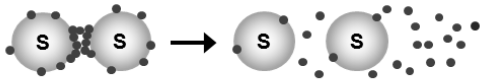
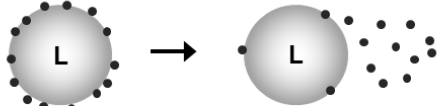
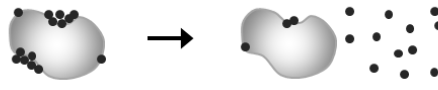
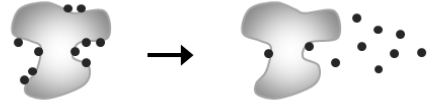
Dispersion during inhalation	SBS	TIO	BUD	FOR
	(+)	(-)	(-)	(-)
	(+)	(-)	(-)	(+)
	(+)(-)	(+)	(+)	(-)
	(-)	(-)	(-)	(+)

Figure 4.47 - Distribution of drug particles on the surface of differently shaped carriers upon blending and dispersion of those drug particles during inhalation (carrier size: S = small / L = large). (+) and (-) indicate how well particles get dispersed from the carriers of different particle shape and size.

Hydrophilic SBS builds hydrogen bonds to the hydrophilic mannitol carrier surface, which results into drug particles that are stronger attached to the surface compared to e.g. lipophilic FOR, whose ability to build such bonds is rather low. Hence, drug entrapment in indentions is favoured for hydrophilic SBS particles, while even low shear or impaction forces during

inhalation last to detach FOR particles even when entrapped in deeper indentions. This concurs with findings described earlier, where SBS detachment was strongly depending on the occurrence of indentions. Even slight indentions lowered the respirable fraction. BUD or TIO containing blends were favoured with those slight indentions as they were not attached as strong as SBS resulting in easier detachment. However, particle-particle interactions of SBS, BUD and TIO particles were strong enough to entrap those drugs in deeper indentions during inhalation. Contrary, lipophilic FOR particles appeared to have the weakest interactive potential, which resulted in adequate dispersion even from deeply indented carriers. However, as mentioned before, there was no effect on the overall FPF of those drugs, but only an effect that suggested the best carrier shape for the different drug particles.

4.3.5 Crystallinity

The influence of crystallinity on drug detachment was gained from experiments performed with micronised and spray dried drug qualities. All spray dried drugs were of fully amorphous quality, while micronised drugs contained crystalline structures. Different mannitol particles were assumed to not affect the drug detachment in terms of crystallinity since all mannitol batches were found to have the same crystalline modification.

Hydrophilic SBS and lipophilic BUD particles were used for powder blends in spray dried and micronised quality as described above. Comparison of crystalline and amorphous particles cannot easily be performed since those different drug qualities are associated with different drug shapes, which are known to affect the aerodynamic performance.

Some assumptions on the effect of crystalline structures can still be made based on the results illustrated here. The use of micronised SBS drug particles lead to increased FPFs compared to amorphous spray dried SBS particles (Figure 4.40). This effect was mainly attributed to different drug shapes as impaction analysis was performed more efficiently for needle-like particles. Nevertheless, amorphous material and its tendency to recrystallise might have an additional reducing effect on the FPF since those particles most likely stay attached to the carrier surface. Experiments in this study were conducted at controlled conditions (21 °C, 35 % rH) to avoid recrystallisation events, which was proved by SEM images (not shown here). Powder blends with spray dried amorphous SBS are more susceptible to recrystallisation than micronised materials that usually show some small amorphous spots at the breaking edges after micronisation even though most of the material appears to be crystalline. Hence, all powder blends, but especially the ones containing spray dried SBS, might be affected by higher relative humidity or uncontrolled conditions, as this allows moisture uptake and recrystallisation.

The comparison of amorphous BUD SD (with higher FPFs) and mostly crystalline micronised BUD (with lower FPFs) cannot directly be correlated to the crystalline state as factors like

particle size or shape exceed effects that possibly arise from crystallinity. The spray dried quality was found with better results than the micronised one even though amorphous structures most likely were expected with lower FPFs due to storage issues.

Conclusively, powder blends with micronised or spray dried SBS are not applicable for devices without desiccants and for the use in everyday life as only low moisture contents keep those products stable. BUD results did most likely not match assumptions for effects arising from crystallinity.

4.3.6 Flowability

SBS drug detachment was further compared to the flow characteristics of the pure mannitol particles as measured with a powder rheometer (Section 4.1.6). Figure 4.48 shows the correlation of powder blends consisting of six different mannitol batches and the three different SBS qualities SBS SD(S/M/L). A clear trend to lower FPFs was observed for rising BFEs or lower mannitol bulk flowability.

These findings can easily be attributed to mannitol properties that were described before since flow characteristics are based on primary particle properties like particle size or shape. As evaluated earlier, the highest BFEs were caused by large indented carrier particles (M97(L)), which in turn provide the deepest indentions for SBS drug particles. The according FPFs are quite low for SBS particles of every size (SBS SD(S/M/L) with an FPF < 12 %). Lowest resistance was found for small spherical carriers (M70(S)) that triggered the best aerodynamic performance for this drug quality. SBS particles were evenly distributed over the whole surface or built drug bridges that were dispersed easily.

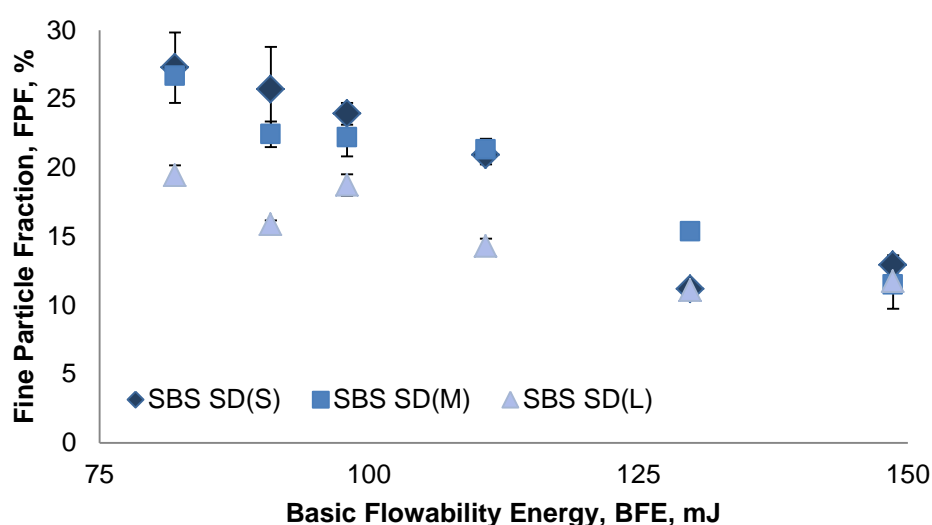


Figure 4.48 - FPF \pm StD in % (y-axis) of powder blends consisting of six chosen mannitol batches (M70(S)/M71(L)/M74(M)/ M80(S)/M80(M)/M97(L)) and SBS SD(S/M/L) related to the BFE in mJ (x-axis) (n=3)

In general, it is important to generate powder blends with appropriate flow properties. All bulk batches used here were of good overall flowability as evaluated with Carrs Index ($CI < 15$), but differed in the BFE due to different particle properties. The delivered mass per shot with the Novolizer[®] was reproducible with a relative standard deviation below 10 % for all powder blends, so that differences in the impaction results can be correlated to carrier properties like size or shape.

4.3.7 Surface Energy

Surface energy measurements were performed for both, mannitol carrier particles and various drug particles. Correlations between dispersive surface energies and according FPFs were hardly detected for any of the different powder blends.

Most mannitol qualities were found with similar dispersive surface energies, where only mannitol quality M71(L) gave reduced values (Section 4.1.8). At the same time, this batch occurred as the most spherical one, so that appropriate findings are assigned to carrier shape rather than to the reduced dispersive surface energy.

Similarly, surface energies of drug particles covered a wide range from 31 mJ m^{-2} for FOR SD to 60 mJ m^{-2} for BUD micronised, but did not enable correlations to FPF level or trends in the detachment of different APIs. Nevertheless, mannitol carrier particles were found to have heterogeneous surfaces in terms of dispersive surface energies, which gave rise to the assumption that some spots on the carrier surface might adhere particles (e.g. drug particles) tighter than other spots which in turn implemented the use of mannitol fines to increase the respirable fraction as discussed in the following section.

4.3.8 Influence of Fines

Based on results that indicated mannitol carrier surfaces to be heterogeneous in dispersive surface energy, mannitol fines were prepared and added prior to the addition of drug particles to generate ternary interactive powder blends consisting of mannitol carrier, mannitol fines and SBS SD(S). Several studies based on lactose monohydrate deal with the addition of fines targeting an increase of the FPF [27,145,146]. One mentions active sites as high energy spots on the surface to bind particles stronger than the rest of the surface [7,72,138]. This theory was used as basis for a row of powder blends containing different concentrations of mannitol fines ($C_{\text{fines}} = 0 - 10 \text{ \% [w/w]}$). Results are summarised in Table 4.12, which gives the FPFs in $\% \pm \text{StD}$, and are further illustrated in Figure 4.49.

Table 4.12 – FPF \pm StD in % of mannitol M80(S) as carrier, SBS SD and different amounts of mannitol fines (n=3)

SBS plus Mannitol Fines

C_{Fines} , % [w/w]	FPF, %	StD
0	19.8	1.1
2	22.9	1.7
4	25.2	0.7
6	26.6	1.4
8	29.5	0.4
10	31.5	0.2

The aerodynamic performances of all powder blends were compared to a blend containing only mannitol M74(M) and SBS SD as a control. Experiments with rising c_{fines} generated constantly rising FPFs starting from 19.8 ± 1.1 % for blends without fines and resulting in blends containing 10 % fines with an FPF of 31.5 ± 0.2 %. The obtained correlation was found to be linear ($R^2 = 0.992$).

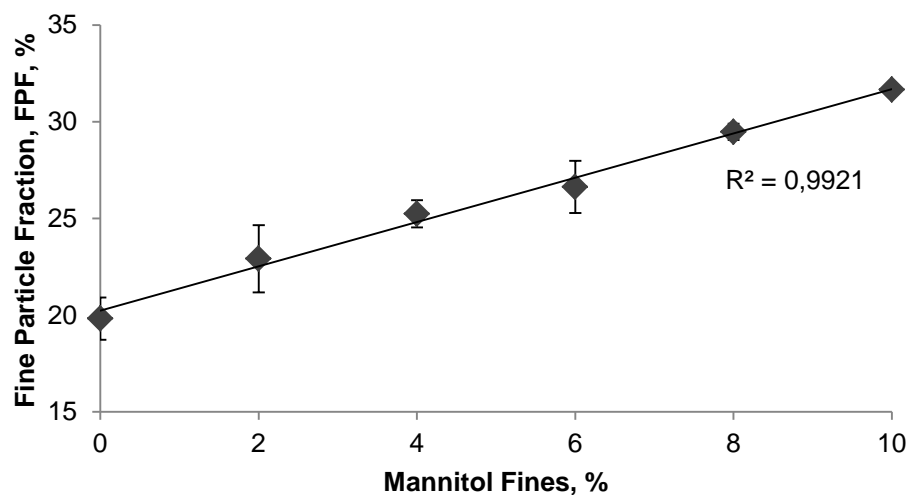


Figure 4.49 – FPF in % \pm StD (y-axis) for powder blends with mannitol M74(M), SBS SD and different concentrations of mannitol fines (x-axis) ($n=3$)

SEM visualisations revealed blends containing 2 % [w/w] mannitol fines (Figure 4.50 – A) to build small bridges consisting of spherical SBS SD and fines. The same bridges were also observed for blends containing 10 % [w/w] mannitol fines, but were supplemented by agglomerates attached to the carrier surface (Figure 4.50 – B).

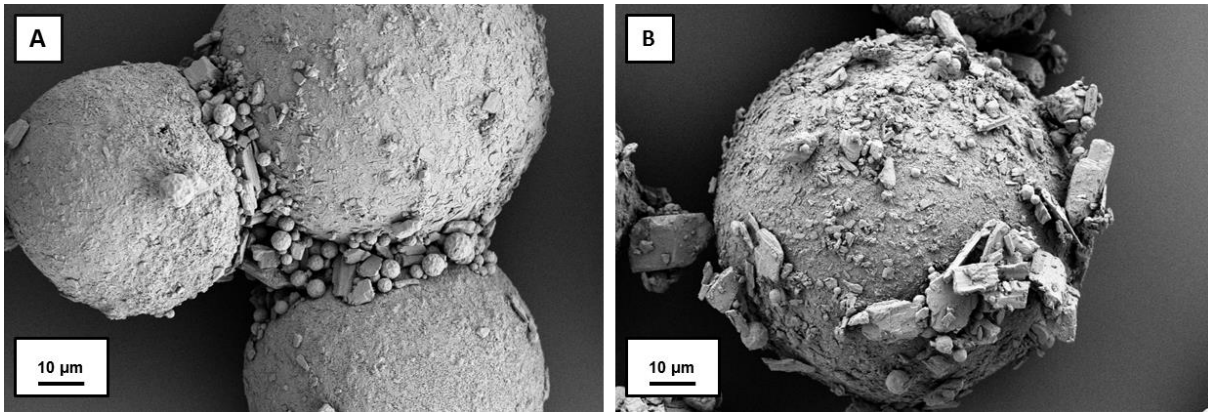


Figure 4.50 – SEM images (1,000-fold magnification) of interactive powder blends consisting of A: 97 % mannitol M74(M), 1 % SBS SD and 2 % mannitol fines; B: 89 % mannitol M74(M), 1 % SBS SD and 10 % mannitol fines

Experiments were performed with a maximum concentration of 10 % [w/w] since powder flow and accurate dosing was not adequate for higher concentrations. The positive effect on drug dispersion increased up to $c_{fines} = 10\%$, while further addition of fines rendered dosing impossible. Following this, the best aerodynamic performance was achieved for interactive powder blends containing the highest fines concentration possible.

Mechanisms behind this improvement can be correlated to theories postulated for blends containing lactose monohydrate [27]. It can be assumed that a small amount of mannitol fines lasts to cover high energy spots with respect to the active sites theory. SBS particles bind at spots of lower energy and detach easier from the surface during inhalation, which in turn results in higher FPFs [27,71].

This theory concurs with the buffer hypothesis, which describes that lactose fines of larger size than the drug particles preserve those drug particles from press-on forces, which in turn results in higher FPFs [24,27]. Mannitol fines were used with a $d_{50.3}$ of 4.1 μm compared to drug particles of $d_{50.3} = 2.4\ \mu\text{m}$ in this study to protect SBS drug particles from press-on forces according to the proposed buffer effect.

Further improvement can be gained, when more fines are added to build agglomerates on the carrier surface. This so-called agglomeration theory indicates that agglomerates of mannitol fines and drug get dispersed easier than formulations consisting of drug and carrier only [7,71]. Mannitol fines were chosen with a size that was small enough to build agglomerates, but large enough to trigger easy dispersion of the drug. These agglomerates supplement the buffer hypothesis as described above [24].

To conclude, the addition of fines to powder blends containing spray dried mannitol particles and drug particles enables reasonable improvements during inhalation. The maximum concentration of fines is restricted by flow properties and with this accurate dosing of the

powder blend when administered with a DPI. Capsule based inhaler devices might be advantageous for such formulations as free powder flow is not necessary during inhalation.

4.3.9 Impact of the device

All powder blends were investigated using the Novolizer[®] as device despite the low apparent density of the mannitol batches used [20,23]. The Novolizer[®] with its impaction walls was mainly constructed for larger carrier particles with higher densities to use appropriate impaction forces for dispersion of the drug [75].

This part of the study dealt with the Easyhaler[®] as an alternative device without cyclone or impaction walls to simplify drug dispersion. Unsurprisingly, experiments resulted in comparably low FPFs as summarised in Table 4.13.

A maximum FPF of 4.2 ± 0.4 % was measured for blends containing mannitol M70(S), which was at the same time the batch performing best with the Novolizer[®] (FPF = 27.3 ± 2.6 %), while the minimum of 1.8 ± 0.0 % for powder blends containing M80(M) matched with the same batch performing worst with the Novolizer[®] (FPF = 11.2 ± 0.3 %).

Table 4.13 – FPF \pm StD in % of six different mannitol batches and SBS SD(S) administered with Novolizer and Easyhaler (n=3)

Mannitol batches			SBS SD(S)			
DoE: Naming		Results: Extra Label- ling	Novolizer [®]		Easyhaler [®]	
Run Order	Exp Name		FPF, %	StD	FPF, %	StD
Run 9	N5	M70(S)	27.3	2.6	4.2	0.4
Run 10	N1	M71(L)	25.7	3.1	3.4	0.1
Run 14	N9	M74(M)	23.9	0.8	3.7	0.2
Run 13	N14	M80(S)	20.9	0.7	2.2	0.2
Run 2	N19	M80(M)	11.2	0.3	1.8	0.0
Run 11	N4	M97(L)	12.9	0.7	3.2	0.3

Trends observed for both inhaler devices were similar but on different levels as illustrated in Figure 4.51. Both revealed mannitol particles dried at higher outlet temperatures (and with more indentions) to perform worse than those with spherical character. Only mannitol M97(L)

did not follow this trend when dispersed with the Easyhaler[®] in accordance to results gained for experiments with the Novolizer[®].

The Easyhaler[®] led to remarkably lower respirable fractions than the Novolizer[®] which can mainly be attributed to the design of the device but also to carrier particle properties. Dispersion with the Easyhaler[®] is mainly based on the laminar air stream during inhalation without any further dispersion mechanisms. Drug particles are preferably detached from large carriers with respective inertia. Low density carrier particles like used in these experiments are disadvantageous as they can easily follow the inspiratory air stream resulting in a low velocity gradient between inhaled air and carrier particle and thus low forces for particle detachment and reduced FPFs. Similarly, low carrier particle densities negatively affect dispersion with the Novolizer[®]. However, the device design compensates the negative effect as cyclone and impaction walls provide adequate dispersion of the interactive powder blends. Larger respirable fractions simplify the correlation of particle properties and arising FPF, which finally reasons the Novolizer[®] to be the first choice device for the experiments described here.

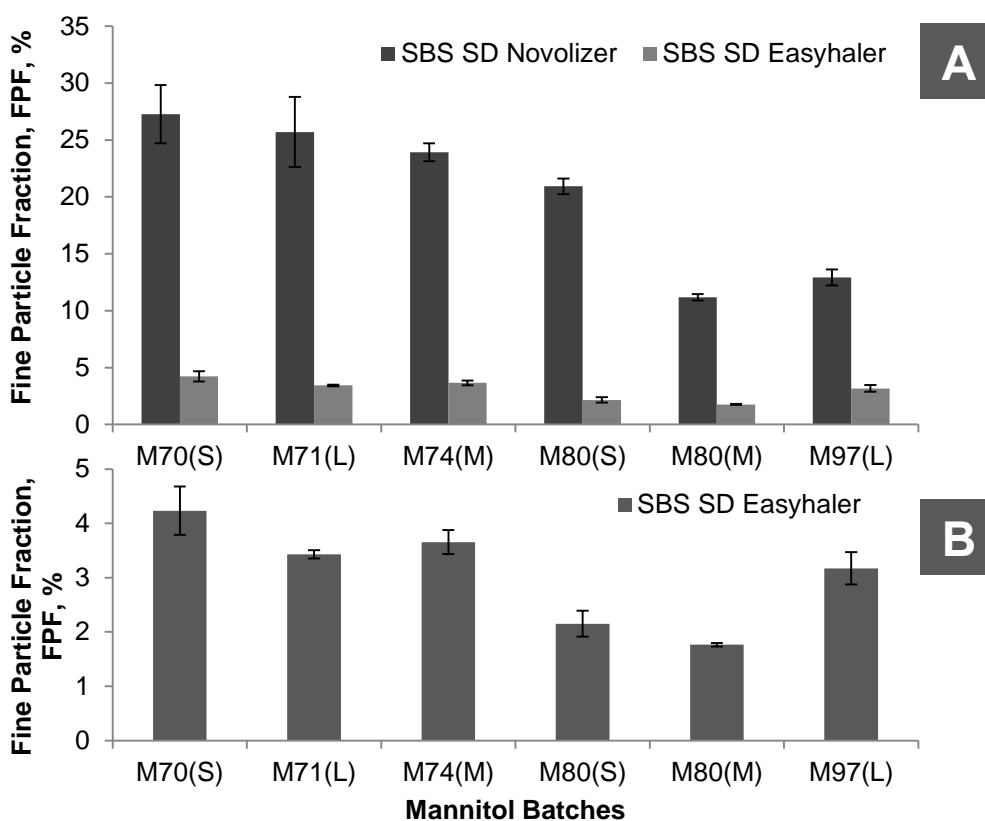


Figure 4.51 – FPF ± StD in % (y-axis) for powder blends consisting of six different mannitol batches (M70(S)/M71(L)/M74(M)/M80(S)/M80(M)/M97(L) and SBS SD. A: results for application with Novolizer[®] and Easyhaler[®]; B: results for application with Easyhaler[®] only (n=3)

5 Overall Findings and Future Perspectives

This work highlights the relevance of process control with respect to the impact on particle-particle interactions in a dry powder formulation for inhalation purposes. The carrier-based dry powder formulations consisted of engineered drug and carrier particles as mostly prepared by spray drying in the scope of this priority program. It could be shown that drug dispersion was crucially influenced by particle properties like size or morphology of both carrier and drug particles. Thus, control over the spray drying process was of tremendous importance to control drug and carrier characteristics.

Engineered mannitol carrier particles were successfully generated with a special spray drying approach that was particularly aiming at narrow particle size distributions to maximise the size control during the process. The laminar rotary atomiser (LamRot) was operated at various rotation speeds to control the droplet size based on according acceleration forces, where the smallest droplets were gained in experiments with the highest rotation speed. Effects on the carrier size were supplementary detected for alternating drying temperatures as these determine the drying rate and therefore the moment of shell formation in association to the surface concentration of the solute mannitol. The drying temperature was further varied to affect the carrier morphology as separately examined for particle shape and surface roughness. Spray drying experiments in collaboration to levitation based single droplet trials performed by Grosshans et al. were successfully conducted to improve knowledge about the drying history of differently shaped spray dried mannitol particles [142].

It was found that indentions that occurred for higher outlet temperatures could be associated to the temperature inside the early particle as this determines the physical condition of the solvent. The appearance of water vapour triggered an expansion of the shell that further resulted into collapsing particle shells during cooling and condensation of the water vapour. Likewise, surface roughness could be correlated to the drying temperature as mannitol solution was pressed through pores in the shell temperature-dependently to finally build rough structures of recrystallised mannitol on the carrier surface.

Profound knowledge about all parameters that influence the product properties enables the preparation of tailor-made carrier particles for inhalation. Particle-particle interactions between drugs and carriers are well-known to be affected by size and morphology so that maximum control over the engineering approach helps to govern these interactions.

In fact, differently shaped and sized mannitol batches were chosen to be blended with four different drugs. Salbutamol sulphate, tiotropium bromide, budesonide and formoterol fumarate were successfully spray dried to gain inhalable particles ranging from 1.8 to 2.5 μm in size. The spray drying approach was chosen to generate spherical particles as controlled

by the shape of the spray dried droplet to idealise the setup for particle-particle interactions during an aerodynamic characterisation of spray dried carrier and drug particles.

Impaction analysis as required by the European Pharmacopoeia to assess the fraction of fine particles indicated that the dispersion of different drug particles during inhalation is based on different drug-depending mechanisms. The carrier shape was found as the main factor of influence on the fine particle fraction. Salbutamol sulphate was the only drug exhibiting a direct correlation between particle shape and respirable drug fraction as indented carriers performed the worst and spherical ones enabled the largest amount of drug to penetrate the stages of interest in the impactor. Tiotropium bromide and budesonide dispersion were influenced with reference to press-on forces, as slight indentions that provide shelter from those forces during blending are preferred to mostly spherical carriers. Budesonide or tiotropium bromide particles were adhered tighter to the surface when no indentions occurred or got trapped when indentation depth was appropriate as observed for large carriers prepared at higher outlet temperatures. An interplay of carrier shape and agglomerate strength was suggested to govern formoterol fumarate dispersion. Deeply indented carriers or large spherical carriers performed best, while slightly indented ones or small spherical ones resulted in reduced fine particle fractions.

Several further carrier or drug properties were examined in this thesis and described with significant effects on the respirable fraction. Carrier size was found to worsen the aerodynamic performance shape dependency as larger carriers comprise deeper indentions for the entrapment of drug particles. Drug size and shape was of importance as it determines where drug particles impact and how well they orientate in the inspiratory air stream to penetrate the deeper airways of the lung. It further affects the tendency to build agglomerates since cohesion proceeds depending on size and contact area.

Coherently, this work concludes that a broad range of particle-particle interactions need to be considered for the development of innovative dry powder formulations. Spray drying was proved as an excellent engineering approach to control particle properties in the preparation of carrier and drug particles and therefore to affect inter-particle forces. However, an overall correlation between drug dispersion and related particle properties that enables prediction for further drugs cannot be drawn since dispersion mechanisms could not be linked to respective properties.

6 Summary

Drug delivery to the lungs for the treatment of respiratory diseases was proved to exceed all other therapeutic strategies and is routinely used in pulmonary therapies today. The lung has further been recognised as a potential target for systemic drug uptake that prevents administered drugs from first-pass metabolisms. Particles for lung penetration require aerodynamic particles sizes between 0.5 μm and 5.0 μm to reach the respiratory zone of the lungs. The European Pharmacopoeia lists nebulisers, pressurised metered-dose inhalers, non-pressurised metered dose inhalers and dry powder inhalers as suitable devices for inhalation. Dry powder formulations as focussed on in this thesis are suggested to be beneficial in terms of long term stability of drugs and administration efficacy due to the absence of a solvent. Most marketed products apply the well-known system of fine drug particles attached to the surface of coarse carrier particles to overcome the cohesiveness of drugs with sizes applicable for lung penetration. The adhered particles are meant to detach from the carrier surface by inspiratory forces during inhalation to follow the air into the lungs. Adhesion of carrier and drug as well as cohesion between several drug particles is known to be affected by a broad range of different particle-particle interactions.

However, only little is known about the mechanistic understanding of those interactions in interactive powder blends and its magnitude of force despite several years of intensive research. This work was therefore designed to particularly focus on adhesion and cohesion as suggested for carrier and various drug particles and to discover how they got affected. Particle preparation was mostly performed by spray drying as an approach that provides maximum control over the targeted particle properties.

Mannitol was chosen as a sugar alcohol for carrier particles instead of the commonly used lactose monohydrate with regards to storage stability since lactose might be incompatible for all formulations containing primary amines and is known to comprise amorphous contents upon spray drying. A laminar rotary atomiser particularly designed to generate very narrow particle size distributions was implemented for the preparation of carrier particles. Spray drying was conducted in the framework of a design of experiments to investigate the drying kinetics of bi-component mannitol water droplets as this provides knowledge about the appearance of the carriers in terms of size and morphology. The carrier size was mainly observed as a function of the rotation speed and, therefore, based on the emerging droplet size with a small supplementary effect by the drying temperature that affected the drying rate resulting in a faster onset of shell formation for higher temperatures. The process temperature was further varied to affect the carrier shape as different particle shapes were described earlier to affect drug dispersion during inhalation. Improved knowledge about how

indentions and surface asperities occur temperature-dependently was investigated by single droplet drying experiments with a levitator at the University of Hamburg as this is of importance for the engineering of tailor-made carrier particles. Higher drying temperatures triggered an expansion of the early shell based on the appearance of water vapour that further condensed during cooling and caused the shell to collapse while lower temperatures enable the preparation of spherical carriers since less water vapour occurs. Further characterisations enabled good correlations for the bulk flowability of these mannitol carriers, where spherical particles performed better than indented ones with regards to mechanical interlocking. Appropriate BET surface areas were successfully linked to particle properties like size and morphology since small, rough, and indented carriers were found with the larger BET surface areas than those of large size and with smooth and spherical character.

A controlled engineering process is of importance not only for carriers but also for drug particles as both might crucially affect the aerodynamic behaviour. Salbutamol sulphate, tiotropium bromide, budesonide and formoterol fumarate were prepared with a commercially available laboratory spray dryer resulting in spherical particles at a size range from 1.8 to 2.4 μm . The drugs were chosen with respect to different intrinsic properties like hydrophilicity, hygroscopicity and surface energies to possibly detect influences by those.

Various mannitol carriers different in size and shape were blended with those drug batches to generate interactive powder blends for aerodynamic characterisations. Investigations on the outer particle properties found the carrier shape to have the main influence on drug dispersion and respirable fraction. The occurrence of indentions influenced the impaction analysis drug-dependently. Different mechanisms were described for salbutamol sulphate that was dispersed best from spherical carriers, tiotropium bromide and budesonide that were preferably detached from slightly indented carriers, and formoterol fumarate that performed best when blended with deeply indented or large and spherical carriers. Different drugs demand different carriers for the best performance based on the mechanisms of dispersion. Tiotropium bromide and budesonide need to be sheltered from press-on forces during blending as those forces reduced the respirable fraction. Formoterol fumarate was generally detached easily, but exhibited tremendous agglomerate strength, so that carriers need to prevent the occurrence of agglomerates. Therefore, large spherical carriers or those with several deep indentions were preferred. A direct correlation between particle shape and drug dispersion was observed for salbutamol sulphate, which performed best when spherical carriers were used. Supplementary, carrier size was of importance for indented carriers as larger carriers provide deeper indentions than smaller ones to finally entrap more drug particles.

The work was extended to further drug properties like size and shape, but also to the influence of properties like crystallinity, hydrophilicity, hygroscopicity or surface energy. Drug particle size was of importance since larger drug batches comprise higher amounts of particles that are larger than 5 μm , which reduced the respirable fraction. The effect of drug shape was tested by comparison to micronised qualities of salbutamol sulphate and budesonide to spray dried batches, resulting in quite divergent but significant results that suggest the shape to have major impact on the fine particle fraction during inhalation. Unfortunately, intrinsic properties like hydrophilicity, crystallinity, hygroscopicity or surface energy could not particularly be correlated to impaction results.

Further, different concentrations of mannitol fines were added to the powder blends to discover whether theorems summarised by Grasmeijer et al. on the basis of lactose monohydrate are applicable for powder blends containing mannitol as a carrier [27]. In fact, rising concentrations were found to steadily increase the respirable drug fraction. Powder blends performed best with 10 % fines since further addition of fines decreased dosing reproducibility.

Supplementary trials with the Easyhaler[®] as another inhaler device found vastly decreased fine particle fractions that however exhibited similar trends in terms of carrier particle shape and respirable fraction. Nevertheless, the Novolizer[®] was acknowledged as the preferred device to detect particle-particle interactions since even low density carrier particles like used here got dispersed adequately due to cyclone and impaction walls of the device.

Overall, results presented in this work allow insight into the accurate preparation of engineered carrier and drug particles and the particle-particle interactions that arise from respective particle properties. However, the effects of intrinsic particle properties on the aerodynamic performance will need further investigations in the future.

7 Summary (German)

Die pulmonale Verabreichung von Arzneistoffen mittels Inhalation ist heutzutage als Routine-Therapie in den Leitfäden zur Behandlung von Asthma oder der chronisch obstruktiven Lungenerkrankung verankert. Zusätzlich ist die Lunge vor allem auf Grund einer möglichen Umgehung des First-Pass-Effektes im Fokus für die systemische Aufnahme von Arzneistoffen und der daraus resultierenden Behandlung weiterer Krankheiten. Eine aerodynamische Partikelgröße von 0.5 – 5.0 μm – die so genannte Feinpartikelfraktion – ist die Grundvoraussetzung, um das Erreichen der Lunge und damit die Aufnahme über das respiratorische Epithel zu ermöglichen. Das Europäische Arzneibuch nennt mit Verneblern, Druckgas-Dosieraerosolen, Normaldruck-Dosieraerosolen und Trockenpulver-Inhalatoren vier verschiedene Devices, die für die Inhalations-Therapie geeignet sind. Formulierungen zur Trockenpulver-Inhalation, wie in dieser Arbeit verwendet, zeigen hierbei ausgeprägte Vorteile in Bezug auf die resultierende Dispergiereffektivität sowie hinsichtlich der Lagerstabilität. Trägerbasierte Systeme, bei denen mikronisierter Arzneistoff an der Oberfläche eines groben Trägerpartikels adhärert, stellen die größte Anzahl der derzeit zugelassenen Produkte, wobei die Arzneistoffpartikel durch Scherkräfte während der Inhalation abgelöst werden, um dem Luftstrom in die Lunge zu folgen. Die hierbei herrschenden Adhäsionskräfte zwischen Träger und Arzneistoff sowie die Kohäsionskräfte zwischen den Arzneistoffpartikeln werden durch viele verschiedene Faktoren beeinflusst.

Die Hintergründe dieser Interaktionen sowie die Intensität der hierbei auftretenden Kräfte sind trotz langjähriger intensiver Forschung nur oberflächlich bekannt. Diese Arbeit zielt daher insbesondere auf Adhäsions- und Kohäsionskräfte zwischen verschiedenen Arzneistoffpartikeln und Trägerpartikeln sowie auf die Mechanismen, die diese Kräfte beeinflussen. Um die resultierenden Partikeleigenschaften zu kontrollieren, wurden die meisten Träger- und Arzneistoffchargen mittels Sprühtrocknung hergestellt.

Die Trägerpartikel wurden aus Mannitol hergestellt, da sich die amorphen Anteile eines sprühgetrockneten Laktose-Produktes nachteilig auf die Lagerstabilität auswirken können sowie die chemische Stabilität von Arzneistoffen durch den reduzierenden Charakter der Laktose beeinflusst werden kann. Die Sprühtrocknung der Trägerpartikel wurde im Rahmen eines Versuchsplanes durchgeführt, wobei ein spezieller laminarer Rotationszerstäuber angewendet wurde, um enge Partikelgrößenverteilungen zu erzeugen. Hierbei wurde zunächst der Einfluss der Trocknungskinetik auf Partikelgröße und –morphologie studiert. Die Trägergröße variierte hierbei vor allem in Abhängigkeit von der Zerstäuber-Rotationsgeschwindigkeit, da diese die Tropfengröße beeinflusst. Ein geringerer zusätzlicher Einfluss wurde für die Prozesstemperatur detektiert, da diese über die Trocknungsrate den

Moment der Hüllbildung bestimmt. Zusätzliches Prozessverständnis hinsichtlich der temperaturabhängig auftretenden Trägermorphologie wurde in Trocknungsexperimenten an levitierenden Einzeltropfen an der Universität Hamburg erlangt, da dies für die Herstellung von Partikeln mit kontrollierten Eigenschaften von großem Interesse ist. Höhere Prozesstemperaturen waren hier ursächlich für eine wasserdampfbasierte Expansion der initialen Hülle, die im Folgenden während des Abkühlens, einhergehend mit der Kondensation des Wasserdampfes, wieder kollabiert und die beobachteten Vertiefungen aufweist. Für niedrigere Prozesstemperaturen wird angenommen, dass kein Wasserdampf entsteht, weshalb sowohl die Partikelexpansion als auch die Eindellungen auf der Oberfläche des Partikels ausbleiben. Im Weiteren wurden Abhängigkeiten für die Fließfähigkeit der hergestellten Trägermaterialien untersucht. Hierbei wurden sphärische Partikel auf Grund des geringeren Potentials zu mechanischer Verzahnung besser bewertet als die eingedellten Pendants. Gleichzeitig wurde die BET Oberfläche sämtlicher Chargen ermittelt, wobei die Oberfläche basierend auf der Partikelgröße, Partikelform und Oberflächenrauheit variierte.

Kontrollierte Prozesstechnik ist in der Trockenpulver-Formulierung nicht nur für die Trägerpartikel von großem Interesse, sondern auch für sämtliche Arzneistoffpartikel, da die Partikel-Partikel-Interaktionen auf einem Zusammenspiel zwischen beiden Komponenten beruhen. Salbutamolsulfat, Tiotropiumbromid, Budesonid und Formoterolfumarat wurden mittels eines kommerziell erhältlichen Sprühtrockners im Größenbereich von $d_{50.3} = 1.8$ bis $2.4 \mu\text{m}$ getrocknet, wobei sie auf ihren intrinsischen Eigenschaften beruhend ausgewählt wurden. Einflüsse seitens Hydrophilie, Hygroskopizität, Kristallinität oder der jeweiligen Oberflächenenergie sollten so untersucht werden.

Ausgewählte Mannitol-Trägerpartikel mit unterschiedlichen Partikelgrößen und -formen wurden im Folgenden mit sämtlichen Arzneistoffchargen gemischt, um interaktive Mischungen für die aerodynamische Charakterisierung zu erzeugen. Einflüsse auf die Feinpartikelfraktion nach erfolgter Impaktionsanalyse wurden vor allem der Form der Trägerpartikel zugeordnet, wobei die Mechanismen der Arzneistoffdispergierung vor allem arzneistoffspezifisch auftraten und keine generellen Schlüsse zuließen. Sphärische Trägerpartikel erzielten die besten Ergebnisse für sprühgetrocknetes Salbutamolsulfat, während Tiotropiumbromid und Budesonid nach Mischung mit leicht eingedellten Mannitolträgern besser dispergiert werden konnten. Die Dispergierung von Formoterolfumarat erfolgte wiederum bevorzugt von tief eingedellten oder großen sphärischen Trägerpartikeln. Verschiedene Arzneistoffpartikel zeigten unterschiedliche Anforderungen an die perfekten Trägerpartikel. Leichte Dellen erwiesen sich als nützlicher Schutz vor Aufpresskräften für Tiotropiumbromid und Budesonid während des Mischvorgangs, was wiederum die Dispergierfähigkeit erhöhte. Die Ablösung von Formoterolfumarat erwies sich als generell vereinfacht, da selbst größere Vertiefungen eine

Ablösung nicht behinderten. Nachteilig erwiesen sich lediglich Trägerpartikel, die eine Agglomeratbildung förderten, so dass große sphärische oder tief eingedellte Träger bevorzugt eingesetzt werden sollten. Salbutamolsulfat zeigte als einziger Arzneistoff eine direkte Korrelation zwischen Feinpartikelfraktion und Partikelform. Die Trägerpartikelgröße war vor allem für eingedellte Partikel von Interesse, da die Tiefe der entsprechenden Dellen und damit die Wahrscheinlichkeit Arzneistoffpartikel festzuhalten von der Trägergröße abhängt.

Im Weiteren wurden Arzneistoffgröße und -form, aber auch Arzneistoffeigenschaften wie die Kristallinität, Hydrophilie, Hygroskopizität und Oberflächenenergie untersucht. Hierbei wurde die Partikelgröße des Arzneistoffs als wichtiger Faktor ausgemacht, da hierüber die Fraktion an Partikeln mit einer Größe $< 5 \mu\text{m}$ bestimmt wird. Die Arzneistoffform, getestet mittels Vergleich von sphärischem und luftstrahl-gemahlenem Salbutamolsulfat und Budesonid, zeigte signifikante Unterschiede in der Feinpartikelfraktion, die einen eindeutigen Einfluss der Partikelform suggerieren. Allgemeingültige Aussagen hinsichtlich eines Einflusses basierend auf den intrinsischen Arzneistoffeigenschaften ließen sich anhand der aerodynamischen Charakterisierung nicht treffen.

Weiterführende Untersuchungen zielten auf die seitens Grasmeijer et al. zusammengefassten Theorien, die feine Laktose zur Unterstützung der Dispergierung während der Inhalation verwendet haben [27]. Die Zugabe von feinem Mannitol zu den Mischungen zeigte eine sich kontinuierlich verbessernde Dispergierung mit steigendem Feinanteil analog zu Ergebnissen für Mischungen mit Laktose-Monohydrat. Ein Feinanteil von 10 % erwies sich als optimal, da die Dosiergenauigkeit bei höherem Feinanteil nicht mehr gegeben war.

Zusätzliche Untersuchungen mit dem Easyhaler[®] als Inhalations-Device zeigten ebenfalls trägerformabhängige Ergebnisse, die jedoch auf weitaus geringerem Feinpartikelfraktions-Niveau beobachtet wurden. Die Verwendung des Novolizers[®] wurde entsprechend bevorzugt, da selbst Partikel mit geringer Dichte – wie in diesem Projekt verwendet – leicht dispergiert wurden, um so auf interpartikuläre Wechselwirkungen zu schließen.

Diese Arbeit bietet einen breit aufgestellten Gesamtüberblick hinsichtlich der reproduzierbaren Herstellung von Träger- und Arzneistoffpartikeln mit maßgeschneiderten Partikeleigenschaften sowie der Partikel-Partikel-Interaktionen zwischen diesen Partikeln basierend auf den jeweiligen Partikeleigenschaften.

8 Appendix

8.1 HPLC Methods

8.1.1 Salbutamol Sulphate

Equipment: Waters HPLC System, Waters Corp., Milford, USA), evaluated with Empower[®] Pro 2 software, Waters Corp., Milford, USA

Stationary phase: LiChroCART[®] 125-4
LiChrospher[®] 100 RP-18 (5 µm)
with pre-column

Mobile phase: 78 % buffer (2.87 g • L⁻¹ sodium heptansulfonate + 2.5 g • L⁻¹ KH₂PO₄ (0.2 mmol), pH adjusted to 3.65 with ortho-phosphoric acid 85 %)
22 % acetonitrile

Flow rate: 0.8 mL • min⁻¹

Detection wavelength: 225 nm

Injection volume: 100 µL

Calibrated range: 0.2 – 120 µg • mL⁻¹

Samples were dissolved in 100 % bi-distilled H₂O.

8.1.2 Tiotropium Bromide

Equipment: Agilent G1316A Colcom 1100 Series (Agilent Technologies, Santa Clara, USA)

Stationary phase: LiChroCART[®] 125-4
LiChrospher[®] 100 RP-18 (5 µm)
with pre-column

Mobile phase: 71 % buffer (1.42 g • L⁻¹ sodium heptanesulphonate, pH adjusted to 3.2 with ortho-phosphoric acid 85 %)

	29 % acetonitrile
Flow rate:	2.0 mL • min ⁻¹
Detection wavelength:	239 nm
Injection volume:	100 µL
Oven temperature	40 °C
Calibrated range:	0.2 – 120 µg • mL ⁻¹

Samples were dissolved in 100 % bi-distilled H₂O.

8.1.3 Budesonide

Equipment:	Waters HPLC System, Waters Corp., Milford, USA), evaluated with Empower [®] Pro 2 software, Waters Corp., Milford, USA
Stationary phase:	LiChroCART [®] 125-4 LiChrospher [®] 100 RP-18 (5 µm) with pre-column
Mobile phase:	75 % methanol 25 % bi-distilled H ₂ O
Flow rate:	1.0 mL • min ⁻¹
Detection wavelength:	248 nm
Injection volume:	100 µL
Calibrated range:	0.2 – 100 µg • mL ⁻¹

Samples were dissolved in a mixture of 75 % methanol and 25 % bi-distilled H₂O.

8.1.4 Formoterol Fumarate

Equipment: Agilent G1316A Colcom 1100 Series (Agilent Technologies, Santa Clara, USA),

Stationary phase: LiChroCART® 125-4
LiChrospher® 100 RP-18 (5 µm)
with pre-column

Mobile phase: 45 % buffer (2.34 g • L⁻¹ sodium octanesulphonate + 1.38 g • L⁻¹ NaH₂PO₄ • H₂O, pH adjusted to 3.2 with ortho-phosphoric acid 85 %)

40 % methanol

15 % acetonitrile

Flow rate: 1.0 mL • min⁻¹

Detection wavelength: 214 nm

Injection volume: 100 µL

Oven temperature 25 °C

Calibrated range: 0.2 – 75 µg • mL⁻¹

Samples were dissolved in bi-distilled H₂O (45 %), methanol (40 %) and acetonitrile (15 %).

8.2 Materials

Acetonitrile (HPLC)	Sigma-Aldrich, Inc., St. Louis, USA
Brij [®] 35	Carl Roth GmbH & Co. KG, Karlsruhe, Germany
Budesonide	Minakem SAS, Dunkerque, France
Decane, GC grade	Sigma-Aldrich, Inc., St. Louis, USA
Dichloromethane	Merck KGaA, Darmstadt, Germany
Bi-distilled H ₂ O	freshly produced with in-house Finn Aqua 75, San- Asalo-Sohlberg Corp., Helsinki, Finland
Ethanol, 96 %	Merck KGaA, Darmstadt, Germany
Formoterol fumarate (Batch: FF0041009)	Vamsi Labs Ltd., Maharashtra, India
Helium 5.0	Linda AG, Munich, Germany
Heptane, GC grade	Merck KGaA, Darmstadt, Germany
Hexane, GC grade	AppliChem, Darmstadt, Germany
Hydrogen 5.0	Linde AG, Munich, Germany
Mannitol (Pearlitol [®] 160C)	Roquette Frères Corp., Lestrem, France
Methanol, HPLC grade	Merck KGaA, Darmstadt, Germany
Nitrogen 5.0	Linde AG, Munich, Germany
Nonane, GC grade	Sigma-Aldrich, Inc., St. Louis, USA
Octane, GC grade	Sigma-Aldrich, Inc., St. Louis, USA
o-Phosphoric acid 85 %	Merck KGaA, Darmstadt, Germany
Potassium dihydrogen phosphate	
Purified H ₂ O	BWT Rondomat Duo 2 DVGW, BWT Wassertechnik, Germany
Salbutamol sulphate	SelectchemieAG, Zurich, Switzerland
Sodium heptanesulphonate	Sigma-Aldrich, Inc., St. Louis, USA
Sodium octanesulphonate	Sigma-Aldrich, Inc., St. Louis, USA
Tiotropium bromide (Batch: 150122)	Hangzhou Hyper Chemicals Ltd., Zhejiang, China

8.3 Abbreviations

API	active pharmaceutical ingredient
BUD	budesonide
CCF	central composite face-centred design
CFC	chlorofluorocarbon
COPD	chronic obstructive pulmonary disease
DoE	design of experiments
DPI	dry powder inhalation
DSC	differential scanning calorimetry
DVS	dynamic vapour sorption
ED	emitted dose
EMA	European Medicines Agency
FDA	Food and Drug Agency
FPD	fine particle dose
FPF	fine particle fraction
FOR	formoterol fumarate
GC	gas chromatography
GINA	Global Initiative for Asthma
GOLD	Global Initiative for Chronic Obstructive Lung Diseases
HFA	hydrofluoroalkanes
RP-HPLC	reversed phase high performance liquid chromatography
ICS	inhaled corticosteroids
iGC	inverse gas chromatography
LABA	long-acting β_2 agonist
m	million
M70(S)	mannitol quality dried at $T_{out} = 70$ °C consisting of small particles
M71(L)	mannitol quality dried at $T_{out} = 71$ °C consisting of large particles
M74(M)	mannitol quality dried at $T_{out} = 74$ °C consisting of medium particles

M80(S)	mannitol quality dried at $T_{out} = 80$ °C and consisting of small particles
M80(M)	mannitol quality dried at $T_{out} = 80$ °C consisting of medium particles
M97(L)	mannitol quality dried at $T_{out} = 97$ °C and consisting of large particles
MMAD	mass median aerodynamic diameter
rH	relative humidity
PSD	particle size distribution
RP	reproducibility
SABA	short-acting β_2 agonist
SBS	salbutamol sulphate
SD	spray dried
SEM	scanning electron microscope
StD	standard deviation
TIO	tiotropium bromide
WHO	World Health Organisation
XRPD	X-ray powder diffraction

8.4 Variables

a_i	coefficient (displaying the statistical significance of the term)
BFE	basic flowability energy, mJ g^{-1}
C_{feed}	feed concentration, % [w/w]
C_{Fines}	concentration of mannitol fines
cp	centre point
D	diameter of the spray tower, m
$d_{10.3}$	10 % quantile of the PSD
$d_{50.3}$	median of the PSD
$d_{90.3}$	90 % quantile of the PSD
d_{adyn}	aerodynamic diameter, μm
d_{cs}	cross-sectional diameter, μm
f	number of factor levels
f_x	factor level
γ_s^d	dispersive surface energy, mJ m^{-2}
H	height of the spray tower
l	sampling length, μm
N	number of factors
n	rotation speed
n/n_m	surface occupancy
p/p_0	partial pressure
Q	volumetric flow rate, L min^{-1}
Q^2	prediction quality
R^2	variation coefficient
rpm	rounds per minute, s^{-1}
rH	relative humidity, % rH
T	temperature, $^{\circ}\text{C}$
t	time, s

T_{ax}	axial air stream temperature, °C
T_{feed}	feed temperature, °C
T_{in}	inlet temperature, °C
t_{inh}	valve opening time, s
T_m	melting point, °C
T_{out}	outlet temperature, °C
T_g	glass transition temperature, °C
T_r	recrystallisation temperature, °C
T_{swirl}	swirl air stream temperature, °C
V_{ax}	axial air stream volume, m ³ h ⁻¹
V_{feed}	feed rate, L h ⁻¹
V_{inh}	absolute inhaled volume, 4 L
V_{swirl}	swirl air stream volume, m ³ h ⁻¹
Y	response to the chosen factors
Y_m	feed concentration, % [w/w]

References

- [1] W. Kamin, F. Erdnuss, I. Kramer, Inhalation solutions--which ones may be mixed? Physico-chemical compatibility of drug solutions in nebulizers--update 2013, *Journal of cystic fibrosis : official journal of the European Cystic Fibrosis Society* 13 (2014) 243–250.
- [2] P.A. Flume, J.P. Clancy, G.Z. Retsch-Bogart, D.E. Tullis, M. Bresnik, P.A. Derchak, S.A. Lewis, B.W. Ramsey, Continuous alternating inhaled antibiotics for chronic pseudomonas infection in cystic fibrosis, *Journal of cystic fibrosis : official journal of the European Cystic Fibrosis Society* (2016).
- [3] H. Heijerman, E. Westerman, S. Conway, D. Touw, G. Doring, Inhaled medication and inhalation devices for lung disease in patients with cystic fibrosis: A European consensus, *Journal of cystic fibrosis : official journal of the European Cystic Fibrosis Society* 8 (2009) 295–315.
- [4] N.R. Labiris, M.B. Dolovich, Pulmonary drug delivery. Part I: Physiological factors affecting therapeutic effectiveness of aerosolized medications, *British Journal of Clinical Pharmacology* 56 (2003) 588–599.
- [5] K. Bechtold-Peters, H. Luessen (Eds.), *Pulmonary drug delivery: Basics, applications and opportunities for small molecules and biopharmaceutics*, ECV - Ed.-Cantor-Verl., Aulendorf, 2007.
- [6] S.M. Setter, T.L. Levien, J.L. Iltz, P.S. Odegard, J.J. Neumiller, D.E. Baker, R.K. Campbell, Inhaled dry powder insulin for the treatment of diabetes mellitus, *Clinical therapeutics* 29 (2007) 795–813.
- [7] M.D. Louey, P.J. Stewart, Particle interactions involved in aerosol dispersion of ternary interactive mixtures, *Pharmaceutical research* 19 (2002) 1524–1531.
- [8] J. Muddle, D. Murnane, I. Parisini, M. Brown, C. Page, B. Forbes, Interaction of Formulation and Device Factors Determine the In Vitro Performance of Salbutamol Sulphate Dry Powders for Inhalation, *Journal of pharmaceutical sciences* 104 (2015) 3861–3869.
- [9] A.H. de Boer, B.H.J. Dickhoff, P. Hagedoorn, D. Gjaltema, J. Goede, D. Lambregts, H.W. Frijlink, A critical evaluation of the relevant parameters for drug redispersion from adhesive mixtures during inhalation, *International Journal of Pharmaceutics* 294 (2005) 173–184.

- [10] A.H. de Boer, H.K. Chan, R. Price, A critical view on lactose-based drug formulation and device studies for dry powder inhalation: which are relevant and what interactions to expect?, *Advanced Drug Delivery Reviews* 64 (2012) 257–274.
- [11] R. Vehring, Pharmaceutical particle engineering via spray drying, *Pharmaceutical research* 25 (2008) 999–1022.
- [12] T.F. Guimarães, A.D. Lanchote, J.S. da Costa, A.L. Viçosa, de Freitas, Luís Alexandre Pedro, A multivariate approach applied to quality on particle engineering of spray-dried mannitol, *Advanced Powder Technology* 26 (2015) 1094–1101.
- [13] T. Schröder, P. Walzel, Design of Laminar Operating Rotary Atomizers under Consideration of the Detachment Geometry, *Chemical Engineering and Technology* 21 (1998) 349–354.
- [14] A. Mescher, A. Möller, M. Dirks, P. Walzel, Gravity affected break-up of laminar threads at low gas-relative-velocities, *Chemical Engineering Science* 69 (2012) 181–192.
- [15] A. Mescher, J. Kamplade, P. Walzel (Eds.), *Spray Drying of Particles with narrow PSD by LAMROT Atomizer and optimized Gas*, 2013.
- [16] E.M. Littringer, A. Mescher, S. Eckhard, H. Schröttner, C. Langes, M. Fries, U. Griesser, P. Walzel, N.A. Urbanetz, Spray Drying of Mannitol as a Drug Carrier—The Impact of Process Parameters on Product Properties, *Drying Technology* 30 (2012) 114–124.
- [17] H. Steckel, N. Bolzen, Alternative sugars as potential carriers for dry powder inhalations, *International Journal of Pharmaceutics* 270 (2004) 297–306.
- [18] H. Larhrib, G.P. Martin, C. Marriott, D. Prime, The influence of carrier and drug morphology on drug delivery from dry powder formulations, *International Journal of Pharmaceutics* 257 (2003) 283–296.
- [19] M.F. Biddiscombe, O.S. Usmani, P.J. Barnes, A system for the production and delivery of monodisperse salbutamol aerosols to the lungs, *International Journal of Pharmaceutics* 254 (2003) 243–253.
- [20] E.M. Littringer, S. Zellnitz, K. Hammernik, V. Adamer, H. Friedl, N.A. Urbanetz, Spray Drying of Aqueous Salbutamol Sulfate Solutions Using the Nano Spray Dryer B-90—The Impact of Process Parameters on Particle Size, *Drying Technology* 31 (2013) 1346–1353.
- [21] S. Nešić, J. Vodnik, Kinetics of droplet evaporation, *Chemical Engineering Science* 46 (1991) 527–537.

- [22] E.M. Littringer, R. Paus, A. Mescher, H. Schroettner, P. Walzel, N.A. Urbanetz, The morphology of spray dried mannitol particles — The vital importance of droplet size, *Powder Technology* 239 (2013) 162–174.
- [23] E.M. Littringer, A. Mescher, H. Schroettner, L. Achelis, P. Walzel, N.A. Urbanetz, Spray dried mannitol carrier particles with tailored surface properties-the influence of carrier surface roughness and shape, *European journal of pharmaceutics and biopharmaceutics : official journal of Arbeitsgemeinschaft für Pharmazeutische Verfahrenstechnik e.V* 82 (2012) 194–204.
- [24] B.H.J. Dickhoff, A.H. de Boer, D. Lambregts, H.W. Frijlink, The effect of carrier surface treatment on drug particle detachment from crystalline carriers in adhesive mixtures for inhalation, *International Journal of Pharmaceutics* 327 (2006) 17–25.
- [25] M.J. Donovan, H.D. Smyth, Influence of size and surface roughness of large lactose carrier particles in dry powder inhaler formulations, *International Journal of Pharmaceutics* 402 (2010) 1–9.
- [26] W. Kaialy, M.N. Momin, M.D. Ticehurst, J. Murphy, A. Nokhodchi, Engineered mannitol as an alternative carrier to enhance deep lung penetration of salbutamol sulphate from dry powder inhaler, *Colloids and surfaces. B, Biointerfaces* 79 (2010) 345–356.
- [27] F. Grasmeijer, A.J. Lexmond, M. van den Noort, P. Hagedoorn, A.J. Hickey, H.W. Frijlink, A.H. de Boer, New mechanisms to explain the effects of added lactose fines on the dispersion performance of adhesive mixtures for inhalation, *PloS one* 9 (2014) e87825.
- [28] J.N. Staniforth, Pre-formulation aspects of dry powder aerosols, *Respiratory Drug Delivery V* (1996) 65–73.
- [29] E. Mutschler, *Mutschler Arzneimittelwirkungen: Lehrbuch der Pharmakologie, der klinischen Pharmakologie und Toxikologie ; mit einführenden Kapiteln in die Anatomie, Physiologie und Pathophysiologie ; mit 257 Tabellen und 1417 Strukturformeln*, 10th ed., WVG Wiss. Verl.-Ges, Stuttgart, 2013.
- [30] E.R. Weibel, *Morphometry of the Human Lung*, 1st ed., Springer Berlin, Berlin, 2014.
- [31] J.B. West, A. Luks, *West's respiratory physiology: The essentials*, Wolters Kluwer, Philadelphia, 2016.
- [32] M.J. Telko, A.J. Hickey, Dry powder inhaler formulation, *Respiratory care* 50 (2005) 1209–1227.

- [33] D.I. Daniher, J. Zhu, Dry powder platform for pulmonary drug delivery, *Particuology* 6 (2008) 225–238.
- [34] K.-H. Frömming, *Biopharmazie-Theorie und Praxis der Pharmakokinetik-*, herausgeg. von J. Meier, H. Rettig und H. Hess, bearb. von L. Dettli, J. W. Faigle, H. Hess, G. F. Kahl, F. Langenbacher, J. Meier, E. Mutschler, E. Nüesch und H. Rettig, 297 Abb., 102 Tab., XV, 473 S., Preis DM 210,00, Georg Thieme Verlag, Stuttgart - New York 1981, *Arch. Pharm. Pharm. Med. Chem.* 315 (1982) 191–192.
- [35] Rote Liste 2016: Arzneimittelverzeichnis für Deutschland (einschließlich EU-Zulassungen und bestimmter Medizinprodukte), 56th ed., Rote Liste Service GmbH, Frankfurt am Main, 2016.
- [36] R.A. Marrie, S. Patten, H. Tremlett, L.W. Svenson, C. Wolfson, B.N. Yu, L. Elliott, J. Profetto-McGrath, S. Warren, S. Leung, N. Jette, V. Bhan, J.D. Fisk, Chronic lung disease and multiple sclerosis: Incidence, prevalence, and temporal trends, *Multiple Sclerosis and Related Disorders* 8 (2016) 86–92.
- [37] R. Rietscher, M. Schroder, J. Janke, J. Czaplewska, M. Gottschaldt, R. Scherliess, A. Hanefeld, U.S. Schubert, M. Schneider, P.A. Knolle, C.-M. Lehr, Antigen delivery via hydrophilic PEG-b-PAGE-b-PLGA nanoparticles boosts vaccination induced T cell immunity, *European journal of pharmaceutics and biopharmaceutics : official journal of Arbeitsgemeinschaft für Pharmazeutische Verfahrenstechnik e.V* 102 (2016) 20–31.
- [38] D. Cipolla, J. Blanchard, I. Gonda, Development of Liposomal Ciprofloxacin to Treat Lung Infections, *Pharmaceutics* 8 (2016).
- [39] M.M. Al-Tabakha, Future prospect of insulin inhalation for diabetic patients: The case of Afrezza versus Exubera, *Journal of controlled release : official journal of the Controlled Release Society* 215 (2015) 25–38.
- [40] Y.S. Nassar, M. Ibrahim, A.G. Salman, T.S. Elgohary, Inhaled ceftazidime and amikacin versus inhaled colistin in the treatment of gram negative ventilator associated pneumonia, *Intensive care medicine experimental* 3 (2015) A380.
- [41] Global Initiative for Asthma (GINA), Global strategy for asthma management and prevention: GINA executive summary (2016 Update), 2016.
<http://ginasthma.org/2016-gina-report-global-strategy-for-asthma-management-and-prevention/>.
- [42] J. Vestbo, S.S. Hurd, A.G. Agustí, P.W. Jones, C. Vogelmeier, A. Anzueto, P.J. Barnes, L.M. Fabbri, F.J. Martinez, M. Nishimura, R.A. Stockley, D.D. Sin, R.

Rodriguez-Roisin, Global strategy for the diagnosis, management, and prevention of chronic obstructive pulmonary disease: GOLD executive summary, *American journal of respiratory and critical care medicine* 187 (2013) 347–365.

- [43] E.D. Bateman, S.S. Hurd, P.J. Barnes, J. Bousquet, J.M. Drazen, M. FitzGerald, P. Gibson, K. Ohta, P. O'Byrne, S.E. Pedersen, E. Pizzichini, S.D. Sullivan, S.E. Wenzel, H.J. Zar, Global strategy for asthma management and prevention: GINA executive summary, *The European respiratory journal* 31 (2008) 143–178.
- [44] Global Initiative for Chronic Obstructive Lung Disease, Pocket guide to COPD diagnosis, management, and prevention. A guide for Health Care Professionals, 2016. <https://www.guidelines.co.uk/gold/copd>.
- [45] European Pharmacopoeia, Preparations for Inhalation, 8th ed., Council of Europe, Strasbourg, 2015.
- [46] S. Newman, P. Anderson, *Respiratory drug delivery: Essential theory and practice*, Respiratory Drug Delivery Online, Richmond, Virginia, 2009.
- [47] D.R. Hess, Nebulizers: principles and performance, *Respiratory care* 45 (2000) 609–622.
- [48] H. Steckel, F. Eskandar, Factors affecting aerosol performance during nebulization with jet and ultrasonic nebulizers, *European journal of pharmaceutical sciences : official journal of the European Federation for Pharmaceutical Sciences* 19 (2003) 443–455.
- [49] P.R. Phipps, I. Gonda, Droplets produced by medical nebulizers. Some factors affecting their size and solute concentration, *Chest* 97 (1990) 1327–1332.
- [50] G. Tiwari, R. Tiwari, B. Sriwastawa, L. Bhati, S. Pandey, P. Pandey, S.K. Bannerjee, Drug delivery systems: An updated review, *International journal of pharmaceutical investigation* 2 (2012) 2–11.
- [51] J. Bell, S. Newman, The rejuvenated pressurised metered dose inhaler, *Expert opinion on drug delivery* 4 (2007) 215–234.
- [52] M. Dolovich, R.E. Ruffin, R. Roberts, M.T. Newhouse, Optimal delivery of aerosols from metered dose inhalers, *Chest* 80 (1981) 911–915.
- [53] L. Borgstrom, E. Derom, E. Stahl, E. Wahlin-Boll, R. Pauwels, The inhalation device influences lung deposition and bronchodilating effect of terbutaline, *American journal of respiratory and critical care medicine* 153 (1996) 1636–1640.

- [54] S.P. Newman, A.W. Weisz, N. Talaei, S.W. Clarke, Improvement of drug delivery with a breath actuated pressurised aerosol for patients with poor inhaler technique, *Thorax* 46 (1991) 712–716.
- [55] G. Pitcairn, S. Reader, D. Pavia, S. Newman, Deposition of corticosteroid aerosol in the human lung by Respimat Soft Mist inhaler compared to deposition by metered dose inhaler or by Turbuhaler dry powder inhaler, *Journal of aerosol medicine : the official journal of the International Society for Aerosols in Medicine* 18 (2005) 264–272.
- [56] R. Dalby, M. Spallek, T. Voshaar, A review of the development of Respimat Soft Mist Inhaler, *International Journal of Pharmaceutics* 283 (2004) 1–9.
- [57] J.H. Bell, P.S. Hartley, J.S. Cox, Dry powder aerosols. I. A new powder inhalation device, *Journal of pharmaceutical sciences* 60 (1971) 1559–1564.
- [58] A.J. Hickey, H.M. Mansour, M.J. Telko, Z. Xu, H.D.C. Smyth, T. Mulder, R. McLean, J. Langridge, D. Papadopoulos, Physical characterization of component particles included in dry powder inhalers. I. Strategy review and static characteristics, *Journal of pharmaceutical sciences* 96 (2007) 1282–1301.
- [59] R.H. Hirst, S.R. Newman, D.A. Clark, M.G.L. Hertog, Lung deposition of budesonide from the novel dry powder inhaler Airmax, *Respiratory medicine* 96 (2002) 389–396.
- [60] F. Lavorini, C.J. Corrigan, P.J. Barnes, P.R.N. Dekhuijzen, M.L. Levy, S. Pedersen, N. Roche, W. Vincken, G.K. Crompton, Retail sales of inhalation devices in European countries: so much for a global policy, *Respiratory medicine* 105 (2011) 1099–1103.
- [61] Asthma Forecast in the US, Japan, and 5EU, 2009.
- [62] Y.S. Cheng, T.C. Marshall, R.F. Henderson, G.J. Newton, Use of a jet mill for dispersing dry powder for inhalation studies, *American Industrial Hygiene Association journal* 46 (1985) 449–454.
- [63] A. Chawla, K. Taylor, J.M. Newton, M. Johnson, Production of spray dried salbutamol sulphate for use in dry powder aerosol formulation, *International Journal of Pharmaceutics* 108 (1994) 233–240.
- [64] E.M. Littringer, M.F. Noisternig, A. Mescher, H. Schroettner, P. Walzel, U.J. Griesser, N.A. Urbanetz, The morphology and various densities of spray dried mannitol, *Powder Technology* 246 (2013) 193–200.
- [65] H. Steckel, H.G. Brandes, A novel spray-drying technique to produce low density particles for pulmonary delivery, *International Journal of Pharmaceutics* 278 (2004) 187–195.

- [66] S.P. Velaga, R. Berger, J. Carlfors, Supercritical fluids crystallization of budesonide and flunisolide, *Pharmaceutical research* 19 (2002) 1564–1571.
- [67] T. Müller, R. Krehl, J. Schiewe, C. Weiler, H. Steckel, Influence of small amorphous amounts in hydrophilic and hydrophobic APIs on storage stability of dry powder inhalation products, *European journal of pharmaceutics and biopharmaceutics : official journal of Arbeitsgemeinschaft für Pharmazeutische Verfahrenstechnik e.V* 92 (2015) 130–138.
- [68] K. Wetterlin, Turbuhaler: a new powder inhaler for administration of drugs to the airways, *Pharmaceutical research* 5 (1988) 506–508.
- [69] A.I. Bot, T.E. Tarara, D.J. Smith, S.R. Bot, C.M. Woods, J.G. Weers, Novel lipid-based hollow-porous microparticles as a platform for immunoglobulin delivery to the respiratory tract, *Pharmaceutical research* 17 (2000) 275–283.
- [70] S.P. Duddu, S.A. Sisk, Y.H. Walter, T.E. Tarara, K.R. Trimble, A.R. Clark, M.A. Eldon, R.C. Elton, M. Pickford, P.H. Hirst, S.P. Newman, J.G. Weers, Improved lung delivery from a passive dry powder inhaler using an Engineered PulmoSphere powder, *Pharmaceutical research* 19 (2002) 689–695.
- [71] P. Lucas, K. Anderson, J.N. Staniforth, Protein deposition from dry powder inhalers: fine particle multiplets as performance modifiers, *Pharmaceutical research* 15 (1998) 562–569.
- [72] F. Grasmeijer, H.W. Frijlink, A.H. de Boer, A proposed definition of the ‘activity’ of surface sites on lactose carriers for dry powder inhalation, *European Journal of Pharmaceutical Sciences* 56 (2014) 102–104.
- [73] C.A. Dunber, A.J. Hickey, P. Holzner, Dispersion and Characterization of Pharmaceutical Dry Powder Aerosols, *KONA* 16 (1998) 7–45.
- [74] S. White, D.B. Bennett, S. Cheu, P.W. Conley, D.B. Guzek, S. Gray, J. Howard, R. Malcolmson, J.M. Parker, P. Roberts, N. Sadrzadeh, J.D. Schumacher, S. Seshadri, G.W. Sluggett, C.L. Stevenson, N.J. Harper, Exubera: pharmaceutical development of a novel product for pulmonary delivery of insulin, *Diabetes technology & therapeutics* 7 (2005) 896–906.
- [75] A.H. de Boer, P. Hagedoorn, D. Gjaltema, J. Goede, H.W. Frijlink, Air classifier technology (ACT) in dry powder inhalation Part 3. Design and development of an air classifier family for the Novolizer multi-dose dry powder inhaler, *International Journal of Pharmaceutics* 310 (2006) 72–80.

- [76] A.H. de Boer, P. Hagedoorn, D. Gjaltema, J. Goede, H.W. Frijlink, Air classifier technology (ACT) in dry powder inhalation Part 4. Performance of air classifier technology in the Novolizer multi-dose dry powder inhaler, *International Journal of Pharmaceutics* 310 (2006) 81–89.
- [77] H. Chrystyn, Closer to an 'ideal inhaler' with the Easyhaler: an innovative dry powder inhaler, *Clinical drug investigation* 26 (2006) 175–183.
- [78] European Pharmacopoeia, 2.9.18, Preparations for Inhalation: Aerodynamic Assessment of Fine Particles, 8th ed., Council of Europe, Strasbourg, 2013.
- [79] X.M. Zeng, G.P. Martin, C. Marriott, J. Pritchard, The effects of carrier size and morphology on the dispersion of salbutamol sulphate after aerosolization at different flow rates, *The Journal of pharmacy and pharmacology* 52 (2000) 1211–1221.
- [80] W. Glover, H.-K. Chan, S. Eberl, E. Daviskas, J. Verschuer, Effect of particle size of dry powder mannitol on the lung deposition in healthy volunteers, *International Journal of Pharmaceutics* 349 (2008) 314–322.
- [81] H. Steckel, B.W. Müller, In vitro evaluation of dry powder inhalers II: Influence of carrier particle size and concentration on in vitro deposition, *International Journal of Pharmaceutics* 154 (1997) 31–37.
- [82] S.G. Maas, G. Schaldach, P.E. Walzel, N.A. Urbanetz, Tailoring dry powder inhaler performance by modifying carrier surface topography by spray drying, *Atomiz Spr* 20 (2010) 763–774.
- [83] S.G. Maas, G. Schaldach, E.M. Littringer, A. Mescher, U.J. Griesser, D.E. Braun, P.E. Walzel, N.A. Urbanetz, The impact of spray drying outlet temperature on the particle morphology of mannitol, *Powder Technology* 213 (2011) 27–35.
- [84] D. El-Sabawi, R. Price, S. Edge, P.M. Young, Novel temperature controlled surface dissolution of excipient particles for carrier based dry powder inhaler formulations, *Drug development and industrial pharmacy* 32 (2006) 243–251.
- [85] H. Steckel, P. Markefka, H. teWierik, R. Kammelar, Effect of milling and sieving on functionality of dry powder inhalation products, *International Journal of Pharmaceutics* 309 (2006) 51–59.
- [86] M.D. Jones, R. Price, The influence of fine excipient particles on the performance of carrier-based dry powder inhalation formulations, *Pharmaceutical research* 23 (2006) 1665–1674.

- [87] F.R. Fronczek, H.N. Kamel, M. Slattery, Three polymorphs (alpha, beta, and delta) of D-mannitol at 100 K, *Acta crystallographica. Section C, Crystal structure communications* 59 (2003) 70.
- [88] L. Tajber, D.O. Corrigan, O.I. Corrigan, A.M. Healy, Spray drying of budesonide, formoterol fumarate and their composites--I. Physicochemical characterisation, *International Journal of Pharmaceutics* 367 (2009) 79–85.
- [89] S. Zellnitz, O. Narygina, C. Resch, H. Schroettner, N.A. Urbanetz, Crystallization speed of salbutamol as a function of relative humidity and temperature, *International Journal of Pharmaceutics* 489 (2015) 170–176.
- [90] G.P. Johari, R.M. Shanker, On the solubility advantage of a pharmaceutical's glassy state over the crystal state, and of its crystal polymorphs, *Thermochimica Acta* 598 (2014) 16–27.
- [91] S. Karner, E.M. Littringer, N.A. Urbanetz, Triboelectrics: The influence of particle surface roughness and shape on charge acquisition during aerosolization and the DPI performance, *Powder Technology* 262 (2014) 22–29.
- [92] S. Karner, M. Maier, E. Littringer, N.A. Urbanetz, Surface roughness effects on the tribo-charging and mixing homogeneity of adhesive mixtures used in dry powder inhalers, *Powder Technology* 264 (2014) 544–549.
- [93] S. Karner, N.A. Urbanetz, Triboelectric characteristics of mannitol based formulations for the application in dry powder inhalers, *Powder Technology* 235 (2013) 349–358.
- [94] S. Kellam, H. Wansbrough, The manufacture of lactose.
<http://nzic.org.nz/ChemProcesses/dairy/3F.pdf>.
- [95] P. Walzel, *Spraying and Atomizing of Liquids*, in: *Ullmann's Encyclopedia of Industrial Chemistry*, Wiley-VCH Verlag GmbH & Co. KGaA, Weinheim, Germany, 2000.
- [96] T. Schröder, P. Walzel, Gestaltung laminar betriebener Rotationszerstäuber unter Berücksichtigung der Abströmgeometrie, *Chemie Ing. Techn.* 70 (1998) 400–405.
- [97] A. Mescher, E.M. Littringer, R. Paus, N.A. Urbanetz, P. Walzel, Homogene Produkteigenschaften in der Sprühtrocknung durch laminare Rotationszerstäubung, *Chemie Ingenieur Technik* 84 (2012) 154–159.
- [98] J. Kamplade, T. Mack, A. Küsters, P. Walzel, Break-Up of Threads From Laminar Open Channel Flow Influenced by Cross-Wind Gas Flow, in: *ASME 2014 4th Joint US-European Fluids Engineering Division Summer Meeting collocated with the ASME 2014 12th International Conference on Nanochannels, Microchannels, and Minichannels*, pp. V002T20A001.

- [99] J. Rayleigh, On the stability of jets 14 (1878).
- [100] T. Schröder, Tropfenbildung an Gerinneströmungen im Schwere- und Zentrifugalfeld. Univ. Gesamthochsch., Diss--Essen, VDI-Verl., Düsseldorf, 1997.
- [101] R. Sarrate, J.R. Ticó, M. Miñarro, C. Carrillo, A. Fàbregas, E. García-Montoya, P. Pérez-Lozano, J.M. Suñé-Negre, Modification of the morphology and particle size of pharmaceutical excipients by spray drying technique, Powder Technology 270 (2015) 244–255.
- [102] D.E. Walton, C.J. Mumford, The Morphology of Spray-Dried Particles, Chemical Engineering Research and Design 77 (1999) 442–460.
- [103] D. Lechuga-Ballesteros, C. Charan, C.L.M. Stults, C.L. Stevenson, D.P. Miller, R. Vehring, V. Tep, M.-C. Kuo, Trileucine improves aerosol performance and stability of spray-dried powders for inhalation, Journal of pharmaceutical sciences 97 (2008) 287–302.
- [104] J. Elversson, A. Millqvist-Fureby, G. Alderborn, U. Elofsson, Droplet and particle size relationship and shell thickness of inhalable lactose particles during spray drying, Journal of pharmaceutical sciences 92 (2003) 900–910.
- [105] N. Rhein, G. Birk, R. Scherließ (Eds.), Characterisation of particle engineered Mannitol as alternative carriers in dry powder inhalation formulations, 2015.
- [106] S. Gaisford, M. Dennison, M. Tawfik, M.D. Jones, Following mechanical activation of salbutamol sulphate during ball-milling with isothermal calorimetry, International Journal of Pharmaceutics 393 (2010) 74–78.
- [107] S.H. Yalkowsky, Y. He, P. Jain, Handbook of aqueous solubility data, 2nd ed., CRC Press, Boca Raton, FL, 2010.
- [108] Hansch, A. Leo, and D. Hoekman, Exploring QSAR: Hydrophobic, Electronic, and Steric Constants C. American Chemical Society, Washington, DC. 1995., J. Med. Chem. 39 (1996) 1189–1190.
- [109] J.S. Patton, R.M. Platz, Routes of delivery: Case studies: (2) Pulmonary delivery of peptides and proteins for systemic action, Advanced Drug Delivery Reviews 8 (1992) 179–196.
- [110] T.B. Y. Peng, Characterization of D-Mannitol by Thermal Analysis, FTIR & Raman Spectroscopy: Application Note, 2016.
https://shop.perkinelmer.com/Content/applicationnotes/app_characterizationofd-mannitol.pdf.

- [111] European Directorate for the Quality of Medicines & HealthCare, European Pharmacopeia 8.0: 8.2 Monographies, 1st ed., Deutscher Apotheker Verlag, Stuttgart, 2016.
- [112] Weltgesundheitsorganisation, Meeting of the WHO Expert Committee on the Selection and Use of Essential Medicines, The selection and use of essential medicines: Report of the WHO Expert Committee, 2013 ; (including the 18th WHO model list of essential medicines and the 4th WHO model list of essential medicines for children) ; [Geneva, Switzerland on 8 - 12 April 2013], World Health Organization, Geneva, 2014.
- [113] T. Herdegen, R. Böhm, Kurzlehrbuch Pharmakologie und Toxikologie, 3rd ed., Thieme, Stuttgart, 2014.
- [114] Drugbank, Budesonide, CAS No. 51333-22-3, 2016.
<http://www.drugbank.ca/drugs/DB01222>.
- [115] Drugbank, Formoterol, CAS No 73573-87-2, 2016. 26.04.2016.
- [116] Drugbank, Tiotropium, CAS No 136310-93-5, 2016.
<http://www.drugbank.ca/drugs/DB01409>.
- [117] US EPA, Estimation Program Interface (EPI) Suite: Version 3.11, 2003.
<http://toxnet.nlm.nih.gov/cgi-bin/sis/search2/r?dbs+hsdb:@term+@rn+@rel+18559-94-9>.
- [118] D. Steinhilber, M. Schubert-Zsilavec, H.J. Roth, Medizinische Chemie: Targets - Arzneistoffe - chemische Biologie ; 191 Tabellen, 2nd ed., Dt. Apotheker-Verl., Stuttgart, 2010.
- [119] B. Dejaegher, Y.V. Heyden, Experimental designs and their recent advances in set-up, data interpretation, and analytical applications, Journal of pharmaceutical and biomedical analysis 56 (2011) 141–158.
- [120] W. Kleppmann, Versuchsplanung: Produkte und Prozesse optimieren, 8th ed., Hanser, München, 2013.
- [121] R. Leardi, Experimental design in chemistry: A tutorial, Analytica Chimica Acta 652 (2009) 161–172.
- [122] MKS Umetrics (Ed.), Modde User Guide, Version 10.1, Umea, Sweden, 2014.
- [123] A. Mescher, Einfluss der Gasführung in Sprühtrocknern auf den Fadenzerfall an Rotationszerstäubern: Analyse und Optimierung. Techn. Univ., Diss.--Dortmund, 2012, 1st ed., Verl. Dr. Hut, München, 2012.

- [124] C. Fritsche, E. Koller (Eds.), Büchi Mini Spray Dryer B-290 - User Manual, Büchi Labortechnik AG, 2009.
- [125] R.A. Storey, I. Ymén (Eds.), Solid state characterization of pharmaceuticals, 1st ed., Wiley & Sons, Chichester, 2011.
- [126] International Organization for Standardization, Particle Size Analysis - Laser Diffraction Methods, 13320th ed., Vernier, Switzerland, 2009.
- [127] European Directorate for the Quality of Medicines & HealthCare, European Pharmacopeia, 8. edition, Ph.Eur. 8.0: Ph. Eur. 2.9.18 Preparations for Inhalation: Aerodynamic Assessment of Fine Particles, 1st ed., Deutscher Apotheker Verlag, Stuttgart, 2016.
- [128] European Committee for Standardization / Deutsches Institut für Normung, Benennungen, Definitionen und Kenngrößen der Oberflächenbeschaffenheit.
- [129] European Directorate for the Quality of Medicines & HealthCare, European Pharmacopeia 8.0: Ph. Eur. 2.9.34 Bulk and Tapped Density of Powders, 1st ed., Deutscher Apotheker Verlag, Stuttgart, 2016.
- [130] K.H. Bauer, B.C. Lippold, Pharmazeutische Technologie: Mit Einführung in die Biopharmazie ; [Lehrbuch] ; mit 91 Tabellen, 9th ed., Wiss. Verl.-Ges, Stuttgart, 2012.
- [131] E. Cordts, H. Steckel, Capabilities and limitations of using powder rheology and permeability to predict dry powder inhaler performance, European journal of pharmaceuticals and biopharmaceutics : official journal of Arbeitsgemeinschaft für Pharmazeutische Verfahrenstechnik e.V 82 (2012) 417–423.
- [132] S. Brunauer, P.H. Emmett, E. Teller, Adsorption of Gases in Multimolecular Layers, J. Am. Chem. Soc. 60 (1938) 309–319.
- [133] European Directorate for the Quality of Medicines & HealthCare, European Pharmacopeia 8.0: Ph. Eur. 2.9.26 - Specific surface area by gas adsorption, 1st ed., Deutscher Apotheker Verlag, Stuttgart, 2016.
- [134] A. Eisazadeh, K.A. Kassim, H. Nur, Morphology and BET surface area of phosphoric acid stabilized tropical soils, Engineering Geology 154 (2013) 36–41.
- [135] J.R. Conder, C.L. Young, Physicochemical measurement by gas chromatography, Wiley & Sons, Chichester u.a., 1979.
- [136] I.M. Grimsey, J.C. Feeley, P. York, Analysis of the surface energy of pharmaceutical powders by inverse gas chromatography, Journal of pharmaceutical sciences 91 (2002) 571–583.

- [137] W. Henry, Experiments on the Quantity of Gases Absorbed by Water, at Different Temperatures, and under Different Pressures, *Philosophical Transactions of the Royal Society of London* 93 (1803) 29–274.
- [138] R. Ho, A.S. Muresan, G.A. Hebbink, J.Y. Heng, Influence of fines on the surface energy heterogeneity of lactose for pulmonary drug delivery, *International Journal of Pharmaceutics* 388 (2010) 88–94.
- [139] M.G. Cares-Pacheco, G. Vaca-Medina, R. Calvet, F. Espitalier, J.-J. Letourneau, A. Rouilly, E. Rodier, Physicochemical characterization of D-mannitol polymorphs: the challenging surface energy determination by inverse gas chromatography in the infinite dilution region, *International Journal of Pharmaceutics* 475 (2014) 69–81.
- [140] S.R. Gopireddy, E. Gutheil, Numerical simulation of evaporation and drying of a bi-component droplet, *International Journal of Heat and Mass Transfer* 66 (2013) 404–411.
- [141] S.R. Gopireddy, Numerical simulation of bi-component droplet evaporation and dispersion in spray and spray drying, Heidelberg, Univ., Diss., 2013, 2013.
- [142] H. Grosshans, M. Griesing, M. Mönckedieck, T. Hellwig, B. Walther, S.R. Gopireddy, R. Sedelmayer, W. Pauer, H.-U. Moritz, N.A. Urbanetz, E. Gutheil, Numerical and experimental study of the drying of bi-component droplets under various drying conditions, *International Journal of Heat and Mass Transfer* 96 (2016) 97–109.
- [143] J. Cornel, P. Kidambi, M. Mazzotti, Precipitation and Transformation of the Three Polymorphs of d -Mannitol, *Ind. Eng. Chem. Res.* 49 (2010) 5854–5862.
- [144] C. Marchioli, M. Fantoni, A. Soldati, Orientation, distribution, and deposition of elongated, inertial fibers in turbulent channel flow, *Phys. Fluids* 22 (2010) 33301.
- [145] X.M. Zeng, G.P. Martin, S.-K. Tee, C. Marriott, The role of fine particle lactose on the dispersion and deaggregation of salbutamol sulphate in an air stream in vitro, *International Journal of Pharmaceutics* 176 (1998) 99–110.
- [146] R. Guchardi, M. Frei, E. John, J.S. Kaerger, Influence of fine lactose and magnesium stearate on low dose dry powder inhaler formulations, *International Journal of Pharmaceutics* 348 (2008) 10–17.

Lebenslauf

Persönliche Daten

Name	Mathias Willi Mönckedieck
Geburtsdatum	18.09.1985
Geburtsort	Cloppenburg
Staatsangehörigkeit	Deutsch

Schulbildung

1992 – 1996	Grundschule Wallschule, Cloppenburg
1996 – 1998	Orientierungsstufe Don-Bosco, Cloppenburg
1998 – 2005	Gymnasium Liebfrauenschule, Cloppenburg
Juni 2005	Erwerb der allgemeinen Hochschulreife

Hochschulstudium

Okt. 2006 – Sept. 2007	Studium der Biologie an der Philipps Universität zu Marburg, Deutschland
Okt. 2007 – Nov. 2011	Studium der Pharmazie an der Christian Albrechts Universität zu Kiel, Deutschland
Jan. 2012 – Jun. 2012	1. Hälfte des Praktischen Jahres in der Privilegierten Adler Apotheke in Hamburg, Deutschland
Jul. 2012 – Dez. 2012	2. Hälfte des Praktischen Jahres an der School of Pharmacy der University of Otago, Dunedin, Neuseeland
Feb. 2013	Abschluss des Pharmazie-Studiums mit dem Erwerb der Approbation zum Apotheker, Kiel, Deutschland
Jan. 2014	Abschluss des Diplom-Studiengangs Pharmazie an der Martin-Luther Universität zu Halle-Wittenberg, Deutschland
Apr. 2013 – März 2014	Promotionsstudium am Research Center for Pharmaceutical Engineering (RCPE) in Graz, Österreich
Seit Apr. 2014	Fortsetzung des Promotionsstudiums an der Christian-Albrechts Universität zu Kiel, Deutschland

Ausbildung

Okt. 2005	Ausbildung zum staatlich anerkannten Rettungssanitäter an der DRK-Rettungsdienstschule in Bodenstein, Deutschland
-----------	---

Beruflicher Werdegang

Sept. 2005 – Aug. 2006	Rettungssanitäter an der DRK Rettungswache in Cloppenburg, Deutschland, im Rahmen eines Freiwilligen Sozialen Jahres
Seit März 2013	Apotheker in der Privilegierten Adler Apotheke in Hamburg, Deutschland

Erklärung nach § 8 der Promotionsordnung

Hiermit erkläre ich gemäß § 8 der Promotionsordnung der Mathematisch-Naturwissenschaftlichen Fakultät der Christian-Albrechts-Universität zu Kiel, dass ich die vorliegende Arbeit, abgesehen von der Beratung durch meinen Betreuer, selbstständig und ohne fremde Hilfe verfasst habe. Weiterhin habe ich keine anderen als die angegebenen Quellen oder Hilfsmittel benutzt und die den benutzten Werken wörtlich oder inhaltlich entnommenen Stellen als solche kenntlich gemacht. Die vorliegende Arbeit ist unter Einhaltung der Regeln guter wissenschaftlicher Praxis entstanden und wurde bei keiner anderen Universität zur Begutachtung eingereicht.

Mathias Mönckedieck

Danksagungen

Abschließend möchte ich die Möglichkeit nutzen Dank an alle auszusprechen, die mich bei der Anfertigung dieser Arbeit direkt oder indirekt unterstützt haben. Mit Hilfe dieser fachlichen aber auch zwischenmenschlichen Unterstützung habe ich an diesem Institut eine sehr lehrreiche und inspirierende Zeit verbringen können.

Mein besonderer Dank gilt hierbei meinem Doktorvater Prof. Dr. Hartwig Steckel, der mich im Rahmen dieses herausfordernden Projektes in seinen Arbeitskreis aufgenommen hat und mir auch trotz der später großen Entfernung immer mit Ratschlägen zur Seite stand.

Ein besonders herzliches Dankeschön gebührt meiner Doktormutter PD Dr. Regina Scherließ, die mich während meiner Promotionszeit vor allem durch immer wiederwährende konstruktive Projektbesprechungen unterstützt hat, aber jederzeit auch für interessante Konversationen über das ferne Neuseeland, den Segelsport oder den ortsansässigen Handball-Bundesligisten Zeit hatte.

Bei PD Dr. Nora Urbanetz möchte ich mich herzlich für die vielen Ideen und Anregungen in den zahlreichen inhaltlich vollgepackten Besprechungen sowie für die Überlassung dieses von ihr initiierten Projektes im Rahmen des DFG-Prioritätsprogrammes bedanken.

Jens Kamplade möchte ich für die fachliche Kompetenz, die Unterstützung bei den Trocknungsversuchen an der TU Dortmund sowie für das entsprechende Rahmenprogramm und den kollegialen Umgang vor Ort danken. In diesem Zuge sei auch Prof. Peter Walzel erwähnt, der mir die experimentellen Voraussetzungen durch die Nutzung des eigens konzipierten institutseigenen Sprühtrockners erst ermöglicht hat.

Matthias Griesing und Holger Großhans möchte ich für fachlich intensive aber auch freundschaftlich feucht-fröhliche Momente während der vergangenen Jahre danken.

Srikanth Gopireddy danke ich für die Einführung in die Simulationswelt sowie für die Hilfe bei der Berechnung der Peclet-Werte im Rahmen dieser Arbeit.

Ein ganz besonderer Dank gilt meinem Master-Studenten Phaniel Fakner, der im Rahmen seiner Masterarbeit mit vollem Einsatz in diesem Projekt mitgearbeitet hat.

Zugleich möchte ich mich bei Jacob Bannow, Saskia Meier und Magdalena Puttnies – sprich bei meinen Hiwis – bedanken, die mir während der Promotionszeit bei einer Großzahl an Impaktionsversuchen zur Seite standen.

Ein ganz spezieller Dank gilt Friederike Gütter, die diese Arbeit Korrektur gelesen hat und auch sonst jederzeit für abwechslungsreiche Abende zu motivieren war (aber natürlich maximal bis 22 Uhr).

Meinem Bürokollegen Mats Hertel danke ich in vielerlei Hinsicht für – wie man so schön sagt – „alles auf und neben dem Platz“. Zu nennen sind hier sowohl fachliche Konversationen als auch auch niveaувolle Momente zu Themen jeglicher Art, die nicht selten in die Vergabe von „Büropunkten“ münden sollten. Ob beim Marathon in Hamburg, beim Angeln in Norwegen oder beim Bier-Bachelor in Bamberg – ich erinnere mich an viele besondere Momente.

Den ehemaligen Kollegen Lars Wagenseil und Gereon Rau danke ich für wertvolle Diskussionen über Fachliches aber manchmal auch weniger Fachliches.

Dem Rest der DDL-Crew um Judith Heidland, Nancy Rhein und Niklas Renner möchte ich für die mentale Unterstützung vor dem Pat Burnell Vortrag aber auch für immer wieder spannende Reisen ins winterlich nasskalte Edinburgh danken. Ebenso danke ich Judith für die Ausrichtung sämtlicher Spieleabende.

Dem technischen Personal danke ich in vielerlei Hinsicht: Hanna Rohwer, Regina Krehl und Maren Rohlf für die unermüdliche Unterstützung bei Problemen an der HPLC-Front, Rüdi Smal für Messungen an XRPD und DSC sowie für die Erstellung von Graphiken, Volkmar Kleppa und Detlef Rödiger für den notwendigen IT-Support und Dirk Böhme für Hilfe bei sämtlichen weiteren technischen Problemen. Kalle Bock möchte ich neben dem technischen Support auch fürs ausdauernde Motivieren sowie für ganz spezielle Momente über den Dächern der Stadt danken.

Generell gebührt dem Arbeitskreis – und damit sind sowohl die aktuellen als auch ehemaligen Kollegen gemeint – ein besonderer Dank für die angenehme Arbeitsatmosphäre während der vergangenen Jahre.

Ein ganz besonderer Dank gilt jedoch meinen Freunden und meiner Familie, ohne die die Anfertigung dieser Arbeit nicht möglich gewesen wäre.

Da sei zunächst meine WG mit Mona Kühling-Thees und Christoph Merschformann genannt, die mich in den letzten Monaten eigentlich selten vor 22 Uhr zu Haus erwarten durften.

Dann möchte ich Momme Imbusch für viele Abende vor Ort aber auch auf See danken. Ich freue mich sehr auf den gemeinsamen Herbst in der Karibik. Ulrike Aumüller danke ich im selben Zuge für die nötige Motivation in der Bibliothek aber auch für die gemeinsamen Ausflüge in die Unischwimmhallen sowie für gemütliche Tatort-Abende.

Leon Fürtges danke ich vor allem für die sportlich schönen Urlaubsmomente der letzten drei Jahre – mögen noch viele weitere Stunden im Sattel oder zu See folgen.

Dann möchte ich hier meinen Jungs aus der Heimat herzlich für jegliche Art der Unterstützung über die vielen gemeinsamen Jahre danken. Gleiches gilt auch für Juliane Frye und Tina Borde, die auch trotz der Entfernung immer erreichbar waren.

Ein ganz spezieller Dank gilt jedem einzelnen aus meiner Familie. Neben meiner Patentante und meinem Patenonkel möchte ich hier vor allem Anita Rolfes danken, die jederzeit ein offenes Ohr hatte.

Mit Jens Mönckedieck möchte ich noch der besten Ablenkung vom Schreiben einer Doktorarbeit danken – es war mir eine Freude mit dir nach Stockholm zu reisen oder einfach nur gegenseitig Motivation für Masterarbeit oder Dissertation zu tanken.

Meiner Schwester Verena Bienek und Ihrem Mann Michael (engl. ausgesprochen) Bienek danke ich für die vielen Nächte, die ich das „Gästezimmer“ bekleiden durfte sowie für die vielen schönen gemeinsamen Momente in den Jahren während der Promotion und für das süßeste Patenkind, das man sich nur wünschen kann

Meinen Eltern gebührt das vermutlich größte und herzlichste „Dankeschön“, da ohne Sie diese Arbeit nie geschrieben worden wäre. Vielen Dank für eure Unterstützung über all die vielen Jahre. Es ist immer wieder schön zu wissen, wo man eigentlich hingehört, auch wenn man das Jahr über viel auf Reisen ist..